EFFECTS OF TRANSITION METAL CATIONIZATION ON PEPTIDE DISSOCIATION BY MASS SPECTROMETRY

by

HEATHER MALONE WATSON

CAROLYN J. CASSADY, COMMITTEE CHAIR
GREGORY J. SZULCZEWSKI
JOHN B. VINCENT
LAURA S. BUSENLEHNER
JANIS M. O'DONNELL

A DISSERTATION

Submitted in partial fulfillment of the requirements
for the degree of Doctor of Philosophy
in the Department of Chemistry
in the Graduate School of
The University of Alabama

TUSCALOOSA, ALABAMA

2011

ABSTRACT

Peptide sequencing is fundamental to understanding a protein's structure and function. The field of proteomics is dedicated to how these aspects relate to human health and disease. Unfortunately, the majority of peptides and proteins are not fully sequenced. In mass spectrometry, this is often due to spectral complications and incomplete fragmentation. There is a need to develop new sample preparation techniques or dissociation methods to increase sequence information. The dissociation of transition metal-cationized peptides by collision-induced dissociation (CID), electron-transfer dissociation (ETD), and electron-transfer collisionally activated dissociation (ETcaD) has been investigated in a quadrupole ion trap (QIT). The resulting mass spectra provide a wealth of information about the primary structures of the peptides.

Using transition metal ions as cationizing reagents proves beneficial to peptide sequencing by CID and, in some cases, is better than the analysis of protonated species. For instance, spectra obtained from CID of singly and doubly charged Cu(II)-heptaalanine ions, $[M + Cu - H]^+$ and $[M + Cu]^{2+}$, are complementary and together provide cleavage at every residue and no neutral losses. This contrasts with protonated heptaalanine, $[M + H]^+$, which results in fewer backbone cleavages by CID and does not allow sequencing of the first three residues.

Multiply charged precursor ions are required in order to carry out ETD and ETcaD. This can be problematic for acidic or neutral peptides. This work demonstrates

that addition of transition metals as a cationizing reagent allows peptides to be submitted to ETD and ETcaD that do not otherwise form multiply charged precursors. ETD spectra were less complex than those produced by CID. ETcaD increases backbone cleavages for all samples studied relative to ETD. In addition, complexes that result in very few cleavages by CID are cleaved at every residue when submitted to ETcaD. Evidence for macrocyclic metallated a- and b-ions is found in ETD and ETcaD spectra in the form of nonsequential product ions.

The sequence (pEEEEGDD) of the peptide component of biologically derived low-molecular-weight chromium binding substance (LMWCr) is obtained as a result of extensive mass spectrometric studies. LMWCr is proposed to be involved in carbohydrate metabolism. The sequencing of the peptide component of LMWCr by MS represents a potentially significant milestone towards understanding the pharmacological role of chromium at a molecular level.

LIST OF ABBREVIATIONS AND SYMBOLS

AC	alternating current
ACN	acetonitrile
ACTH	adrenocorticoptropic hormone
$AgBF_4$	silver tetrafluoroborate
Ala	alanine
Asp	aspartic acid
BF_4	tetrafluoroborate
CAD	collisionally activated dissociation
CCA	α-cyano-4-hydroxycinnamic acid
CID	collision-induced dissociation
Cys	cysteine
Da	Dalton
DC	direct current
ddH_2O	doubly deionized water
DE	delayed extraction
DHB	2,5-dihydroxybenzoic acid
DIC	1, 4-diisopropylcarbodiimide
DMF	N,N-dimethylformamide
e^-*	low energy electron

ECD	electron capture dissociation
EDTA	ethylenediaminetetraacetic acid
E_k	kinetic energy
EM	electron multiplier
E_p	potential energy
ESI	electrospray ionization
ET	electron-transfer
ETcaD	electron-transfer collisionally activated dissociation
ETD	electron-transfer dissociation
ETnoD	electron-transfer no dissociation
eV	electron volt
FA	formic acid
Fmoc	9-fluoroenylmethoxycarbonyl
g	grams
Glu	glutamic acid
Gly	glycine
GP	graphite powder
HCT	high capacity trap
Hobt	1-hydroxybenzotriazole hydrate
HPLC	high performance liquid chromatography
Hz	hertz
ICC	ion charge control

IE2	second ionization energy
IE3	third ionization energy
IRMPD	infrared multiphoton dissociation
kV	kilovolts
L	liters
LC	liquid chromatography
LMWCr	low-molecular-weight chromium-binding substance
$[M - H]^-$	deprotonated peptide
$[M + H]^+$	protonated peptide
$[M + Met]^{n+}$	metallated peptide
m/z	mass-to-charge
MALDI	matrix-assisted laser desorption ionization
mbar	millibar
MeOH	methanol
Met	Metal
MHz	megahertz
mM	millimolar
mmol	millimoles
mol	mole
MS	mass spectrometry
ms	milliseconds
MS/MS	tandem mass spectrometry
MS^2	tandem mass spectrometry

MS^n	tandem MS on product ion formed by $MS^{(n-1)}$
mTorr	millitorr
nA	nanoamperes
nanoESI	nanoelectrospray ionization
nCI	negative chemical ionization
nm	nanometers
NMP	N-methyl-2-pyrrolidinone
NMR	nuclear magnetic resonance
pE	pyroglutamate
PIP	piperidine
PSD	post-source decay
PTM	post-translational modification
QIT	quadrupole ion trap
r	radius
rad	radians
RE	recombination energy
RF	radiofrequency
RI	relative intensity
SPPS	solid phase peptide synthesis
t	time
TFA	trifluoracetic acid
THF	tetrahydrofuran
TIS	triisopropylsilane

TM	transition metal
TOF	time-of-flight
UV	ultraviolet
z	component perpendicular to r in a QIT
μL	microliters
μm	micrometers
ω	angular frequency

ACKNOWLEDGMENTS

This dissertation would not have been possible without the training and guidance of my research advisor, Dr. Carolyn J. Cassady. I sincerely appreciate her support and encouragement throughout my studies.

I would also like to thank my committee members, Drs. Gregory Szulczewski, John B. Vincent, Laura S. Busenlehner, and Janis M. O'Donnell for their valuable advice and suggestions throughout my graduate studies. An additional thank you goes to Dr. Vincent whose suggestion that I do undergraduate research for him many years ago started me down this path.

The financial support of the National Institutes of Health (R21-AT003 485-01) and the National Science Foundation (CHE-0848470) is gratefully acknowledged. The National Science Foundation CRIF program is acknowledged for purchase of the Bruker HCTultra PTM discovery system (CHE 0639003). I am also appreciative of the support from The University of Alabama National Alumni Association's License Tag Fellowship.

I would also like to acknowledge the current and past group members of Dr. Cassady's lab, in particular Dr. Junjie Gao for his patience during my initial training and Samantha Bokatzian-Johnson without whom I would be in the Department of Education right now. I am also grateful to members of Dr. Shaughnessy's lab, Drs. Scott Brown and Steven Raders for assistance in the hexakis(tetrahydrofuran)chromium(III) tris(tetrafluoroborate) synthesis.

Finally, I would like to thank my family, Brad, Emma, and Sara Kate, for their patience, love, and support. I would also like to acknowledge my mom, Connie, for keeping me grounded and for her invaluable assistance with my girls, and my dad, Kenny for instilling in me curiosity, a love of math, and reminding me that “if it were easy, everyone would do it”.

CONTENTS

ABSTRACT ii

LIST OF ABBREVIATIONS AND SYMBOLS..... iv

ACKNOWLEDGMENTS……..ix

LIST OF TABLES…….……...xvi

LIST OF SCHEMES xvii

LIST OF FIGURES..... xviii

CHAPTER 1. AN OVERVIEW OF THE DISSERTATION 1

REFERENCES 5

CHAPTER 2. INSTRUMENTATION AND EXPERIMENTAL PROCEDURES……...7

2.1 Electrospray Ionization/Quadrupole Ion Trap Mass Spectrometry 7

2.1.1 ESI/nanoESI..... 7

2.1.2 Quadrupole Ion Trap Mass Spectrometry..... 11

2.1.3 Collision-Induced Dissociation (CID) 17

2.1.4 Electron-Transfer Dissociation (ETD)..... 19

2.1.5. Electron-Transfer Collisionally-Activated Dissociation (ETcaD)..... 24

2.2 Matrix-Assisted Laser Desorption Ionization/Time-of-Flight (MALDI/TOF) 25

2.2.1 MALDI 25

2.2.2 TOF MS 31

2.2.3 Post-Source Decay 37

2.3 Peptide Synthesis Protocol..... 39

2.4 Peptide Sequencing Nomenclature 44

REFERENCES 47

CHAPTER 3. THE EFFECTS OF COLLISION-INDUCED DISSOCIATION ON TRANSITION METAL-PEPTIDE COMPLEXES..... 52

3.1 Introduction..... 52

3.2 Experimental 55

3.2.1 Preparation of Transition Metal-Peptide Complexes..... 55

3.2.2 Mass Spectrometry..... 57

3.2.3 UV-Visible Spectroscopy 58

3.2.4 Reagents 59

3.3 Results and Discussion 59

3.3.1 CID of Protonated and Deprotonated Polyalanines 64

3.3.2 CID of Cr(III) Bound to Heptaalanine 72

3.3.3 CID of Fe(II) and Fe(III) Bound to Heptaalanine 75

3.3.4 CID of Co(II) Bound to Heptaalanine 80

3.3.5 CID of Ni(II) Bound to Heptaalanine 83

3.3.6 CID of Cu(I) and Cu(II) Bound to Heptaalanine 85

3.3.7 Coordination of Transition Metal Ions to Tri- and Hepta-Alanine Methyl Ester 95

3.3.8 Confirmation of Product Ion Assignments 95

3.3.9 Metallated a-ions 96

3.4 Conclusions 107

REFERENCES 108

CHAPTER 4. COMPARISON OF ELECTRON-TRANSFER DISSOCIATION TO COLLISION-INDUCED DISSOCIATION OF TRANSITION METAL-CATIONIZED PEPTIDES 115

4.1 Introduction 115

4.2 Experimental 120

4.2.1 Synthesis of Peptides and Preparation of TM-Peptide Complexes 120

4.2.2 Mass Spectrometry 120

4.2.3 Reagents 121

4.3 Results and Discussion 122

4.3.1 Metal Ion Effects on Sequencing/Backbone Cleavages 126

4.3.2 Comparisons to CID 142

4.3.3 Macrocyclic a- and b-ions. Do They Exist? Do They Scramble Sequence Information? 144

4.4 Conclusions 148

REFERENCES 150

CHAPTER 5. ELECTRON-TRANSFER COLLISIONALLY-ACTIVATED DISSOCIATION OF TRANSITION METAL-CATIONIZED PEPTIDES ... 156

5.1 Introduction 156

5.2 Experimental 158

5.3 Results and Discussion 158

5.3.1 Effectiveness of ETcaD on Transition Metallated Peptides 158

5.3.2 ETcaD of Cr(III)-AAAAAGA 160

5.3.3 ETcaD of Fe(II)-AAAAAGA 167

5.3.4 ETcaD of Co(II)-AAAAAGA 167

5.3.5 ETcaD of Ni(II)-AAAAAGA 168

5.3.6 ETcaD of Cu(II)-AAAAAGA 169

5.3.7 Loss of Carbon by ETcaD of Cu(II)-Peptides 169

5.4 Conclusions 171

REFERENCES 172

CHAPTER 6. CHARACTERIZATION AND SEQUENCING OF LMWCr 174

6.1 Introduction 174

6.2 Experimental 177

6.2.1 Preparation of Samples 177

6.2.2 Mass Spectrometry 178

6.3 Results and Discussion 179

6.3.1 Mass Spectrometric Analysis of Acidic and LMWCr Candidate Peptides .. 179

6.3.2 Synthesis of $Cr(THF)_6(BF_4)_3$ hexakis(tetrahydrofuran)chromium(III) tris(tetrafluoroborate) 181

6.3.3 Reactions of $Cr(THF)_6(BF_4)_3$ with EDGEECDCGE 182

6.4 Smaller Heptapeptide Fragments of LMWCr 183

6.4.1 Production of Apo-Oligopeptide of LMWCr 183

6.4.2 MALDI/TOF MS of Model Peptides and LMWCr 188

6.4.3 Analysis of LMWCr Using ESI/QIT MS 190

6.4.4 Supporting Evidence for the Proposed Sequence Belonging to LMWCr..... 194

6.5 Conclusions 195

REFERENCES 197

CHAPTER 7. CONCLUDING REMARKS 200

LIST OF TABLES

3.1 CID products formed from transition metal-cationized heptaalanine where z is the charge on the product ion. 60

3.2 Transition metal cationized heptaalanine products formed by CID. 61

3.3 Product ions obtained by CID of transition metal-cationized ^{13}C-labeled heptaalanine 65

3.4 Product ions formed by CID of transition metal-cationized AAAAAGA. 68

3.5 Product ions formed by CID of Cu(II)-cationized peptides 89

4.1 ETD products from $[M + Cr - H]^{2+}$ and $[M + Met]^{2+}$ for heptaalanine cationized by Met = Fe(II), Co(II), Ni(II), and Cu(II) 127

4.2 The ionic radii, exchange rates, electron configurations, and ionization energies of the transition metals studied in this chapter. 130

LIST OF SCHEMES

3.1 Mechanism of a-ion formation from b-ions via elimination of CO …….....98

3.2 Vachet-Glish mechanism illustrating loss of ammonia from the a_4^+ ion of YGGF. ..…….....105

3.3 Proton bound dimer mechanism illustrating ammonia loss from the a_4^+ ion of YGGF. ..…….....106

LIST OF FIGURES

2.1 ESI ion formation and ESI source shown for the production of protonated ions. 9

2.2 Magnified image (10 x) of fused silica emitter tips used in nanoESI (a) in working condition, (b) with partially blocked flow, and (c) completely blocked flow…….....12

2.3 Cross section of the HCTultra's quadrupole ion trap 14

2.4 Schematic of the Bruker HCTultra PTM discovery system 18

2.5 Peptide fragmentation nomenclature based on Roepstorff and Fohlman's original nomenclature..... 20

2.6 Reactant anions are generated in a negative chemical ionization (nCI) source in two steps: (a) generating low energy electrons and (b) attaching the low energy electrons to fluoranthene. 22

2.7 Electron transfer dissociation is an ion/ion reaction that typically results in c- and z-type product ions and neutral reactant molecules. 23

2.8 Common MALDI matrices and abbreviations..... 27

2.9 Dried samples spots magnified 10x of (a) CCA and (b) DHB 28

2.10 Ionization by MALDI from the surface of a sample target 30

2.11 Diagram of MALDI/TOF MS equipped with reflectron 32

2.12 Simplified diagram illustrating delayed extraction and reflectron TOF. 36

2.13 Fmoc protective group used in peptide synthesis 40

2.14 Steps of SPPS peptide synthesis 41

2.15 Structures of the amino acids used in this work 43

2.16 Blocking the C-terminus of a peptide with a methyl ester..... 41

3.1 Structures of some of the heptapeptides studied in this chapter including (a) heptaalanine, (b) ^{13}C-labeled heptaalanine, (c) GGAAAAA, and (d) AAAAAGA……...56

3.2 Low-energy CID spectra obtained from (a) protonated, $[M + H]^+$, and (b) deprotonated, $[M - H]^-$, heptaalanine. 71

3.3 Low-energy CID spectrum obtained from $[M + Cr - H]^{2+}$, produced by a mixture of heptaalanine and $CrCl_3$. 73

3.4 Low-energy CID spectrum obtained from $[M + Fe - H]^+$, produced by a mixture of heptaalanine and $FeCl_2$. 76

3.5 Low-energy CID spectrum obtained from $[M + Fe]^{2+}$, produced by a mixture of heptaalanine and $FeCl_2$. 77

3.6 Low-energy CID spectrum obtained from $[M + Fe - H]^{2+}$, produced by a mixture of heptaalanine and $FeCl_3$. 79

3.7 Positive MS^3 CID spectrum on a_4^+ product formed from $[M + Fe - H]^{2+}$ for $FeCl_3$ and heptaalanine. Note * refers to loss of NH_3…….81

3.8 Low-energy CID spectrum obtained from $[M + Co]^{2+}$, produced by a mixture of heptaalanine and $CoCl_2$..... 82

3.9 Low-energy CID spectrum obtained from $[M + Ni]^{2+}$, produced by a mixture of heptaalanine and $NiCl_2$. 84

3.10 Low-energy CID spectrum obtained from $[M + Cu - H]^+$, produced by a mixture of heptaalanine and $CuCl_2$. 87

3.11 Low-energy CID spectrum obtained from $[M + Cu - H]^+$, produced by a mixture of ^{13}C-labeled heptaalanine and $CuCl_2$ 91

3.12 Positive MS^3 CID spectra obtained from the $[M + Cu - H - 12]^+$ product formed from $[M + Cu - H]^+$ for a mixture of Cu(II) with (a) heptaalanine and (b) ^{13}C-labeled heptaalanine. 92

3.13 Low-energy CID spectrum obtained from $[M + Cu]^{2+}$, produced by a mixture of heptaalanine and $CuCl_2$. 93

3.14 Structures of b-ions for peptides. 99

3.15 Positive MS^3 CID spectrum on $[b_6 + Cu - H]^{2+}$ product formed from $[M + Cu]^{2+}$ for $CuCl_2$ and heptaalanine. 100

3.16 Positive MS^3 CID spectrum on $[a_6 + Fe - H]^{2+}$ product formed from $[M + Fe]^{2+}$ for a mixture of heptaalanine and $FeCl_2$. 101

3.17 Positive MS^4 CID spectrum on $[a_5 + Fe - H]^{2+}$ product formed from CID on $[a_6 + Fe - H]^{2+}$ for $FeCl_2$ and heptaalanine. 102

4.1 ETD spectrum of $[M + Cr - H]^{2+}$ produced from heptaalanine cationized by Cr(III). ... 123

4.2 ETD spectra of $[M + Met]^{2+}$ produced from heptaalanine cationized by (a) Fe(II), (b) Co(II), and (c) Ni(II) 124

4.3 ETD spectrum of $[M + Cu]^{2+}$ produced from heptaalanine cationized by Cu(II) ..... .125

4.4 Comparison of (a) ETD and (b) CID spectra of heptaalanine cationized by Cr(III), $[M + Cr - H]^{2+}$ 128

4.5 Comparison of (a) ETD and (b) CID spectra from heptaalanine cationized by Fe(II), $[M + Fe]^{2+}$ 132

4.6 Comparison of (a) ETD and (b) CID spectra of heptaalanine cationized by Co(II), $[M + Co]^{2+}$ 133

4.7 Comparison of (a) ETD and (b) CID spectra of heptaalanine cationized by Ni(II), $[M + Ni]^{2+}$ 135

4.8 Comparison of (a) ETD and (b) CID spectra resulting from heptaalanine cationization by Cu(II), $[M + Cu]^{2+}$ 137

4.9 ETD produced from AAAAAGA cationized by Cr(III), $[M + Cr - H]^{2+}$ 139

4.10 ETD of AAAAAGA cationized by (a) Fe(II), (b) Co(II), and (c) Ni(II), $[M + Met]^{2+}$ ...140

4.11 ETD produced from AAAAAGA cationized by Cu(II), $[M + Cu]^{2+}$ ……..141

4.12 ETD spectra of (a) $[M + 2H]^{2+}$ and (b) $[M + Co]^{2+}$ from fibrinopeptide B..... 143

4.13 Different sequence scrambling possibilities that can follow ring opening from a macrocyclic ion. Amino acid residues can also be eliminated in the process…….145

4.14 CID five protonated, $[M + H]^{+}$, heptapeptides. Note the loss of nonsequential ions indicated in red……147

5.1 Comparing the sequencing efficacy of (a) ETD, (b) CID, and (c) ETcaD on Cr-cationized heptaalanine, $[M + Cr - H]^{2+}$ 159

5.2 Backbone cleavages produced by ETcaD of heptaalanine cationized by transition metals 161

5.3 ETcaD spectrum obtained from ETD on $[M + Cr - H]^{2+}$, where M = AAAAAGA, followed by CID on the ETnoD product $[M + Cr - H]^{+}$. Nonsequential product ions are marked in red……...162

5.4 ETcaD spectrum obtained from ETD on $[M + Fe]^{2+}$, where M = AAAAAGA, followed by CID on the ETnoD product $[M + Fe]^{+}$. Nonsequential product ions are marked in red. ……163

5.5 ETcaD spectrum obtained from ETD on $[M + Co]^{2+}$, where M = AAAAAGA, followed by CID on the ETnoD product $[M + Co]^{+}$. Nonsequential product ions are marked in red. ……164

5.6 ETcaD spectrum obtained from ETD on $[M + Ni]^{2+}$, where M = AAAAAGA, followed by CID on the ETnoD product $[M + Ni]^{+}$. Nonsequential product ions are marked in red. ……165

5.7 ETcaD spectrum obtained from ETD on $[M + Cu]^{2+}$, where M = AAAAAGA, followed by CID on the ETnoD product $[M + Cu]^{+}$. Nonsequential product ions are marked in red. ……166

6.1 Positive MALDI mass spectra obtained from (a) protonated DAAAD, $[M + H]^{+}$ and (b) the Cr^{3+}-adducted DAAAD, $[M + Cr - 2H]^{+}$ 180

6.2 Positive MALDI MS spectra obtained after mixing EDGEECDCGE candidate peptide with $CrCl_3 \bullet 6H_2O$ and $Cr(THF)_6(BF_4)_3$ 184

6.3 Structure of the LMWCr candidate sequence EDGEECDCGE with acidic sites circled ……..185

6.4 Negative MALDI/TOF MS of treated LMWCr samples from (a) human urine, (b) bovine liver, (c) alligator liver, and (d) chicken liver 186

6.5 Negative PSD spectra of the $[M - H]^{-}$ from (a) treated bovine LMWCr, and its candidate sequences, (b) pEEEEGDD, and (c) pEEEGEDD 187

6.6 Negative ESI/QIT spectrum of (a) bovine LMWCr and the candidate sequences, (b) pEEEEGDD, and (c) pEEEGEDD 191

6.7. Negative MS^3 spectra obtained from CID of the $[M - H - H_2O]^{+}$ for M = (a) bovine LMWCr, (b) pEEEEGDD, and (c) pEEEGEDD 193

CHAPTER 1

AN OVERVIEW OF THE DISSERTATION

Mass spectrometry has evolved over the last century into one the most powerful tools in analytical chemistry. Since J. J. Thomson's early experiments,[1, 2] mass spectrometry has contributed to a range of fields from atomic physics to molecular and clinical biology. This evolution has led to modern mass spectrometers that incorporate various configurations of ion sources, mass analyzers, and detectors. Although the technique is now more than a century old, only since the 1980s has it become useful in peptide and protein analysis.[3, 4] Since that time, interest in the field of mass spectrometry has rapidly increased, especially in the field of proteomics.[5] Investigations into the fundamental processes occurring during peptide dissociations in the mass spectrometer are a small part of the ongoing evolution of the technique.

The studies presented in this dissertation focus on the behaviors of transition metal-peptide complexes in mass spectrometry. An emphasis is placed on how different types of dissociation techniques affect the gas-phase chemistry of these complexes. The goals of this research are to obtain a more fundamental understanding of how transition metals affect the dissociation of peptides and to investigate the potential use of transition metals as cationizing reagents in peptide sequencing. An example of how this fundamental knowledge can be applied to de novo sequencing is given through the

successful sequencing of the major fragment of low molecular weight chromium-binding substance (LMWCr) by mass spectrometry.

Chapter 2 lays the foundation for subsequent chapters. The instrumentation and experimental techniques and conditions employed throughout this research are described. The ionization methods, electrospray ionization (ESI), nanoESI, and matrix-assisted laser desorption ionization, and mass analyzers, quadrupole ion trap (QIT) and time-of-flight (TOF), are presented. Dissociation methods for QIT: collision-induced dissociation (CID) and electron-transfer dissociation (ETD) and for TOF: post-source decay (PSD) are explained. The solid phase peptide synthesis protocol, structures of the amino acids used in this work, and the peptide sequencing nomenclature is given.

Collision-induced dissociation (CID) is the most common form of tandem mass spectrometry utilized in the sequencing of peptides and proteins. Incomplete backbone fragmentation, loss of post-translational modifications, sequence scrambling, and neutral losses are some of the obstacles of CID.[6-10] Adding transition metals to peptides was carried out in an effort to minimize all or some of the obstacles. Additionally the behaviors of these transition metal-peptide complexes in the mass spectrometer is of interest since many biologically derived peptides are metallated.

The findings presented in Chapter 3 have been selected as a Special Feature Perspectives article in the *Journal of Mass Spectrometry* as a way to increase sequence informative ions by simply adding a cationization reagent. The CID spectra of transition metal-cationized peptides and protonated peptides are compared. The effect of changing the complexed transition metal, Cr(III), Fe(III), Fe(II), Co(II), Ni(II), and Cu(II), to heptaalanine is explored. Backbone cleavages resulting in b- and a- type ions are

primarily produced by CID of protonated peptides. These studies focus on the type and relative abundances of product ions that form by CID on transition metallated complexes as well as on how the various metal ions alter the formation of sequence informative ions.

New studies[8, 11] highlighting the complimentary nature of electron-transfer dissociation (ETD) and CID have sparked interest in subjecting samples to both techniques then comparing the sets of spectra to optimize sequence information. However, applying ETD to neutral and acidic peptides is limited by its requirement of multiply charged precursor ions (for example, $[M + 2H]^{2+}$ and $[M + 3H]^{3+}$).[12] The addition of di- and tri-valent transition metals is expected to increase the number of peptides that can be submitted to ETD by giving them the multiple charges required by ETD.

Electron-transfer dissociation of transition metal-cationized peptides is explored in Chapter 4. The heptapeptides examined contain only alanine and glycine and, as expected, do not readily accept multiple protons. As a result, the study of these heptapeptides by ETD, which requires multiply charged precursors, could only be carried out after transition-metal cationization. This allowed ETD spectra to be obtained and compared to CID of the same complexes. The ETD spectra were cleaner and easier to interpret than those produced by CID. Ni(II) cationization resulted in complete sequence coverage by ETD. Macrocyclic structured product ions can eliminate a residue after ring reopening. Since the residue can be eliminated from any position in the ring, the product ion formed may be nonsequential. Identification of these nonsequential losses was made possible in spectra obtained with Co(II) and Ni(II). This is the first evidence of metallated, macrocyclic a- and b-ions produced by ETD.

Chapter 5 applies a novel dissociation technique called electron-transfer collisionally activated dissociation (ETcaD)[13] to transition metal-peptide complexes. ETcaD involves utilizing CID to enhance ETD product ion formation. Overall spectral quality and ease of interpretation is greatly improved in ETcaD over CID and sequence coverage is improved over ETD. In fact, Cr(III)-heptaalanine submitted to ETD gives only two sequence informative ions, and the same complex submitted to ETcaD results in complete sequence identification. However, the technique does produce more nonsequential losses than those identified during ETD.

To further illustrate the importance of fundamental studies into transition metal-peptide complexes, the sequencing of a biologically derived peptide, low-molecular weight chromium-binding substance (LMWCr) is presented in Chapter 6. The LMWCr findings were selected as Editor's Pick by the *Journal of Nutrition*. The sequencing of LMWCr is important to understanding the potential role LMWCr plays in the metabolism of carbohydrates. Proposed sequences for the peptide were synthesized, and various methods of replicating the biologically derived peptide, which contains four Cr(III), were carried out. A Cr complex with easily exchangeable ligands was synthesized to increase the number of bound Cr(III). Different dissociation methods were carried out on both the model peptides and the biologically derived peptides. The spectra were compared to finally elucidate the primary structure of a large fragment of the apo-peptide.

Chapter 7 highlights the major contributions of this dissertation and offers some interesting starting points for extending these studies in the future.

REFERENCES

1. J. J. Thomson, Rays of positive electricity. *Proc. R. Soc.* **1913,** A89, 1-20.

2. I. W. Griffiths, J.J. Thomson-The centenary of his discovery of the electron and of his invention of mass spectrometry. *Rapid Commun. Mass Spectrom.* **1997,** 11, 3-16.

3. D. F. Hunt; A. M. Buko; J. M. Ballard; J. Shabanowitz; A. B. Giordani, Sequence analysis of polypeptides by collision activated dissociation on a triple quadrupole mass spectrometer. *Biomed. Mass Spectrom.* **1981,** 8, 397-408.

4. K. Biemann; F. Gapp; J. Seibl, Application of mass spectrometry to structure problems, 1. Amino acid sequence in peptides. *J Am. Chem. Soc.* **1959,** 81, 2274-2275.

5. R. Service, PROTEOMICS: New database to track protein locations. *Science* **2005,** 309, 1310.

6. A. G. Harrison; A. B. Young; C. Bleiholder; S. Suhai; B. Paizs, Scrambling of sequence information in collision-induced dissociation of peptides. *J. Am. Chem. Soc.* **2006,** 128, 10364-10365.

7. I. Riba-Garcia; K. Giles; R. H. Bateman; S. J. Gaskell, Evidence for structural variants of a- and b-type peptide fragment ions using combined ion mobility/mass spectrometry. *J. Am. Soc. Mass Spectrom.* **2008,** 19, 609-613.

8. F. Sobott; S. Watt; J. Smith; M. Edelmann; H. Kramer; B. Kessler, Comparison of CID versus ETD based MS/MS fragmentation for the analysis of protein ubiquitination. *J. Am. Soc. Mass Spectrom.* **2009,** 20, 1652-1659.

9. C. Bleiholder; S. Osburn; T. D. Williams; S. Suhai; M. Van Stipdonk; A. G. Harrison; B. Paizs, Sequence-scrambling fragmentation pathways of protonated peptides. *J. Am. Chem. Soc.* **2008,** 130, 17774-17789.

10. B. J. Bythell; D. F. Barofsky; F. Pingitore; M. J. Polce; P. Wang; C. Wesdemiotis; B. Paizs, Backbone cleavages and sequential loss of carbon monoxide and

ammonia from protonated AGG: A combined tandem mass spectrometry, isotope labeling, and theoretical study. *J. Am. Soc. Mass Spectrom.* **2007,** 18, 1291-1303.

11. R. Zubarev; A. Zubarev; M. Savitski, Electron capture/transfer versus collisionally activated/induced dissociations: Solo or duet? *J. Am. Soc. Mass Spectrom.* **2008,** 19, 753-761.

12. R. A. Zubarev; N. L. Kelleher; F. W. McLafferty, Electron Capture Dissociation of Multiply Charged Protein Cations. A Nonergodic Process. *J. Am. Chem. Soc.* **1998,** 120, 3265-3266.

13. D. Swaney; G. C. McAlister; M. Wirtala; J. C. Schwartz; J. E. P. Syka; J. J. Coon, Supplemental activation method for high-efficiency electron-transfer dissociation of doubly protonated peptide precursors. *Anal. Chem.* **2007,** 79, 477-485.

14. Press Release: The 1989 Nobel Prize in Physics In Nobelprize.org: 1989; 2011.

15. P. Roepstorff; J. Fohlman, Proposal for a common nomenclature for sequence ions in mass spectra of peptides *Biol. Mass Spectrom.* **1984,** 11, 601.

CHAPTER 2

INSTRUMENTATION AND EXPERIMENTAL PROCEDURES

An overview of the experimental procedures and instrumental methodology used throughout this work are discussed in this chapter including ionization techniques and quadrupole ion trap and time-of-flight mass analyzers. Procedures for synthesizing model peptides, sequencing nomenclature, and the structures of relevant amino acids are also described.

2.1 Electrospray Ionization/Quadrupole Ion Trap Mass Spectrometry

2.1.1 ESI/nanoESI

To analyze peptides and other large biological molecules by mass spectrometry, one must be able to produce intact ions of these samples. Until the advent of electrospray ionization (ESI) and matrix-assisted laser desorption ionization (MALDI), the analysis of peptides and proteins by mass spectrometry was difficult. Electrospray ionization was developed by Yamashita and Fenn[1, 2] in the 1980s based on a concept first introduced by Dole[3] in 1968. ESI is a soft ionization technique used to ionize large molecules by taking advantage of Dole's idea that solvent evaporation from a droplet yields a net electric charge. This idea was combined with earlier knowledge of droplet behavior explained by Rayleigh in 1882[4]; as solvent evaporates from droplet surfaces, the density of charges on

the droplet surface increases until it reaches a critical value, dubbed the "Rayleigh Limit." At this time Coulombic repulsion overcomes surface tension, and the droplet breaks apart in an "explosion" that results in smaller droplets.[4] Dole extended this idea further and suggested that each of the newly produced "offspring" droplets should also evaporate until reaching their Rayleigh limits and also undergo Coulombic explosions with the cycle continuing until a free gas-phase ion is formed.[3]

ESI as a mass spectrometric ionization source was developed by Yamashita and Fenn,[2] who applied bigger vacuum systems and faster pumps, along with an understanding of free jet expansions, to Dole's initial results. Several modifications to the technique were made including adding a counter current of drying gas to the incoming stream of sample droplets, which prevented ion resolvation before entering the vacuum system. Fenn was awarded part of the Nobel Prize in Chemistry in 2002 for his work on the development of ESI and for demonstrating its usefulness by applying ESI MS to the study of large molecules.[1, 5]

Sample is introduced into an ESI source through a needle and transfer line using a syringe pump at a flow rate of ~120 μL/min. The ESI process involves several steps including solvent evaporation from the sample and droplet fission once the Rayleigh limit is reached. The process continues until a desolvated quasi-molecular ion (for example, $[M + nH]^{n+}$) is produced as shown in Figure 2.1. ESI produces multiply charged species dependent on the size of the molecule. This is especially beneficial for the analysis of biomolecules whose large molecular weights are outside the mass-to-charge (*m/z*) range of mass analyzers. The increase in charge means that species with even very high masses

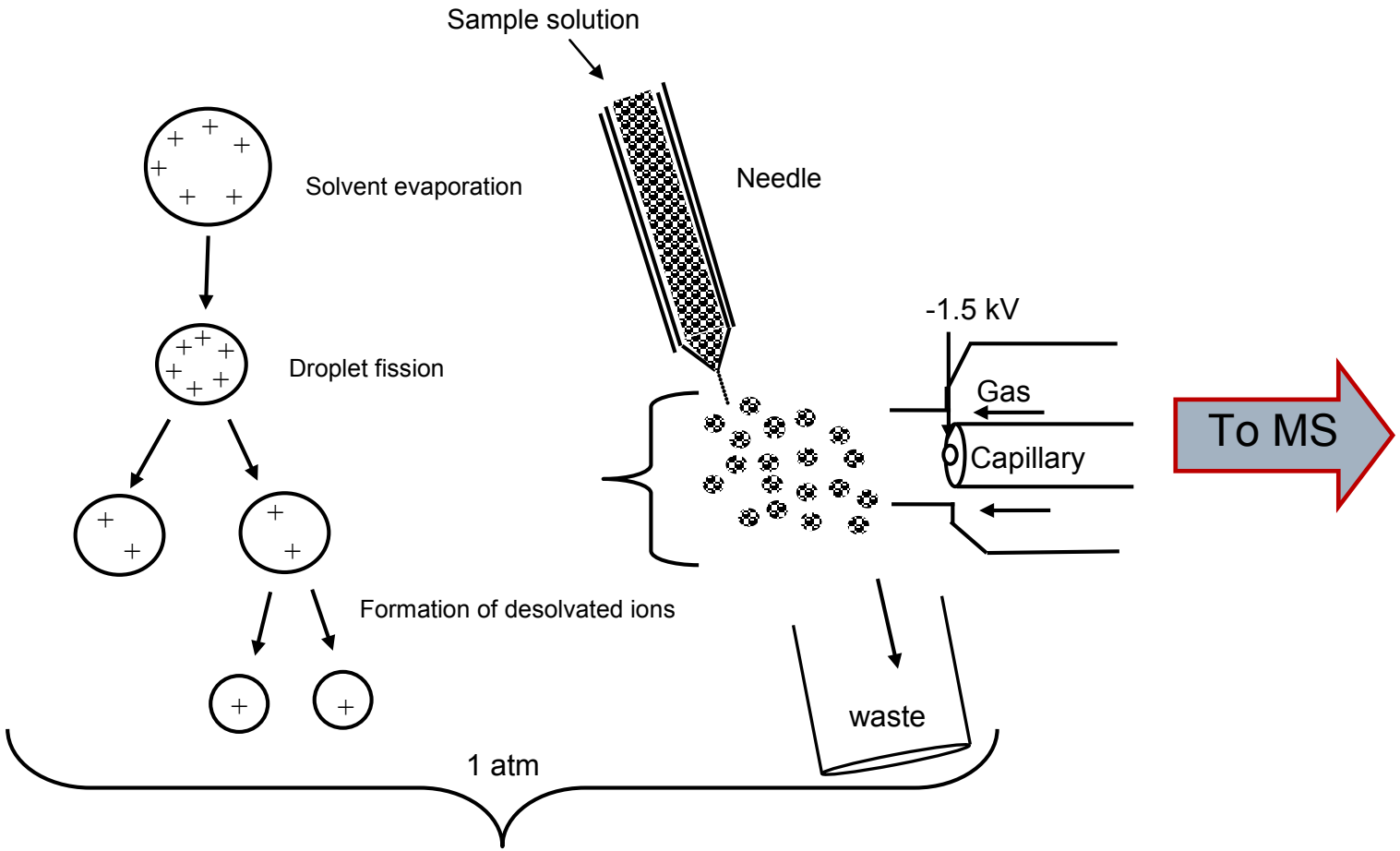

Figure 2.1. ESI ion formation and ESI source shown for the production of protonated ions.

result in ions with *m/z* that lie within the range of most mass analyzers. For example, a protein with a mass of ~89,000 Da and a charge of 33 has a *m/z* of 2,697.

By controlling the sample preparation, the nature of the analyte ions can be manipulated. For example, changing the solvent and/or addition of salts can aid the formation of ions in the solution or during the nebulization/desolvation process itself. A typical ESI sample contains the analyte and a solvent such as MeOH, ACN, H_2O or combinations of these. Additives can alter ion formation by adding/removing hydrogens, cations, and anions. For example, salts can serve as cation sources; acids can serve as proton sources; and bases can promote the abstraction of protons from the analyte (negative mode). With the aid of nitrogen nebulizing sheath gas, sample droplets enter the ESI source (Figure 2.1) as an aerosol into a high electric field gradient, which is formed by keeping the nebulizer at ground and applying a voltage to the capillary of ~ 1-5 kV. The charged droplets contain solvent molecules and both positive and negatively charged ions. The ions of one polarity are forced to the surface of the droplet due to the attraction to the applied field. The droplets migrate toward the capillary where a counter flowing, heated bath gas enhances solvent evaporation. Analyte ions are guided toward the glass capillary by electrostatic gradients. Once the capillary entrance is reached, the pressure differential between the ion source and the ion focusing and transfer region forces ions though the capillary toward the analyzer.

When low volumes of sample need to be analyzed, a nanoESI source can be installed in place of the ESI source. NanoESI, introduced by Wilm and Mann[6, 7], allows extremely small sample volumes to be analyzed with increased tolerance to salt contaminations[8-10]. Low flow rates of ~ 50 nL/min - 500 nL/min are used allowing

samples of only 30 μL to be studied for an hour. NanoESI involves a silica transfer line and emitter with inner and outer diameters around 75 and 15 μm, respectively. No nebulizer gas is necessary due to the small initial droplet sizes, which are much smaller than those formed from traditional ESI. NanoESI was employed in this work when salt backgrounds suppressed the intensities of precursor ions of interest because nanoESI has been found to be more tolerant of salts.[9]

While nanoESI tends to decrease salt backgrounds and requires very little sample volume, it has some drawbacks. The delicate transfer lines and emitters are made of fused silica, which is easily pinched, crushed, or clogged, as shown in Figure 2.2. All of these things render them useless. In order for nanoESI to result in good MS signal, the flow must be consistent and the spray steady. Any variation in the geometry of the spray in relation to the capillary results in signal loss due to the small nature of the spray. Therefore, any silica crystal that breaks off into the transfer line or "shear" crack in the wall of the line itself can block the flow altogether or divert it so that the spray is no longer near the orifice of the capillary.

2.1.2 Quadrupole Ion Trap Mass Spectrometry

Quadrupole ion traps (QITs) were originally called the Paul trap after Wolfgang Paul who won the 1989 Nobel Prize in Physics for its development.[11] Quadrupole ion traps are extremely versatile devices that can perform many stages of tandem mass analysis (MS^n) all in one space the size of a napkin ring. A QIT can store gas-phase ions of a selected *m/z* range for a period of time and only require pressures of around 1 mTorr (He buffer gas background). Once transferred into the trap, the ions oscillate at their

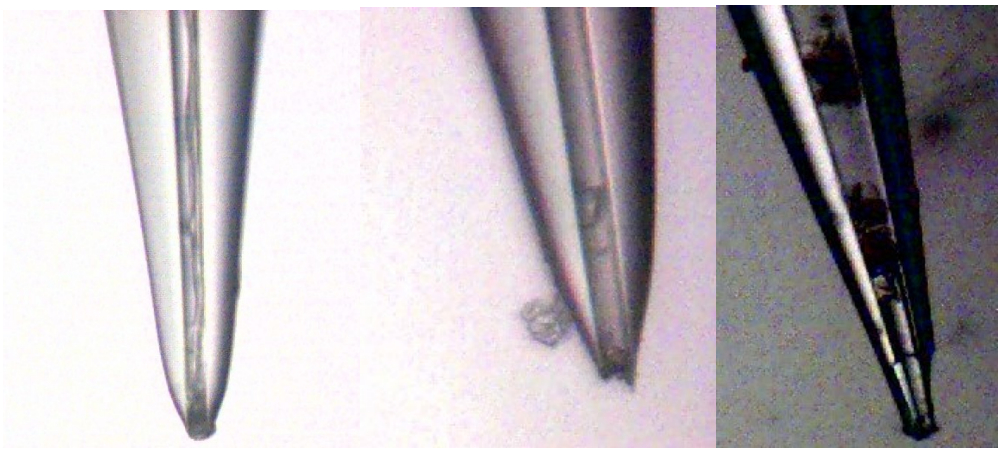

(a) (b) (c)

Figure 2.2. Magnified image (10 x) of fused silica emitter tips used in nanoESI (a) in working condition, (b) with partially blocked flow and (c) completely blocked flow.

secular frequency, which is dependent on their *m/z* and the amplitude and frequency of the applied radiofrequency (RF) voltage (to the ring electrode, see Figure 2.3). QITs have been used to trap both positive and negative ions in order to study them in the absence of solvent in a "potential well" by applying the appropriate potentials to the trap's electrodes. In essence, a QIT is a beaker or test tube used to study gas-phase ions.

The QIT is made of stainless steel machined with two identical end cap electrodes and a hyperbolic ring electrode between them (see cross section in Figure 2.3). When the end caps are held at ground and a potential is applied to the ring electrode, charged ions transferred from the capillary can be confined to the center of the trap. Helium buffer gas at pressures of ~ 3×10^{-3} mbar is present at all times in the trap to dampen ion motion and prevent energetic collisions. Ion motion inside this "trapping" field is best described by Mathieu's second-order linear differential equation shown in Equation 2.1 where *u* represents *x,y*, and *z* axes, ξ is a dimensionless parameter (ξ =ωt/2 where ω is frequency and *t* is time), and a_u and q_u are known as dimensionless trapping parameters.[12]

$$\frac{d^2u}{d\xi^2} + (a_u - 2q_u \cos 2\xi)\, u = 0 \tag{2.1}$$

Substitution of ωt/2 into Equation 2.1 for ξ gives

$$\frac{d^2u}{dt^2} = \frac{\omega^2}{4}\frac{d^2u}{d\xi^2} \tag{2.2}$$

Substitution of Equation 2.2 into Equation 2.1 and multiplying by mass of the ion *m* and rearranging gives

$$m\frac{d^2u}{dt^2} = -m\frac{\omega^2}{4}(a_u - 2q_u \cos \omega t)u \tag{2.3}$$

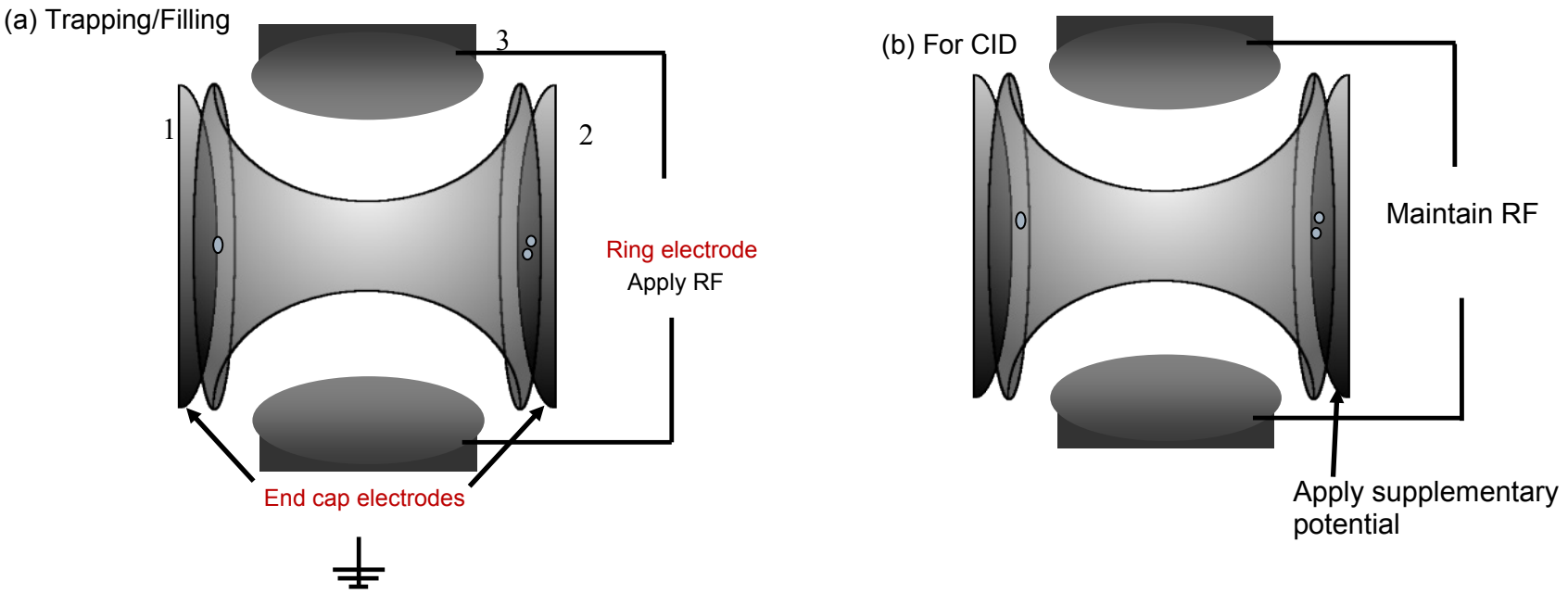

Figure 2.3. Cross section of the HCTultra's quadrupole ion trap where 1) indicates the entrance end cap electrode, 2) is the exit end cap electrode, and 3) is the ring electrode. Two modes are shown (a) the trapping and filling and (b) the addition of supplementary potential to the exit electrode during CID.

Since the above equation represents the force on an ion in directions *u* (all dimensions *x, y, z*), the left hand side of Equation 2.3 can be considered force *F,* which equals mass times acceleration (F = ma). The forces in each of the coordinate directions are not coupled so that the forces in each direction may be determined separately. If considering the *x* direction, F_x, the force in the x-direction experienced by an ion of mass *m* with charge *e,* and acceleration *a,* is equal to Equation 2.4 at any point within a quadrupolar field, then

$$F_x = ma = m\frac{d^2x}{dt^2} = -e\frac{\partial\phi}{\partial x} \tag{2.4}$$

The electric potential is applied to the ring electrode as either radiofrequency (RF) potential, V cos ωt, or combined with a direct current (DC) potential, U, according to Equation 2.5. Here, the angular frequency ω is defined as 2Π*f* (where *f* is in Hz) and describes the alternating current (AC) field, which is in the RF region in rad s^{-1}.

$$\Phi_0 = (U + V cos\omega t) \tag{2.5}$$

U and V are the amplitudes of the DC and AC voltages, respectively, and ω is the angular frequency (in rad s^{-1}). The inner cylindrical cavity (coordinates *r, z*) of the QIT has a radius across the ring electrode *r* and a *z* component perpendicular to *r* that defines the shortest distance from the center of the trap to the end cap electrodes. Taking the applied electric potential (Equation 2.5) and differentiating with respect to *x* leads to Equation 2.6, which is representative of the potential gradient.

$$\frac{\partial \phi}{\partial x} = \frac{2x}{r_0^2}\left(U + V\cos\omega t\right) \tag{2.6}$$

Substitution of Equation 2.6 into Equation 2.4 gives an expression for the force on an ion (Equation 2.7).

$$m\frac{\mathrm{d}^2 x}{\mathrm{d}t^2} = \frac{-2e}{r_0^2}\left(U + V\cos\omega t\right)x \tag{2.7}$$

The right hand sides of Equations 2.3 and 2.7 can be compared, keeping in mind that *u* represents *x* and allows the force in *x* direction to be expressed in terms of *a* and *q* (the dimensionless trapping parameters) as shown in Equations 2.8 and 2.9.

$$a_x = \frac{8zeU}{mr_0^2\omega^2} \tag{2.8}$$

$$q_x = \frac{-4zeV}{mr_0^2\omega^2} \tag{2.9}$$

This derivation can be repeated to obtain the force that the ion experiences in the *y* and *z* directions in the same manner. These forces experienced by the ion in the combined *x*, *y*, and *z* directions are what govern the ion's motion in the QIT. In order to keep this complex ion motion and thus keep the ions trapped, the potential difference has to oscillate in the megahertz (MHz) range. The Mathieu stability diagram[12] illustrates the stable regions in a QIT experienced by ions of certain *m/z* as a function of the voltage and frequency applied to the ion trap electrodes. This relates directly to the a_x and q_x values equated in 2.8 and 2.9 and allows the *m/z* relationship to be defined by this voltage and frequency after q_{max} is established for the given instrument as Equation 2.10. Ion motion in a quadrupolar field in a_z, q_z space is only stable in the regions defined by the stability

diagram. The intersection of q_z with boundary created by $\beta_z = 1$ for most QITs is 0.908, which is also called q_{max} in mass selective instability mode.

$$\frac{m}{z} = \frac{4eV}{q_{max}\omega^2 r_0^2} \qquad (2.10)$$

Mass-to-charge detection is accomplished during the scan of the quadrupolar and dipolar fields (changing V and ω from Equation 2.10). This is accomplished via auxiliary voltage applied to the exit end-cap (this additional voltage is also used during precursor ion isolation, dissociation, and mass analysis phases of scan sequences). During this time the fields are increased incrementally to eject ions from low to high *m/z* values out of the trap through the holes in the exit end cap. Once the ions have left the QIT, they enter a region of higher vacuum (~5 x 10^{-6} mbar) to prevent further collisions before detection by an electron multiplier (EM). A conversion dynode allows for the detection of negative ions.

The overall utility of the QIT to trap and react both positive and negative ions in the same space make it attractive and versatile for applications involving peptide sequencing. With a wide range of ionization and dissociation techniques, the ion trap design used in the work of this dissertation is particularly good. The QIT employed for the presented research is a high capacity spherical trap (see Figure 2.4 for Bruker HCTultra PTM Discovery System diagram).[13] This trap's electrodes have optimized geometries that force ions to the center of the trap and into a spherical shape. This increases both the storage capacity of the trap and the likelihood of an ion/ion reaction during electron-transfer dissociation (ETD). In the HCTultra QIT, the RF potential can be applied to all three electrodes (the ring and end-cap electrodes) causing the resultant

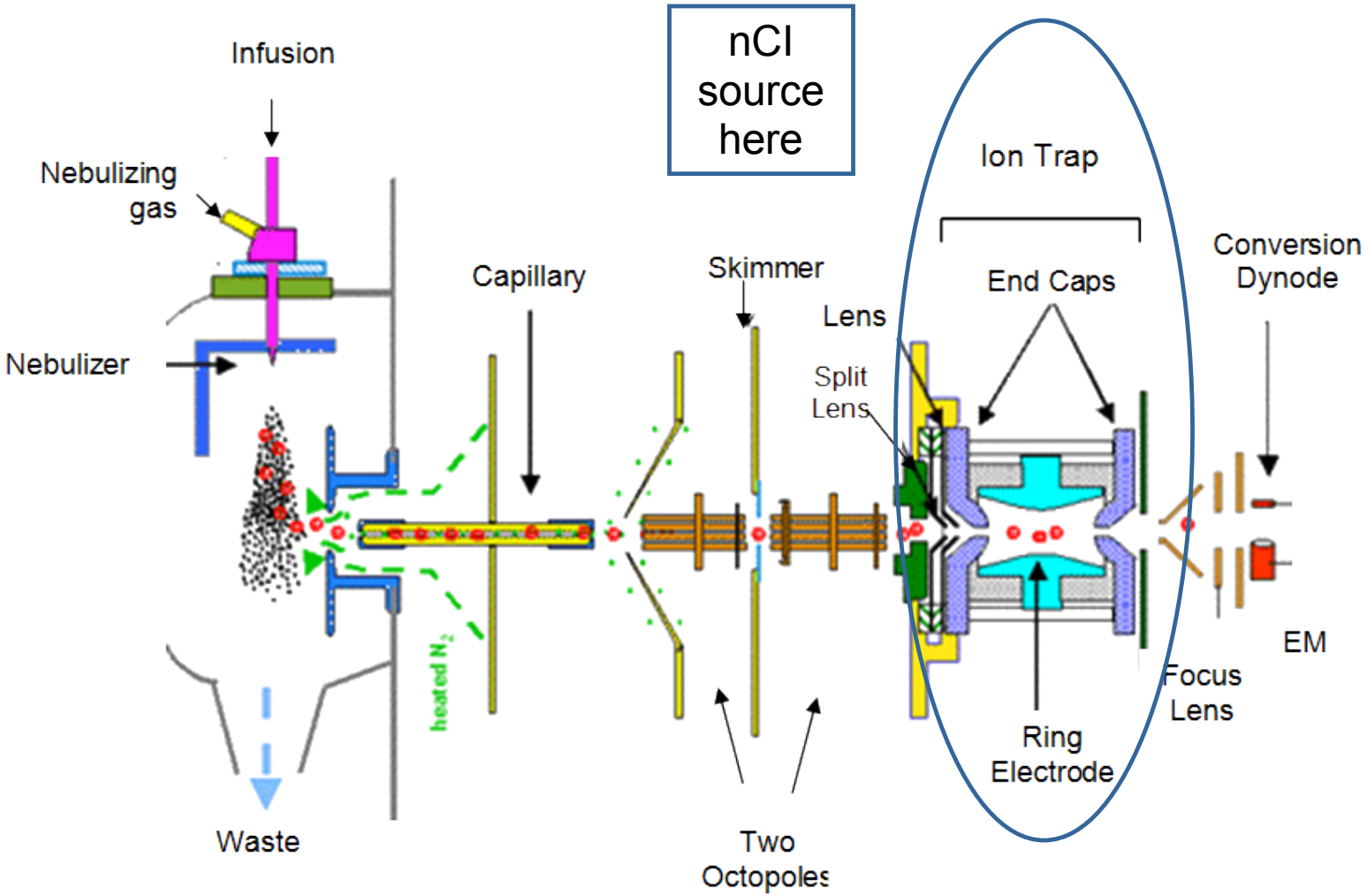

Figure 2.4 Schematic of the Bruker HCTultra PTM Discovery System.

electric fields to mimic the behaviors of a hexapole giving the operator more control of ion motion and interactions during reactions such as ETD.

2.1.3 Collision-Induced Dissociation (CID)

Ionization methods such as ESI and nanoESI generally produce intact protonated peptides, $[M + nH]^{n+}$, that can be fragmented by collision-induced dissociation (CID) into primarily b_n/y_n pairs (Figure 2.5).[14] Peptide fragmentation nomenclature will be discussed in section 2.4.

Low energy (1-100 eV) CID, the most common form of tandem mass spectrometry[15], is based on the principle that ions given a high kinetic energy will dissociate after collisions with a neutral bath gas. CID is a slow heating technique that, in a QIT, involves isolating the ion of interest by applying a RF voltage at the resonance frequency band just above and below the resonance frequency required to cause excitation of the selected ions. By applying an excitation frequency at the resonance frequency of the *m/z* of interest, the ion's kinetic energy is increased, accelerating the ions into helium atoms. Thus, in a QIT, helium serves as both the buffer gas and the CID collision gas. The kinetic energy of these inelastic collisions is in the range of 1-100 eV and results in transfer of some kinetic energy to vibrational energy, which is distributed along the backbone of the peptide. Equation 2.11 is a representation of CID where m_1 is the precursor ion, m_2 is a product ion, m_3 is a neutral product, and * is excess energy. This energy is redistributed internally resulting in breakage of bonds in the peptide.

$$m_1^+ + He \rightarrow [m_1^+]^* \rightarrow m_2^+ + m_3 \qquad (2.11)$$

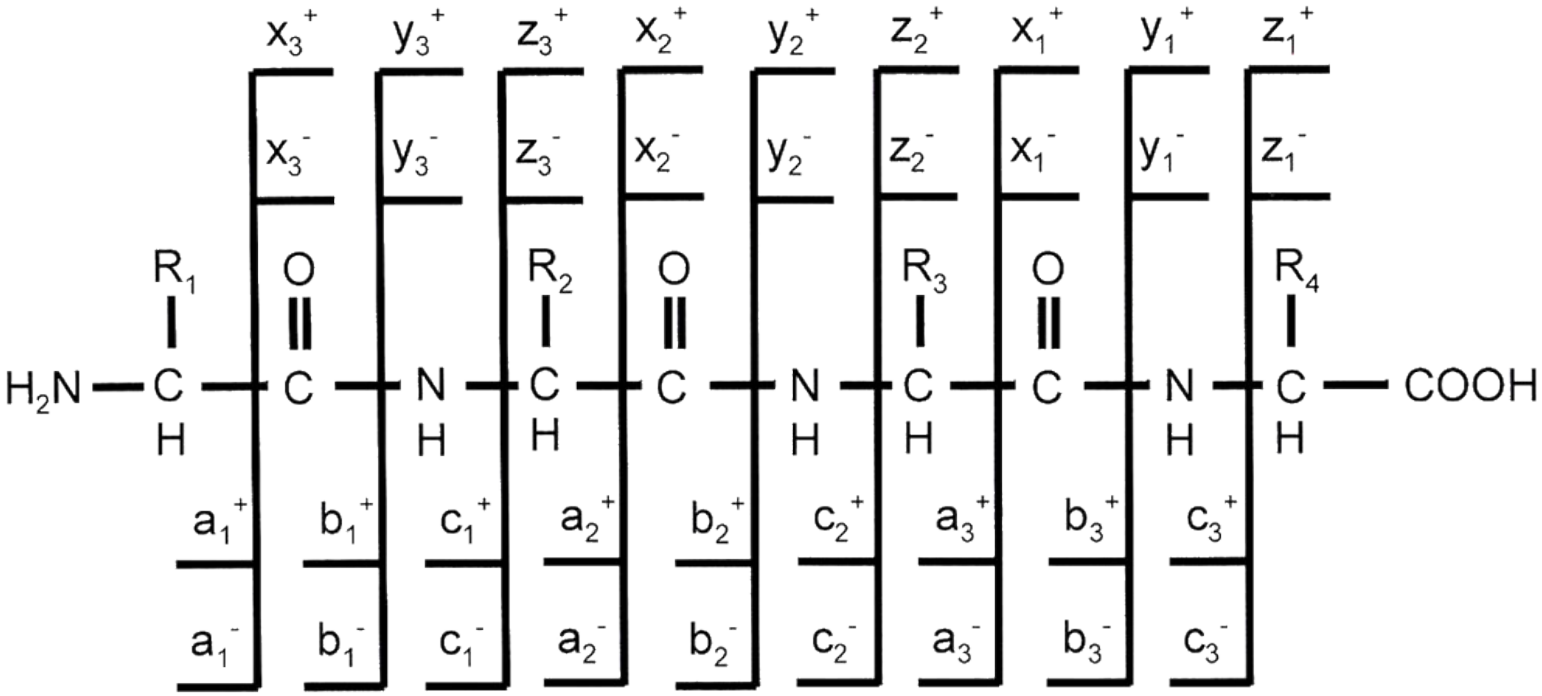

Figure 2.5. Peptide fragmentation nomenclature based on Roepstorff and Fohlman's original nomenclature.[53]

2.1.4 Electron-Transfer Dissociation (ETD)

Unlike CID, electron-transfer dissociation (ETD) is a nonergodic process that leads to more randomized cleavages and higher peptide sequence coverage by utilizing ion/ion reactions.[16, 17] The sites of post translational modifications (PTMs) such as glycosylations, phosphorylations and sulfations are preserved and can be identified with ETD but are lost during the CID process.[18-21] The two dissociation methods are complimentary and when used together give more information about a peptide's primary sequence than either technique alone.

Electron-transfer dissociation is a recently introduced[22] fragmentation technique accomplished by reacting a positive, multiply charged ($[M + nH]^{n+}$, $n \geq 2$) precursor ion with a radical anion to transfer a low energy electron to the precursor ion. This reduced species, $[M + nH]^{(n-1)+\bullet}$, is unstable and typically undergoes dissociation of the N-Cα bonds of peptides/proteins. Therefore, ETD generally produces c- and z-type product ions, which will be discussed in section 2.4.

Prior to an ETD reaction, electrons from a filament (~ 75 eV) interact with methane gas in a negative chemical ionization chamber to produce low energy electrons (e^{-}*, < 1 eV) that are transferred to a reactant, in this work, fluoranthene. This process is shown in Figure 2.6. During an ETD reaction, these fluoranthene anions serve as a mediator to transfer the low energy electrons to multiply charged precursor ions (Figure 2.7). The reduced precursor undergoes dissociation via a free radical reaction cascade. The exact mechanism for ETD is unclear and is under debate. Two proposed mechanisms currently being examined include the Cornell mechanism[16] and the Utah-Washington

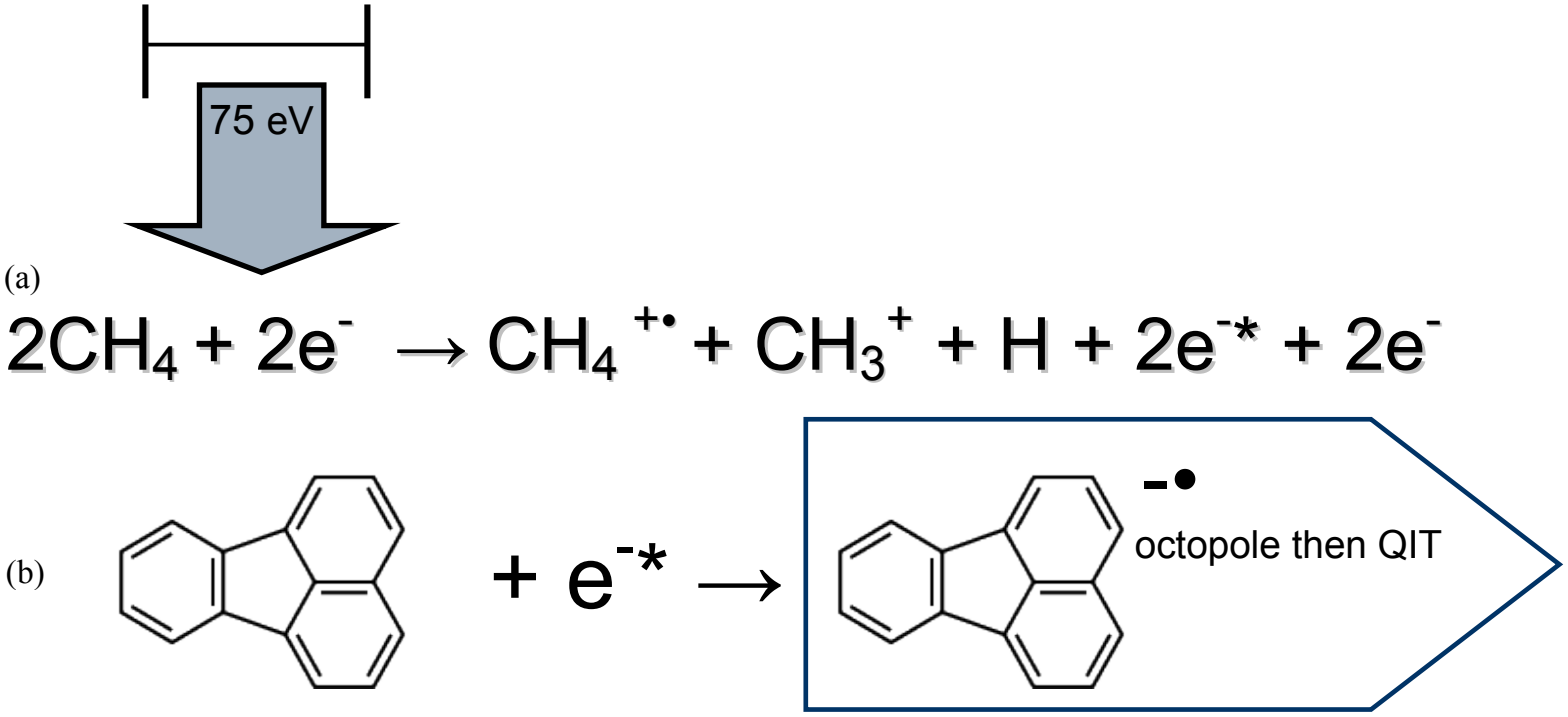

Figure 2.6. Reactant anions are generated in a negative chemical ionization (nCI) source in two steps: (a) generating low energy electrons and (b) attaching the low energy electrons to fluoranthene.

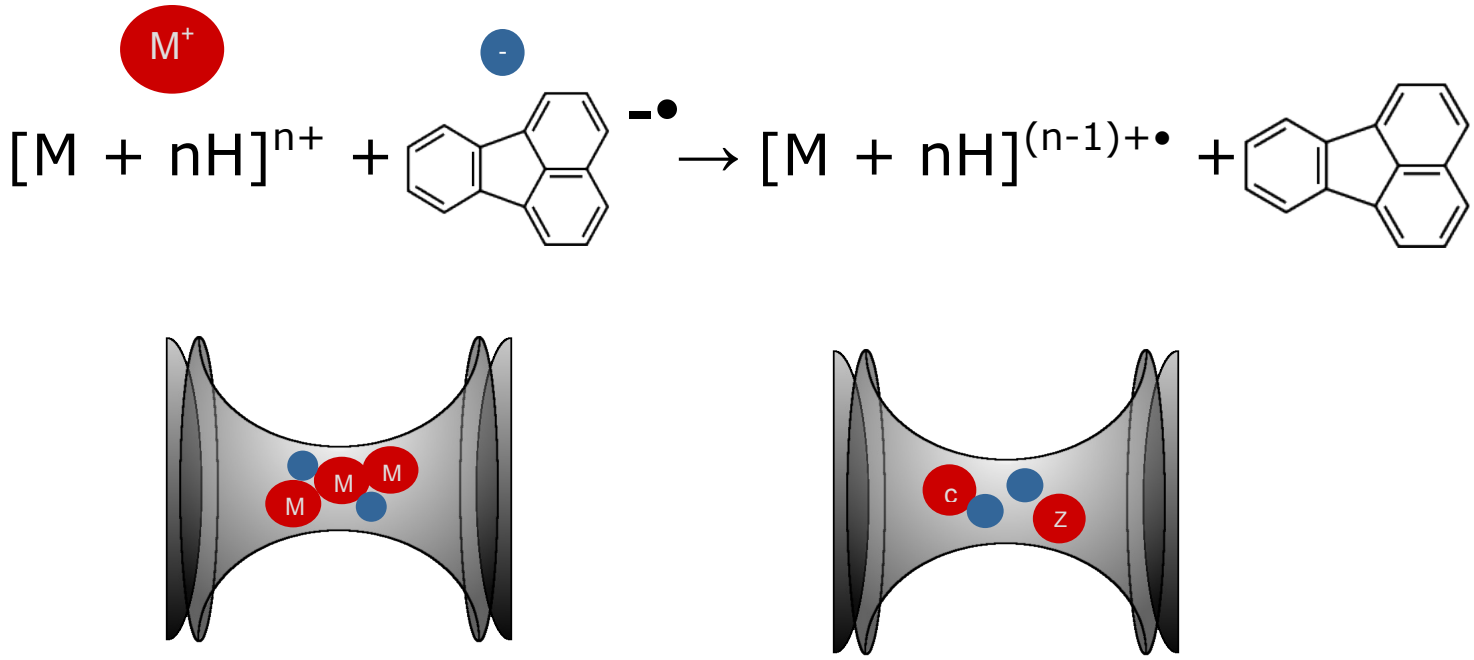

Figure 2.7. Electron transfer dissociation is an ion/ion reaction that typically results in c- and z-type product ions and neutral reactant molecules.

mechanism[23]. According to the Cornell mechanism, the electron is initially captured at a positive site to form a Rydberg radical center. As the electron relaxes to the ground Rydberg level a hydrogen atom is released that can attach the oxygen atom of the backbone carbonyl. This allows a C-N Π bond to form as the N-Cα bond is broken.[16, 24] Alternatively, the Utah-Washington mechanism suggests that the hydrogen atom is not necessary for N-Cα bond cleavage. In this mechanism, the electron is captured either directly at the amide Π* orbital or at a the Rydberg orbital of a positively charged site and subsequently undergoes intra-molecular transfer to the amide Π* orbital both resulting direct cleavage of the N-Cα bond.[23, 24] A typical ETD reaction only takes between 50-300 ms and provides randomized cleavage to yield good peptide sequence coverage. However, the overall efficiency (i.e., percentage of precursor ion that is dissociated) is low and depends strongly on the overlap between reactant anions and the precursor cations in the trap.

2.1.5. Electron-Transfer Collisionally-Activated Dissociation (ETcaD)

Both CID and ETD can be implemented in the quadrupole ion trap to perform tandem mass spectrometry (MS^n, $n \geq 2$). This allows multiple stages of MS to be carried out in time. Dissociation of product ions can lead to structural information and can be used to obtain further sequence information of ambiguous ions. Low product ion intensities are common in ETD spectra often because the ion/ion reaction efficiencies are low.[25] As a result unreacted precursor, $[M + nH]^{n+}$, and the reduced precursor, $[M + nH]^{(n-1)+\bullet}$, are often the most intense ions in the spectra. These reduced ions have been called electron-transfer no dissociation (ETnoD).[26, 27]

In order to glean more information about the precursor ion, a new method called ETD/CID[28] or ETcaD[26] has been introduced. This involves trapping the reduced precursor produced by ETD, the ETnoD ion, and submitting it to supplemental activation, in this case CID. The extra energy given to the reduced precursor by collisions with helium gas allows further dissociations. ETcaD is being investigated as a method that may preserve post-translational modifications (PTMs) and also increase the overall intensities of product ions.[26]

2.2 Matrix-assisted Laser Desorption Ionization/Time-of-Flight (MALDI/TOF)

2.2.1 MALDI

MALDI is also a "soft" ionization technique that allows large molecules such as proteins and glycans to be ionized without breaking bonds in the process. Tanaka et al. introduced the technique after finding that mixtures of analyte, glycerol, and fine powdered metal irradiated by a laser could ionize analyte without inducing fragmentation.[29] This earned Tanaka a share of the Nobel Prize in Chemistry in 2002. Improvements to this technique include work by Karas and Hillenkamp, who found that mixing a light absorbing media with a nonabsorbing analyte allowed the ionization of proteins of 100,000 Daltons and decreased unwanted fragmentation.[30, 31]

Compared to electrospray ionization (ESI), MALDI requires smaller sample volumes and is more tolerant to contaminations. A typical sample spot requires only ~1 μL of sample solution on the target plate, and when stored properly, the target can be analyzed multiple times over months if necessary. The MALDI process also produces

singly charged ions whereas ESI can produce multiply charged and singly charged ions, which can complicate spectral interpretation.

Optimum ionization conditions and spectral results are dependent on sample preparation with MALDI as with ESI. Many factors should be considered when preparing samples such as selecting the right matrix, optimizing the matrix to analyte ratio, choosing a sample plate of appropriate composition, and even the method of putting the sample onto the plate. All of these factors contribute to the overall quality of the resulting spectrum.[32] The matrix also serves to reduce intermolecular contact between analyte molecules, which reduces desorption energy, and acts as a protonation agent.

Choosing the correct MALDI matrix is important. The most commonly used matrices 2, 5-dihydroxybenzoic acid (DHB), α-cyano-4-hydroxycinnamic acid (CCA), and sinapinic acid (SA) are shown in Figure 2.8. A good matrix must possess several qualities.[33, 34] First, it must absorb light at the wavelength of the ionizing laser in order to transfer energy to the dissolved analyte to cause ionization. Second, a good matrix is soluble in common solvents so that analytes and the matrix are together while remaining chemically inert with the analyte. For peptides and proteins, CCA and DHB are the most commonly used matrices. CCA is best for lower mass range peptides and is soluble in common organic solvents.[35] CCA generally imparts more energy to the analyte upon desorption and ionization than DHB and, as a result, is particularly good if post-source decay (PSD) spectra are desired. An advantage of CCA is that it dries in a thin layer of homogeneous small crystals (Figure 2.9) leading to increased resolution. If the analyte tends to dissociate from the extra energy imparted by CCA, or if it is water soluble, DHB is a good option. DHB is a good matrix for peptides, glycoproteins, and glycans.[34] It is

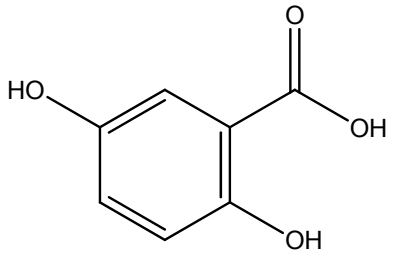

2, 5-dihydroxybenzoic acid (DHB)

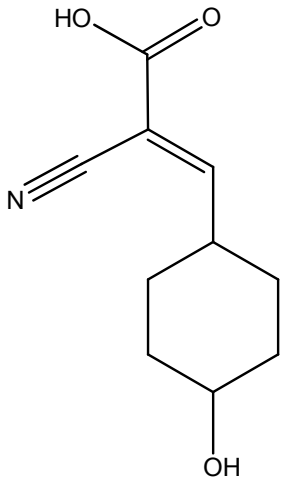

a-cyano-4-hydroxycinnamic acid (CCA)

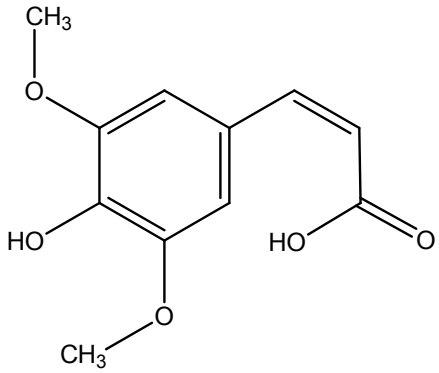

sinapinic acid (SA)

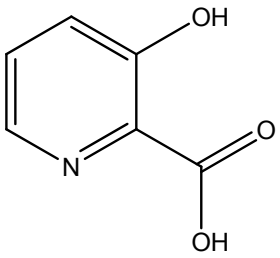

3-hydroxypicolinic acid (HPA)

Figure 2.8. Common MALDI matrices and abbreviations.

soluble in both water and organic solvents. The main drawback is revealed when DHB is dried. A typical DHB sample dries into ring of jagged inhomogeneous crystals near the rim of the sample spot, as shown in Figure 2.9. The best signals are typically attained in between these large crystals but near the rim of the spot. Because *m/z* resolution can be affected by heterogeneity of the sample layer, DHB spectra tend to show less resolution but are more tolerant to salt or detergent contaminations. For the analysis of high mass proteins, sinapinic acid is usually the best choice. The higher energy imparting CCA tends to fragment higher mass peptides before detection unlike the "softer" SA.

Once the best matrix is chosen, the matrix dissolved into the appropriate solvent (ACN for CCA and ACN/H_2O for DHB). Sonication aids in preparing a saturated solution followed by centrifugation to remove excess solid. Samples are prepared by mixing various ratios of analyte to matrix. Usually a 1:1 through 1:10, sample to matrix ratio is a good starting point. Unlike many techniques an increase in the concentration of analyte may not directly result in signal increase. This is because the matrix molecules must surround the analyte in order to transfer energy. If the analyte is increased to the point that the matrix can not surround it, the chance of ionizing the analyte decreases.

For the work presented in this dissertation, the matrices DHB and CCA were used, and the optimum ratio was usually around 1:5 analyte to matrix where the initial concentration of the peptide samples were μM. DHB matrices were prepared with 0.1 % TFA to aid protonation in 1/1 v/v ACN H_2O. Once samples were applied to the sample plate (or target), they were allowed to dry on a bench top or, for less volatile solvents, under gentle nitrogen. After drying, the sample spots were inspected under high magnification for homogeneity and loaded into the MALDI source. A Bruker Daltonics

(Billerica, MA, USA) Reflex III MALDI/TOF mass spectrometer equipped with delayed extraction and a two stage reflectron was used in this work.

A pulsed laser, in this case a 337 nm nitrogen laser with ca. 3 ns pulse length, was focused onto the sample spot (ca. 10^4 μm^2) of interest. Each pulse generates a plume of matrix and analyte from the target surface (see Figure 2.10).

Although not completely understood, several theories have been offered to try to explain the desorption of such large molecules by MALDI, including the photochemical ionization model,[36] the cluster ionization mechanism,[37-40] the pneumatic assistance model,[40] and, more recently, the energy-transfer induced disproportionation (ETID) model.[41]

2.2.2 TOF MS

The first time-of-flight (TOF) mass analyzer was developed in 1948 by Cameron and Eggers.[42] The mass analyzer did not gain widespread usage until the development of MALDI, whose pulsed laser ionization is very compatible with TOF. Though TOF requires pulsed ionization, it can be used with both pulsed and continuous ion sources by gating continuous sources such as ESI and electron ionization (EI); this creates a pulsed effect of incoming ions. This combined with extreme sensitivity (because all ions make it through the flight tube) makes TOF a very versatile and commonly used mass analyzer.

Time-of-flight is the simplest of the mass analyzers to explain in terms of theory. TOF measures the *m/z* of ions in a field-free flight tube based on how long it takes for ions to reach a detector (Figure 2.11). Given the same initial kinetic energy and removing all

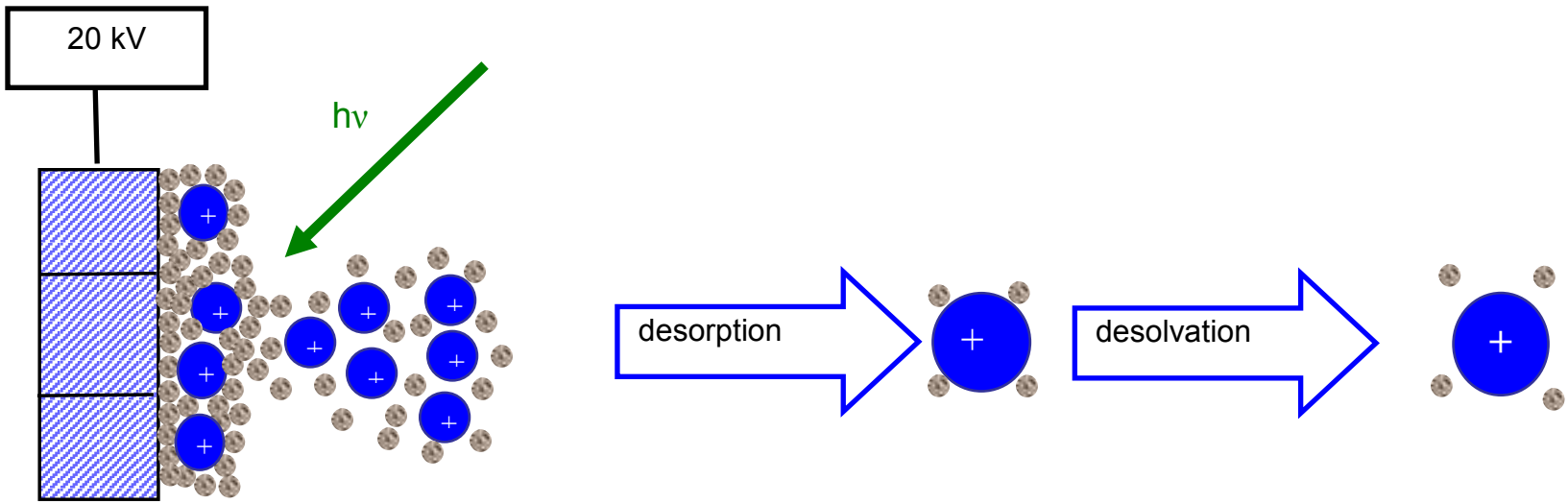

Figure 2.10. Ionization by MALDI from the surface of a sample target.

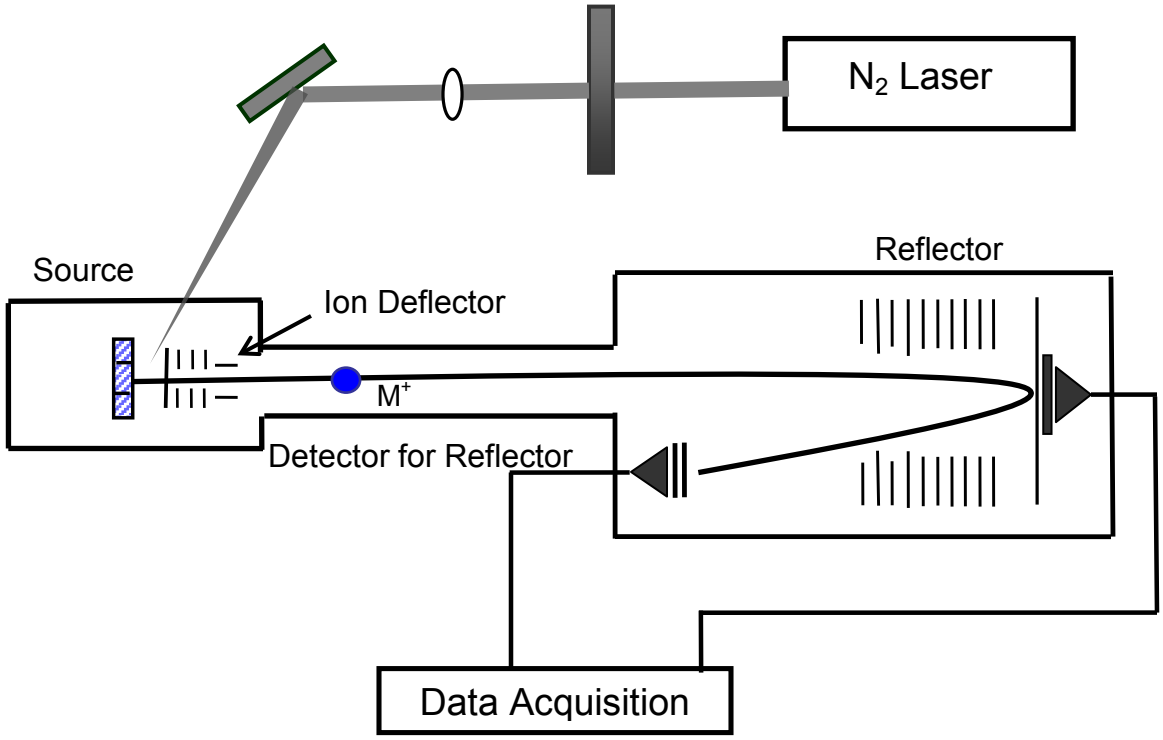

Figure 2.11. Diagram of MALDI-TOF MS equipped with reflector.

obstacles (vacuum), larger ions will take longer to traverse the same distance as smaller ions.

A charged particle in an electric field has a potential energy (E_p) related to the strength of the electric field (V_1) and nominal charge of the particle (*z*, usually 1 in MALDI) as shown in Equation (2.12).

$$E_p = zV_1 \tag{2.12}$$

Once irradiated by the incoming laser pulse, ions of interest (negative or positive) are accelerated from the sample plate by the application of high voltage (V_1) as shown in Figure 2.12. For positive/negative mode analysis typical accelerating potential is ~ +/- 20-30 kV, respectively, where like charges repel.

In theory, all ions receive the same initial kinetic energy and leave the source at the same time. This initial kinetic energy (E_k) is related to the ion's mass (*m*) according to Equation (2.13), which demonstrates that lighter ions have a higher velocity (*v*). As a result, ions with a lower mass reach the detector sooner.

$$E_k = \frac{1}{2}mv^2 \tag{2.13}$$

This acceleration due to V_1 converts the ion's potential energy into kinetic energy, which can be equated as shown in Equation (2.14) to provide a relationship between the ion's mass, charge and velocity shown in Equation (2.15).

$$E_p = E_k \tag{2.14}$$

$$zV_1 = \frac{1}{2}mv^2 \tag{2.15}$$

The length (L) between initial acceleration of the ions from the sample plate and the detector is known. Also, the ions' velocity (*v*) in an evacuated tube does not change. Therefore, velocity can be determined by relating the distance (L) and the measured time it takes to reach the detector (t) as given in Equation 2.16.

$$v = \frac{L}{t} \tag{2.16}$$

Substitution of L/t into Equation (2.15) for velocity gives Equation 2.17 and rearrangement of this equation to solve for time gives Equation 2.18.

$$\frac{m}{z} = 2\frac{V_1}{v^2} = \frac{2V_1t^2}{L^2} \tag{2.17}$$

$$t = \left(\frac{L}{\sqrt{2V_1}}\right)\sqrt{\frac{m}{z}} \tag{2.18}$$

Because L and V_1 are known they can be considered constant *k* and a simplified as Equation (2.19) that directly relates the ion's arrival time *t*, which is measured, to its mass to charge ratio.

$$t = k\sqrt{\frac{m}{z}} \tag{2.19}$$

Combining MALDI with TOF allows not only high sensitivity but unlimited mass range. However, early instrument designs had poor *m/z* resolution. This was due to combined effects of ions receiving slightly different amounts of kinetic energy from the high voltage before being accelerated from the source and the uneven surface of sample spots. Slight distributions in initial kinetic energy leads to ions of the same mass reaching the detector at slightly different times, which results in peak broadening. In addition, uneven surface geometry of crystalline matrices such as DHB can cause ions forming from different heights above the crystalline surface to experience a different electric field. This shifts the apparent *m/z* of the ions in the mass spectrum.

Delayed extraction (DE) and improvements to sample preparation techniques have increased TOF resolution. The original concept for delayed extraction in MALDI/TOF originated from a technique called "time-lag focusing" proposed by Wiley et al.[43] in 1955. In 1995 the technique was first applied to MALDI/TOF (as DE) to increase resolution by delaying the extractions of ions from the source by less than a microsecond. This is achieved by applying a second high voltage (V_2) that is slightly lower than V_1 a few hundred nanoseconds later. This allows all desorbed ions to leave the source at the same time and compensates for the initial spread of ion velocity (see Figure 2.12), thus improving mass resolution. The incorporation of DE into MALDI/TOF not only improves resolution, but evidence of improved signal-to-noise, reduction and sometimes elimination of matrix background, and decreased effects of laser intensities on flight times have been reported.[44]

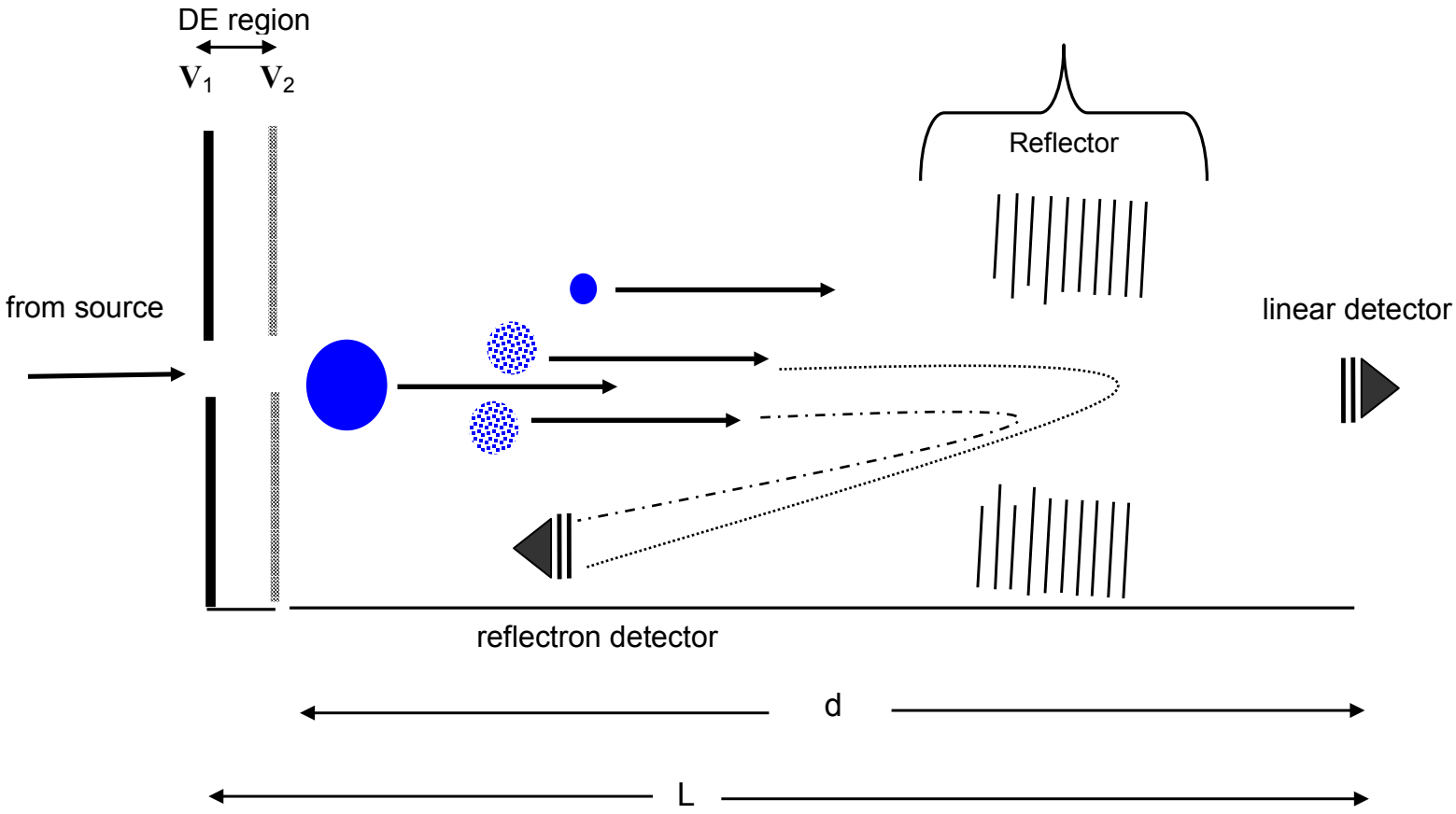

Figure 2.12. Simplified diagram illustrating delayed extraction and reflectron TOF. The textured ions have the same *m/z* but slightly different velocities. The faster ion travels further into the field to correct for this. Therefore, ions with the same *m/z* arrive at the detector at the same time.

To further correct for kinetic energy spreads of ions with the same *m/z*, electrostatic fields are applied along the flight tube of the Bruker Reflex IV. This process is called reflectron TOF. Reflectron TOF mass analyzers were first introduced by Mamyrin and coworkers,[45] and several variations and improvements have been made since that time.[46] As shown in Figure 2.12, electrostatic lenses with increasing potential are used to slow down ions entering the field and reverse their direction back toward a detector. To compensate for the kinetic energy spread, the more energetic ions penetrate the field deeper whereas less energetic ions travel into the field less. The overall effect is that ions of the same *m/z* travel slightly different paths; but because of the initial E_k spread, they ultimately reach the detector at the same time. Reflectron TOF has a separate detector from linear TOF, in this work a microchannel plate, located at the point where ions of the same mass; but different kinetic energies hit the surface of the detector at the same time. This greatly increases the resolution and mass accuracy of the resulting spectra.

2.2.3 Post-Source Decay

Initial investigations into the MALDI/TOF process determined that the ionization process was so "soft" that few fragment ions were observed. However, a large portion of these ions was soon discovered to dissociate after desorption but prior to detection[47] and was termed post-source decay.[48] Post-source decay (PSD) is a process that allows tandem MS spectra to be obtained by MALDI/TOF. With PSD, the identification of structurally informative fragment ions (that form in the field free region of the flight tube after leaving the ion source) is possible. Because MALDI allowed the ionization of large peptides and

PSD allowed tandem MS to be accomplished by MALDI/TOF, PSD was soon successful in peptide sequencing.[49]

During the MALDI process, excess internal energy can be imparted to analyte ions by elevated laser power. For some ions this energy is enough to cause them to fragment in the field free region of the flight tube. This excess energy can be increased by increasing the irradiating laser power resulting in more ions fragmenting. For a PSD experiment, a precursor ion is chosen by applying an ion gate between the ion source and the field free region. The ion gating selection process chooses various *m/z* based on the knowledge that ions of different *m/z* have different velocities (Equation 2.12). The gating voltage is applied at a specific time so that only the ions of the selected *m/z* are transmitted into the flight tube. The fragment ions formed in the flight tube have the same velocity as the precursor ion chosen but have different kinetic energies because their masses are smaller. In order to differentiate the fragment ions from the precursor ion and each other, a modification to the voltages applied to the ion lenses of the reflectron is made. In this work, post-source decay (PSD) spectra were obtained in the negative mode after precursor ion isolation by stepping down the reflectron voltages in stages, -21.0, -19.55, -15.75, -11.82, -8.86, -6.64, -4.98, -3.74, and -2.80 kV, and the resulting spectral segments were stitched together into a PSD spectrum with the processing software Flexanalysis.

The MALDI/TOF MS work presented in Chapter 5 was carried out on a Bruker Daltonics (Billerica, MA, USA) Reflex III MALDI/TOF mass spectrometer equipped with delayed extraction and a two stage reflectron. Samples were desorbed/ionized by a 337 nm nitrogen laser from Laser Science (Franklin, MA, USA) model VSL-337ND-S from sample plates. Positive and negative spectra were obtained using linear and reflectron

modes with accelerating voltages of +/- 20-22 kV for positive or negative mode respectively. Mass-to-charge calibration was carried out with ACTH (18-39) for positive mode analysis[50] and a mixture of renin substrate, angiotensin II, and fibrinopeptide B (human)[51] in the negative mode.

2.3 Peptide Synthesis Protocol

Standard peptide synthesis based on Fmoc procedures involving solid phase peptide synthesis (SPPS) first developed by R. B. Merrifield.[52] In 1984 Merrifield was honored with the Nobel Prize in chemistry for this contribution. Fmoc is the more commonly used of the SPPS techniques because of its higher yields and refers to the solid support Wang resin consisting of the base labile 9-fluorenylmethyloxycarbonyl (Fmoc). Unlike peptides made naturally in biological systems, SPPS starts with the C-terminal amino acid and the peptide is lengthened step-wise by adding additional amino acids until the sequence is completed with the N-terminus. The C-terminus is bound to an insoluble resin. This resin or "bead" prevents the C-terminus from reacting with other amino acids. The N-terminus of the amino acid is blocked with a protecting group, like Fmoc, (see Figure 2.13) until ready to react with the next amino acid in the synthesis.

The overall process involves repeated cycles of coupling and deprotection as outlined in Figure 2.14. The free N-terminal amine of a solid phase peptide (still bound to resin support) is coupled to an incoming N-protected amino acid unit. After coupling (creating a new peptide bond), the newly added amino acid's N-terminus is deprotected revealing a reactive site to which the next amino acid is coupled to. Once the coupling/deprotecting cycles have added the desired number and types of amino acids, the

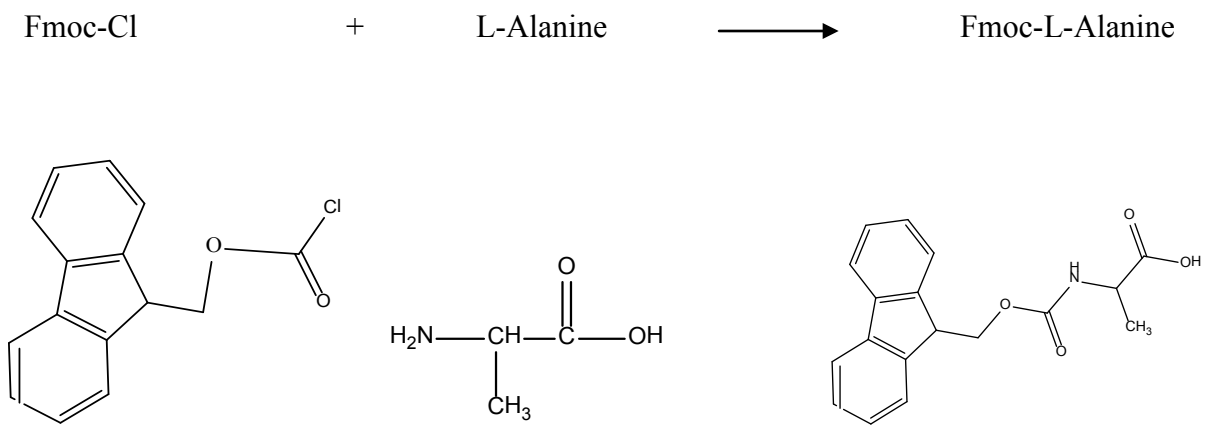

Figure 2.13. Fmoc protective group used in peptide synthesis.

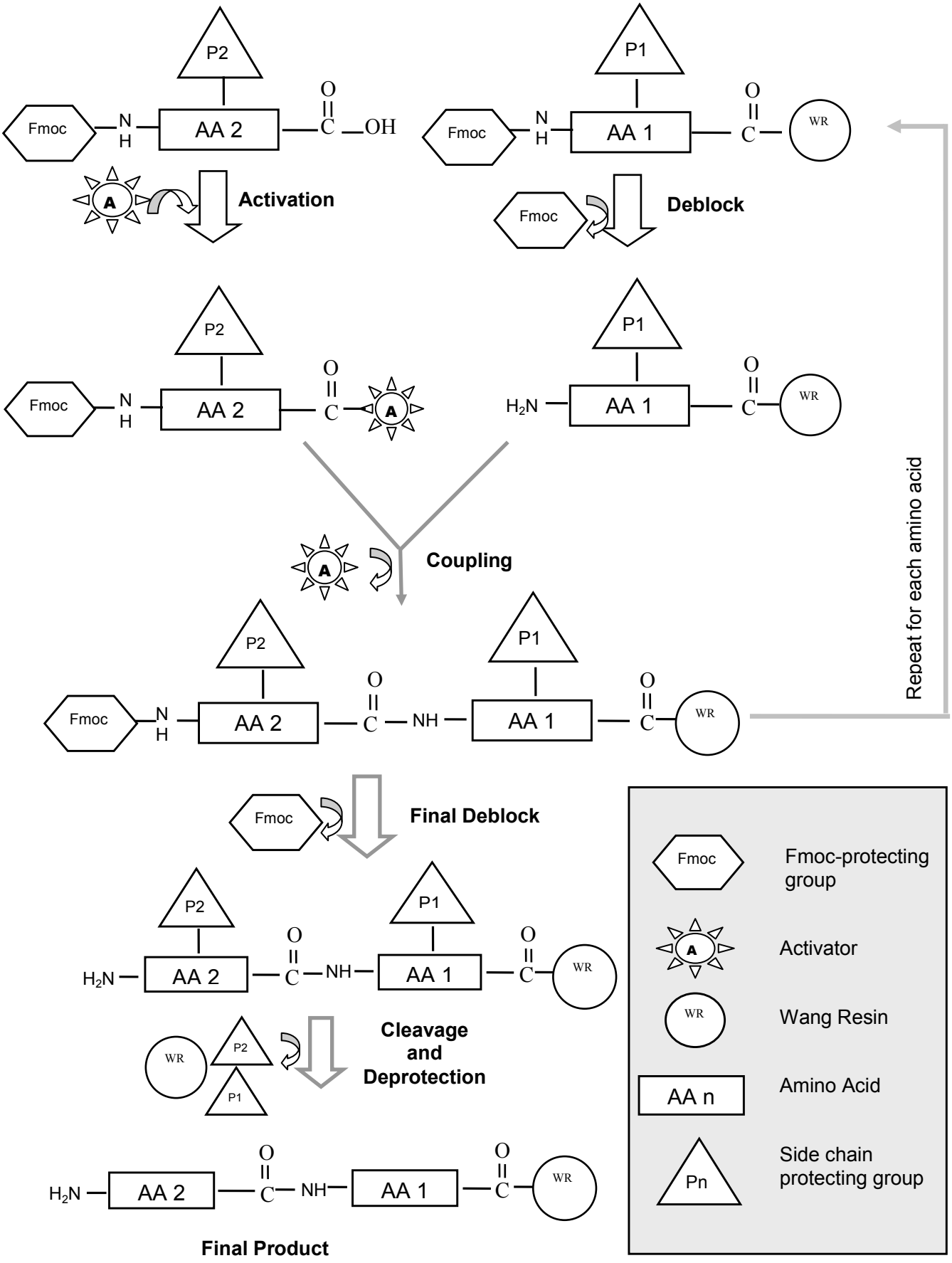

Figure 2.14. Steps of SPPS peptide synthesis

new peptide is cleaved from its resin support; and, concurrently, all side chain protecting groups are cleaved from their protecting groups to yield crude free peptide.

In particular, the peptides used in Chapters 3-6 of this dissertation were synthesized with the aid of an Advanced ChemTech (Louisville, KY, USA) Model 90 peptide synthesizer. The chemicals involved were purchased from various sources including AnaSpec (Fremont, CA, USA) for amino acid residues, Wang resins, and 1-hydroxybenzotriazole hydrate (HOBt) and Fisher Scientific (Pittsburg, PA, USA) for N,N-dimethylformamide (DMF), piperidine (PIP), N-methyl-2-pyrrolidinone (NMP), 1, 3-diisopropylcarbodiimide (DIC), trifluoracetic acid (TFA), ethyl ether, and triisopropylsilane (TIS). The amino acid structures are shown in Figure 2.15. The amino acids used in peptide synthesis typically contained the Fmoc protecting group as shown in Figure 2.13. The C-terminal amino acids contain the Fmoc protecting group and Wang resin.

The Fmoc protecting groups were removed with a 20% (v/v) PIP in DMF solution. The amino acid residues were prepared as solutions of 0.5 M in HOBt (prepared as 0.5 M in NMP) and added to deblocked residues along with DIC (prepared as 0.5 M in NMP) that serves as the activator for the coupling reaction. Coupling was allowed to occur via mechanical shaking for 90-120 minutes. Once all residues were added, the removal of side chain protecting groups and the C-terminal resin was achieved via a cleavage reaction. The cleavage cocktail, consisting of 9.5 mL of TFA, 0.5 mL of MQ H_2O, and 0.3 ml of TIS, was mixed with the protected peptide and allowed to stir for a minimum of three hours. The mixture was then filtered directly into ~30 mL ethyl ether, which had been cooled to -78 °C on a dry ice/ACN slurry. This solution was allowed to incubate in a

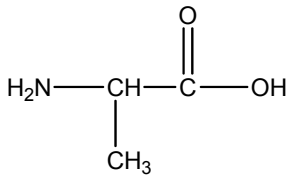

Alanine (A)

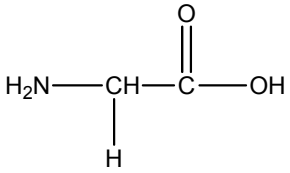

Glycine (G)

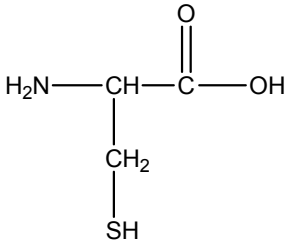

Cysteine (C)

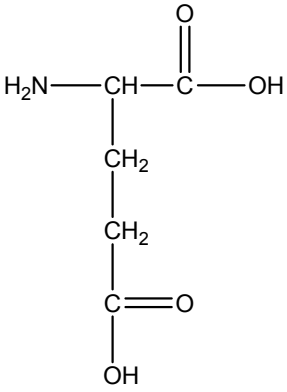

Glutamic Acid (E)

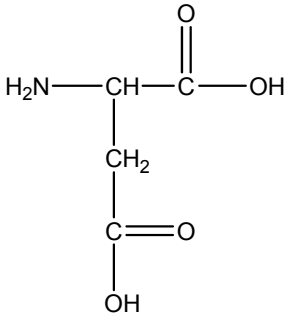

Aspartic Acid (D)

Figure 2.19. Structures of the amino acids used in this work.

freezer for a minimum of three hours and then centrifuged at 3000 rpm for 20 minutes. After decanting from the gel-like peptide, another volume of cold ethyl ether was added, and the incubation, centrifugation, and decanting steps were repeated once more. The remaining gel was then put into a desiccator until dry, usually overnight, and the remaining solid peptide used for further experiments.

Peptides studies involving a "blocked" C-terminus were carried out by methyl esterification of the C-terminus of synthesized peptide (Figure 2.16). This was accomplished by mixing 69 μL of dry methanol, 5 μL of acetic anhydride, 6 μL of 12 M hydrochloric acid for five minutes and then adding 1.2 mg of solid peptide. The mixture was stirred for two hours and then refrigerated for 24 hours.

2.4 Peptide Sequencing Nomenclature

In order to more clearly discuss the spectra presented in Chapters 3-6, the peptide cleavage symbolism (a, b, c, and y) used in the dissertation refers to the location of cleavage sites along the backbone. It is based on Roepstorff and Fohlman's original nomenclature[53] and is illustrated in Figure 2.5. Many different types of product ions form in tandem mass spectrometry and the various dissociation techniques are known for producing some types more than others. For example, the most common CID products are b-and y-type ions formed from C-N cleavage of the peptide bond. ETD products are most often c-and z-type ions formed from dissociation of the N-Cα bond. These are not hard and fast rules. Often times other ion types appear in each method.

Cleavage along the peptide backbone produces a charged product, appearing in the spectrum, and a neutral that goes undetected. If the charge remains on the N-terminal

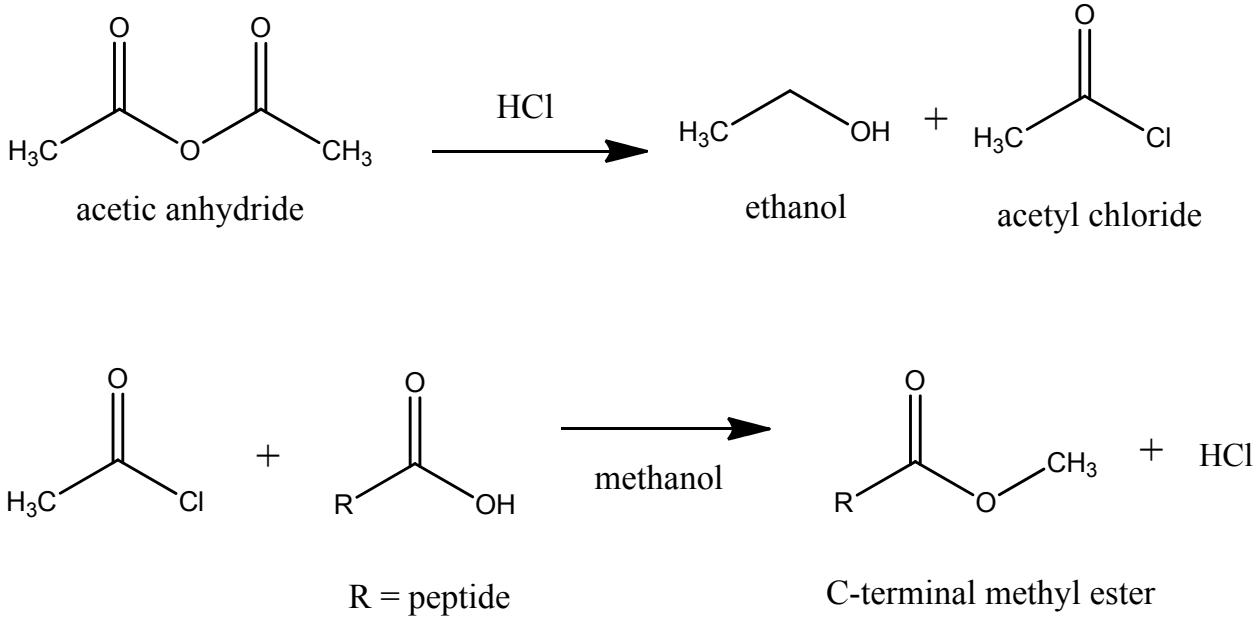

Figure 2.16. Blocking the C-terminus of a peptide with a methyl ester.

product, the ion is defined as a_n, b_n, or c_n. If the charge remains with the C-terminal product, the ion is defined as x_n, y_n, or z_n. The subscript "n" refers to "n-th" amino acid residue where cleavage occurs. Numbering depends on whether the product is from the N- or C-terminus and begins with that termini's amino acid. Any loss or addition of hydrogen from these products will be specifically noted. For example, in positive mode, protonated y-ions form with two additional hydrogens and will be referred to as $[y + 2H]^+$. This is done to keep track of hydrogen atoms because metal ions can displace a varying number of hydrogen atoms. Each label also distinguishes whether or not the product contains the metal ion. For example, $[a_4 + Cu - 2H]^{2+}$ is a doubly charged product ion formed after cleavage of the Cα-C bond after the fourth amino acid residue.

REFERENCES:

1. J. B. Fenn, Electrospray wings for molecular elephants (Nobel lecture). *Angew. Chem. Int. Ed.* **2003,** 42, 3871-3894.

2. M. Yamashita; J. B. Fenn, Electrospray ion source. Another variation on the free-jet theme. *J. Phys. Chem.* **1984,** 88, 4451-4459.

3. M. Dole; R. L. Hines; R. C. Mack; R. C. Mobley; L. D. Ferguson; M. B. Alice, Molecular beams of macroions *J Chem. Phys.* **1968,** 49, 2240-2249.

4. J. W. Strutt, On the equilibrium of liquid conducting masses charged with electricity. *Philos Mag.* **1882,** 14, 184-186.

5. T. Frängsmyr, The Nobel Prizes. August 20, 2011. http://www.nobelprize.org/nobel_prizes/physics/laureates

6. M. Wilm; M. Mann, Electrospray and Taylor-cone theory, Dole's beam of macromolecules at last? *Int. J. Mass Spectrom. Ion Process.* **1994,** 136, 167.

7. M. Wilm; M. Mann, Analytical properties of the nanoelectrospray ion source. *Anal. Chem.* **1996,** 68, 1-8.

8. T. L. Constantopoulos; G. S. Jackson; C. G. Enke, Effects of salt concentration on analyte response using electrospray ionization mass spectrometry. *J Am. Soc. Mass Spectrom.* **1999,** 10, 625-634.

9. R. Juraschek; T. Dülcks; M. Karas, Nanoelectrospray-More than just a minimized-flow electrospray ionization source. *J. Am. Soc. Mass Spectrom.* **1999,** 10, 300-308.

10. M. Karas; U. Bahr; T. Dülcks, Nano-electrospray ionization mass spectrometry: addressing analytical problems beyond routine. *Fresnius. J. Anal. Chem.* **2000,** 366, 669-676.

11. The 1989 Nobel Prize in Physics. August 20, 2011. http://www.nobelprize.org/nobel_prizes/physics/laureates/1989/press.html

12. R. E. March, An introduction to quadrupole ion trap mass spectrometry. *Journal of Mass Spectrometry* **1997,** 32, 351-369.

13. Bruker Daltonics, *HCTultra PTM Discovery System User Manual*. Billerica, MA, 2006.

14. I. A. Papayannopoulos, The interpretation of collision-induced dissociation tandem mass spectra of peptides. *Mass Spectrometry Reviews* **1995,** 14, 49-73.

15. J. Wells; S. McLuckey, Collision-induced dissociation (CID) of peptides and proteins. *Methods Enzymol.* **2005,** 402, 148-185.

16. R. A. Zubarev; K. F. Haselmann; B. Budnik; F. Kjeldsen; F. Jensen, Towards an understanding of the mechanism of electron-capture dissociation: a historical perspective and modern ideas. *Eur. J. Mass Spectrom.* **2002,** 8, 337-349.

17. R. A. Zubarev; D. M. Horn; E. K. Fridriksson; N. L. Kelleher; N. A. Kruger; M. A. Lewis; B. K. Carpenter; F. W. McLafferty, Electron Capture Dissociation for Structural Characterization of Multiply Charged Protein Cations. *Anal. Chem.* **2000,** 72, 563-573.

18. H. J. Cooper; K. Hakansson; A. G. Marshall, The role of electron capture dissociation in biomolecular analysis. *Mass Spectrom. Rev.* **2005,** 24, 201-222.

19. F. Meng; A. J. Forbes; L. Miller; N. L. Kelleher, Detection and localization of protein modifications by high resolution tandem mass spectrometry. *Mass Spectrom. Rev.* **2005**, 57-77.

20. R. A. Zubarev, Reactions of polypeptide ions with electrons in the gas phase. *Mass Spectrom. Rev.* **2003,** 22, 57-77.

21. R. A. Zubarev, Electron-capture dissociation tandem mass spectrometry. *Curr. Opin. Biotechnol.* **2004,** 15, 12-16.

22. J. E. P. Syka; J. J. Coon; M. J. Schroeder; J. Shabanowitz; D. F. Hunt, Peptide and protein sequence analysis by electron transfer dissociation mass spectrometry. *Proc. Nat. Acad. Sci. USA* **2004,** 101, 9528-9533.

23. X. Chen; F. Turecek, The arginine anomaly: arginine radicals are poor hydrogen atom donors in electron transfer induced dissociations. *J. Am. Chem. Soc.* **2006,** 38, 12520-12530.

24. J. Simons, Mechanisms for S-S and N-Cα bond cleavage in peptide ECD and ETD mass spectrometry. *Chem. Phys. Lett.*, **2010**, 484, 81-95.

25. S. J. Pitteri; P. A. Chrisman; J. M. Hogan; S. A. McLuckey, Electron transfer ion/ion reactions in a three-dimensional quadrupole ion trap: reactions of doubly and triply protonated peptides with SO_2dot^-. *Anal. Chem.* **2005,** 77, 1831-1839.

26. D. L. Swaney; G. C. McAlister; M. Wirtala; J. C. Schwartz; J. E. P. Syka; J. J. Coon, Supplemental activation method for high-efficiency electron-transfer dissociation of doubly protonated peptide precursors. *Anal. Chem.* **2006,** 79, 477-485.

27. Y. Xia; H. Han; S. A. McLuckey, Activation of intact electron-transfer products of polypeptides and proteins in cation transmission mode ion/ion reactions. *Anal. Chem.* **2008,** 80, 1111-1117.

28. J. L. Campbell; J. W. Hager; J. C. Y. Le Blanc, On performing simultaneous electron transfer dissociation and collision-induced dissociation on multiply protonated peptides in a linear ion trap. *J. Am. Soc. Mass Spectrom.* **2009,** 20, 1672-1683.

29. K. Tanaka; Y. Ido; S. Akita; Y. Yoshida; T. Yoshida, Detection of high mass molecules by laser desorption time-of-flight mass spectrometry. *Second Japan-China Joint Symposium on Mass Spectrometry* **1987**, 185-187.

30. M. Karas; D. Bachmann; F. Hillenkamp, Influence of the wavelength in high-irradiance ultraviolet-laser desorption mass-spectrometry of organic-molecules. *Anal. Chem.* **1985**, 2935-2939.

31. M. Karas; F. Hillenkamp, Laser desorption ionization of proteins with molecular masses exceeding 10,000 daltons. *Anal. Chem.* **1988**, 2299-2301.

32. F. Hillenkamp; M. Karas; D. Holtkamp; P. Klüsener, Energy deposition in ultraviolet laser desorption mass spectrometry of biomolecules. *Int. J. Mass Spectrom. Ion Proc.* **1986,** 69, 265-276.

33. M. C. Fitzgerald; G. R. Parr; L. M. Smith, Basic matrixes for the matrix-assisted laser desorption/ionization mass spectrometry of proteins and oligonucleotides. *Anal. Chem.* **1993,** 65, 3204-3211.

34. P. Juhasz; C. E. Costello; K. Biemann, Matrix-assisted laser desorption ionization mass spectrometry with 2-(4-hydroxyphenylazo)benzoic acid matrix. *J. Am. Soc. Mass Spectrom.* **1993,** 4, 399-409.

35. S. L. Cohen; B. T. Chait, Influence of Matrix Solution Conditions on the MALDI-MS Analysis of Peptides and Proteins. *Anal. Chem.* **1996,** 68, 31-37.

36. H. Ehring; M. Karas; F. Hillenkamp, Role of photoionization and photochemistry in ionization processes of organic molecules and relevance for matrix-assited laser desorption ionization mass spectrometry. *Org. Mass Spectrom.* **1992**, 472-480.

37. M. Karas; M. Gluckman; J. Schafer, Ionization in matrix-assisted laser desorption/ionization: singly charged molecular ions are the lucky survivors. *J. Mass Spectrom.* **2000,** 35, 1-12.

38. M. Karas; R. Kruger, Ion formation in MALDI: The cluster ionization mechanism *Chem. Rev.* **2003,** 103, 427-439.

39. R. Kruger; A. Pfenninfer; I. Fournier; M. Gluckman; M. Karas, Analyte incorporation and ionization in matrix-assisted laser desorption/ionization visualized by pH indicator molecular probes. *Anal. Chem.* **2001,** 73, 5812-5821.

40. V. Talroze; R. Jacob; A. Burlingame; M. Baldwin, Insight into the MALDI mechanism. Matrix decomposition and pneumatic assistance in plume formation. *Adv. Mass Spectrom.* **2001,** 15, 481-482.

41. W. C. Chang; L. C. L. Huang; Y.-S. Wang; W.-P. Peng; H. C. Chang; N. Y. Hsu; W. B. Yang; C. H. Chen, Matrix-assted laser desorption/ionization (MALDI) mechanism revisted. *Anal. Chim. Acta.* **2007,** 582, 1-9.

42. A. E. Cameron; D. Eggers, An ion "velocitron". *Rev. Sci. Instrum.* **1948,** 19, 605-607.

43. W. C. Wiley; I. H. McLaren, Time-of-flight mass spectrometer with improved resolution. *Rev. of Sci. Instrum.* **1955,** 26, 1150-1157.

44. M. L. Vestal; P. Juhasz; S. A. Martin, Delayed extraction matrix-assisted laser-desorption time-of-flight mass-spectrometry. *Rapid Commun. Mass Spectrom* **1995,** 9, 1044-1050.

45. B. A. Mamyrin; V. I. Karataev; D. V. Shmikk; V. A. Zagulin, The mass-reflectron, a new nonmagnetic time-of-flight mass spectrometer with high resolution. *Sov. Phys. JETP* **1973,** 37, 45-48.

46. B. A. Mamyrin, Time-of-flight mass spectrometry (concepts, achievements, and prospects) *Int. J. Mass Spectrom.* **2001,** 206, 251-266.

47. B. Spengler; D. Kirsch; R. Kaufmann, Metastable decay of peptides and proteins in matrix-assisted laser-desorption mass-spectrometry. *Rapid Commun. Mass Spectrom* **1991,** 5, 198-202.

48. R. Kaufmann; B. Spengler; F. Lutzenkirchen, Mass-spectrometric sequencing of linear peptides by product-ion analysis in a reflectron time-of-flight mass-spectrometer using matrix-assisted laser-desorption ionization. *Rapid Commun. Mass Spectrom* **1993,** 7, 902-910.

49. B. Spengler; D. Kirsch; R. Kaufmann; E. Jaeger, Peptide sequencing by matrix-assisted laser-desorption mass-spectrometry. *Rapid Commun. Mass Spectrom* **1992**, 105-108.

50. J. C. Rouse; W. Yu; S. Martin, A comparison of the peptide fragmentation obtained from a reflector matrix-assisted laser desorption-ionization time-of-flight and a tandem four sector mass spectrometer. *J. Am. Soc. Mass Spectrom.* **1995**, 822-835.

51. J. Jai-nhuknan; C. J. Cassady, Negative ion matrix-assisted laser desorption/ionization time-of-flight post-source decay calibration by using fibrinopeptide b. *J. Am. Soc. Mass Spectrom.* **1998**, 540-544.

52. R. B. Merrifield, Solid phase peptide synthesis I. Synthesis of a tetrapeptide. *J. Am. Chem. Soc.* **1963,** 85, 2149-2154.

53. P. Roepstorff; J. Fohlman, Proposal for a common nomenclature for sequence ions in mass spectra of peptides. *Biological Mass Spectrometry* **1984,** 11, 601.

CHAPTER 3

THE EFFECTS OF COLLISION-INDUCED DISSOCIATION ON TRANSITION METAL-PEPTIDE COMPLEXES

3.1 Introduction

Metal ions affect the structure, conformation, and function of many proteins. Biological activity of peptides and proteins is frequently dependent on activation by metal ion binding. Often these metals are transition metals with redox active properties that aid in electron transfer processes.[1] Individual transition metals have unique chemical properties and, as a result, various biological functions. For example, cobalt is the cofactor to vitamin B_{12} and its enzymes, while copper-containing proteins are involved in the transport and activation of dioxygen, reduction of inorganic molecules, electron transfer and several other processes.[2] Iron is essential in hemes and is also involved in other storage and transport proteins.[3] Evidence suggests that chromium activates insulin receptor kinase in the presence of insulin.[4, 5] Transition metals are also known to interfere with zinc finger binding.[6]

Interest in metallopeptides and metalloproteins has increased since completion of the human genome project. Protein and peptide sequencing is seen as the next large scale biological challenge.[7] Structural characterization of metalloproteins can be difficult at times due to the small sample amounts typically isolated and the intolerance of many

analytical techniques to impure samples. Mass spectrometry (MS) is becoming the preferred method to investigate primary structures of metal-peptide complexes because of its sensitivity and ability to analyze impure samples. Electrospray ionization (ESI) and nanoelectrospray ionization (nanoESI) allow ionization and subsequent mass analysis of such samples. The introduction of nanoESI by Wilm and Mann[8, 9] allows extremely small sample volumes to be analyzed and also provides increased tolerance to salt contaminations.[10-12]

Ionization methods such as ESI and nanoESI generally produce intact protonated peptides, $[M + nH]^{n+}$, that can be fragmented by collision-induced dissociation (CID) into primarily b_n/y_n pairs.[13] Such protonated peptides do not always dissociate sufficiently along their backbones to give full sequence information. Metal attachment to peptides and other biomolecules has been studied in an attempt to increase backbone fragmentation and gain more sequence information than is obtained from the protonated precursors.[14-23] Mass spectrometry studies have also provided information on metal ion-protein stoichiometry[24] and identified the specific metal binding sites of proteins.[25] Other research has focused on the correlation between gas-phase metal-protein interactions and the solvated complexes.[16, 17] In addition, elucidating fundamental information such as gas-phase fragmentation pathways is important in the development of predictive models used in bioinformatics.[26]

Past work focusing on the interactions of alkali and alkaline earth metals with peptides suggests that metal ions potentially coordinate to the most basic site of the peptide such as the N-terminus or a basic side chain,[22] to carbonyl oxygens,[14, 27] or even to the C-terminus.[14] No clear trends have been reported for gas-phase metal binding

sites. This may be because the past studies have involved variation in peptide amino acid composition and possibly also due to the nature of the metal ions themselves.

Evidence exists that transition metals not only coordinate with peptides[28, 29] but can also insert into the backbone by direct cleavage.[18, 30] Investigations into the gas-phase ion/molecule reaction chemistry of transition metal ions with many organic molecules reveal that they can insert into a variety of different bonds.[31-37] For example, gas-phase Co(I) inserts into the C-C bonds of alkanes,[37] the C-H, C-C, C-N, and N-O bonds of nitroalkanes,[34] and the C-H, N-H, and C-C bonds of secondary and tertiary amines.[35] Gas-phase reactions of Fe^+ with aldehydes and ketones involve elimination of H_2 and insertion into C-H and C-C bonds.[31] The trends are that Fe(I) is less selective and inserts into a variety of different bonds, whereas Ni(I) is considered very selective while Mn(I) and Cr(I) are unreactive with alkanes.[32]

Studies involving transition metallated-peptide complexes (Co, Ni, Mn, and Fe) have shown that both positive and negatively charged ions form by fast atom bombardment (FAB).[16] Matrix-assisted laser desorption ionization/time-of-flight (MALDI/TOF) and FAB MS of these complexes reveal information such as cysteine residue positions[38, 39] and the effects of aromatic side chain involvement in directing fragmentation.[40]

Cassady and coworkers[19] found that ionic Cr-peptide complexes demonstrate significantly less fragmentation by CID than protonated peptides. These peptides contained highly acidic residues. Cr(III) is thought to bind tightly through multiple carboxylate or carbonyl groups preventing facile backbone cleavage. Fragmentation of

these complexes generated exclusively metallated product ions, as well as extensive carbon monoxide (CO) loss from both the precursor and metallated y-series ions.

The formation of metal ion-polyalanine, $(Ala)_n$, complexes (Met = Li, Na, K, Rb, Cs, Mg, Ca, Sr, and Ba) by ESI was investigated by Kohtani et al.[41] They observed the coordination of mono- and di-valent metals to $(Ala)_n$ for n = 14-25. This number of alanine residues results in a helical conformation leaving only the dangling C-terminus available for metal ion coordination. These researchers also reported that the trivalent metals, In(III), Sc(III), and Y(III), did not form complexes with polyalanines.

In the present study, the effects of several first row transition metals on CID are explored for peptides with no steric hindrances or acidic or basic side chains that might influence dissociation. Because the side chain of alanine is a methyl group, which should not serve as a ligand in metal binding, metal coordination to polyalanine is thought to occur through the backbone amide groups and possibly the termini. The focus is on gaining insight into the gas-phase chemistry of transition metal-cationized peptides and understanding how specific transition metal ions affect dissociation of the peptide backbone.

3.2 Experimental

3.2.1 Preparation of Transition Metal-Peptide Complexes

Peptides were synthesized using an Advanced Chemtech (Louisville, KY, USA) model 90 synthesizer according to the standard Fmoc solid phase synthesis protocols.[42] The peptide synthesis procedure is discussed in Chapter 2. The peptides studied were AAAAAAA, AAAAAA, AAAAA, AAGGAAA, GGAAAAA, AAAAAGA, AAA-OMe,

AAAAAAA-OMe, and ^{13}C-labeled AAAAAAA (labeled at the side chains of the first and sixth residues from the N-terminus) as shown in Figure 3.1. Each peptide was prepared as a 2 mM solution in methanol/water at 1:1 volume:volume ratio. Metal solutions were prepared by dissolving the chloride salts of Cr(III), Fe(II), Fe(III), Co(II), Ni(II), Cu(I), and Cu(II) in water to bring the final metal salt concentration to 0.5 M. Transition metal-peptide complexes were formed by adding a few microliters of metal solution to 1 mL of peptide solution to yield a metal to peptide mole ratio of 25:1. Solutions for ESI were 5-10 μM in peptide and were prepared in acetonitrile (ACN):water at a 1:1 volume:volume ratio.

Methyl esterification of the C-terminus of trialanine (AAA) and heptaalanine (AAAAAAA) was accomplished by mixing 69 μL of dry methanol, 5 μL of acetic anhydride, and 6 μL of 12 M hydrochloric acid for five minutes and then adding 1.2 mg of crystalline peptide (Figure 2.20). The mixture was stirred for two hours, followed by 24 hours of refrigerated incubation.[43]

3.2.2 Mass Spectrometry

The mass spectra of positively charged transition metal-peptide complexes were acquired with a Bruker (Billerica, MA, USA) HCTultra PTM Discovery System. The mass spectrometer is discussed in Chapter 2. Samples were ionized with ESI and on-line nanoESI. In order to minimize sodium and potassium ion contamination, the nanoESI transfer lines were equilibrated with approximately 50 μL of the appropriate metal salt solutions (in ACN:H_2O) before sample introduction. The ESI capillary voltage was adjusted from -2500 to -3000 V to maintain a capillary current of approximately 20 nA

(a)

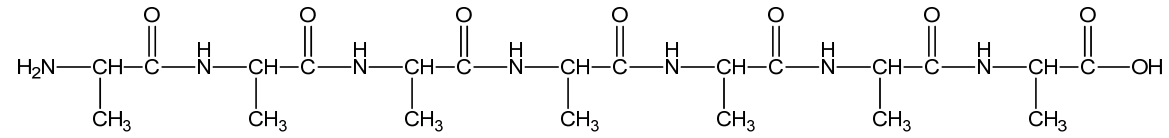

(b)

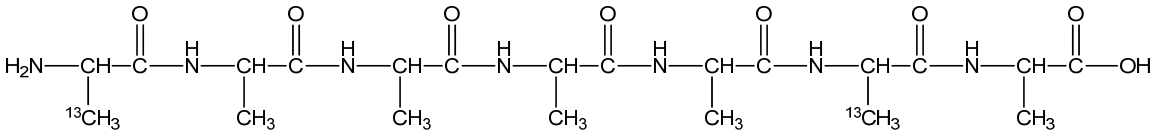

(c)

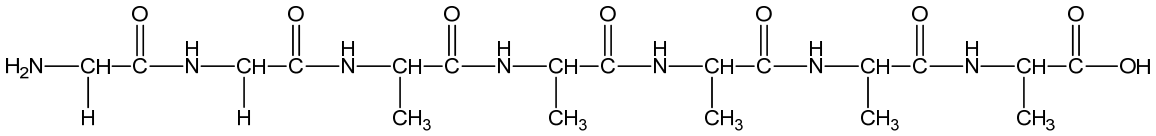

(d)

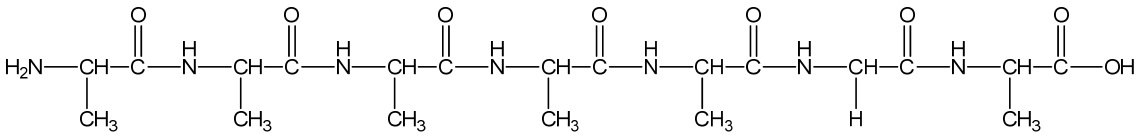

Figure 3.1. Structures of some of the heptapeptides studied in this chapter including (a) heptaalanine, (b) ^{13}C-labeled heptaalanine, (c) GGAAAAA, and (d) AAAAAGA.

with ESI flow rates ranging from 125-175 μL/h. Drying gas temperatures were optimized between 220-250 °C. A syringe pump connected to fused silica transfer tubing (360 μm x 50 μm) and emitters (360 μm x 75 μm x 15 μm) were used to introduce sample by nanoESI. NanoESI emitters were purchased from New Objective (Woburn, MA, USA). NanoESI conditions were optimized with flow rates of 5-20 μL/h. No nebulizer gas was used with nanoESI; however, nitrogen was used as the drying gas. For nanoESI, drying gas temperatures were 120-150 °C, and flow rates ranged from 3 to 10 L/min. The capillary voltage was adjusted between -1200 and -2000 V so that the capillary and end plate offsets gave a needle current of approximately 15 nA.

All mass spectra were acquired in the positive ion mode. CID experiments were performed in helium gas with a 30% to 200% collision energy sweep and amplitudes of 0.8 to 1.2 V. The high capacity trap was filled with the optimum number of ions (approximately 200,000) during an accumulation time of approximately 200 ms. Precursor ion isolation widths were adjusted from 1.0 to 4.0 *m/z* to allow maximum intensity while excluding nearby ions. The lowest *m/z* scanned for CID product ions was 50 *m/z*. Spectra shown are typically averages of 100 to 200 scans.

3.2.3 UV-visible Spectroscopy

Optical absorption spectra in the range of 190 to 800 nm were obtained with a DU-800 UV-vis spectrophotometer (Beckman Coulter, Inc, Fullerton, CA, USA). All samples studied by UV-visible spectroscopy were dissolved in the ESI solvent (ACN/H_2O). Samples examined include $CuCl_2$, glycine, $CuCl_2$ mixed with glycine, $CuCl_2$ mixed with L-alanine, and $CuCl_2$ mixed with heptaalanine.

3.2.4 Reagents

HPLC grade acetonitrile, acetic anhydride, hydrochloric acid, and HPLC grade methanol were purchased from Fisher Scientific (Hampton, NH, USA). Water was purified with a Barnstead (Dubuque, IA, USA) water purification system. Transition metal chlorides were obtained from various sources and used without further purification: $FeCl_3 \bullet 6\ H_2O$, $NiCl_2 \bullet 6\ H_2O$ (Sigma Aldrich, St. Louis, MO, USA), $FeCl_2 \bullet 4\ H_2O$ (Acros Organics, Liège Area, Belgium), CuCl (B & A, Morristown, NJ, USA), $CuCl_2$ (Johnson Matthey, Malvern, PA, USA), $CoCl_2 \bullet 6\ H_2O$ (J. T. Baker, Phillipsburg, NJ, USA), and $CrCl_3 \bullet 6\ H_2O$ (Fisher Scientific, Hampton, NH, USA). Peptide synthesis reagents were obtained from Advanced ChemTech (Louisville, KY, USA) and AnaSpec (Fremont, Ca, USA) and were Fmoc-Ala-OH $\bullet\ H_2O$, Fmoc-Gly-OH, Fmoc-Ala Wang resin, Fmoc-Ala-OH (3-^{13}C) , N-hydroxybenzotrizole, 1, 3-diisopropyl carbodiimide, piperidine, N-methyl-2-pyrrolidone, triisopropyl silane, and trifluoracetic acid.

3.3 Results and Discussion

The current study involved penta-, hexa-, and heptaalanines. The three peptides behaved in a similar manner. Therefore, throughout this manuscript the focus will be on heptaalanine. Product ions formed from CID on complexes of transition metal ions complexed with heptaalanine are summarized in Table 3.1, and a more expanded summary, including ion abundances, is included in Table 3.2. For comparison purposes, Table 3.1 also includes CID products for protonated and deprotonated heptaalanine. The peptide cleavage symbolism (a, b, c, and y) used in this manuscript refers only to the

Table 3.1. CID products formed from transition metal-cationized heptaalanine (M = AAAAAAA) where z is the charge on the product ion.

		CID Product Ions	
Salt	**Precursor Ion**	**z = 1+**	**z = 2+**
$CrCl_3$• 6H_2O	**$[M+Cr-H]^{2+}$**	a_5+Cr-H, a_6+Cr-H, a_6+Cr-3H, c_5+Cr, c_6+Cr, c_4+Cr-H	a_6+Cr-2H, a_7+Cr-2H, b_6+Cr-2H, b_7+Cr-2H, c_6+Cr+H, y_3, y_5
$FeCl_3$•6 H_2O	**$[M+Fe-H]^{2+}$**	a_4, a_3-NH_3, a_4-NH_3, b_2, b_3, b_2+Fe-2H, c_6+Fe+H	a_6+Fe-H, a_7+Fe-H, b_7+Fe, c_6+Fe
$FeCl_2$•4 H_2O	**$[M+Fe-H]^{+}$**	a_4+Fe-2H, a_5+Fe-2H, a_6+Fe-2H, a_7+Fe-2H, a_4+Fe-2H-NH_3, a_5+Fe-2H-NH_3, b_4+Fe-2H, b_5+Fe-2H, b_6+Fe-2H, b_7+Fe-2H, b_6+Fe-2H-17, b_7+Fe-2H-17, b_7+Fe-2H-NH_3&H_2O, c_5+Fe+H, c_6+Fe+H, c_4+Fe, x_3, x_4	
$FeCl_2$•4 H_2O	**$[M+Fe]^{2+}$**	a_2, a_4, a_3-NH_3, b_2, b_3+Fe-2H, c_4+Fe+H, c_5+Fe+H, c_6+Fe+H, c_5+Fe+H-H_2O	a_6+Fe-H, a_7+Fe-H, b_6+Fe-H, b_7+Fe-H
$CoCl_2$•6 H_2O	**$[M+Co]^{2+}$**	a_4+Co-2H, a_5+Co-2H, a_6+Co-2H, b_4+Co-2H, b_5+Co-2H, b_6+Co-2H, c_4+Co+H, c_5+Co+H, c_6+Co+H	a_5+Co-H, a_6+Co-H, a_7+Co-H, b_6+Co-H, b_5+Co-H, b_7+Co-H, b_7+Co-2H-17, c_6+Co
$NiCl_2$•6 H_2O	**$[M+Ni]^{2+}$**	a_2, a_4, a_4+Ni-2H, a_5+Ni-2H, b_4+Ni-2H, b_5+Ni-2H, b_6+Ni-2H, y_7, y_3+Ni, y_2+Ni-H	a_6+Ni-H, b_6+Ni-H, c_5+Ni
$CuCl_2$	**$[M+Cu-H]^{+}$**	a_4+Cu, a_5+Cu, a_6+Cu, a_7+Cu, b_4+Cu-2H, b_5+Cu-2H, b_6+Cu-2H, c_3+Cu+H, c_4+Cu+H, c_5+Cu+H	
$CuCl_2$	**$[M+Cu]^{2+}$**	a_2, a_2+Cu, a_4+Cu, a_5+Cu, a_6+Cu, b_2, b_4+Cu-2H, b_5+Cu-2H, b_6+Cu-2H, c_4+Cu+H, c_5+Cu+H, y_2	b_5+Cu-H, b_6+Cu-H, b_7+Cu-H
		z = 1+	**z = 1-**
CH_3COOH	**$[M+H]^{+}$**	a_4, a_5, a_6, a_7, a_3-NH_3, a_4-NH_3, a_5-NH_3, a_6-NH_3 a_7-NH_3, b_3, b_4, b_5, b_6, b_7, b_6-H_2O, b_7-H_2O	
NH_4OH	**$[M-H]^{-}$**		a_4, a_5, b_6-2H, b_7-2H, c_2, c_3, c_4, c_5, c_3-H_2O, c_4-H_2O, y_4, y_5, y_6

Table 3.2. Transition metal cationized heptaalanine (AAAAAAA) products formed by CID.

Cr(III)					***[M+Cr-H]*$^{2+}$ [a]**			
	charge	**A , n=1**	**A , n=2**	**A , n=3**	**A , n=4**	**A , n=5**	**A , n=6**	**A , n=7**
a_n+Cr-H	1					w[b]	w	
a_n+Cr-2H	2						s	s
a_n+Cr-3H	1						w	
b_n+Cr-2H	2						w	m
c_n+Cr+H	2						w	
c_n+Cr	1					m	w	
c_n+Cr-H	1				w			
y(8-n)	2			m		w		
neutral loss:	s, $[M+Cr-H-CO]^{2+}$							
	m, $[M+Cr-H-H_2O]^{2+}$							

Fe(III)					***[M+Fe-H]*$^{2+}$**			
	charge	**A , n=1**	**A , n=2**	**A , n=3**	**A , n=4**	**A , n=5**	**A , n=6**	**A , n=7**
a_n	1				s			
a_n-NH_3	1			w	m			
a_n+Fe-H	2						w	w
b_n	1		w	s				
b_n+Fe	2							w
b_n+Fe-2H	1		w					
c_n+Fe+H	1						w	
c_n+Fe	2						w	

Fe(II)					***[M+Fe-H]*$^{+}$**			
	charge	**A , n=1**	**A , n=2**	**A , n=3**	**A , n=4**	**A , n=5**	**A , n=6**	**A , n=7**
a_n+Fe-2H	1				w	w	s	w
a_n+Fe-2H-NH_3	1				w	w		
b_n+Fe-2H	1				w	m	m	m
b_n+Fe-2H-17	1						w	s
b_n+Fe-2H-17-H_2O	1							w
c_n+Fe+H	1					s	w	
c_n+Fe	1				w			
$x_{(8-n)}$	1				w	w		

Table 3.2 Continued

Fe(II)					*[M+Fe]$^{2+}$*			
	charge	**A , n=1**	**A , n=2**	**A , n=3**	**A , n=4**	**A , n=5**	**A , n=6**	**A , n=7**
a_n	1		w[a]		m			
a_n-NH_3	1			w				
a_n+Fe-H	2						s	w
b_n	1		w					
b_n+Fe-H	2						w	w
b_n+Fe-2H	1			w				
c_n+Fe+H	1				w	w	w	
c_n+Fe+H-H_2O	1					w		

Co(II)					*[M+Co]$^{2+}$*			
	charge	**A , n=1**	**A , n=2**	**A , n=3**	**A , n=4**	**A , n=5**	**A , n=6**	**A , n=7**
a_n+Co-2H	1				w	w	w	
a_n+Co-H	2					w	s	w
b_n+Co-2H	1				w	w	w	
b_n+Co-H	2						w	w
b_n+Co-2H-17	2							w
c_n+Co+H	1				w		w	
c_n+Co	2						w	

Ni(II)					*[M+Ni]$^{2+}$*			
	charge	**A , n=1**	**A , n=2**	**A , n=3**	**A , n=4**	**A , n=5**	**A , n=6**	**A , n=7**
a_n	1		w		**w**			
a_n+Ni-2H	1				w	w		
a_n+Ni-H	2						s	
b_n+Ni-2H	1				w	w	w	
b_n+Ni-H	2						s	
c_n+Ni	2					w		
$y_{(8-n)}$	1							w
$y_{(8-n)}$+Ni	1			w				
$y_{(8-n)}$+Ni-H	1		w					

Table 3.2 Continued

Cu(II)					***[M+Cu-H]$^+$***			
	charge	**A , n=1**	**A , n=2**	**A , n=3**	**A , n=4**	**A , n=5**	**A , n=6**	**A , n=7**
a_n+Cu	1				w	w	s	s
b_n+Cu-2H	1				w	w	m	
c_n+Cu+H	1			w	w	w		

Cu(II)					***[M+Cu]$^{2+}$***			
	charge	**A , n=1**	**A , n=2**	**A , n=3**	**A , n=4**	**A , n=5**	**A , n=6**	**A , n=7**
a_n	1		w					
a_n+Cu	1		w		w	m	w	
b_n	1		w					
b_n+Cu-2H	1				w	w	s	
b_n+Cu-H	2					w	s	w
c_n+Cu+H	1				w	w		
$y_{(8-n)}$	1						w	

[a] Precursor ion.

[b] Relative intensities where w is weak (<30%), m is medium (30-59%), and s is strong > 60%.

cleavage sites along the peptide backbone (following original Roepstorff and Fohlman nomenclature[44]). Any loss or addition of hydrogen from these fragments is specifically noted; e.g., positive mode protonated y-ions will be referred to as $[y_n + 2H]^+$. This is done to keep track of hydrogen atoms because a varying number may be displaced by the metal ions.

When product ion assignment was ambiguous, heptapeptides were studied in which glycine residues (57 Da), or ^{13}C-labeled alanine residues (72 Da) were substituted for alanine residues (71 Da). CID of the peptides AAAAAGA, AAGGAAA, GGAAAAA, and ^{13}C-labeled AAAAAAA mixed with the transition metal salts produced the same types of product ions as those formed with heptaalanine. The product ions formed from CID on complexes of transition metal ions complexed with ^{13}C-labeled heptaalanine and AAAAAGA are summarized in Tables 3.3 and 3.4.

3.3.1 CID of Protonated and Deprotonated Polyalanines

Polyalanines were examined to determine how peptides with no sterically hindered or acidic or basic side chains dissociate in the gas phase prior to metal coordination. Protonated, $[M + H]^+$, and deprotonated, $[M - H]^-$, polyalanines were isolated and submitted to CID.

Protonated heptaalanine, $[M + H]^+$, dissociates to yield primarily members of the b- and a-ion series as shown in Figure 3.2a. The base peak is b_6^+, followed in intensity by b_5^+. Other ions are formed at less than 30% relative intensity (RI) and include a_n^+, n = 4-7; $[a_n - NH_3]^+$, n = 3-7; b_n^+, n = 3-7; $[b_n - H_2O]^+$, n = 5-7; and $[y_n + 2H]^+$, n = 4-5.

Table 3.3. Products obtained by CID of transition metal-cationized ^{13}C-labeled heptaalanine.

Cr(III)					***[M+Cr-H]*$^{2+}$** [b]			
	charge	***A, n=1**	**A, n=2**	**A, n=3**	**A, n=4**	**A, n=5**	***A, n=6**	**A, n=7**
a_n	1		w[c]	m				
a_n+Cr	2					m		
a_n+Cr-H	1					w		
a_n+Cr-2H	2						s	s
a_n+Cr-2H	1						w	
b_n	1		w					
b_n+Cr-H	2						w	
b_n+Cr-2H	1					w	w	
c_n+Cr	1				w	w	w	
$y_{(8-n)}$	1						w	w
neutral loss:	s, $[M+Cr-H-CO]^{2+}$ m, $[M+Cr-H-H_2O]^{2+}$							

Fe(II)					***[M+Fe]*$^{2+}$**			
	charge	***A, n=1**	**A, n=2**	**A, n=3**	**A, n=4**	**A, n=5**	***A, n=6**	**A, n=7**
a_n	1		w					
a_n+Fe-H	2						s	w
b_n	1		w					
b_n+Fe-H	2						w	
b_n+Fe-2H	1					w	w	
c_n+Fe+H	1					w	w	
$y_{(8-n)}$+Fe	2					w		

Table 3.3 Continued

Co(II)					$[M+Co]^{2+}$			
	charge	***A, n=1**	**A, n=2**	**A, n=3**	**A, n=4**	**A, n=5**	***A, n=6**	**A, n=7**
a_n+Co-2H	1				w	w	w	
a_n+Co-H	2					w	s	w
b_n+Co-2H	1				w	w	w	
b_n+Co-H	2						w	
c_n+Co+H	1					w	w	
neutral loss: m, $[M+Co-H-H_2O]^{2+}$								

Ni(II)					$[M+Ni]^{2+}$			
	charge	***A, n=1**	**A, n=2**	**A, n=3**	**A, n=4**	**A, n=5**	***A, n=6**	**A, n=7**
a_n	1		w		w			
a_n-NH_3	1			w				
a_n+Ni-2H	1				w	w		
a_n+Ni-H	2						m	w
b_n	1		w					
b_n+Ni-2H	1				w	w	w	
b_n+Ni-H	2						m	
c_n+Ni	2					w		
c_n+Ni+H	1					w	w	
$y_{(8-n)}$	1							w
$y_{(8-n)}$+Ni-H	1		w					

Table 3.3 Continued

Cu(II)					$[M+Cu]^{2+}$			
	charge	***A, n=1**	**A, n=2**	**A, n=3**	**A, n=4**	**A, n=5**	***A, n=6**	**A, n=7**
$\mathbf{a_n}$	1		w					
$\mathbf{a_n}$**+Cu**	1				w	m	w	
$\mathbf{a_n}$**+Cu**	2		w			w		s
$\mathbf{a_n}$**+Cu-H**	2						m	
$\mathbf{b_n}$	1		w					
$\mathbf{b_n}$**+Cu-2H**	1				w	w	m	
$\mathbf{b_n}$**+Cu-H**	2						m	
$\mathbf{c_n}$**+Cu+H**	1					w	w	
$\mathbf{y_{(8-n)}}$	1							w

[a] Where * indicates residues containing ^{13}C side chains.

[b] Precursor ion.

[c] Where relative intensities 1-29 %, 30-59 %, and 60-100 % are indicated by w, m, and s respectively.

Table 3.4. Products formed by CID of transition metal-cationized AAAAAGA.

CID		*[M+Cr-H]$^{2+}$*						
	charge	**A, n=1**	**A, n=2**	**A, n=3**	**A, n=4**	**A, n=5**	**G, n=6**	**A, n=7**
a_n^+	1		w[a]					
a_n+Cr	2						m	
a_n+Cr-2H	2							s
a_n+Cr-14	2							
a_n+Cr-2H-H_2O	2							
a_n+Cr-3H	1						w	
a_n+Cr-H	1						w	
b_n+Cr-2H	2						w	s
c_n+Cr-H	2					s		
c_n+Cr-2H	1				w	w		
c_n+Cr-3H	1							
y(8-n)+Cr-2/3H	1		w	w				
$y_{(8-n)}$+Cr-2H	2		w					
$y_{(8-n)}$	1						w	
also: $[M+Cr-Co]^{2+}$	s							

CID		*[M+Fe]$^{2+}$*						
	charge	**A, n=1**	**A, n=2**	**A, n=3**	**A, n=4**	**A, n=5**	**G, n=6**	**A, n=7**
a_n	1							
a_n+Fe							w	
a_n+Fe-H	2						s	w
b_n	1							
b_n+Fe-H	2						w	w
b_n+Fe-2H							w	
c_n+Fe+2H	2							
c_n+Fe+H	1					w	w	
c_n+Fe+H-H_2O	1							

Table 3.4 continued.

CID				*[M+Co]$^{2+}$*				
	charge	**A, n=1**	**A, n=2**	**A, n=3**	**A, n=4**	**A, n=5**	**G, n=6**	**A, n=7**
a_n+Co-2H	1				w	w		
a_n+Co	1						w	
a_n+Co-H	2					w	s	m
b_n+Co-2H	1						w	
b_n+Co-H	2						s	
c_n+Co+H	1				w		s	
c_n+Co	1					w		
[$y_{(8-n)}$+Co-2H]	1			w	w			

CID				*[M+Ni]$^{2+}$*				
	charge	**A, n=1**	**A, n=2**	**A, n=3**	**A, n=4**	**A, n=5**	**G, n=6**	**A, n=7**
a_n			w					
a_n+Ni	1				w	w		
a_n+Ni-H	2						s	w
b_n+Ni-2H	1				w	w	w	
b_n+Ni-H	1							
b_n+Ni-H	2						s	w
c_n+Ni+H	1						w	
c_n+Ni+2H	2						w	
$y_{(8-n)}^{+}$	1							w
$y_{(8-n)}$+Ni-2H	1			w	w			

Table 3.4 continued.

CID		*[M+Cu]$^{2+}$*						
	charge	**A, n=1**	**A, n=2**	**A, n=3**	**A, n=4**	**A, n=5**	**G, n=6**	**A, n=7**
a_n+	1		m					
a_n+Cu	1						w	
a_n+Cu-H	2						w	s
a_n+Cu-H	1		w					
a_n+Cu-Ala	1						s	
a_n+Cu-2Ala	1						w	
a_n+Cu-Ala-Gly	1						w	
b_n	1		m					
b_n+Cu-2H	1				w	w	w	
b_n+Cu-H	2						s	
c_n+Cu+H	1					w	w	
$y_{(8-n)}^+$	1							w
$y_{(8-n)}$+Cu-2H	1			w				

[a] Relative intensities 0-29%, 30-59%, and 60-100% are indicated by w, m, and s respectively.

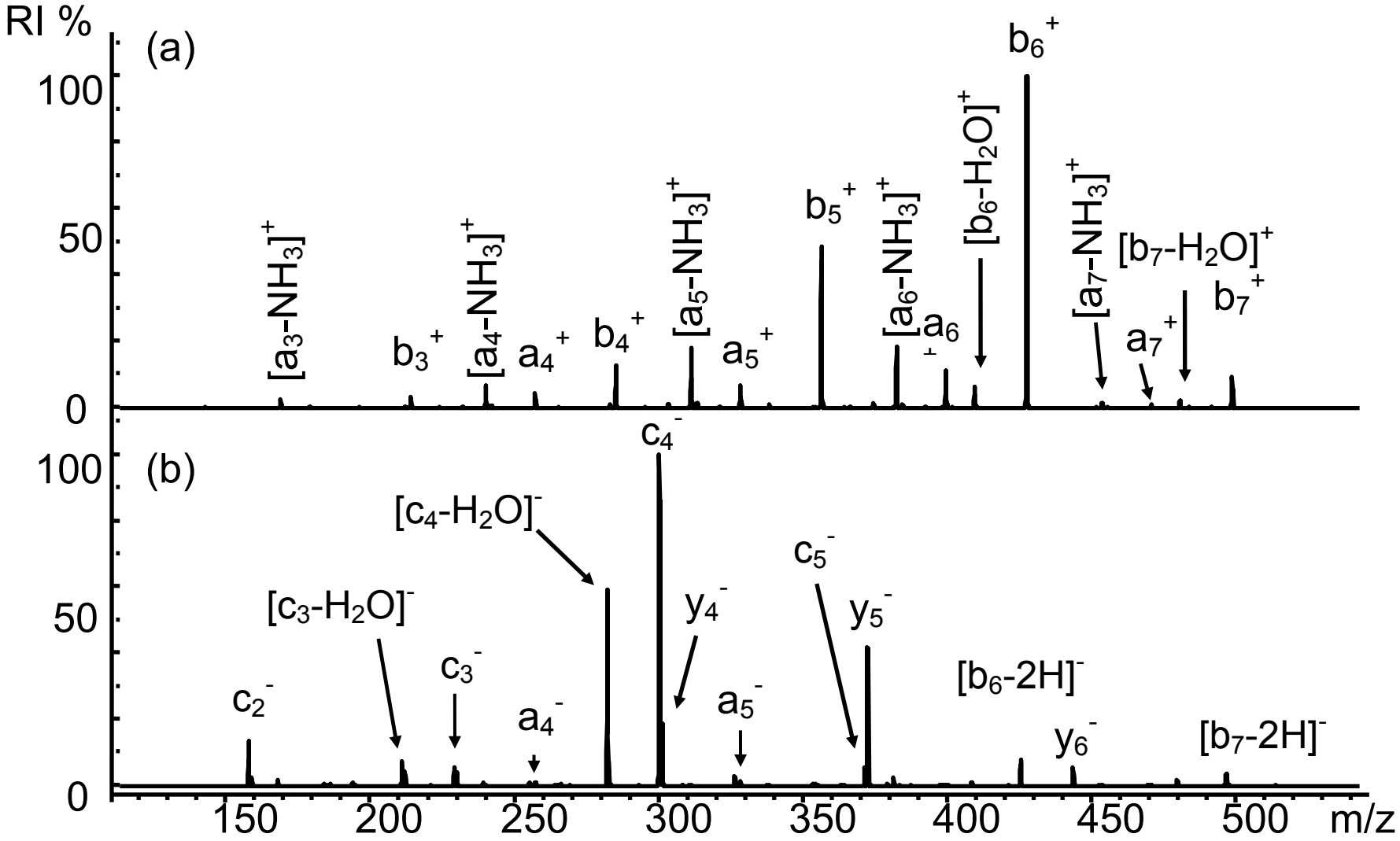

Figure 3.2. Low-energy CID spectra obtained from (a) protonated, $[M + H]^+$, and (b) deprotonated, $[M - H]^-$, heptaalanine.

The a-ion intensities are always less than that of the corresponding b-ions. These a-ions subsequently lose NH_3.

Metal coordination to peptides can displace one or more protons resulting in complexes that may behave more like $[M - H]^-$ than $[M + H]^+$. For comparison, a CID spectrum was obtained from deprotonated heptaalanine, $[M - H]^-$, and is shown in Figure 3.2b. The base peak is c_4^-; water loss from this ion is the second most intense peak. A prominent y_5^- forms, as well as c_n^-, n = 2-4, which result from cleavages of the distal amide bonds with no added or displaced hydrogens. Also, a_n^-, n = 4-5; b_n^-, n = 6-7; and y_n^-, n = 2-6, are present in lower intensities.

3.3.2 CID of Cr(III) bound to Heptaalanine

Mixtures of Cr(III) and polyalanines produce $[M + Cr - H]^{2+}$ by ESI for penta- through heptaalanine. A small amount of triply charged ions formed with heptaalanine as $[M + Cr]^{3+}$; its low intensity prevented further study.

As shown in Figure 3.3, CID of $[M + Cr - H]^{2+}$ yields a complex spectrum containing a mixture of doubly and singly charged products. The spectrum is the most difficult to interpret compared to those from the other species under study, and numerous peaks are unassigned. The precursor ion loses small neutrals to form $[M + Cr - CO]^{2+}$ and $[M + Cr - H_2O]^{2+}$ at approximately 75 and 35 % relative intensity, respectively. This is similar to loss of CO and water that was observed in the dissociation of Cr-bound acidic peptides by Cassady and coworkers.[19] They proposed that CO loss originated from side-chain or C-terminal carboxylic acid groups coordinated to Cr(III). The most intense product ion is $[a_7 + Cr - 2H]^{2+}$, which is due to loss of both CO and H_2O (loss of 46 Da)

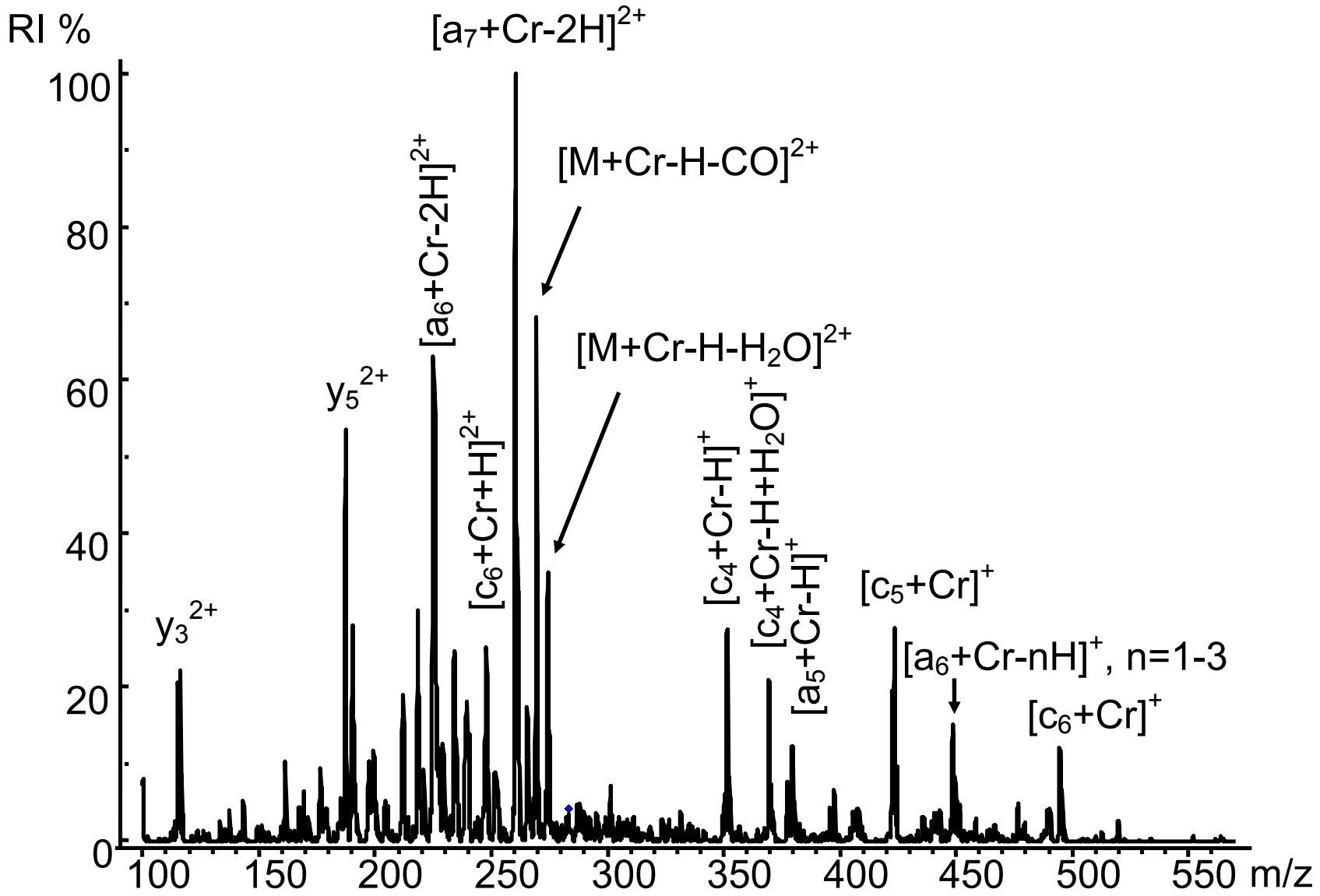

Figure 3.3. Low-energy CID spectrum obtained from $[M + Cr - H]^{2+}$, produced by a mixture of heptaalanine and $CrCl_3$.

from the precursor. This has also been reported by Lavanant and Hoppilliard from studies involving Cu(I) and Cu(II) cationized arginine- and lysine- containing dipeptides.[45]

All a-ions in the spectrum are coordinated to Cr; some with no deprotonation while others lose up to three hydrogens. Cr-complexed a-ions are the most intense of the doubly charged products, whereas the metallated c-ions are the most intense singly charged products. A series of $[a_6 + Cr - nH]^+$, n = 0-3, forms. In contrast, b-ions only appear as doubly charged products and only with elimination of two hydrogens, $[b_n + Cr - 2H]^{2+}$. Metallated c-ions form as $[c_n + Cr + H]^{2+}$and $[c_n + Cr]^+$, n = 5-6, and as $[c_4 + Cr - H]^+$.

While most of the product ions are metallated, abundant y_3^{2+} and y_5^{2+} also form. This mixture of metallated and non-metallated products could hinder sequencing because no clear indication is present as to whether a product ion contains Cr. This is because Cr has only one major isotope. Of all of the transition metal ions studied here, the data suggests that Cr(III) is the least suitable for peptide sequencing.

The addition of chromium(III) chloride to the peptide solutions also has an interesting effect on the ESI spectra. Not only are Cr(III)-peptide adduct ions produced, but protonation is enhanced. For example, doubly protonated heptaalanine ions, $[M + 2H]^{2+}$, are formed in sufficient intensity for MS/MS analysis in the presence of Cr(III); in contrast, addition of acetic acid to the solution does not produce sufficient $[M + 2H]^{2+}$ for study. Cr(III) has an acid dissociation constant, pK_a, of ~3.4 and reacts with water to produce $CrOH^{2+}$ and $H^+(aq)$.[46] Therefore, Cr(III) is more acidic than organic acids such as acetic acid ($pK_a \sim 4.8$) or formic acid ($pK_a \sim 3.7$)[47] that are common

solution additives to enhance protonation by ESI. Numerous other metal ions are also more acidic than organic acids.[46] Consequently, the use of metal salts to promote both metal-adduction and protonation of peptides may be part of a multi-faceted approach to peptide sequencing.

3.3.3 CID of Fe(II) and Fe(III) Bound to Heptaalanine

When heptaalanine is mixed with Fe(II) salts, ESI produces both $[M + Fe - H]^+$ and $[M + Fe]^{2+}$. The formation of these ions indicates that iron remains in the 2+ oxidation state.

Analysis of $[M + Fe - H]^+$ by CID yields primarily metallated N-terminal product ions, as shown in Figure 3.4. For $n \geq 4$, intense members of the a-, b-, and c- series form, which is very useful for sequencing. These ions include $[a_n + Fe - 2H]^+$, n = 4-7; $[b_n + Fe - 2H]^+$, n = 3-7; $[b_n + Fe - 2H - 17]^+$, n = 6-7; $[a_n + Fe - 2H - NH_3]^+$, n = 4-5; $[c_4 + Fe]^+$ and $[c_n + Fe + H]^+$, n = 5-6. No product ions totally dominate the spectrum, reducing relative intensities of other ions; instead, a useful consistency in overall ion abundances exists. This contrasts with the dominance of metallated a-ions produced from the dissociation of $[M + Fe]^{2+}$, which is shown in Figure 3.5. Because $[M + Fe - H]^+$ is singly charged, all product ions are singly charged; this also makes product ion assignments easier. The only drawback to using $[M + Fe - H]^+$ for peptide sequencing is the abundance of CID product ions that include elimination of the small neutrals H_2O or NH_3 (or both). This adds complexity to peak assignment.

For $[M + Fe]^{2+}$ generated by adding Fe(II) to heptaalanine, the CID spectrum has prominent metallated and non-metallated members of the a-, b-, and c-series. The

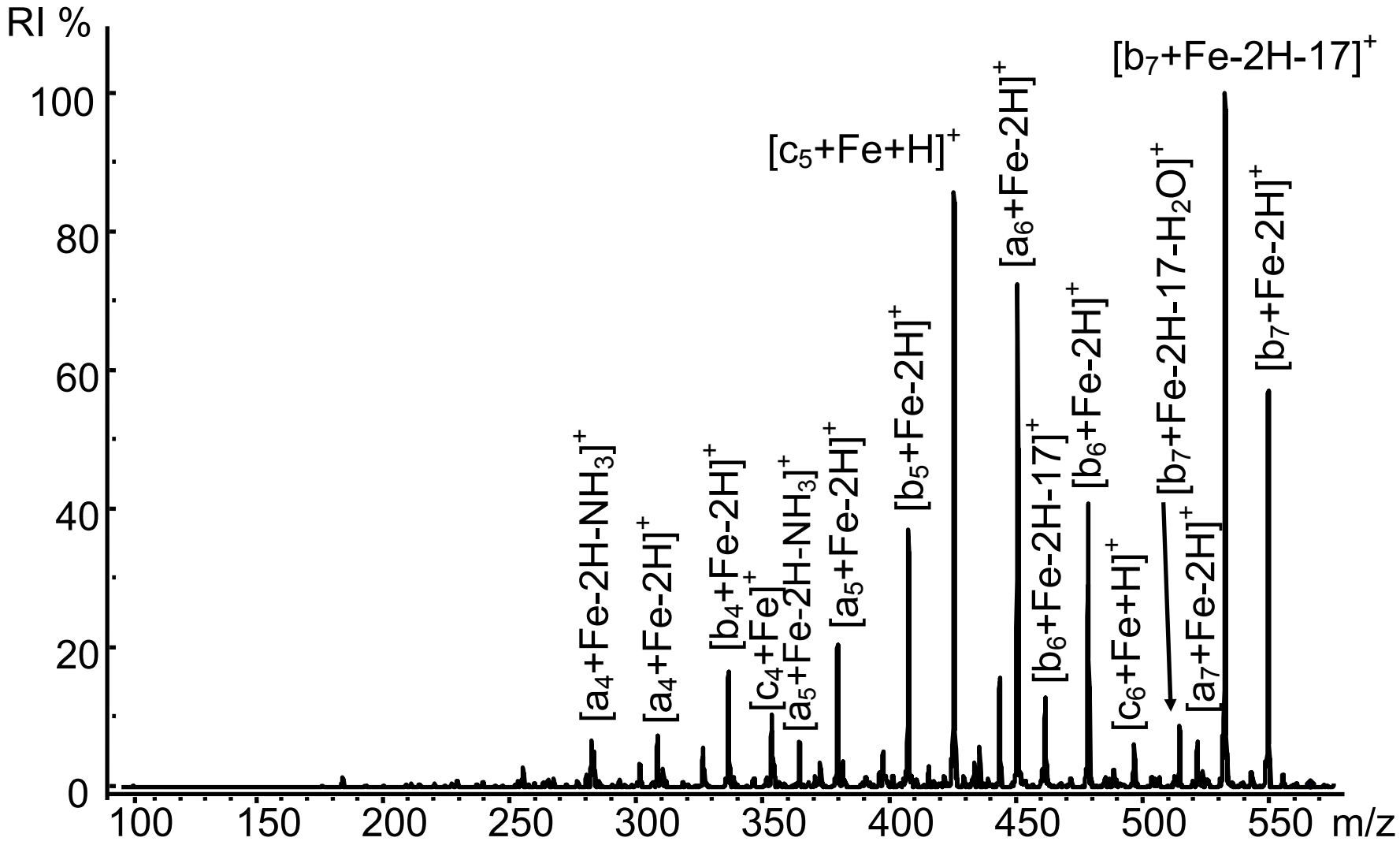

Figure 3.4. Low-energy CID spectrum obtained from $[M + Fe - H]^+$, produced by a mixture of heptaalanine and $FeCl_2$.

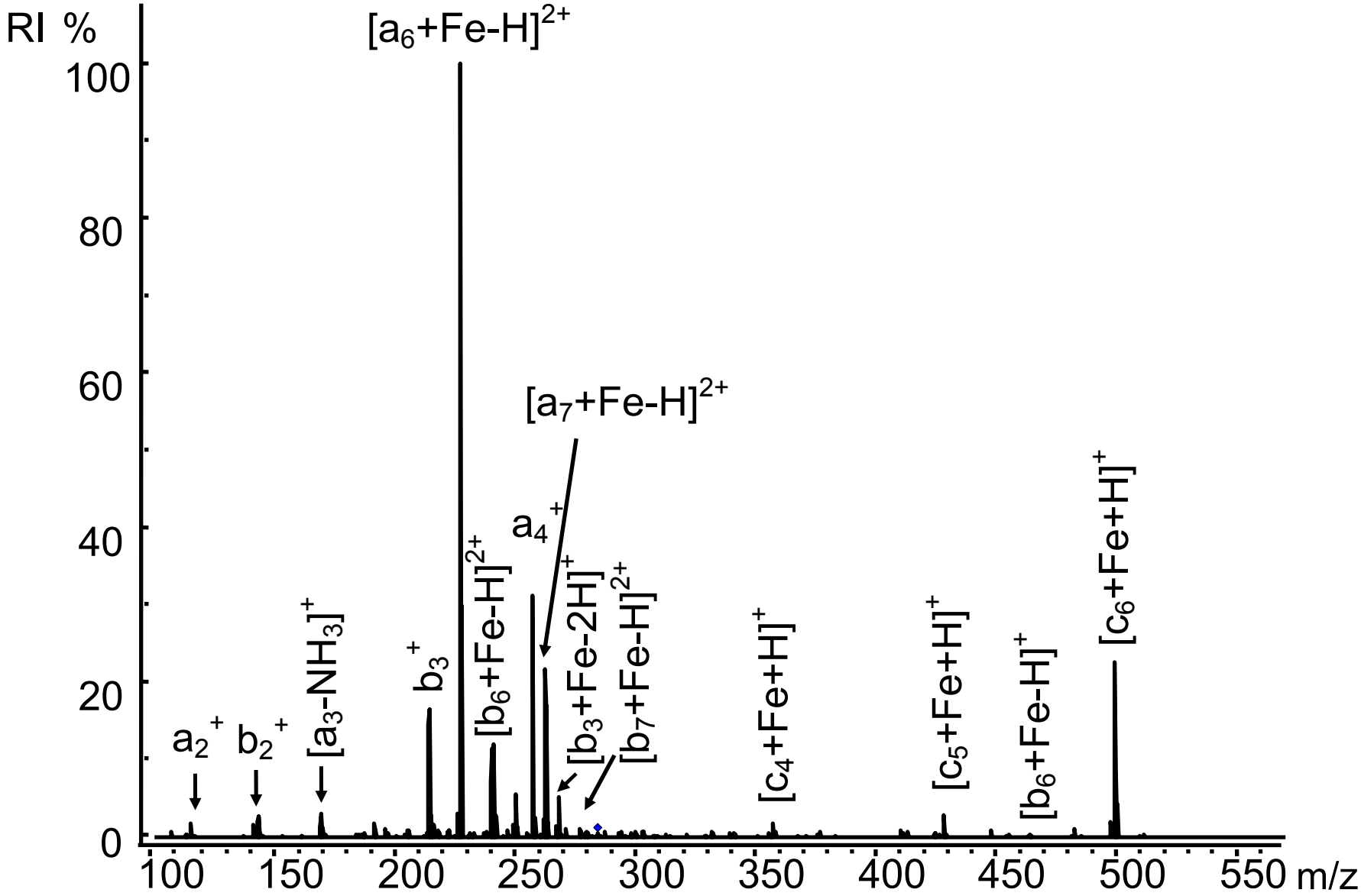

Figure 3.5. Low-energy CID spectrum obtained from $[M + Fe]^{2+}$, produced by a mixture of heptaalanine and $FeCl_2$.

spectrum differs greatly from that of protonated heptaalanine (Figure 3.2a) because the dominant products are $[a_n + Fe - H]^{2+}$ rather than b-ions. The base peak is $[a_6 + Fe - H]^{2+}$, which might be due to elimination of CO from $[b_6 + Fe - H]^{2+}$, as could $[a_7 + Fe - H]^{2+}$ from $[b_7 + Fe - H]^{2+}$. Singly charged metallated products include $[b_n + Fe - H]^+$, n = 3, 6, and $[c_n + Fe + H]^+$, n = 4-6. Several non-metallated products form, including, a_n^+, n = 2-4; $[a_3 - NH_3]^+$ and b_n^+, 2-3, with a_4^+ being relatively intense. The production of both metallated and non-metallated CID products make spectral interpretation more difficult for metals lacking more than one major isotope, as was the case for both Fe and Cr. However, an advantage for the dissociation of $[M + Fe]^{2+}$ is that non-metallated product ions form for n = 2-4, while metallated products occur for n = 4-7. Thus, the combination of products provides greater sequence coverage and includes cleavage throughout the backbone except between residues 1 and 2. Also, unlike $[M + Fe - H]^+$, the spectrum of $[M + Fe]^{2+}$ contains very little neutral loss; this should aid in sequencing. However, like the other doubly charged precursor ions, CID on $[M + Fe]^{2+}$ yields product ions that are both singly and doubly charged. While this does increase spectral complexity, it does not prevent spectral interpretation.

Addition of Fe(III) to polyalanines produces $[M + Fe - H]^{2+}$, which is consistent with the charge on the metal remaining at 3+. CID of $[M + Fe - H]^{2+}$ produces a unique spectrum. Figure 3.6 shows that non-metallated a- and b-series ions dominate and neutral loss is also common. Interestingly, the most prominent product ion is a_4^+, followed by b_3^+, $[a_4 - NH_3]^+$, and $[a_3 - NH_3]^+$. $[M + Fe - H]^{2+}$ is the only metallated heptaalanine studied where the CID spectrum is dominated by non-metallated product ions. Several metallated products do form at lesser intensities. Singly charged products such as

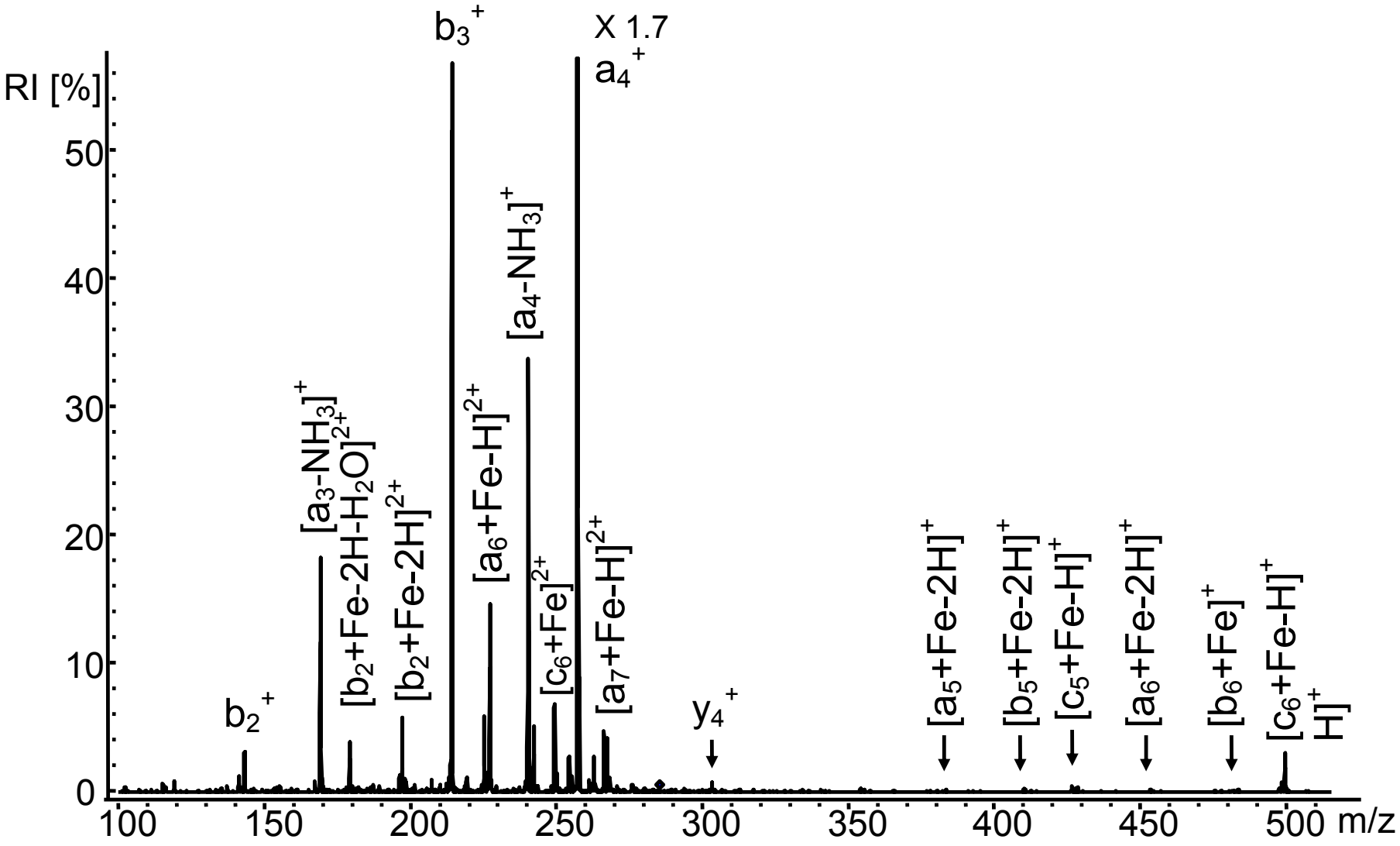

Figure 3.6. Low-energy CID spectrum obtained from $[M + Fe - H]^{2+}$, produced by a mixture of heptaalanine and $FeCl_3$.

$[a_n + Fe - 2H]^+$, n = 5-6; $[b_n + Fe - 2H]^+$, n = 5-6; and $[c_n + Fe + H]^+$, n = 5-6, appear. In addition, doubly charged $[a_n + Fe - H]^{2+}$, n = 6-7, $[b_2 + Fe - 2H]^{2+}$, and $[c_6 + Fe + 2H]^{2+}$ form in similar abundances to the singly charged, metallated product ions.

The most abundant metallated product has a relative intensity of only approximately 12 % relative to the base peak a_4^+. A possible explanation for the low yield of metallated product ions is that Fe(III) may be coordinating to the carboxylic acid group on the C-terminus, which is incorporated in the neutral product that the mass spectrometer does not detect. To confirm the peak assignment of a_4^+, the ion was submitted to CID (MS^3, Figure 3.7) and demonstrates the same dissociation products as a_4^+ generated by CID of the protonated heptaalanine. However, the only other triply charged metal ion studied, Cr(III), does not have this large propensity to form non-metallated products. Also, CID on $[M + Fe - H]^{2+}$ does not provide uniform sequence coverage in terms of ion intensity; for example, all n = 5 product ions are very weak and barely distinguishable from the background noise. Consequently, CID of $[M + Fe - H]^{2+}$ does not appear promising for peptide sequencing.

3.3.4 CID of Co(II) Bound to Heptaalanine

Electrospray on mixtures with Co(II) produces $[M + Co]^{2+}$ for penta- through heptaalanine. A less intense $[M + Co + H]^{3+}$ forms with heptaalanine but not at an intensity suitable for study by CID.

Dissociation of $[M + Co]^{2+}$ produced from heptaalanine yields both singly and doubly charged metallated product ions, as shown in Figure 3.8. The dominant product, $[a_6 + Co - H]^{2+}$, forms 28 Da lower in mass (CO elimination) from the second most

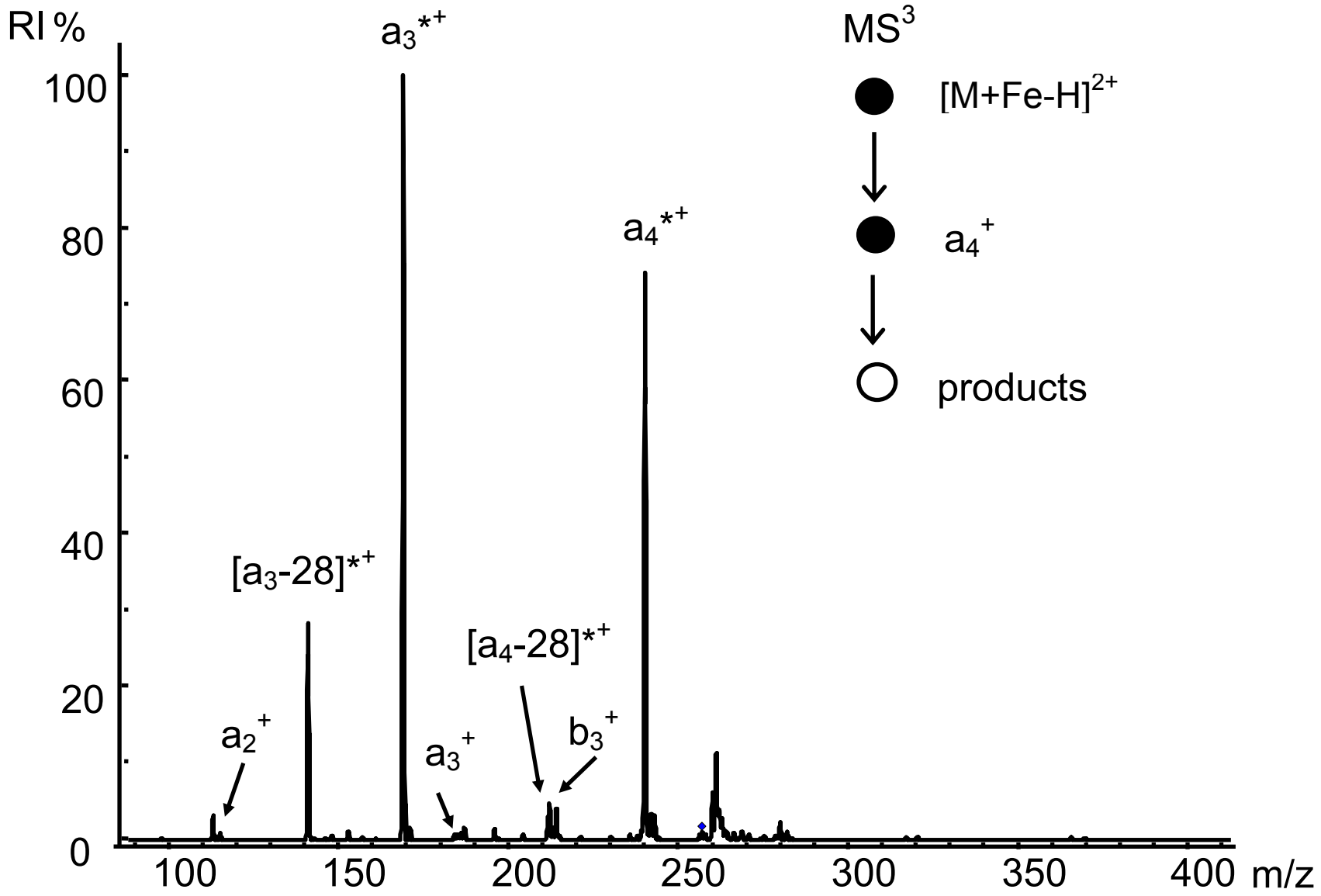

Figure 3.7. Positive MS^3 CID spectrum on a_4^+ product formed from $[M + Fe - H]^{2+}$ for $FeCl_3$ and heptaalanine. Note * refers to loss of NH_3.

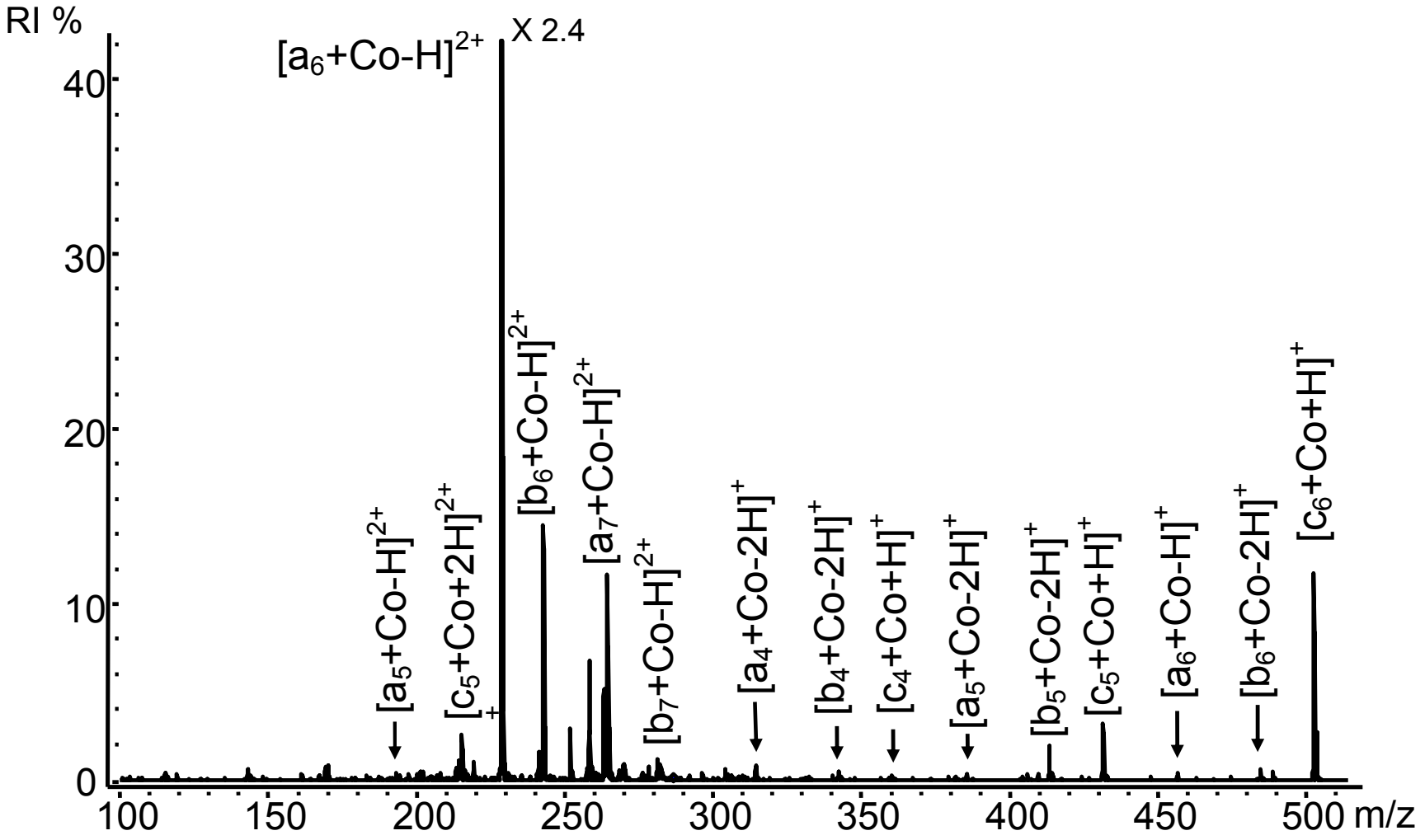

Figure 3.8. Low-energy CID spectrum obtained from $[M + Co]^{2+}$, produced by a mixture of heptaalanine and $CoCl_2$.

intense product, $[b_6 + Co - H]^{2+}$. Doubly charged CID products include $[a_n + Co - H]^{2+}$, n = 5-7; $[b_n + Co - H]^{2+}$, n = 6-7; and $[c_5 + Co + 2H]^{2+}$. Most singly charged products are less than 5% relative intensity. These include $[a_n + Co - 2H]^{+}$, n = 4-6; $[b_n + Co - 2H]^{+}$, n = 4-6; and $[c_n + Co + H]^{+}$, n = 4-6.

Several factors make this spectrum relatively easy to interpret: neutral loss does not occur from any backbone cleavage products, all product ions are metallated, and only one type of a-ion is produced. Less desirable features are the lack of cleavage for n < 4 (limiting the ability to sequence the first four residues of the peptide) and the fact that many of the assigned product ions are of very low intensity because the spectrum is dominated by $[a_6 + Co - H]^{2+}$, which is five times more intense than any other product ion. Also, a mixture of singly and doubly charged product ions, which adds complexity, is present, although in some cases it may also increase the quantity of structurally informative ions.

3.3.5 CID of Ni(II) Bound to Heptaalanine

Ionization of a mixture of Ni(II) and heptaalanine by ESI produces doubly charged $[M + Ni]^{2+}$. The CID spectrum of $[M + Ni]^{2+}$, shown in Figure 3.9, is dominated by $[a_6 + Ni - H]^{2+}$. A medium intensity $[b_6 + Ni - H]^{2+}$ forms 28 Da lower in mass (CO loss). All other product ions are of low intensity and include doubly charged $[c_5 + Ni]^{2+}$ and $[a_7 + Ni]^{2+}$. Singly charged products include $[b_n + Ni - 2H]^{+}$, n = 4-6; $[a_n + Ni - 2H]^{+}$, n = 4-5; $[c_6 + Ni + H]^{+}$; and $[y_n + Ni]^{+}$, n = 5-6. The metallated y-ions are the only C-terminal products and do not have 2 additional hydrogens, $[y_n + 2H]^{+}$, as would be

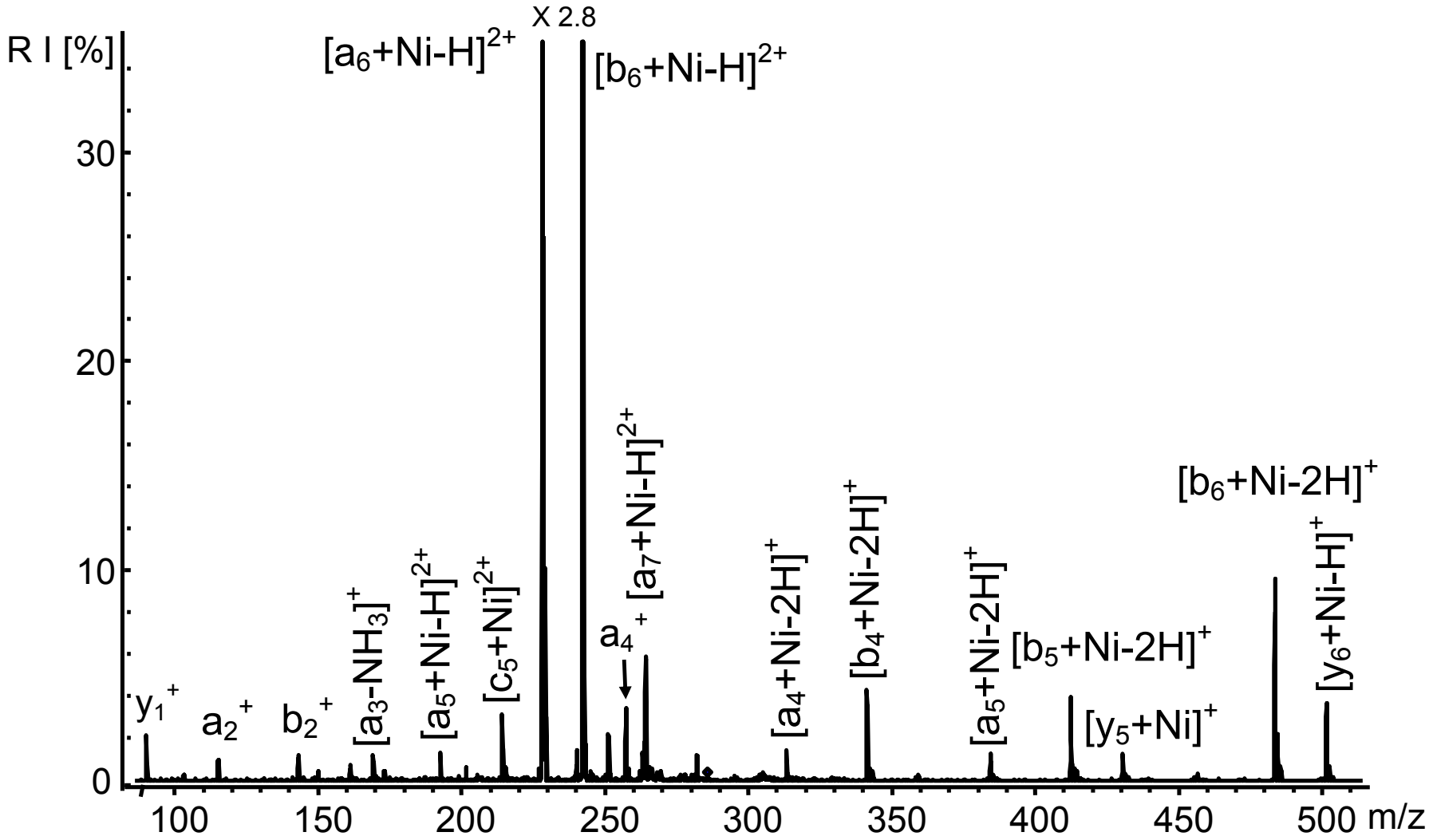

Figure 3.9. Low-energy CID spectrum obtained from $[M + Ni]^{2+}$, produced by a mixture of heptaalanine and $NiCl_2$.

expected with protonated species in positive mode. Non-metallated products include a_n^+, n = 2, 4; $[a_3 - NH_3]^+$, and b_2^+.

The CID spectrum of $[M + Ni]^{2+}$ resembles the spectra of $[M + Fe]^{2+}$ and $[M + Co]^{2+}$. This is not unexpected because these three metals comprise the "iron triad" and are known to have similar chemical and physical properties. Like its Fe- and Co-complexed counter parts, $[M + Ni]^{2+}$ dissociates to yield singly and doubly charged products, the loss of small neutral molecules does not occur, and only one a-series is produced. A unique feature for $[M + Ni]^{2+}$ is the formation of two metallated y-ions, which are the only metallated C-terminal ions observed in this study. Like $[M + Fe]^{2+}$, $[M + Ni]^{2+}$ produces a mixture of metallated and non-metallated products. However, Ni has the advantage of possessing two major isotopes, Ni-58 and Ni-60; this causes metallated products to appear in duplicate, allowing them to be readily distinguished from non-metallated products. Also, as was the case for Fe(II), the combination of these products increases sequence coverage. With Ni(II), non-metallated products form for n = 2-4 and metallated products for n = 4-6.

3.3.6 CID of Cu(I) and Cu(II) Bound to Heptaalanine

Electrospray on heptaalanine mixed with either Cu(I) or Cu(II) produces $[M + Cu]^{2+}$ and $[M + Cu - H]^+$. Nearly identical CID spectra indicate that mixtures of Cu(I) and Cu(II) generate the same ion structures by ESI. That is, Cu(I) is being oxidized to Cu(II). To determine if this is occurring before or after the ESI process, UV-visible absorption spectra were acquired for a series of solutions. Cu(II) from $CuCl_2$ in ACN/H_2O solvent has a d → d transition around 660 nm. In contrast, Cu(I) from CuCl

does not absorb in this region. When Cu(I) is mixed with either glycine, alanine, or heptaalanine, the visible absorption band at 660 nm for Cu(II) appears. Therefore, the presence of these small peptides and amino acids in solution (i.e., not the ESI process) is oxidizing Cu(I) to Cu(II). Consequently, the mass spectra discussed here all involve complexes with Cu(II).

Electrospray on a mixture containing Cu(II) and heptaalanine produces both singly and doubly charged metal-cationized precursors. CID of $[M + Cu - H]^+$ yields exclusively N-terminal fragments, as shown in Figure 3.10. Unlike $[M + Fe - H]^+$, the only other singly charged metallated complex studied, this spectrum contains prominent $[a_n + Cu]^+$, n = 4-7, and no loss of hydrogen or small neutrals. The b-series ions form only 26 Da lower than the a-series as $[b_n + Cu - 2H]^+$, n = 4-6. The c-ion series is generated with one additional hydrogen, as $[c_n + Cu + H]^+$, n = 3-5, and is in much lower abundance than the a- and b-series. Like $[M + Fe - H]^+$, the spectrum of $[M + Cu - H]^+$ is relatively "clean", with a series of easily assigned a-, b-, and c-ions starting at n = 3. However, $[M + Cu - H]^+$ generates no H_2O or NH_3 losses from the backbone cleavage ions. Dissociation of $[M + Cu - H]^+$ forms only singly charged CID products form (with sequence coverage from n = 3-7); this makes the spectrum easier to interpret than those of the various doubly charged $[M + Met]^{2+}$.

Interestingly, a small amount of methyl side chain loss from $[a_n + Cu]^+$, n = 6-7, and loss of carbon from the precursor, to form $[M + Cu - H - C]^+$, occurs (Figure 3.10). To further investigate this unusual behavior, heptapeptides were synthesized containing glycine residues in various positions: AGAGAAA, AAAAAGA, and AAAGGAA. In addition, heptaalanine with ^{13}C-labeling of the alanine side chain (methyl groups) on the

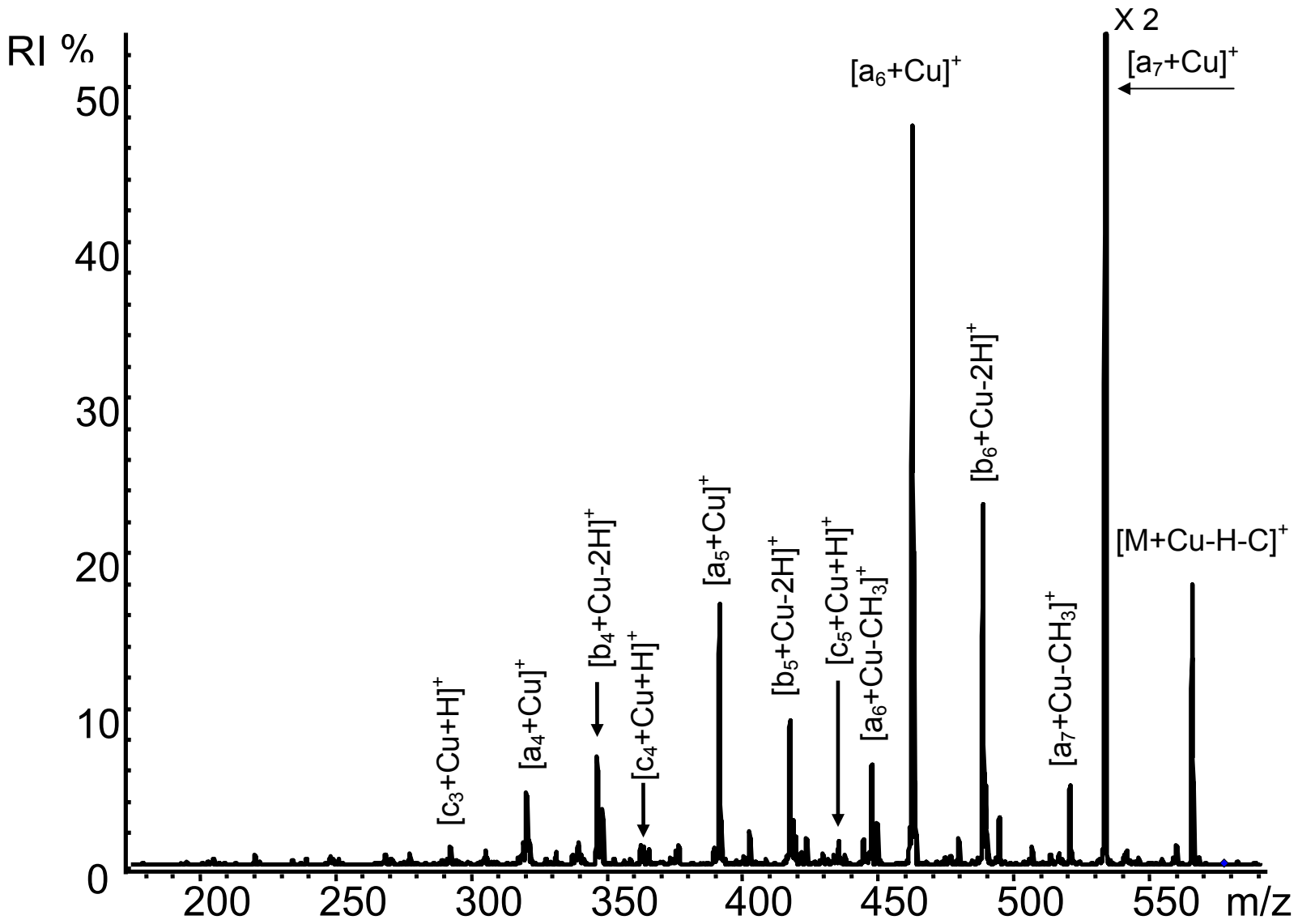

Figure 3.10. Low-energy CID spectrum obtained from $[M + Cu - H]^+$, produced by a mixture of heptaalanine and $CuCl_2$.

first and sixth residues was studied. Products formed by CID of these Cu(II) cationized peptides are summarized in Table 3.5. Mixtures of these peptides with Cu(II) also produced $[M + Cu]^{2+}$ and $[M + Cu - H]^{+}$. CID of each $[M + Cu - H]^{+}$ produce exclusively $[M + Cu - H - 12]^{+}$. If the carbon lost came from the side chain carbon of alanine, elimination of 13 Da or a mixture of 12 Da and 13 Da for the ^{13}C-labeled heptaalanine is expected (Figure 3.11). $[M + Cu - H - C]^{+}$ was submitted to CID and yielded a loss of 34 Da for each peptide studied (see Figure 3.12). This could be elimination of the small neutrals H_2 and O_2 or H_2O_2. $[M + Cu - H - C - 34]^{+}$ dominates the MS^3 spectra and is the only product ion of greater than 10 % relative intensity. The results suggest that carbon loss is not coming from the side chain of alanine. Also, the only location for facile elimination of H_2 and O_2 (or combinations of these atoms) is from the C-terminus. In a gas-phase ion chemistry study of the reactions of Cu(I) with organic aldehydes, ketones, carboxylic acids, and esters, Freiser and coworkers[48] found that a variety of small neutral molecules (e.g. H_2O, H_2, CO, CH_2O, and CH_2) and radicals were eliminated as the neutral product. They proposed a mechanism where the metal ion coordinates to both oxygens of a carboxylic acid or ester group, with the result being rearrangements that lead to the neutral losses. Similar processes may be occurring in low abundance at the C-terminal carboxylic acid group during CID on peptides complexed to Cu(II).

N-terminal product ions form by CID of $[M + Cu]^{2+}$, as shown in Figure 3.13. The doubly charged products are $[b_n + Cu - H]^{2+}$, n = 5-7, and $[a_n + Cu - H]^{2+}$, n = 5-7. The base peak is $[b_6 + Cu - H]^{2+}$, followed in intensity by $[a_6 + Cu - H]^{2+}$. A 28 Da difference (CO loss) is associated with each of these $[b_n + Cu - H]^{2+}$ and $[a_n + Cu - H]^{2+}$

Table 3.5. Product ions formed by CID of Cu(II)-cationized peptides.

GGAAAAA		$[M+Cu]^{2+a}$						
	charge	**G, n=1**	**G, n=2**	**A, n=3**	**A, n=4**	**A, n=5**	**A, n=6**	**A, n=7**
$\mathbf{a_n}$**+Co-H**	2						s[b]	w
$\mathbf{b_n}$**+Co-2H**	1					w	w	
$\mathbf{b_n}$**+Co-2H-17**	2							w
$\mathbf{c_n}$**+Co+H**	1						w	
$\mathbf{y_{8-n}}$**+Co-2H**	1			w			w	

AAGGAAA		$[M+Cu]^{2+}$						
	charge	**A, n=1**	**A, n=2**	**G, n=3**	**G, n=4**	**A, n=5**	**A, n=6**	**A, n=7**
$\mathbf{a_n}$	1		m		w			
$\mathbf{a_n}$**+Cu**	1					s	m	
$\mathbf{a_n}$**+Cu-H**	2						s	
$\mathbf{b_n}$	1		w					
$\mathbf{b_n}$**+Cu-2H**	1				w	m	s	
$\mathbf{b_n}$**+Cu-H**	2						s	
$\mathbf{c_n}$**+Cu+H**	1					w	w	
$\mathbf{y_{(8-n)}}$	1						w	m

Table 3.5 Continued

AAAGGAA		$[M+Cu]^{2+}$						
	charge	**A, n=1**	**A, n=2**	**A, n=3**	**G, n=4**	**G, n=5**	**A, n=6**	**A, n=7**
$\mathbf{a_n}$	1		m					
$\mathbf{a_n}$**+Cu**	1					s	m	
$\mathbf{a_n}$**+Cu-H**	2						m	
$\mathbf{b_n}$	1							
$\mathbf{b_n}$**+Cu-2H**	1					w	s	
$\mathbf{b_n}$**+Cu-H**	2					w	m	
$\mathbf{c_n}$**+Cu**	1			w				
$\mathbf{c_n}$**+Cu+H**	1					m	w	
$\mathbf{y_{(8-n)}}$	1						w	m
other products:	w, $[M+Cu-H_2O]^{2+}$ m, $[M+Cu-CO_2]^{2+}$							

AGAGAAA		$[M+Cu]^{2+}$						
	charge	**A, n=1**	**G, n=2**	**A, n=3**	**G, n=4**	**A, n=5**	**A, n=6**	**A, n=7**
$\mathbf{a_n}$	1							
$\mathbf{a_n}$**+Cu**	1				w	w	w	
$\mathbf{a_n}$**+Cu-H**	2						m	
$\mathbf{b_n}$	1		w					
$\mathbf{b_n}$**+Cu-2H**	1				w	w	m	
$\mathbf{b_n}$**+Cu-H**	2					w	m	
$\mathbf{c_n}$**+Cu+H**	1					w	w	
$\mathbf{y_{(8-n)}}$	1							w
other products:	w, $[M+Cu-H_2O]^{2+}$ w, $[M+Cu-CO_2]^{2+}$ w, $[a_6+Cu-Gly]^{+}$ m/z: s, 145.0 and	m,	401.8			s		m

[a] Precursor ion.

[b] Where relative intensities 1-29%, 30-59%, and 60-100% are indicated by w, m, and s respectively.

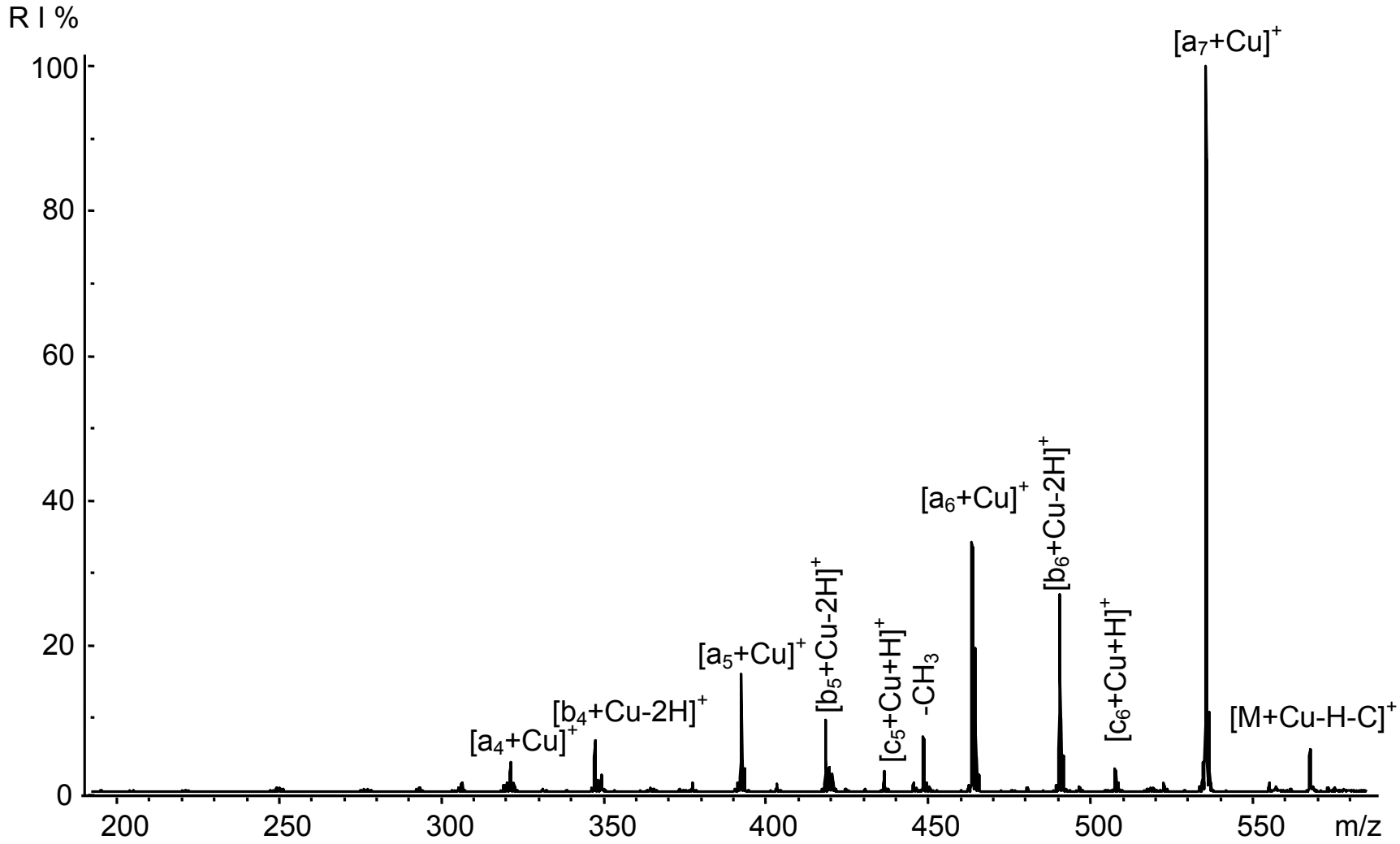

Figure 3.11. Low-energy CID spectrum obtained from $[M + Cu - H]^+$, produced by a mixture of ^{13}C-labeled heptaalanine and $CuCl_2$.

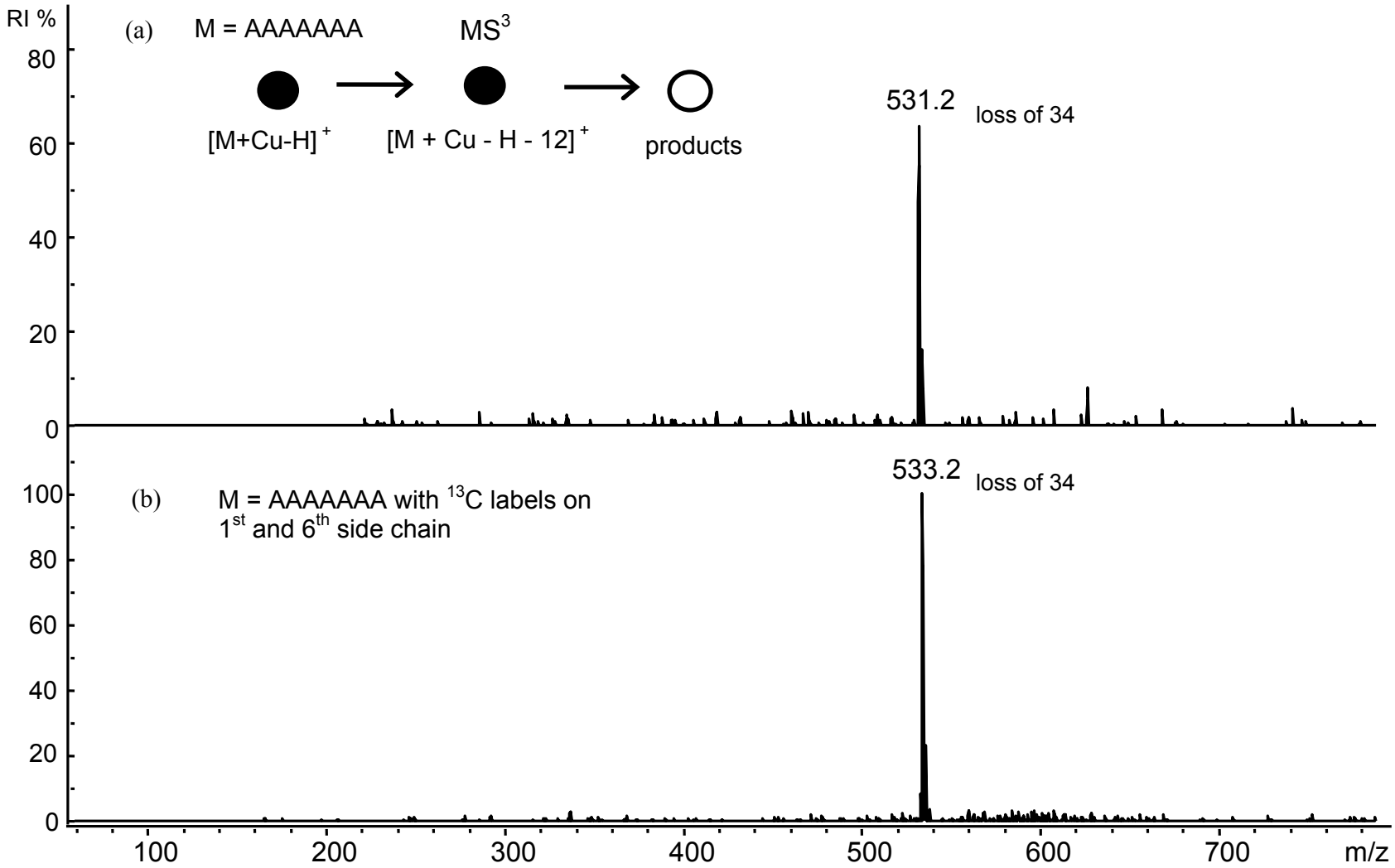

Figure 3.12. Positive MS^3 CID spectra obtained from the $[M + Cu - H - 12]^+$ product formed from $[M + Cu - H]^+$ for a mixture of Cu(II) with (a) heptaalanine and (b) ^{13}C-labeled heptaalanine.

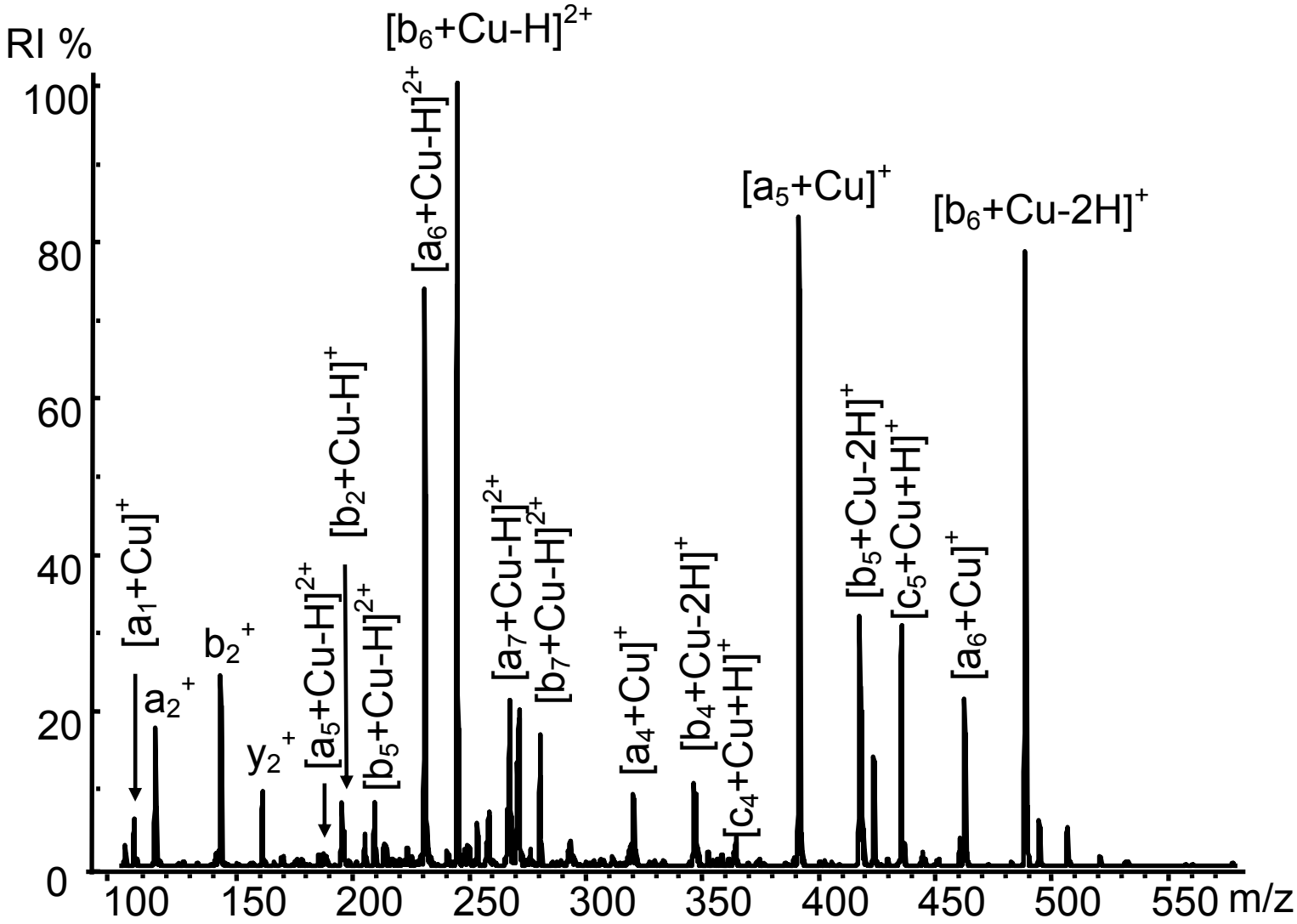

Figure 3.13. Low-energy CID spectrum obtained from $[M + Cu]^{2+}$, produced by a mixture of heptaalanine and $CuCl_2$.

pairs. In contrast, the singly charged a-ions, $[a_n + Cu]^+$, n = 4-6, are 26 Da lower in mass than the corresponding b-ions, $[b_n + Cu - 2H]^+$, n = 4-6. Singly charged c-ions form as $[c_n + Cu + H]^+$, n = 3-6.

The spectrum shown in Figure 3.13 is unique in that some b-ions are slightly more abundant than a-ions. Also, singly and doubly charged products are in near equal abundances; for the other $[M + Met]^{2+}$ studied, doubly charged products were far more abundant. As was the case for the other $[M + Met]^{2+}$, neutral loss products that complicate spectral interpretation are absent. In addition, like the Fe(II) and Ni(II) analogs, $[M + Cu]^{2+}$ produces non-metallated products that assist in sequencing residues near the N-terminus. The presence of peaks containing the two major Cu isotopes, Cu-63, and Cu-65, allow metallated and non-metallated ions to be readily distinguished. Another unique feature is the formation of $[a_1 + Cu]^+$, the only n = 1 ion found in this study, which allows identification of the N-terminal residue.

The CID results for penta-, hexa-, and heptaalanine mixed with several first row transition metal chlorides suggest that the best metal for peptide sequencing is Cu(II). Because both $[M + Cu - H]^+$ and $[M + Cu]^{2+}$ are produced by ESI on a mixture of $CuCl_2$ and peptide, analysis of a single solution allows both CID spectra to be obtained. Also, the two spectra are complimentary: $[M + Cu - H]^+$ generates an easily interpreted spectrum of singly-charged metallated ions produced from the N-terminus for $n \geq 3$, while $[M + Cu]^{2+}$ allows the first three residues to be sequenced and provides confirming information on the remainder of the sequence. This is more sequence information than is provided by CID on protonated heptaalanine (Figure 3.2a), where cleavage only occurs for $n > 3$ so that the first three residues cannot be sequenced.

These results for penta-, hexa-, and heptaalanine mixed with several first row transition metal chlorides suggests that the best metal for peptide sequencing is Cu(II). In particular, performing CID on both $[M + Cu - H]^+$ and $[M + Cu]^{2+}$ in a complimentary manner provides the greatest sequence coverage and the most readily interpretable spectra.

3.3.7 Coordination of Transition Metal Ions to Tri- and Hepta-alanine Methyl Ester

Studies were also performed on polyalanines where the C-terminal carboxylic acid group was replaced with a methyl ester to hinder coordination of transition metal ions to the C-terminus. ESI mass spectra on mixtures of metal salts with AAA-OMe and AAAAAAA-OMe show that metallated peptide ions form in the absence of a carboxylic acid group. This demonstrates that the metals can coordinate to the peptide through sites such as the N-terminus and/or backbone amide groups. In addition, the formation of almost exclusively metallated N-terminal CID product ions strongly suggests that the transition metals are coordinating with the N-terminus. This is consistent with computational studies for Co(II)[49] and Cu(II)[50] and IRMPD studies involving $(Ala)_n$, n = 2-5 with Met^{3+} (Met = La, Ho, and Eu),[51] which indicate that metals are coordinated to an N-terminal nitrogen and further solvated by carbonyl oxygens.

3.3.8 Confirmation of Product Ion Assignments

Substitution of glycine residues (57 Da) for alanine residues in several heptapeptides was carried out when product ion assignment was ambiguous. In addition,

^{13}C-labeled alanine residues (72 Da) were substituted into different positions of the heptaalanine chain (alanine residue = 71 Da). For example, the masses of c-series ions are 0.98 Da lower than y-series ions in polyalanines. Because addition and loss of hydrogens is common when working with metals, unambiguous assignments of these ions required such "mass labeling" near the termini. This changes the c- and y-series ion masses and makes clear that the products are metallated c-ions. Studies of the peptides AAAAAGA, AAGGAAA, GGAAAAA, and ^{13}C-labeled AAAAAAA mixed with the transition metal salts give the same types of product ions as those formed with heptaalanine.

3.3.9 Metallated a-ions

When complexed to first row transition metal ions, the most abundant CID products from polyalanines are a-ions. This contrasts with CID on $[M + H]^+$ and $[M - H]^-$ where b- and y-ions are produced in much greater abundance than a-ions. For protonated peptides, recent structural and mechanistic studies involving infrared multiphoton dissociation (IRMPD)[52, 53] and ion mobility spectrometry (IMS)[54] have focused on the isomers of a_n^+, which can be linear or macrocyclic. Several studies suggest that these a_n^+ are produced directly from oxazalone-structured b-ions via elimination of CO; [55-57] these ions usually further eliminate NH_3.[58, 59]

With the exception of $[M + Cu - H]^+$, all of the metallated peptide ions produce at least one a-series ion that is 28 Da lower in mass than a b-series ion. For example, the following a-ions have corresponding b-series that are 28 Da lower in mass: $[a_n + Cr - 2H]^{2+}$ from Figure 3.3, $[a_n + Fe - 2H]^+$ and $[a_n + Fe - H]^{2+}$ from Figures 3.4-5,

$[a_n + Co - H]^+$ from Figure 3.8, $[a_n + Ni - 2H]^+$ from Figure 3.9, and $[a_n + Cu - H]^{2+}$ from Figure 3.13. This is analogous to what is seen for protonated peptides where CO is eliminated to form a-ions as proposed by Yalcin et al. [55] (see Scheme 3.1) and suggests a mechanism where metallated a-ions are produced by CO elimination from metallated b-ions. CID and computational studies involving argentinated peptides found that $[b_2 - H + Ag]^+$ produced from GGG has a metallated oxazalone structure and $[a_2 - H + Ag]^+$ is a metallated immonium ion.[23, 60] The $[b_n + Met - H]^{2+}$ and $[a_n + Met - H]^{2+}$ formed here probably have the metallated oxazalone and immonium structures (Figure 3.14) because the b-ions eliminate CO when subjected to a further stage of CID (MS^3) as shown in Figure 3.15. Interestingly, $[b_n + OH + Ag]^+$ that form by CID of argentinated (i.e. silver-containing) peptides[23] were not produced from any of the metallated polyalanine complexes studied here.

Metallated a-ions were also selected for multistage CID studies and yielded similar results. For example, $[a_6 + Fe - H]^{2+}$ generated by CID of $[M + Fe]^{2+}$ was isolated and submitted to a further stage of CID (MS^3), as shown in Figure 3.16. The most prominent product is loss of an alanine residue to produce $[a_5 + Fe - H]^{2+}$. Several products form, including elimination of ammonia from the precursor, $[a_6 + Fe - H - NH_3]^{2+}$. The remaining products are all singly charged. The base peak, $[a_5 + Fe - H]^{2+}$, formed in MS^3, was submitted to CID (MS^4). This eliminates water, forming $[a_5 + Fe - H - H_2O]^{2+}$ (Figure 3.17). Water loss is interesting because the N-terminal side of the peptide has no hydroxyl groups.

Other metallated a- and b-ions were selected for multiple-stage CID studies and yield similar results. For example, CID (MS^2 stage) of the precursor ion, $[M + Met]^{2+}$,

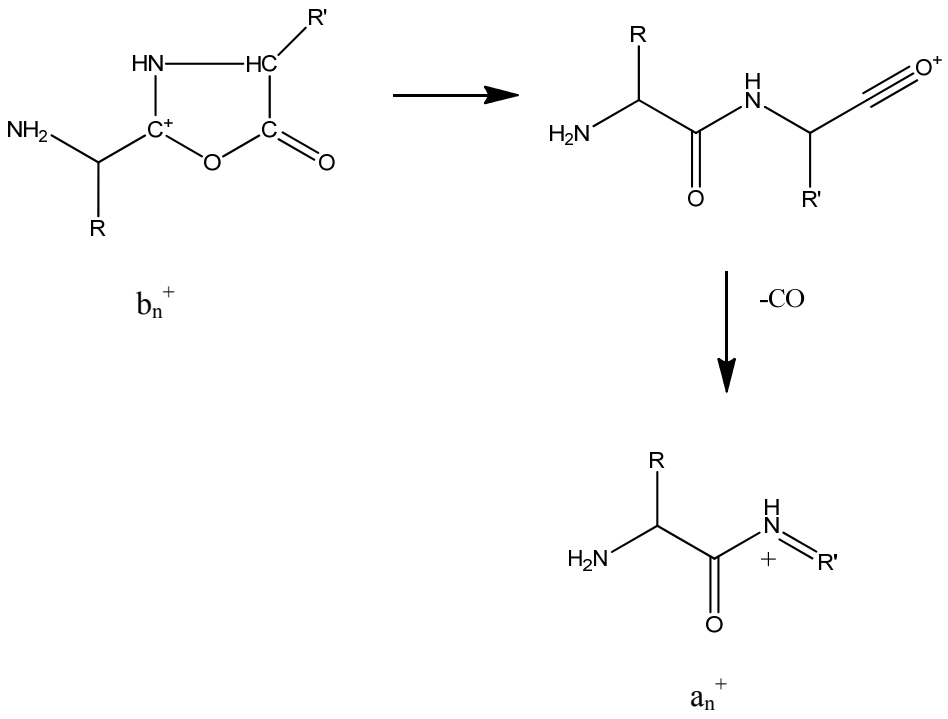

b_n^+

a_n^+

Scheme 3.1. Mechanism of a-ion formation from b-ions via elimination of CO.

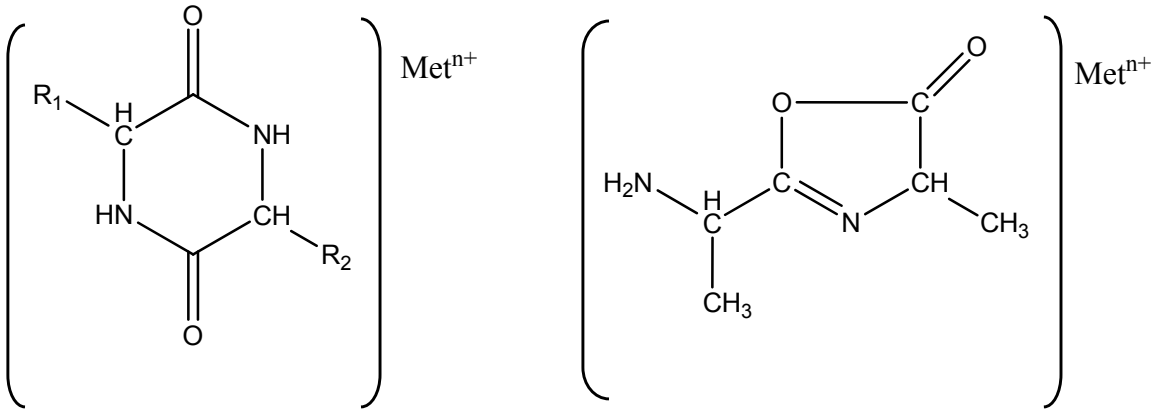

diketopiperazine structured b-ion

oxazalone structured b-ion

Figure 3.14. Structures of b-ions for peptides.

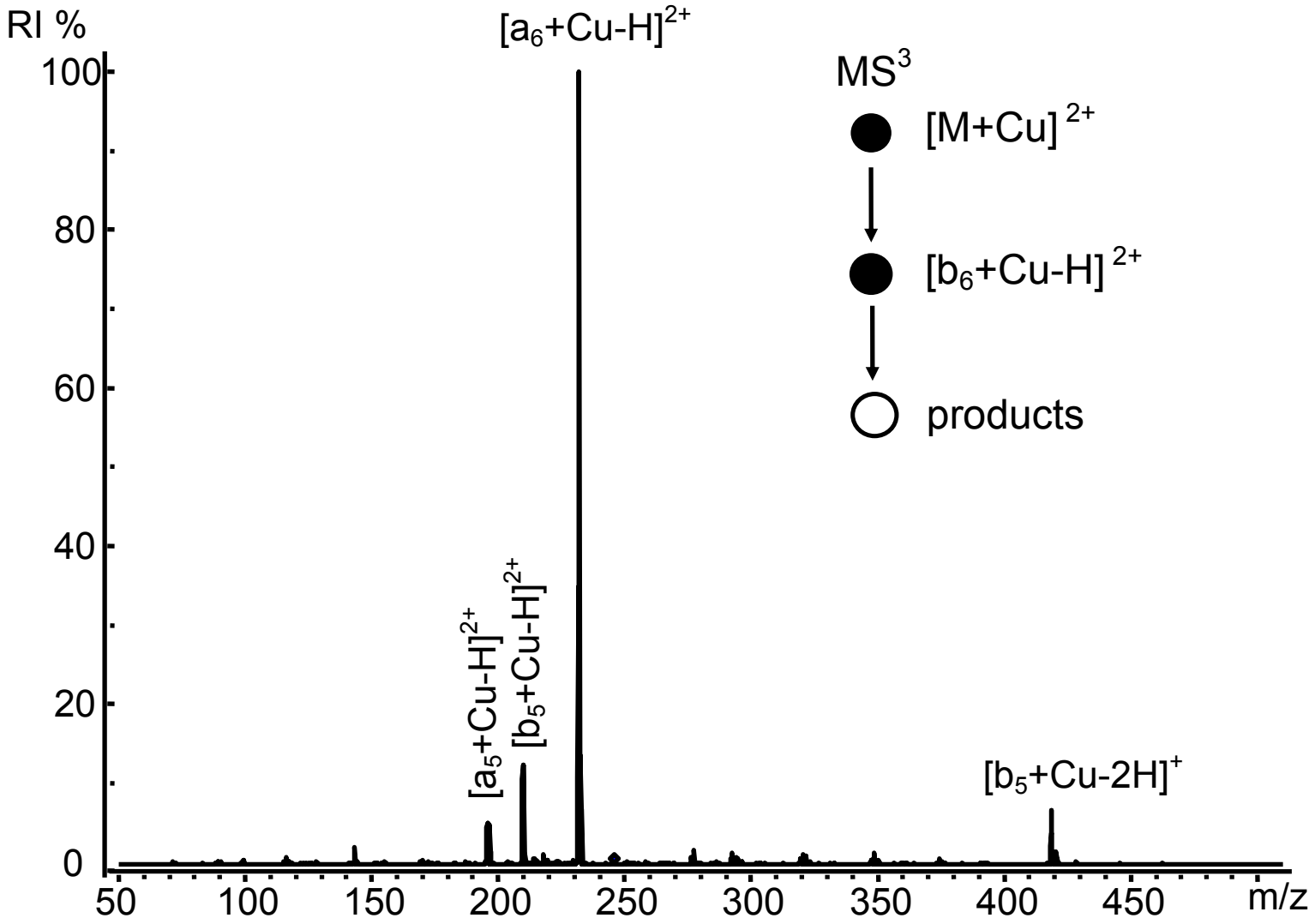

Figure 3.15. Positive MS^3 CID spectrum on $[b_6 + Cu - H]^{2+}$ product formed from $[M + Cu]^{2+}$ for $CuCl_2$ and heptaalanine.

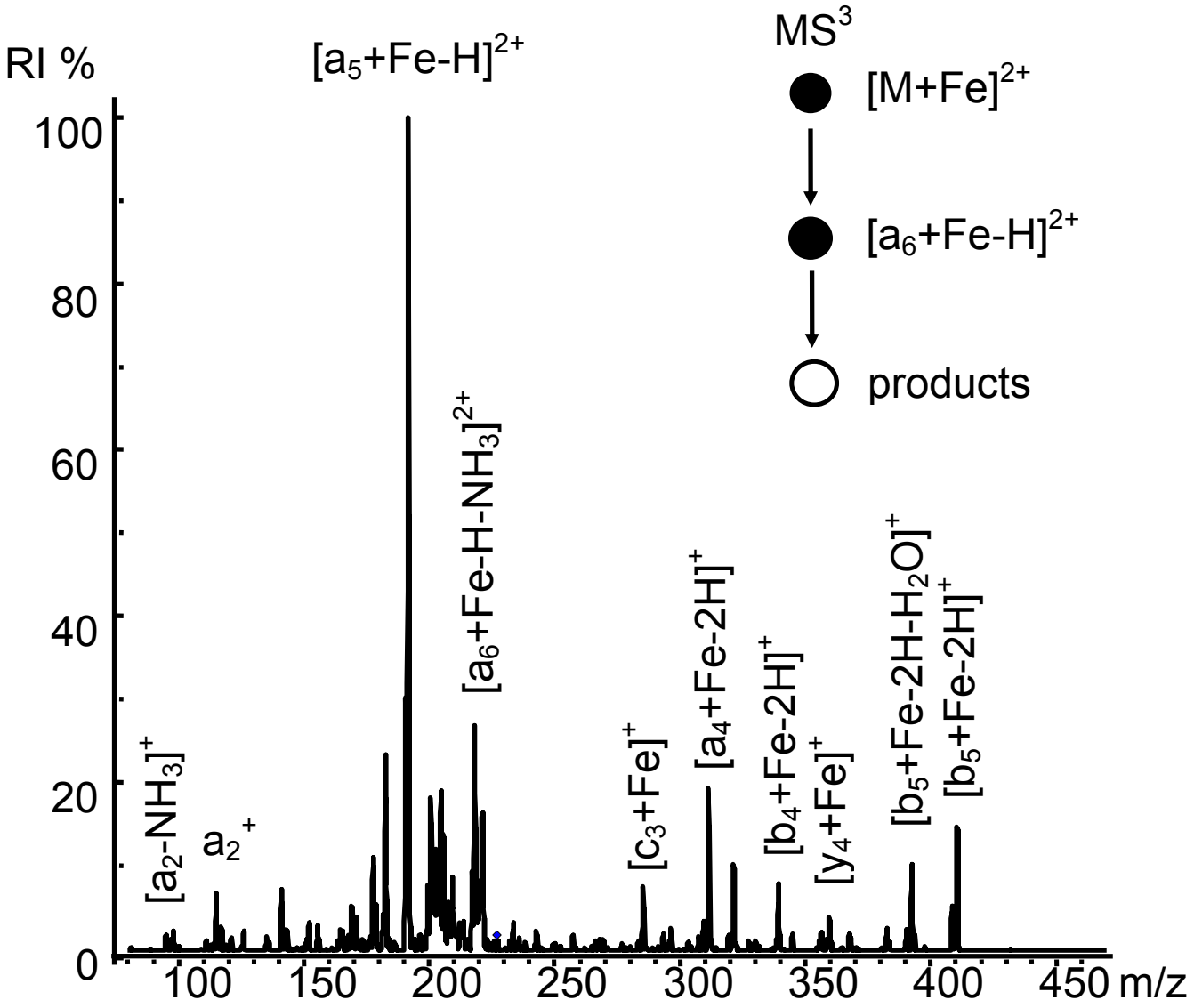

Figure 3.16. Positive MS^3 CID spectrum on $[a_6 + Fe - H]^{2+}$ product formed from $[M + Fe]^{2+}$ for a mixture of heptaalanine and $FeCl_2$.

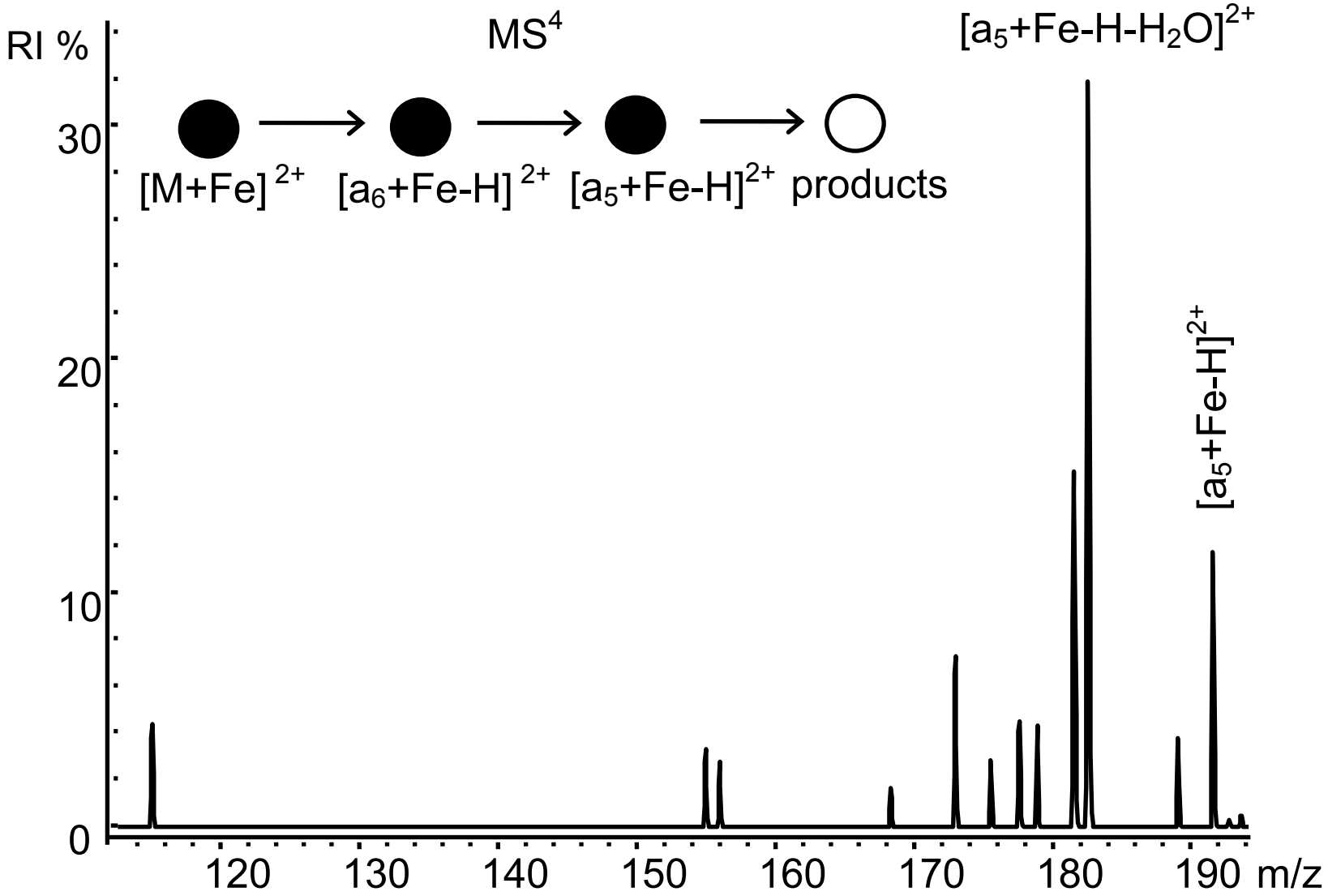

Figure 3.17. Positive MS^4 CID spectrum on $[a_5 + Fe - H]^{2+}$ product formed from $[a_6 + Fe - H]^{2+}$ for $FeCl_2$ and heptaalanine.

yields $[a_6 + Met - H]^{2+}$, which was isolated and dissociates (MS^3 stage) to produce $[a_5 + Met - H]^{2+}$ for Met = Fe, Co, and Ni. CID (MS^3) of $[b_6 + Cu - H]^{2+}$ produced by $[M + Cu]^{2+}$ (MS^2) generates predominantly $[a_6 + Cu - H]^{2+}$ (Figure 3.15). CID on metallated heptapeptides containing both alanine and glycine residues revealed that the residue lost from a-ions is located exclusively at the C-terminus. This suggests that submitting metallated a-ions to further stages of CID may be helpful in peptide sequencing. Similar MS^3 on b-ions from Fe(II), Co(II), and Ni(II) complexes also show that they dissociate to produce predominately a-ions by loss of CO.

Submitting metallated a-ions to further stages of mass spectrometry may be helpful in elucidating sequence information because these product ions primarily lose one amino acid residue. For example, $[a_n + Met - H]^{2+}$, n = 6-7, lose exactly the mass of an alanine residue to give $[a_{n-1} + Met - H]^{2+}$ for Met = Fe, Co, and Ni. However, the larger metallated b-series ions, $[b_n + Met - H]^{2+}$, n = 5-7, dissociate to eliminate CO generating almost exclusively $[a_n + Met - H]^{2+}$.

An unusual feature of the CID spectra is that some metallated a-ions appear 26 or 27 Da lower in mass than b-ions. In these instances, a mechanism involving b-ions undergoing a secondary dissociation to generate a-ions can not be occurring. For example, $[a_n + Cr]^{2+}$ in Figure 3.2 can not be forming from the b-series, which is $[b_n + Cr - 2H]^{2+}$. Also, $[a_n + Cu]^{+}$ and $[a_n + Cu]^{2+}$ of Figures 3.10, 3.11, and 3.13 do not have corresponding b-series. Here a-ion formation appears to result from direct dissociation of the precursor ion; that is, the precursor ion is producing a-ions with no b-ion intermediate. The exact mechanism is unclear and may even vary depending on the nature of the transition metal ion. Transition metal ions can coordinate at electron pairs

on heteroatoms such as oxygen.[23, 45, 51] Therefore, metal ion coordination at carbonyl oxygens along the peptide backbone may be leading to cleavage of C-C bonds alpha to the carbon. Metal ions are also possibly inserting into bonds along the peptide backbone, producing a- or b-ions or both. Studies of gas-phase ion chemistry have established that singly charged metal ions often insert into C-C and C-N bonds[18, 31-37, 61-63] and doubly or triply charged metal ions should be even more reactive due to their greater electron deficiency.

Another interesting observation is that none of the metallated a-ions lose NH_3 with the exception of a few species from $[M + Fe - H]^+$ and $[M + Ni]^{2+}$. In contrast, every a-ion produced by protonated polyalanines eliminates NH_3 (see Figure 3.2a). Two mechanisms for the elimination of NH_3 from a-ions have been suggested: the Vachet Glish (VG) and the proton bound dimer (PBD) mechanisms (See Schemes 3.2 and 3.3).[59, 64, 65] In the VG mechanism, ammonia loss from a-ions comes from the N-terminal amino group.[59] The PBD mechanism proposes elimination of the amide nitrogen atom from the oxazalone ring of a corresponding b-ion.[64, 65] The lack of NH_3 elimination for metallated polyalanines does not support a specific mechanism. Regarding the VG mechanism, if the metal ion is coordinated to the N-terminus, this could prevent NH_3 elimination. Regarding the PBD mechanism, it should not occur with metallated polyalanines because they do not have a mobile proton available for proton bound dimer formation.

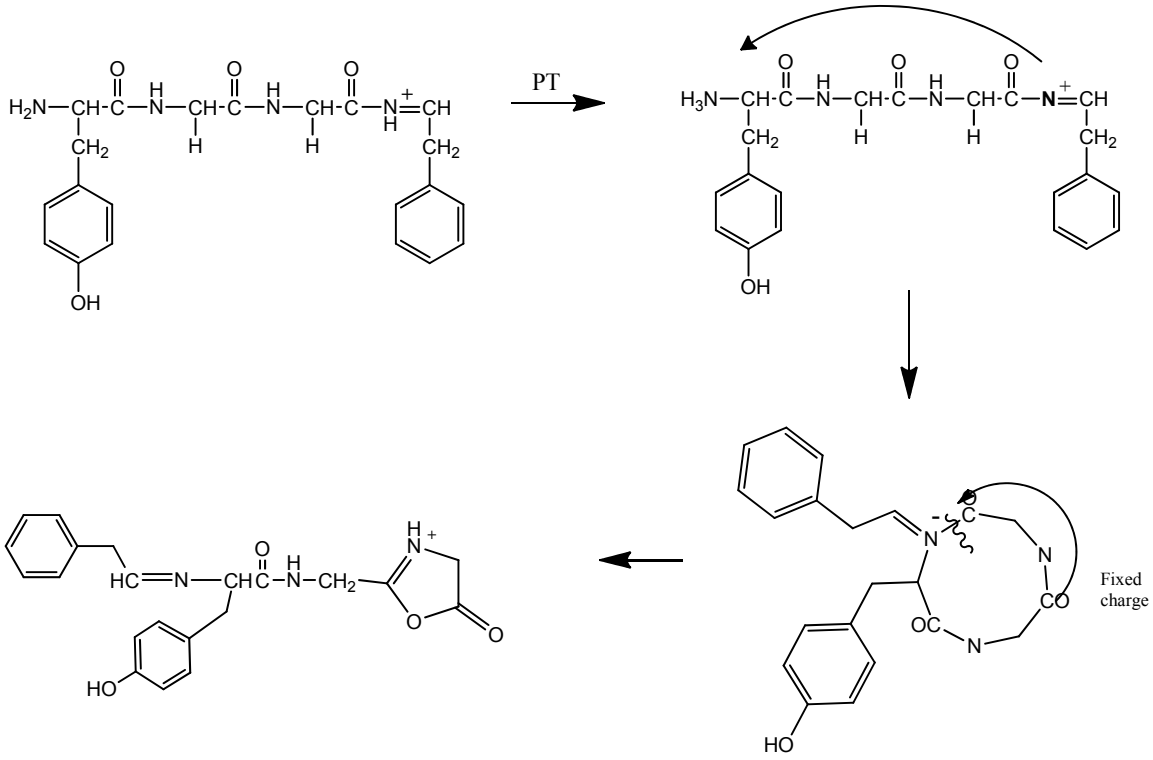

Scheme 3.2. Vachet-Glish mechanism illustrating loss of ammonia from the a_4^+ ion of YGGF.

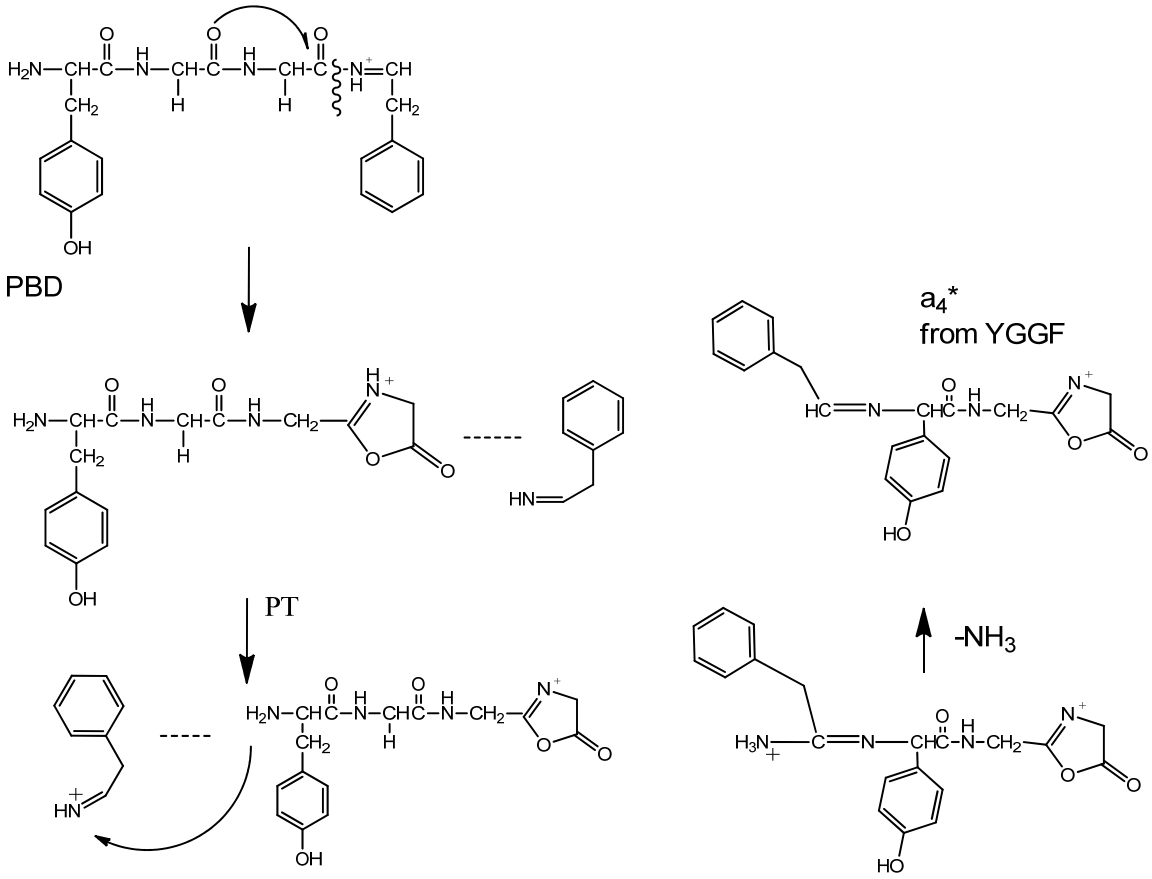

Scheme 3.3. Proton bound dimer mechanism illustrating ammonia loss from the a_4^+ ion of YGGF.

3.4 Conclusions

Peptides containing no acidic, basic, or sterically hindering side chains, such as those containing all alanine or combinations of only alanine and glycine, react with transition metals to produce complexes that ionize by ESI to produce singly, doubly, and occasionally triply charged ions. These metallated precursor ions dissociate by CID much differently than their protonated and deprotonated counterparts.

Collision-induced dissociation of transition metal-peptide complexes yields primarily metallated N-terminal fragment ions with the major products being metallated a-, b-, and c-ions. Metallated polyalanines dissociate to give doubly and singly charged products as well as metallated and non-metallated products. The overall type and abundances of product ions is dependent of both the identity of the metal and the precursor ion charge. For example, CID of $[M + Fe - H]^{2+}$ from Fe(III) gives mostly non-metallated product ions and less sequence coverage than the other metals studied, whereas the $[M + Met]^{2+}$ from Fe(II), Co(II), and Ni(II) give relatively "clean" spectra with many sequence informative products. Fundamental understanding of how these metals affect CID of polyalanines may assist in mass spectrometry analysis of biologically derived samples that contain these metals. A promising cationizing reagent for sequencing is Cu(II). CID of $[M + Cu - H]^{+}$ and $[M + Cu]^{2+}$ produce complimentary spectra that provide full sequencing of the model peptides studied and are easy to study as both precursor ions are produced from one sample.

REFERENCES

1. E. I. Solomon; M. J. Baldwin; M. D. Lowery, Electronic structures of active sites in copper proteins: contributions to reactivity. *Chem. Rev.* **1992,** 92, 521-542.

2. I. Bertini; A. Sigel; H. Sigel, *Handbook on Metalloproteins*. Marcel Dekker, Inc.: New York City, 2001.

3. J. A. Gutierrez; M. Wessling-Resnick, Molecular mechanisms of iron transport. *Crit. Rev. Eukaryot. Gene Expr.* **1996,** 6, 1-14.

4. J. B. Vincent, The biochemistry of chromium. *J. Nutr.* **2000,** 130, 715-718.

5. Z. Q. Wang; X. H. Zhang; J. C. Russell; M. Hulver; W. T. Cefalu, Chromium picolinate enhances skeletal muscle cellular insulin signaling in vivo in obese, insulin-resistant JCR:LA-cp rats. *J. Nutr.* **2006,** 136, 415-420.

6. H.-J. Thiesen; C. Bach, Transition metals modulate DNA-protein interactions of SP1 zinc finger domains with its cognate target site. *Biochem. Biophys. Res. Commun.* **1991,** 176, 551-557.

7. R. F. Service, PROTEOMICS: New database to track protein locations. *Science* **2005,** 309, 1310.

8. M. Wilm; M. Mann, Electrospray and Taylor-cone theory, Dole's beam of macromolecules at last? *Int. J. Mass Spectrom. Ion Proc.* **1994,** 136, 167-180.

9. M. Wilm; M. Mann, Analytical properties of the nanoelectrospray ion source. *Anal. Chem.* **1996,** 68, 1-8.

10. R. Juraschek; T. Dülcks; M. Karas, Nanoelectrospray-More than just a minimized-flow electrospray ionization source. *J. Am. Soc. Mass Spectrom.* **1999,** 10, 300-308.

11. T. L. Constantopoulos; G. S. Jackson; C. G. Enke, Effects of salt concentration on analyte response using electrospray ionization mass spectrometry. *J. Am. Soc. Mass Spectrom.* **1999,** 10, 625-634.

12. M. Karas; U. Bahr; T. Dülcks, Nano-electrospray ionization mass spectrometry: addressing analytical problems beyond routine. *Fresnius. J. Anal. Chem.* **2000,** 366, 669-676.

13. I. A. Papayannopoulos, The interpretation of collision-induced dissociation tandem mass spectra of peptides. *Mass Spectrom. Rev.* **1995,** 14, 49-73.

14. R. P. Grese; R. L. Cerny; M. L. Gross, Metal ion-peptide interactions in the gas phase: a tandem mass spectrometry study of alkali metal cationized peptides. *J. Am. Chem. Soc.* **1989,** 111, 2835-2842.

15. T. Vaisar; C. L. Gatlin; F. Turecek, Oxidation of peptide-copper complexes by alkali metal cations in the gas phase. *J. Am. Chem. Soc.* **1996,** 118, 5314-5315.

16. P. Hu; M. L. Gross, Gas-phase interactions of transition-metal ions and di- and tripeptides: a comparison with alkaline-earth-metal-ion interactions. *J. Am. Chem. Soc.* **1993,** 115, 8821-8828.

17. A. Reiter; J. Adams; H. Zhao, Intrinsic (gas-phase) binding of Co^{2+} and Ni^{2+} by peptides: A direct reflection of aqueous-phase chemistry. *J. Am. Chem. Soc.* **1994,** 116, 7827-7838.

18. D. M. Crizer; Y. Xia; S. A. McLuckey, Transition metal complex cations as reagents for gas-phase transformation of multiply deprotonated polypeptides. *J. Am. Soc. Mass Spectrom.* **2009,** 20, 1718-1722.

19. D. Pu; J. B. Vincent; C. J. Cassady, The effects of chromium(III) coordination on the dissociation of acidic peptides. *J. Mass Spectrom.* **2008,** 43, 773-781.

20. V. Anbalagan; B. A. Perera; A. T. M. Silva; A. L. Gallardo; M. Barber; J. M. Barr; S. M. Terkarli; E. R. Talaty; M. J. Van Stipdonk, Formation of $[b_n + 17 + Ag]^+$ product ions from Ag^+ cationized native and acetylated peptides. *J. Mass Spectrom.* **2002,** 37, 910-926.

21. L. M. Teesch; J. Adams, Metal ions as special reagents in analytical mass spectrometry. *Org. Mass Spectrom.* **1992,** 27, 931-943.

22. L. M. Mallis; D. H. Russell, Fast-atom-bombardment-tandem mass spectrometry studies of alkali-metal ions of small peptides. *Anal. Chem.* **1986,** 58, 1076-1080.

23. I. K. Chu; T. Shoeib; X. Guo; C. F. Rodriquez; T.-C. Lau; A. C. Hopkinson; K. W. M. Siu, Characterization of the product ions from the collision-induced dissociation of argentinated peptides *J. Am. Soc. Mass Spectrom.* **2001,** 12, 163-175.

24. J. A. Loo, Studying noncovalent protein complexes by electrospray ionization mass spectrometry. *Mass Spectrom. Rev.* **1997,** 16, 1-23.

25. L. C. M. Ngoka; M. L. Gross, Location of alkali metal binding sites in endothelin a selective receptor antagonists, cyclo(D-Trp-D-Asp-Pro-D-Val-Leu) and cyclo(D-Trp-D-Asp-Pro-D-Ile-Leu), from multistep collisionally activated decompositions. *J. Mass Spectrom.* **2000,** 35, 265-276.

26. K. C. Barlow; R. A. J. O'Hair, Gas-phase peptide fragmentation: how understanding the fundamentals provides a springboard to developing new chemistry and novel proteomic tools. *J. Mass Spectrom.* **2008,** 43, 1301-1319.

27. L. M. Teesch; J. Adams, Fragmentations of gas-phase complexes between alkali metal ions and peptides: metal ion binding to carbonyl oxygens and other neutral functional groups. *J. Am. Chem. Soc.* **1991,** 113, 812-820.

28. H. Sigel; R. B. Martin, Coordinating properties of the amide bond. Stability and structure of metal ion complexes of peptides and related ligands. *Chem. Rev.* **1982,** 82, 385-426.

29. W. Bal; H. Kozlowski; G. Kupryszewski; Z. Mackiewicz; L. Pettit; R. Robbins, Complexes of Cu(II) with Asn-Ser-Phe-Arg-Tyr-NH_2; an example of metal ion-promoted conformational organization which results in exceptionally high complex stability. *J. Inorg. Biochem.* **1993,** 52, 79-87.

30. S. J. Shields; B. K. Bluhm; D. H. Russell, Fragmentation chemistry of $[M + Cu]^+$ peptide ions containing an N-terminal arginine. *J. Am. Soc. Mass Spectrom.* **2000,** 11, 626-638.

31. R. C. Burnier; G. D. Byrd; B. S. Freiser, Gas-phase reactions of iron(1^+) with ketones and ethers. *J. Am. Chem. Soc.* **1981,** 103, 4360-4367.

32. P. B. Armentrout; L. F. Halle; J. L. Beauchamp, Periodic trends in transition metal-hydrogen, metal-carbon, and metal-oxygen bond dissociation energies.

Correlation with reactivity and electronic structure. *J. Am. Chem. Soc.* **1981,** 103, 6501-6502.

33. R. R. Corderman; J. L. Beauchamp, Ion cyclotron resonance investigation of the decarbonylation of aldehydes by (n5-C_5H_5)Ni^+. *J. Am. Chem. Soc.* **1976,** 98, 5700-5702.

34. C. J. Cassady; B. S. Freiser; S. W. McElvany; J. Allison, Gas-phase reactions of cobalt(1^+) ion and Co(ligand)$_n^+$ with nitroalkanes. *J. Am. Chem. Soc.* **1984,** 106, 6125-6135.

35. B. D. Radecki; J. Allison, Parallels in the formation of transition metal-amide bonds in solution and in the gas phase: an ion cyclotron resonance study of cobalt ion chemistry with amines. *J. Am. Chem. Soc.* **1984,** 106, 946-952.

36. S. J. Babinec; J. Allison, The chemistry of first-row transition-metal ions with primary amines in the gas phase: correlations of reactivity with electronic structure. *J. Am. Chem. Soc.* **1984,** 106, 7718-7720.

37. J. Allison; R. B. Freas; D. P. Ridge, Cleavage of alkanes by transition metal ions in the gas phase. *J. Am. Chem. Soc.* **1979,** 101, 1332-1333.

38. Z. Wu; F. A. Fernandez-Lima; D. H. Russell, Amino acid influence on copper binding to peptides: Cysteine versus arginine. *J. Am. Soc. Mass Spectrom.* **2010,** 21, 522-533.

39. O. V. Nemirovskiy; M. L. Gross, Gas phase studies of the interactions of Fe^{2+} with cysteine-containing peptides. *J. Am. Soc. Mass Spectrom.* **1998,** 9, 1285-1292.

40. P. Hu; C. Sorensen; M. L. Gross, Influences of peptide side chains on the metal ion binding site in metal ion-cationized peptides: participation of aromatic rings in metal chelation. *J. Am. Soc. Mass Spectrom.* **1995,** 6, 1079-1085.

41. M. Kohtani; M. F. Jarrold; S. Wee; R. A. J. O'Hair, Metal ion interactions with polyalanine peptides. *J. Phys. Chem. B* **2004,** 108, 6093-6097.

42. W. Chan; P. White, *Fmoc Solid Phase Peptide Synthesis: A Practical Approach*. Oxford University Press: New York, 2000.

43. P. G. Wuts; T. W. Greene, *Greene's Protective Groups in Organic Synthesis*. 4 ed.; John Wiley & Sons, Inc.: Hoboken, NJ, 2006.

44. P. Roepstorff; J. Fohlman, Proposal for a common nomenclature for sequence ions in mass spectra of peptides. *Biol. Mass Spectrom.* **1984,** 11, 601.

45. H. Lavanant; Y. Hoppilliard, Fragmentation of arginine- and lysine-containing dipeptides cationized by Cu^{+} and Cu^{2+}. *Eur. Mass Spectrom.* **1999**, 41-50.

46. R. E. Mesmer; C. F. Baes Jr., *The hydrolysis of cations: A critical review of hydrolytic species and their stability constants in aqueous solution*. Wiley-Interscience: New York, 1976.

47. A. E. Martell; R. M. Smith, *Critical Stability Constants*. Plenum Press: New York, 1974-1989; Vol. 1-6.

48. R. C. Burnier; G. D. Byrd; B. S. Freiser, Copper (I) chemical ionization-mass spectrometric analysis of esters and ketones. *Anal. Chem.* **1980,** 52, 1641-1650.

49. E. Constantino; A. Rimola; M. Sodupe; L. Rodriguez-Santiago, Coordination of $(Glycyl)_n$ glycine (n = 1-3) to Co^{+} and Co^{2+}. *J. Phys. Chem. A* **2009,** 113, 8883-8892.

50. A. Rimola; E. Constantino; L. Rodriguez-Santiago; M. Sodupe, Binding Properties of $Cu^{+/2+}$ -(glycyl)nglycine Complexes (n = 1-3). *J. Phys. Chem. A* **2008,** 112, 3444-3453.

51. J. S. Prell; T. G. Flick; J. Oomens; G. Berden; E. R. Williams, Coordination of Trivalent Metal Cations to Peptides: Results from IRMPD Spectroscopy and Theory. *J. Phys. Chem. A* **2009,** 114, 854-860.

52. N. C. Polfer; J. Oomens; S. Suhai; B. Paizs, Infrared spectroscopy and theoretical studies on gas-phase protonated Leu-enkephalin and its fragments: direct experimental evidence for the mobile proton. *J. Am. Chem. Soc.* **2007,** 129, 5887-5897.

53. N. C. Polfer; B. C. Bohrer; M. D. Plasencia; B. Paizs; D. E. Clemmer, On the dynamics of fragment isomerization in collision-induced dissociation of peptides. *J. Phys. Chem. A* **2008,** 112, 1286-1293.

54. I. Riba-Garcia; K. Giles; R. H. Bateman; S. J. Gaskell, Evidence for structural variants of a- and b-type peptide fragment ions using combined ion mobility/mass spectrometry. *J. Am. Soc. Mass Spectrom.* **2008,** 19, 609-613.

55. T. Yalcin; I. G. Csizmadia; M. R. Peterson; A. G. Harrison, The structure and fragmentation of B_n (n >= 3) ions in peptide spectra. *J. Am. Soc. Mass Spectrom.* **1996,** 7, 233-242.

56. J. Yague; A. Paradela; M. Ramos; S. Ogueta; A. Marina; F. Barahona; J. Lopez de Castro; J. VÃzquez, Peptide rearrangement during quadrupole ion trap fragmentation: Added complexity to MS/MS spectra. *Anal. Chem.* **2003,** 75, 1524-1535.

57. B. Paizs; Z. Szlávik; G. Lendvay; K. Vékey; S. Suhai, Formation of a_2^+ ions of protonated peptides. An ab initio study. *Rapid Commun. Mass Spectrom.* **2000,** 14, 746-755.

58. T. Yalcin; C. Khouw; I. G. Csizmadia; M. R. Peterson; A. G. Harrison, Why are b-ions stable species in peptide spectra? *J. Am. Soc. Mass Spectrom.* **1995,** 6, 1165-1174.

59. R. W. Vachet; B. M. Bishop; B. W. Erickson; G. L. Glish, Novel peptide dissociation: Gas-phase intramolecular rearrangement of internal amino acid residues. *J. Am. Chem. Soc.* **1997,** 119, 5481-5488.

60. V. W. M. Lee; H. Li; T.-C. Lau; K. W. M. Siu, Structures of b and a Product Ions from the Fragmentation of Argentinated Peptides. *J. Am. Chem. Soc.* **1998,** 120, 7302-7309.

61. D. Wen; T. Yalcin; A. G. Harrison, Fragmentation reactions of Cu^+ -cationated α-amino acids. *Rapid Commun. Mass Spectrom.* **1995,** 9, 1155-1157.

62. H. Lavanant; Y. Hoppilliard, Formation and fragmentation of α-amino acids complexed by Cu^+. *J. Mass Spectrom.* **1997,** 32, 1037-1049.

63. Q. P. Lei; I. J. Amster, The reactions of ground state Cu^{+1} and Fe^{+1} with the 20 common amino acids. *J. Am. Soc. Mass Spectrom.* **1996,** 7, 722-730.

64. T. Cooper; E. Talaty; J. Grove; M. Van Stipdonk; S. Suhai; B. Paizs, Isotope labeling and theoretical study of the formation of a_3^* ions from protonated tetraglycine. *J. Am. Soc. Mass Spectrom.* **2006,** 17, 1654-1664.

65. B. J. Bythell; D. F. Barofsky; F. Pingitore; M. J. Polce; P. Wang; C. Wesdemiotis; B. Paizs, Backbone cleavages and sequential loss of carbon monoxide and ammonia from protonated AGG: A combined tandem mass spectrometry, isotope labeling, and theoretical study. *J. Am. Soc. Mass Spectrom.* **2007,** 18, 1291-1303.

CHAPTER 4

COMPARISON OF ELECTRON-TRANSFER DISSOCIATION TO COLLISION-INDUCED DISSOCIATION OF TRANSITION METAL-CATIONIZED PEPTIDES

4.1 Introduction

The field of proteomics is challenged with the task of understanding what proteins are present, what their structures and functions are, and how they interact within a cell, tissue, or organism.[1] Identifying the primary structures, or amino acid sequences, of proteins and peptides is considered the next big biological challenge since the completion of the Human Genome Project.[2] In order to tackle the large scale problem presented by proteomics, automated high-throughput tandem mass spectrometry techniques are often used to sequence and quantify proteins and peptides. De novo sequencing is the process of assigning amino acid sequences by examining product masses of fragments of the original peptide created by degradation or dissociation. The term "de novo" in peptide sequencing is specific to sequencing without prior knowledge of the original peptide sequence. This form of sequencing is viewed as the only way to accomplish large-scale mass spectrometry based proteomics.[3]

Key limitations in high-throughput proteomics are the incomplete datasets available to search engines and incomplete fragmentation of the peptides. One way to increase confidence in sequence matches made through these search engines is to

increase the number of fragments along a peptide/protein backbone, ideally at every amino acid residue, while decreasing the number of uninformative product ions such as neutral losses and rearrangements. Although the most common method of tandem MS is collision-induced dissociation (CID),[4] a newer technique, electron-transfer dissociation (ETD),[5] offers several advantages. Understanding the complementary nature of these techniques and the fundamental principles that govern the gas-phase chemistry that occurs during each is essential to de novo sequencing.[3] This knowledge can also be used to increase sequence coverage in peptides and improve predictive models in bioinformatics.

ETD is a relatively new MS/MS technique whereby fragmentation is a result of ion/ion reaction during which a multiply charged analyte receives a very low energy electron from a radical anion. ETD requires multiply charged precursor ions, $[M + nH]^{n+}$, because electron transfer to the precursor produces the charged reduced product $[M + nH]^{(n-1)+\bullet}$. For a singly charged precursor, this would result in a neutral and therefore be useless in mass spectrometry, which can only detect charged species. The resulting reduced species is unstable and typically fragments at the N-Cα bond producing c/z-type ions.[6, 7] (This nomenclature is explained further in Chapter 2.) Despite investigations into ETD mechanisms, the process is still not fully understood, but is proposed to involve electron capture at a positively charged site (usually at a Rydberg orbital).[8-11] After initial electron transfer/capture the electron can relax back down to lower energy Rydberg orbitals causing H release or the electron can be transferred to the Π* orbital of the peptide bond (leading to N-Cα cleavage) before relaxation. In addition to c/z-type ions, a-, b-, and y- ion formation also occurs.[10, 12] ETD has some drawbacks

including low product ion intensities that result from the low efficiency of the process itself, which results from poor spatial overlap of the radical anion species with the precursor ions within the trap.[13, 14] A primary product results from electron transfer to peptide $[M + nH]^{n+}$ species, which produces the charge reduced $[M + nH]^{(n-1)+\bullet}$; this has been called electron-transfer no dissociation (ETnoD).[15]

Collision-induced dissociation involves colliding activated precursor ions of interest into a neutral such as helium, which results in rapid redistribution of vibrational energy, equivalent to internal heating, of the precursor ions. Once this internal energy has reached the fragmentation threshold, the ions cleave at the weakest bonds. This includes the bonds at post-translational modifications (PTMs), side chains, and the weakest part of the peptide backbone itself to give primarily b/y-ions.[16] In contrast and to its complement, ETD cleavage occurs quickly, before energy has time to be distributed along all the degrees of freedom of molecule. This results in more randomly distributed N-Cα cleavage and thus typically higher sequence coverage.[11, 17] In addition, ETD leads to retention of labile PTMs so that phosphorylation and glycosylations sites can be identified.[8, 18-20] CID and ETD are said to be complementary and, when used together, increase peptide sequence and PTM identification over either technique alone.

Typically a more highly protonated precursor leads to more fragmentation by ETD (due to Coulombic factors) and several papers indicate that ETD is particularly inefficient for the dissociation of dications.[13, 14] Often times, as is the case for peptides containing only neutral amino acid side chains such as glycine and alanine, multiple protonation by electrospray ionization (ESI) is not possible due to lack of basic side chains that serve as protonation sites.[21]

In order to study such peptides by ETD, metal ions can be added as a charge carrier. This not only allows study by ETD, but varying the type of metal has recently been studied as a tunable parameter for energy deposition during the ET process or as a way to direct ETD behavior.[22] ETD has also been implemented in the identification of drug metallation sites. The anticancer agent cisplatin and a promising new organoruthenium complex contain platinum and ruthenium, respectively, whose binding sites to the peptide substance P, have been identified by CID and ETD mass spectrometry.[23] Studies of metal-peptide complexes by electron capture dissociation (ECD), a similar technique, show abundant c- and z-type product ions similar to those produced by ECD on protonated precursor ions.[9, 24, 25] These are not the only ion types formed during ECD of metal-peptide complexes. A study involving the ECD of substance P complexed with divalent transition metals and alkaline earth metals reveal both metallated and nonmetallated product ions from the a-, b-, c-, y-, and z-ion series.[22] The type of product ions that form was directly affected by the identity of the metal ion. Heeren and coworkers found that varying the type of metal (Ni, Co, Cu, and Zn ions) complexed to oxytocin also changed the products formed by ECD on $[M + Met]^{2+}$.[26, 27] No studies have clearly indicated the type of metal (alkali, alkaline earth, transition) that may be the most beneficial to peptide sequencing. Why some peptide-metal combinations form c-and z-type ions whereas other combinations form only a-, b-, y-type ions is not clear. Another complexity to consider is why some product ions form with and others without retaining the metal ion.

Some studies involving dissociation of metal-ligand-peptide complexes by ECD and ETD have been reported. Useful sequence information has been obtained this way.

However, the addition of ligands, such as heptadentate species, add to the complexity of the resulting spectra.[28] ETD of small peptides complexed with metal-2,2′-bipyridines (bpy) have been useful in the study of energetics and structures involved in dissociation.[29, 30] Products related to the bpy ligand and elimination of small neutrals form during ETD of these complexes. Small peptides complexed with platinum-ligands have been studied by ECD and reveal elimination of the intact peptide as the primary product.[31] These investigations suggest that the addition of organic ligands to metal-peptide complexes hinders peptide sequencing and increases spectral complexity. The work presented in this dissertation utilizes metal salts and not complex organic ligands to minimize these effects.

A more fundamental reason to study metal-cationized peptides is that many biological peptides depend on interactions with metal ions to maintain activity and catalytic properties.[32-37] Understanding how this metal binding affects fragmentation during various mass spectrometric techniques may lead to improvement to predictive models for bioinformatics. Improvement to search algorithms can be made with fundamental understanding of dissociation mechanisms and product ion structures, especially of how these two techniques complement each other.

The focus of this study is on the effects of transition metals on the ETD process. Comparisons to recent CID studies, which are discussed in Chapter 3, of transition metal-cationized peptides are also made. Alanine and glycine were used in the polypeptides studied to highlight the intrinsic differences of the metal ions interacting with the peptide backbone and their effects on ETD. Di- and tri-valent transition metals Cr(III), Fe(II), Co(II), Ni(II), and Cu(II) were used to cationize several heptapeptides by ESI. Of

particular interest was how the different metal ion properties, such as electron configurations and recombination energies, might prohibit or alter the transferred electron's participation in the ETD process.

4.2 Experimental

4.2.1 Synthesis of Peptides and Preparation of TM-peptide Complexes

Peptides were synthesized using an Advanced Chemtech (Louisville, KY, USA) model 90 synthesizer according to the standard Fmoc solid phase synthesis protocols as discussed in Chapter 2 Section 3.[38] The peptides studied were AAAAAAA, AAGGAAA, AAAGGAA, GGAAAAA, AAAAAGA, AGAGAAA, and ^{13}C-labeled AAAAAAA (labeled at the side chains of the first and sixth residues from the N-terminus). Each peptide was prepared as a 2 mM solution in 1:1 methanol:water . Metal solutions were prepared by dissolving the chloride salts of Cr(III), Fe(II), Co(II), Ni(II), and Cu(II) in water to bring the final metal salt concentration to 0.5 M. Transition metal-peptide complexes were formed by adding a few microliters of metal solution to one mL of peptide solution to yield a metal to peptide mole ratio of 25:1. Solutions for ESI were 5-10 μM in peptide and were prepared in 1:1 acetonitrile (ACN):water.

4.2.2 Mass Spectrometry

All experiments were performed with a Bruker (Billerica, MA, USA) HCTultra PTM Discovery System as discussed in Chapter 2. Samples were ionized by electrospray ionization (ESI) and introduced through a nebulizer into the source region. The ESI capillary voltage was adjusted from -2500 to -3000 V to maintain a capillary current of approximately 20 nA with ESI flow rates ranging from 125-175 μL/h. Drying gas

temperatures were optimized between 220-250 °C. The high capacity trap was filled with the optimum number of ions (approximately 200,000) during an accumulation time of approximately 200 ms.

All mass spectra were acquired in the positive ion mode. ETD experiments were performed utilizing radical anions of fluoranthene (*m/z* 202) produced by negative chemical ionization (Chapter 2 Section 1.4) with methane and electrons (71-75 eV). The precursor cation ICC target (Bruker's ion charge control utility that maximizes trapping efficiency) ranged from 100,000-200,000 while a value of 50,000-200,000 was used for the anion population. The ion/ion reaction times ranged from 100 to 500 ms. CID experiments were performed in helium gas with a 30 % to 200 % collision energy sweep and amplitudes of 0.8 to 1.2 V. Precursor ion isolation widths were adjusted from 1.0 to 4.0 *m/z* to allow maximum intensity while excluding nearby ions. The lowest *m/z* scanned for product ions was 50 *m/z*. Spectra shown are typically averages of 100 to 200 scans.

4.2.3 Reagents

Peptide synthesis reagents were obtained from Advanced ChemTech (Louisville, KY, USA) and AnaSpec (Fremont, Ca, USA) and were Fmoc-Ala-OH • H_2O, Fmoc-Gly-OH, Fmoc-Ala Wang resin, Fmoc-Ala-OH (3-^{13}C) , N-hydroxybenzotrizole, 1, 3-diisopropyl carbodiimide, piperidine, N-methyl-2-pyrrolidone, triisopropyl silane, and trifluoracetic acid. HPLC grade acetonitrile, acetic anhydride, hydrochloric acid, and HPLC grade methanol were purchased from Fisher Scientific (Hampton, NH, USA). Water was purified with a Barnstead (Dubuque, IA, USA) water purification system.

Transition metal chlorides were obtained from various sources and used without further purification: $FeCl_3 \cdot 6\ H_2O$, $NiCl_2 \cdot 6\ H_2O$ (Sigma Aldrich, St. Louis, MO, USA), $FeCl_2 \cdot 4\ H_2O$ (Acros Organics, Liège Area, Belgium), CuCl (B & A, Morristown, NJ, USA), $CuCl_2$ (Johnson Matthey, Malvern, PA, USA), $CoCl_2 \cdot 6\ H_2O$ (J. T. Baker, Phillipsburg, NJ, USA), and $CrCl_3 \cdot 6\ H_2O$ (Fisher Scientific, Hampton, NH, USA).

4.3 Results and Discussion

Electrospray ionization on mixtures of peptides and transition metal chloride salts forms both protonated and metallated peptide ions. The metallated peptides primarily form doubly charged ions. For example, peptides mixed with trivalent Cr form $[M + Cr - H]^{2+}$ and with divalent Fe, Co, Ni, and Cu form $[M + Met]^{2+}$. In addition, heptapeptides cationized by Fe(II) and Cu(II) also form small amounts of $[M + Met - H]^{+}$ by ESI. This is consistent with the charge on these metals remaining at 2+.

Figures 4.1-4.3 show ETD spectra obtained from heptaalanine (AAAAAAA) cationized by Cr(III), Fe(II), Co(II), Ni(II), and Cu(II). The experimental mass-to-charge (*m/z*) values of the assigned products are within +/- 0.5 Da from predicted *m/z*. Nomenclature is similar to Roepstorff and Fohlman[7] (as discussed in Chapter 2 Section 4) where a, b, and c denote charge remaining on the N-terminal products and x, y, and z for C-terminal products. Any added or removed hydrogen atoms or metal ions will be indicated in the label for clarity. For example, $[a_4 + Cu - H]^{+}$ denotes a singly charged product ion produced by cleavage of the Cα-C bond after the fourth amino acid residue, incorporation of the copper ion, and loss of one hydrogen.

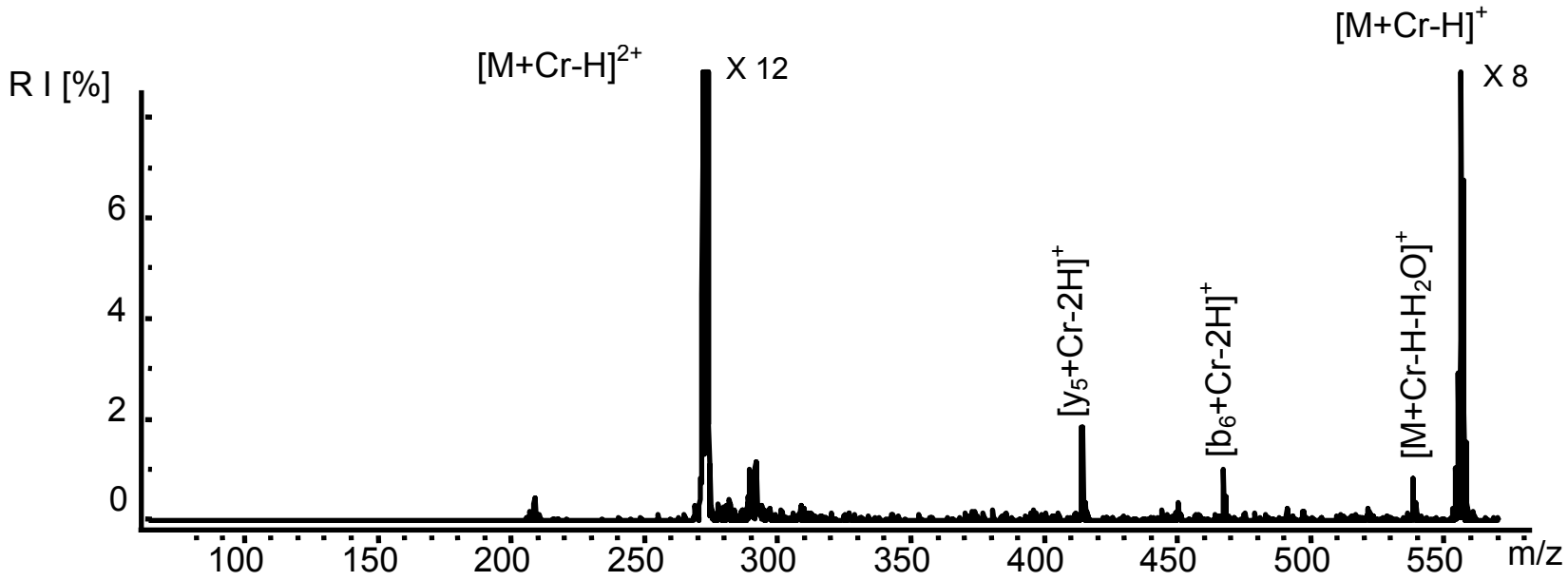

Figure 4.1. ETD spectrum of $[M + Cr - H]^{2+}$ produced by heptaalanine cationized by Cr(III).

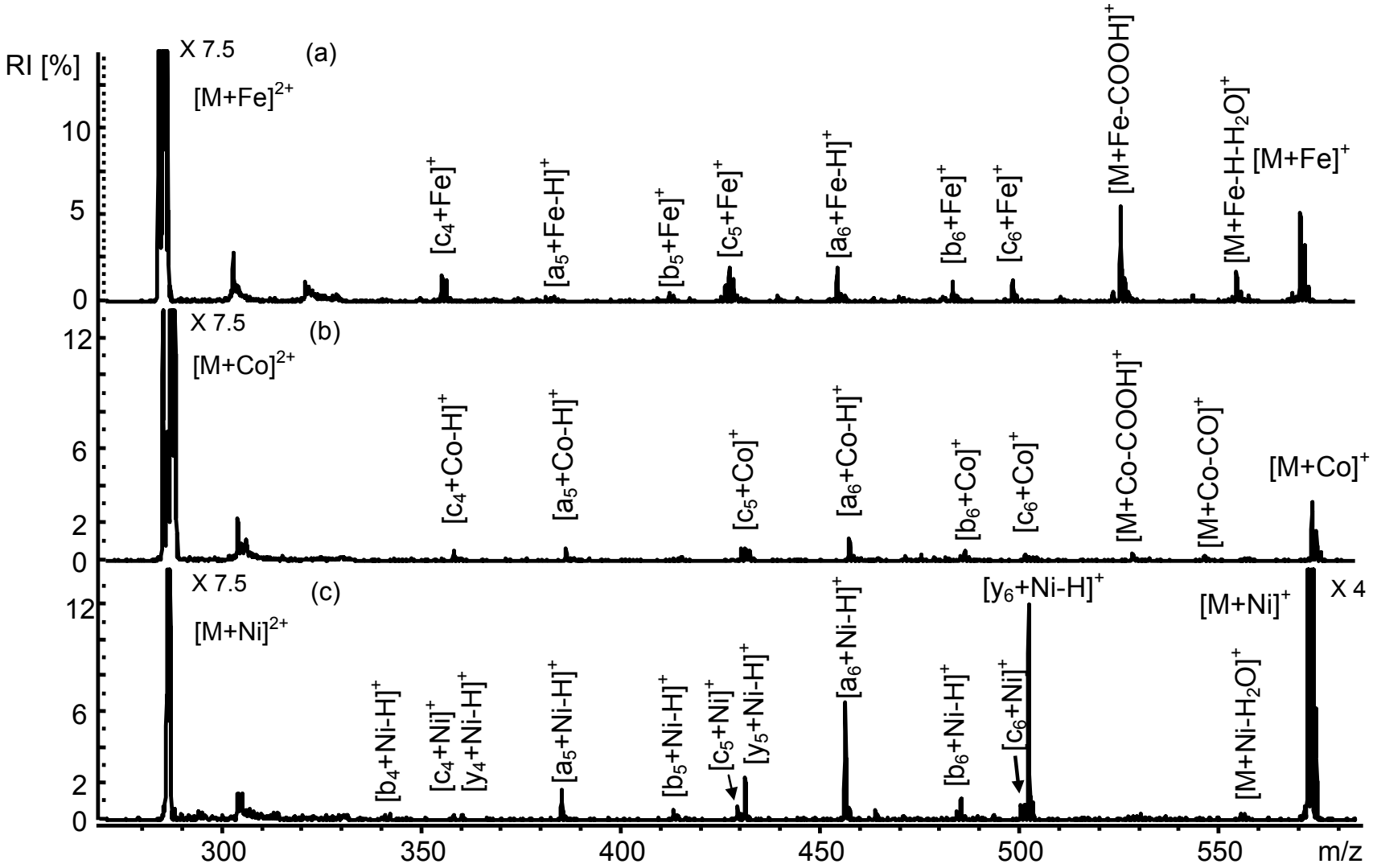

Figure 4.2. ETD spectra of $[M + Met]^{2+}$ produced from heptaalanine cationized by (a) Fe(II), (b) Co(II), and (c) Ni(II).

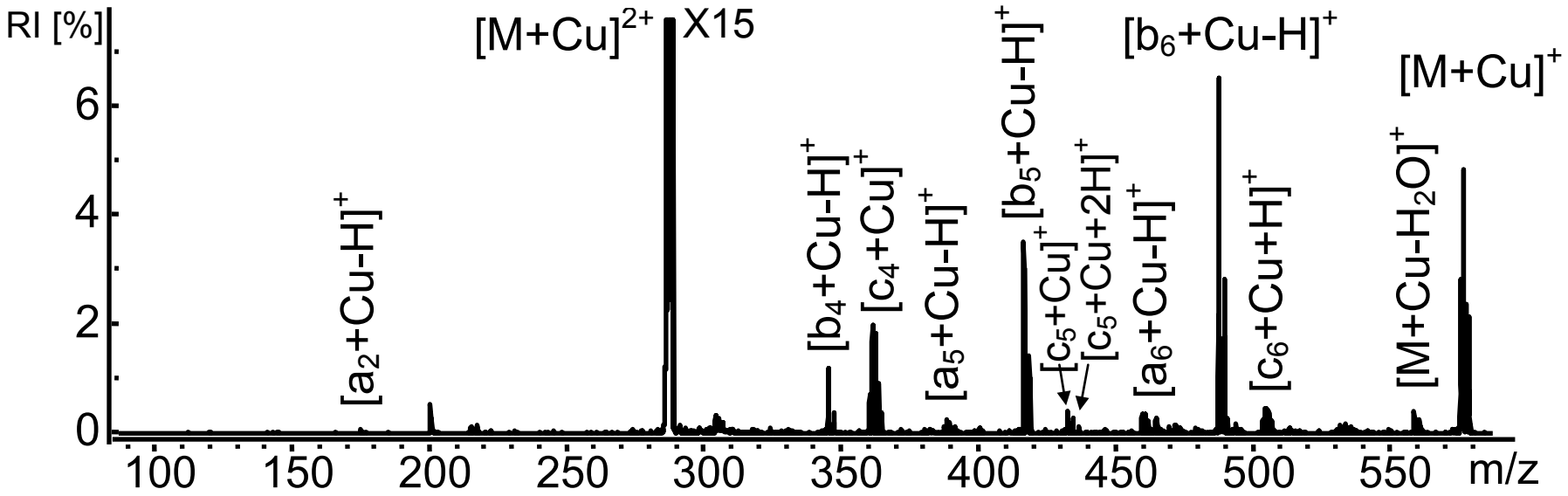

Figure 4.3. ETD spectrum of $[M + Cu]^{2+}$ produced from heptaalanine cationized by Cu(II).

4.3.1 Metal Ion Effects on Sequencing/Backbone Cleavages

Interestingly, heptaalanine cationized by different transition metal ions produce different ETD tandem mass spectra. Typical ETD product ions from protonated peptides such as c- and z-ions[39] are not the most prevalent products after transition metal-cationization. For transition metal-cationized peptides, c-ions form but are not the most prominent product ions and z-ions do not form. The spectrum produced from Cr(III) cationization is drastically different from those produced by members of the "iron triad" (Fe, Co, and Ni) and different still from those produced by Cu(II). Products formed by ETD of all transition metallated heptaalanines and their relative intensities are given in Table 4.1.

ETD of $[M + Cr - H]^{2+}$ produced from a mixture of Cr(III) chloride salt and heptaalanine provides very little sequence information (Figure 4.1). The most prominent feature is the reduced precursor ion, $[M + Cr - H]^{+}$, which loses water forming $[M + Cr - H - H_2O]^{+}$. The loss of water and limited fragmentation is similar to what is observed during the CID of the same precursor, as discussed in Chapter 3, (see Figure 4.4) but even less fragmentation is observed by ETD. More product ions are formed by ETD on all other transition metals studied than with Cr(III).

Highly protonated species may lead to more fragmentation as a result of Coulombic repulsions between the protons.[40] In contrast, increasing ion charge with di- and tri-valent metals may not follow this trend since the charge results from the metal only on a given precursor ion and the charge is not spread among multiple locations. Attempts to carry out ETD on Fe(III) complexes were unsuccessful due to difficulties

Table 4.1. ETD products from $[M + Cr - H]^{2+}$ and $[M + Met]^{2+}$ for heptaalanine cationized by Met = Fe(II), Co(II), Ni(II), and Cu(II).

$[M+Cr-H]^{2+}$ [a]

	A (n=1)	A (n=2)	A (n=2)	A (n=3)	A (n=4)	A (n=5)	A (n=6)	A (n=7)
b_n+Cr-2H							1[b]	
y_{8-n}+Cr-2H				2				
Neutral loss: $[M-H_2O]^+$								

$[M+Co]^{2+}$

	A (n=1)	A (n=2)	A (n=2)	A (n=3)	A (n=4)	A (n=5)	A (n=6)	A (n=7)
a_n+Co-H							0.5	
a_n+Co-H-CO						0.5		
b_n+Co							0.7	
c_n+Co						0.8	0.5	
Neutral loss: $[M+Co-CO]^+$ $[M+Co-COOH]^+$								

$[M+Cu]^{2+}$

	A (n=1)	A (n=2)	A (n=2)	A (n=3)	A (n=4)	A (n=5)	A (n=6)	A (n=7)
a_n+Cu-H						0.3	0.1	
b_n+Cu-H					1.2	3.3	6.5	
c_n+Cu+H					1.8		0.5	
c_n+Cu					2	0.2		
Neutral loss: $[M+Cu-H_2O]^+$								

$[M+Fe]^{2+}$

	A (n=1)	A (n=2)	A (n=3)	A (n=4)	A (n=5)	A (n=6)	A (n=7)
a_n+Fe-H					0.2	2	5
b_n+Fe					0.5	1	2
c_n+Fe				1.2	2	1	

$[M+Ni]^{2+}$

	A (n=1)	A (n=2)	A (n=3)	A (n=4)	A (n=5)	A (n=6)	A (n=7)
a_n+Ni-H					2.2	6	
b_n+Ni-H					0.75	1.4	
c_n+Ni				0.4	3	1.1	
$[y_{(8-n)}$+Ni-2H]		12	2.5	0.5			

[a] Precursor ion.

[b] Values are % relative intensity where the base peak is undissociated precursor ion.

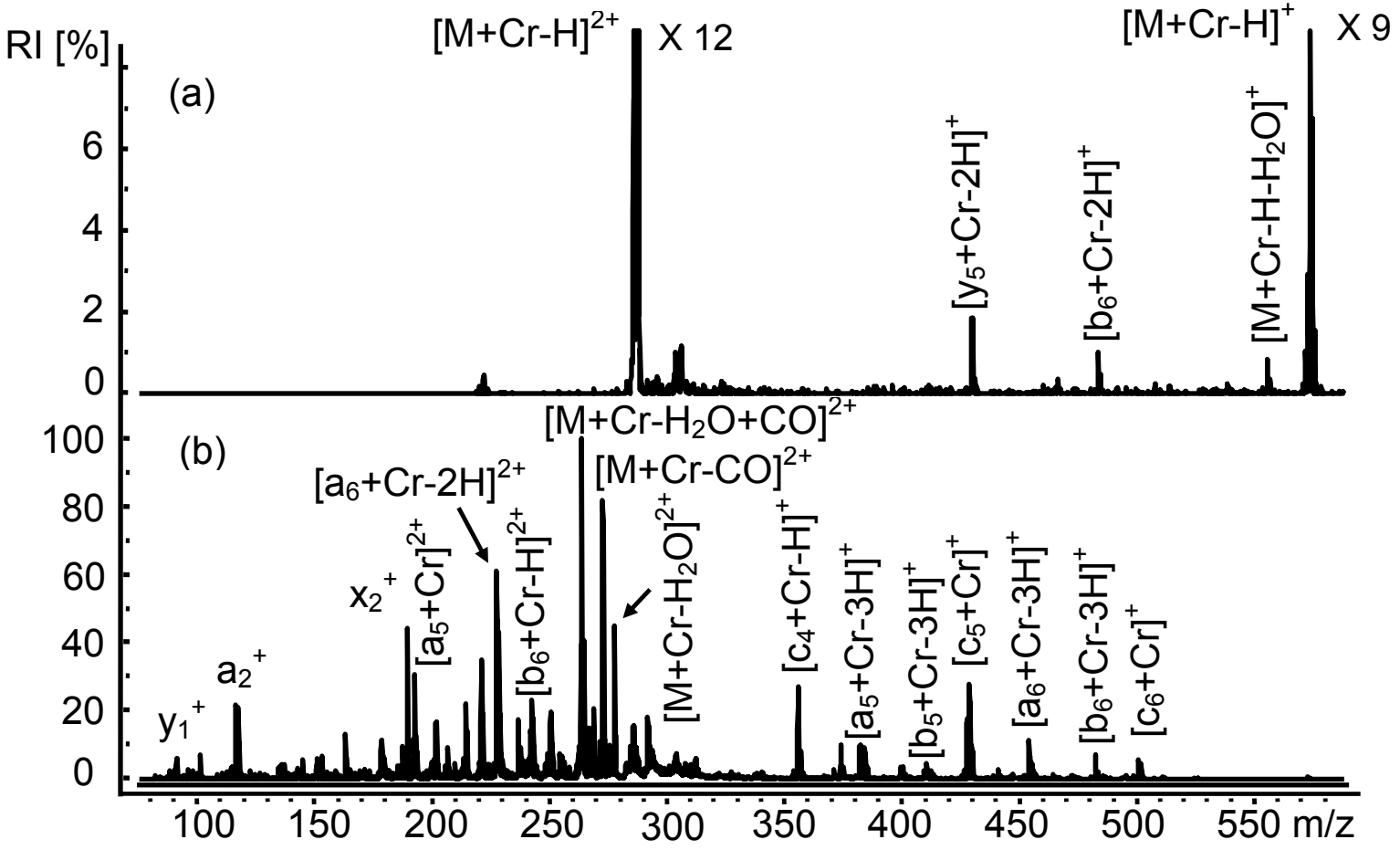

Figure 4.4. Comparison of (a) ETD and (b) CID of heptaalanine cationized by Cr(III), $[M + Cr - H]^{2+}$.

ionizing the samples with ESI and nanoESI. The low intensities of $[M + Fe - H]^{2+}$ produced during ionization were difficult to perform ETD reactions with. As a result, Cr(III) was the only trivalent metal studied. The higher affinity of Cr(III) for the transferred electron (than the divalent metal ions) may have reduced the metal to Cr(II). This could result in the charge becoming localized at the metal ion preventing extensive dissociation along the peptide backbone.

In ETD, a correlation of ionization energy (IE) values to recombination energy (RE, energy released when an electron is added to an ionized molecule) is applicable because the energy involved is the reverse process of vertical ionization energy. Theoretical and experimental studies have investigated the RE effects on ETD.[9, 29, 30, 41] Iavarone et al.[9] found that electron capture occurs at the site with the highest RE and Jensen et al.[41] observed that the likelihood of N-Cα cleavage decreases as the RE of the charge site increases. According to these findings, metal ions with higher RE are more likely to be the site of electron capture and the product ions that appear in the resulting ETD spectra are less likely to be c- and z-type ions.

Cr(III) has a third ionization energy (IE3) of 31 eV. This is 10-15 eV larger than the second ionization energies (IE2s) of the divalent metals studied here (Table 4.2).[42, 43] In the case of Cr(III), an electron that is added to the trivalent chromium may release enough energy to cause vibrational type dissociation at the weakest part of the peptide bond (based on bond energies, C-N[44]) to give b- and y-ions, similar to CID.

The ETD spectra obtained after cationization by Fe(II) and Co(II) are very similar in both ion types and abundances as shown in Figure 4.2. The most prominent peaks are of the precursors $[M + Met]^{2+}$ that did not undergo ETD. This is not unexpected because

Table 4.2. The ionic radii, ligand exchange rates, electron configurations, and ionization energies of the transition metal ions studied.

	Ionic Radii (Å)[a]						
Metal	**4-Coordinate**	**6-Coordinate (low/high spin)**	**8-Coordinate**	**Exchange rates[b] (k_1, sec^{-1})**	**# of d electrons[b]**	**IE2 (eV)[a]**	**IE3 (eV)[a]**
Cr^{3+}				2×10^{-6}	3		30.96
Fe^{2+}	0.77	0.75/0.92	1.06	4×10^{6}	6	16.2	
Co^{2+}	0.72	0.75/0.88	1.04	3×10^{6}	7	17.1	
Ni^{2+}	0.69	0.83	----	4×10^{4}	8	18.2	
Cu^{2+}	0.71	0.87	----	1×10^{9}	9	20.3	

[a]Values are from CRC Handbook of Chemistry and Physics.[42]
[b]Values are from Principles of Bioinorganic Chemistry[43] and based on exchange rates for water molecules from the first coordination sphere of metal ions at 25°C.

protonated peptides also have low ETD reaction efficiencies and intense unreacted precursor ion peaks.[13, 14] Both $[M + Fe]^{2+}$ and $[M + Co]^{2+}$ lose COOH and also exhibit minimal H_2O and CO loss for Fe(II) and Co(II), respectively. All backbone cleavage products are singly charged, retain the metal ion, and include the N-terminus (a-, b-, and c-ions) with no neutral losses. Simple cleavage is observed for b- and c-ions, $[b_n + Met]^+$ and $[c_n + Met]^+$, whereas a-series ions form by addition of the metal and loss of one hydrogen, $[a_n + Met - H]^+$. For both Fe(II) and Co(II), the same three out of six possible backbone cleavages occur by ETD (at n = 4-6). While fewer neutral losses occur and fewer complexities are formed with these two ions compared to CID of the same complexes (Figures 4.5 and 4.6), they only lead to 50% sequence coverage. The similarities of spectra produced by Fe(II) and Co(II) are not unexpected considering the similar properties of these ions as shown in Table 4.2. Consider the lability of the metal-ligand interactions by using the ligand exchange rates shown in Table 4.2. These values demonstrate the vast difference (15 orders of magnitude between Cr(III) and Cu(II)), in the rates at which bonds between the metal ions and ligands are breaking and reforming. The ligand exchange rates of Fe(II) and Co(II), relative to the other metal ions studied, are very similar and may indicate that these metal ions share similar coordination geometries and coordination sites on the peptides.

The ETD spectrum of $[M + Ni]^{2+}$, Figure 4.2, has higher product ion intensities than those typically formed with the other metals; some products have greater than 10% relative intensity (RI). The reduced precursor is at 50% RI. Metallated N-terminal products form for $n \geq 4$ as with other transition metals studied and include $[a_n + Ni - H]^+$ for n = 5-6; $[b_n + Ni - H]^+$ for n = 4-6; and $[c_n + Ni]^+$ for n = 4-6. In addition to

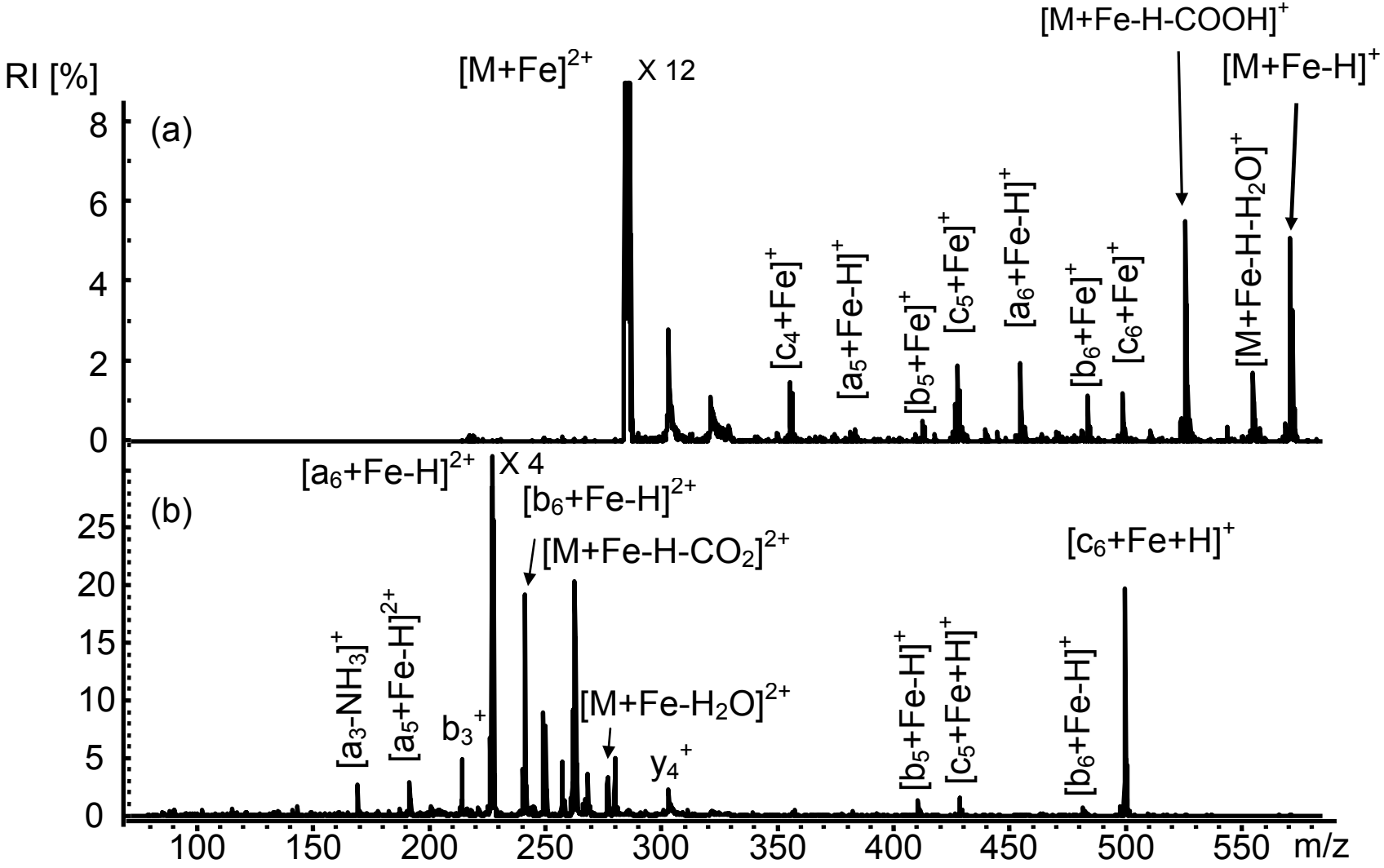

Figure 4.5. Comparison of (a) ETD and (b) CID spectra from heptaalanine cationized by Fe(II), $[M + Fe]^{2+}$.

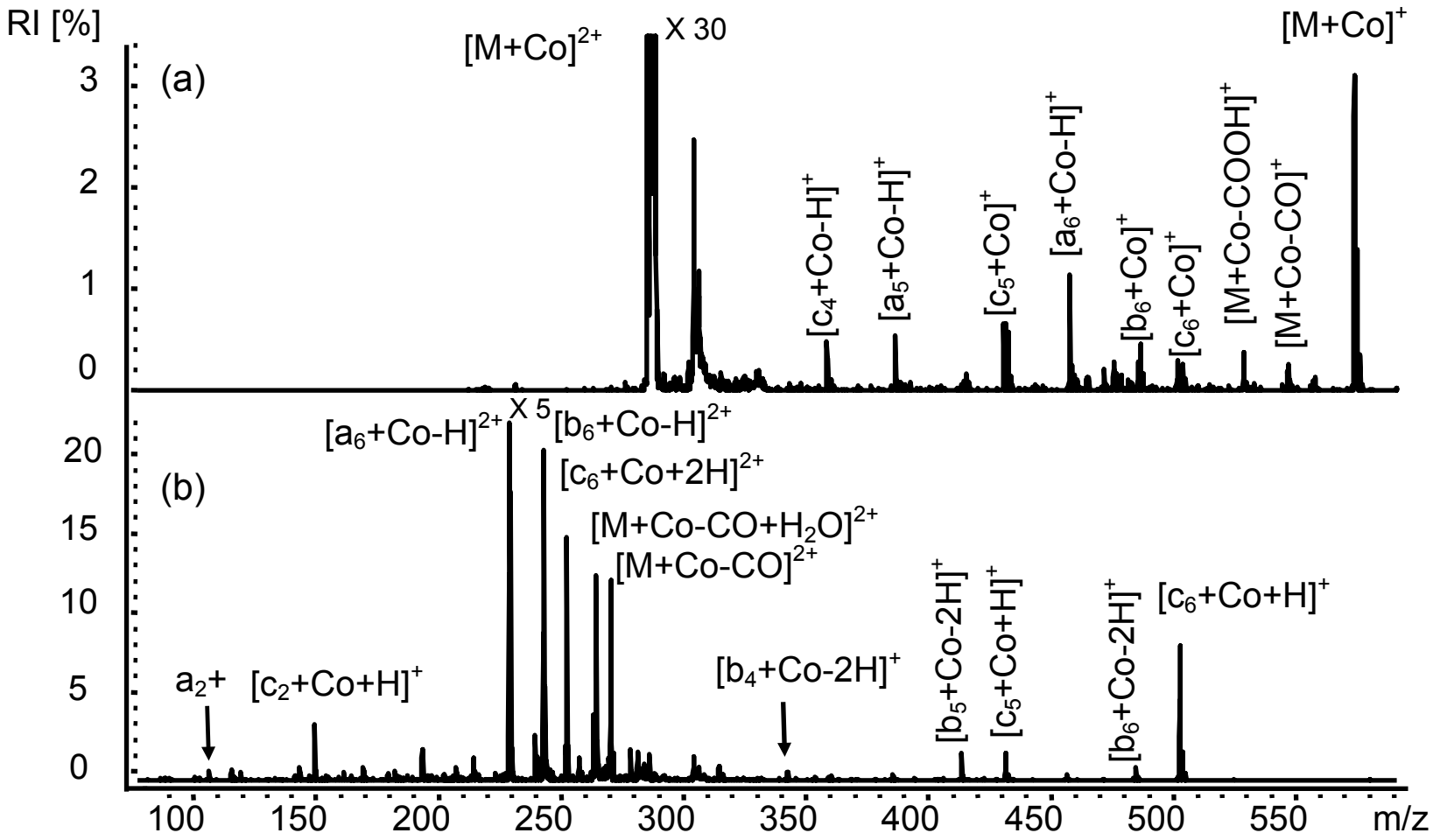

Figure 4.6. Comparison of (a) ETD and (b) CID of heptaalanine cationized by Co(II), $[M + Co]^{2+}$.

metallated N-terminal products, Ni(II) complexes give metallated y-ions, which formed as $[y_n + Ni - 2H]^+$ for n = 4-6. The formation of these additional C-terminal products allows complete sequence coverage (six out of six backbone cleavages) to be attained, whereas CID of the same complex gives five out of six possible backbone cleavages as shown in Figure 4.7. Metallated N-terminal ions form in the CID spectra with Ni(II) peptide complexes as well (see Figure 3.9).

The formation of metallated y-ions by ECD on Ni(II)-oxytocin complexes has been observed by Kleinnijenhuis et al.,[26] where the most intense metallated y-ion forms from cleavage between S-S bonds. ECD preferentially cleaves protonated species between S-S bonds. Therefore the electron capture preference for the oxytocin S-S bonds during ECD is likely driving this intense y-ion production. However, less intense metallated y-ions also form with Ni(II)-oxytocin complexes at locations that have no S-S bonds.[26] The alanine- and glycine- containing peptides studied in this work do not have the complexity of S-S bonds to consider. Therefore, the y-ions produced are a result of Ni(II) cationization. Initial Ni(II)-peptide complexes may have Ni(II) coordinated to the N- and the C-termini based on the propensity of Ni(II), whether by CID or ETD, to form metallated C- and N-terminal product ions.

Electron-transfer dissociation of $[M + Cu]^{2+}$ produces $[M + Cu]^+$ as well as $[M + Cu - H_2O]^+$. The a- and c-ions form in similar abundances to analogous ions produced from ETD of $[M + Co]^{2+}$ and $[M + Fe]^{2+}$; however, the b-series ions produced in the Cu(II) spectra are more intense. Kleinnijenhuis et al.[26] noted only metallated b-ions (and neutral losses) in their ECD work with oxytocin Cu^{2+} complexes. They proposed that the electron was captured at the metal, reducing Cu^{2+} to Cu^+, resulting in a

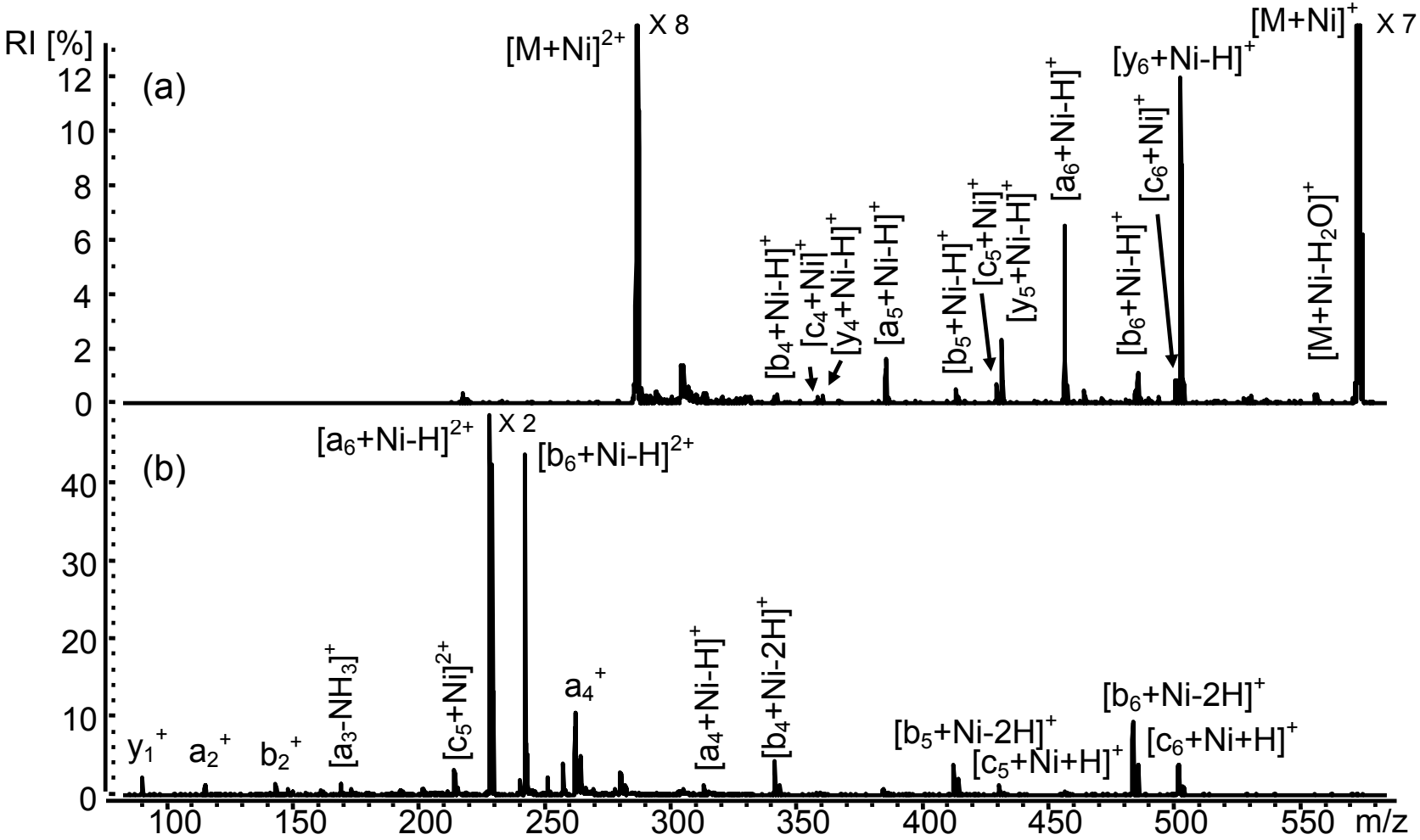

Figure 4.7. Comparison of (a) ETD and (b) CID of heptaalanine cationized by Ni(II), $[M + Ni]^{2+}$.

closed d-shell (See Table 4.2) and preventing electron participation in the radical-driven dissociation typical of ECD and ETD. The resulting reduced species is vibrationally excited, and typical CID products form as result of the recombination energy, not by expected ETD pathways. Similarly in this ETD work, the relatively intense metallated b-ions may be forming as a result of Cu(II) reduction. In ETD, the recombination energy effect is less than in ECD[45] because of the low electron binding energy of the ETD reagent (fluoranthene); however, the presence of metal cations with higher IE2s, like Cu(II) and Cr(III) (see Table 4.2) likely increases the RE effects because of the high affinities of metal cations for the transferred electron. The presence of metallated a- and c-ions suggests that competing pathways exist: one by redistribution of vibrational energy, and another involving either the transferred electron or a released $H^{\bullet}$ as expected by typical ECD/ETD pathways.

The presence of $[a_2 + Cu - H]^+$ allows identification of the peptide's second amino acid residue, which is not possible in the spectra of $[M + Fe]^{2+}$ and $[M + Co]^{2+}$. The addition of zero, one, or two H to metallated c-ions occurs. Similarly, the loss of H for metallated c-ions has been noted for alkaline earth metal ion-peptide complexes.[22, 24] Note that ETD of $[M + Cu]^{2+}$ produces an a-ion series that is 28 Da (CO elimination) lower in mass than b-ions. This is unlike the same complex dissociated by CID (Figure 4.8), which forms an a-ion series 26 Da lower in mass than b-ions ($[a_n + Cu]^+$ and $[b_n + Cu - 2H]^+$). This is also unlike the b-ions formed from Fe(II) and Co(II) complexes by ETD (Figure 4.2) where a-ions form 29 Da lower in mass than b-ions. This may lead to easier interpretation because there is only one type of a-ion to consider. However,

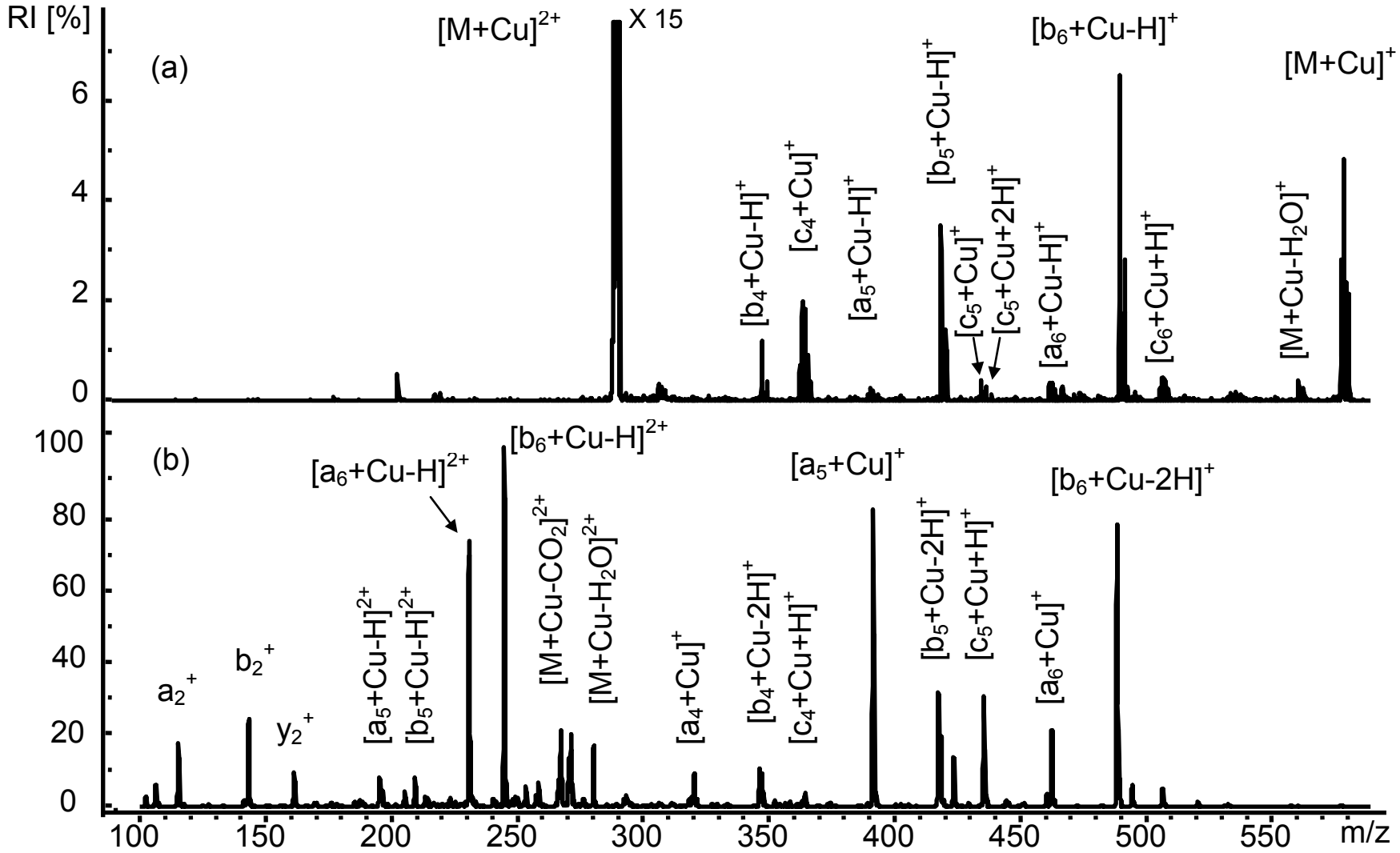

Figure 4.8. Comparison of (a) ETD and (b) CID spectra resulting from heptaalanine cationization by Cu(II), $[M + Cu]^{2+}$.

different types of c-ions are forming, all metallated, some with no additional hydrogens and others with one and two additional hydrogens.

The atypical ETD spectra produced with Cu(II)-peptide complexes may also be attributed to ligand exchange rates, as shown in Table 4.2. Of all of the metal ions studied here, Cu(II) has the fastest ligand exchange rate. The unusual reactivity of Cu(II) with peptides to produce increased fragmentation by CID, and to eliminate carbon by CID and ETD, may result from greater mobility of the Cu(II) in the gas phase. This, combined with the stable $3d^{10}$ electron configuration and a comparatively higher IE2 value for Cu(II), makes it difficult to determine the exact cause for the unusual spectra. Further investigation of these properties is clearly needed to distinguish true contributing factors.

The trend observed by Jensen et al.[41] for a decrease in N-Cα cleavages with increasing RE is consistent with the results obtained in this work. N-Cα cleavage in peptides leads to formation of c- and z-type product ions in mass spectra. Therefore, as the RE of the metal ions increase, the number of N-Cα cleavages (c-ions) decrease. This can be seen in Figures 4.9 - 4.11, where the RE of Cr(III) > Cu(II) > Ni(II) > Co(II) > Fe(II).

ETD Fibrinopeptide B-Cu(II)

Observations of b-ions in the ETD spectra of peptides containing no or few basic amino residues have been made. Liu and Hakansson[46] suggest that these b-ions form from either vibrationally excited precursor ions or from nitrogen-protonated conformers, which directly result from the peptide's low basicity. To investigate whether it is the

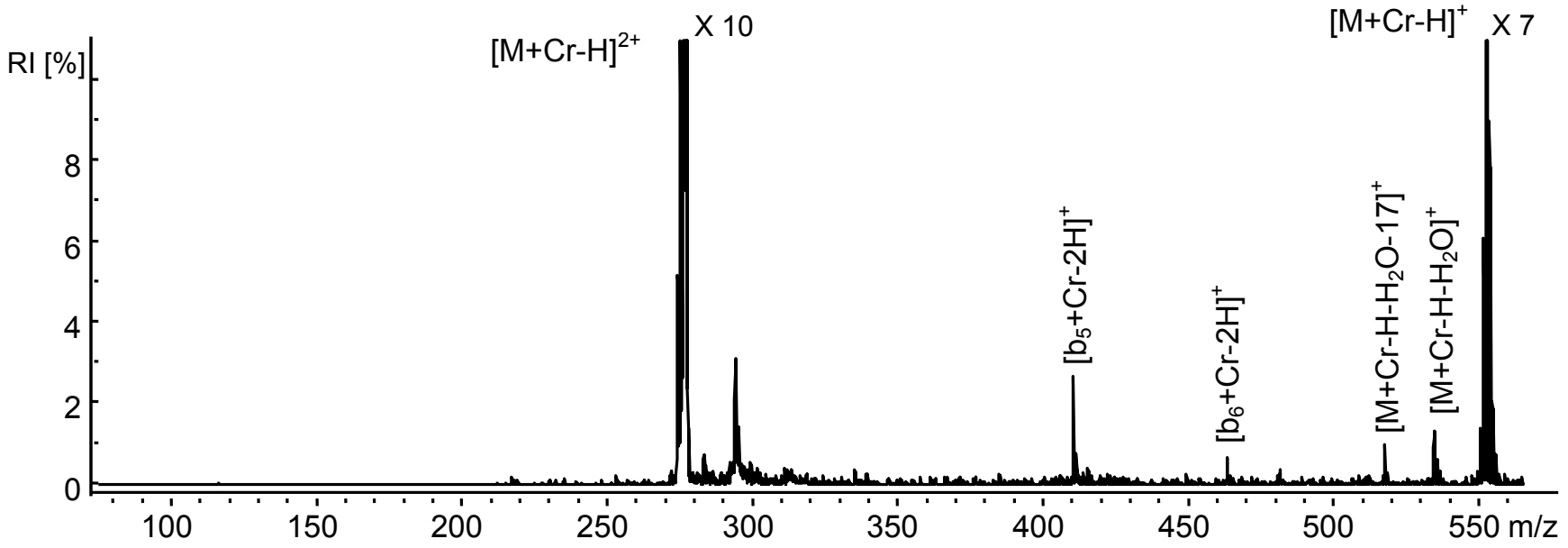

Figure 4.9. ETD spectra produced from AAAAAGA cationized by Cr(III), $[M + Cr - H]^{2+}$.

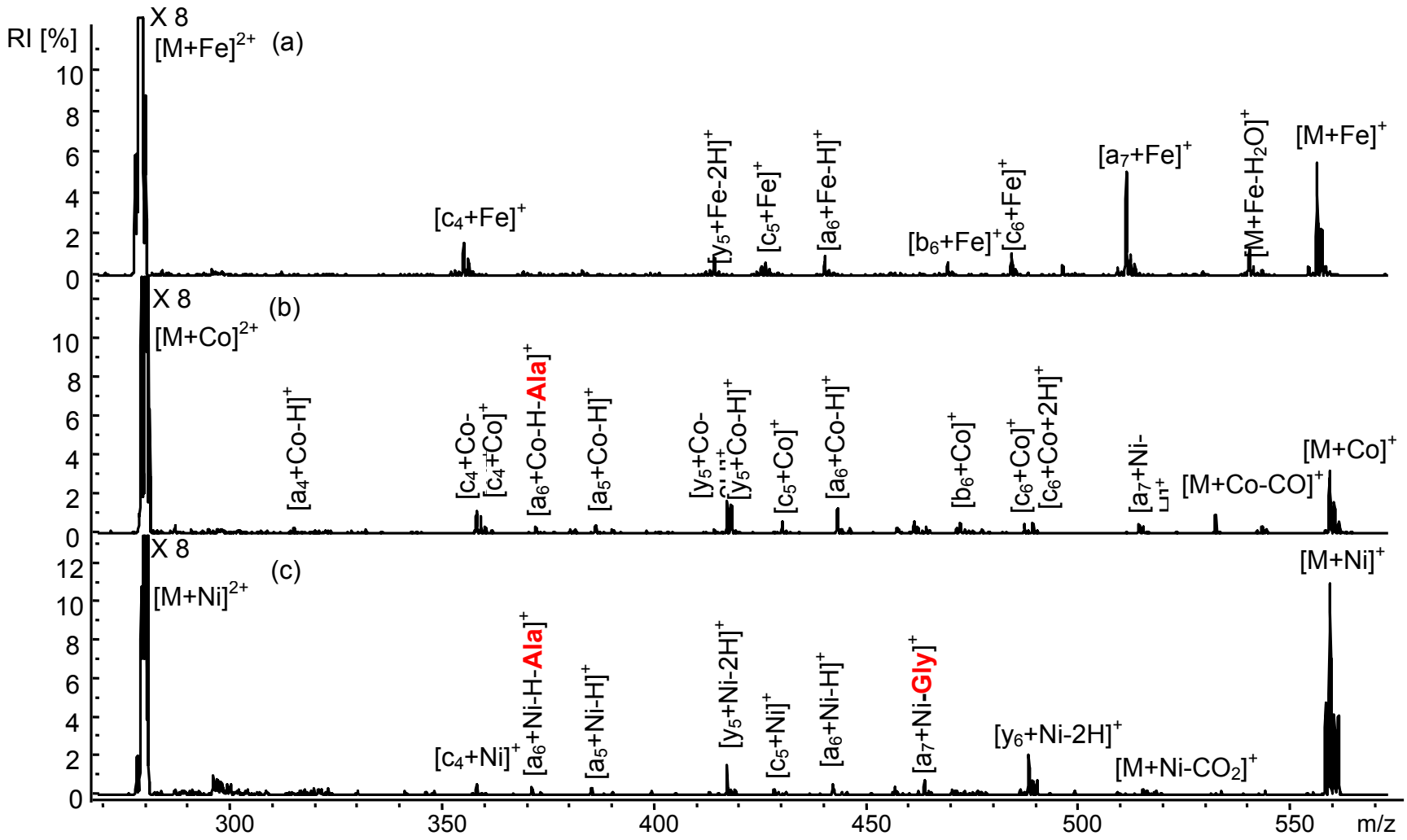

Figure 4.10. ETD spectra of AAAAAGA cationized by (a) Fe(II), (b) Co(II), and (c) Ni(II), $[M + Met]^{2+}$. Note nonsequential losses in red (or bold).

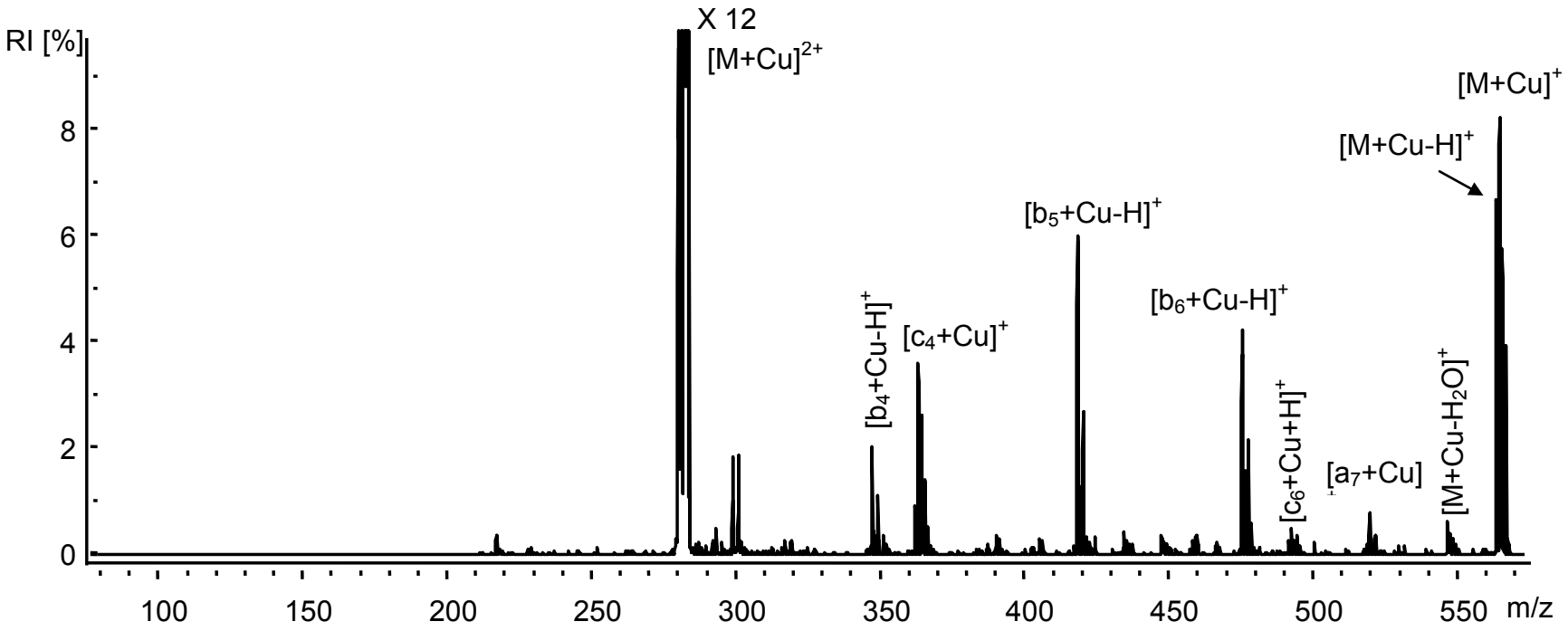

Figure 4.11. ETD spectrum of AAAAAGA cationized by Cu(II), $[M + Cu]^{2+}$.

metal ions or the lack of basic amino acid residues that is contributing to the increased b-ion formation in the ETD spectra of this work, fibrinopeptide B (containing one basic residue arginine) was complexed with Co(II) and submitted to ETD. The spectrum of $[M + 2H]^{2+}$ from fibrinopeptide B (pEGVNDNEEGFFSAR) contains the z-ion series; no b-ions are produced, as shown in Figure 4.12. For comparison, $[M + Co]^{2+}$ (M = fibrinopeptide B) was submitted to ETD and resulted in b- and y-ion formation and no z-ions. This data on $[M + Co]^{2+}$ of fibrinopeptide B suggests that metal cationization and not the lack of basic amino acid residues is contributing to the b-ion formation in these studies. However, additional studies with more basic peptides will be necessary to conclusively state that the presence of a metal ion promotes b- and y-ion formation.

4.3.2 Comparisons to CID

As with CID of the transition metal-peptide complexes, which are discussed in Chapter 3, metallated products dominate the ETD spectra. However in CID, a mixture of both metallated and nonmetallated products are present. ETD spectra are cleaner and less complex with no need to consider multiply charged products, but product ions are also less intense than with CID. The intense metallated a-ions that dominate all CID spectra are not as prevalent in ETD spectra. The metal ions chosen for study play a role in the mechanism of ion production in both techniques. For example, the mechanism of metallated a-ion formation could involve the elimination of CO from metallated b-ions in the case of ETD of Ni(II)- and Cu(II)-peptide complexes (Figure 4.2 and 4.3) whereas with Fe(II)- and Co(II)-peptide complexes, the metallated a-ions are produced 29 Da lower in *m/z* than metallated b-ions (Figure 4.2). Utilizing the CID and ETD spectra

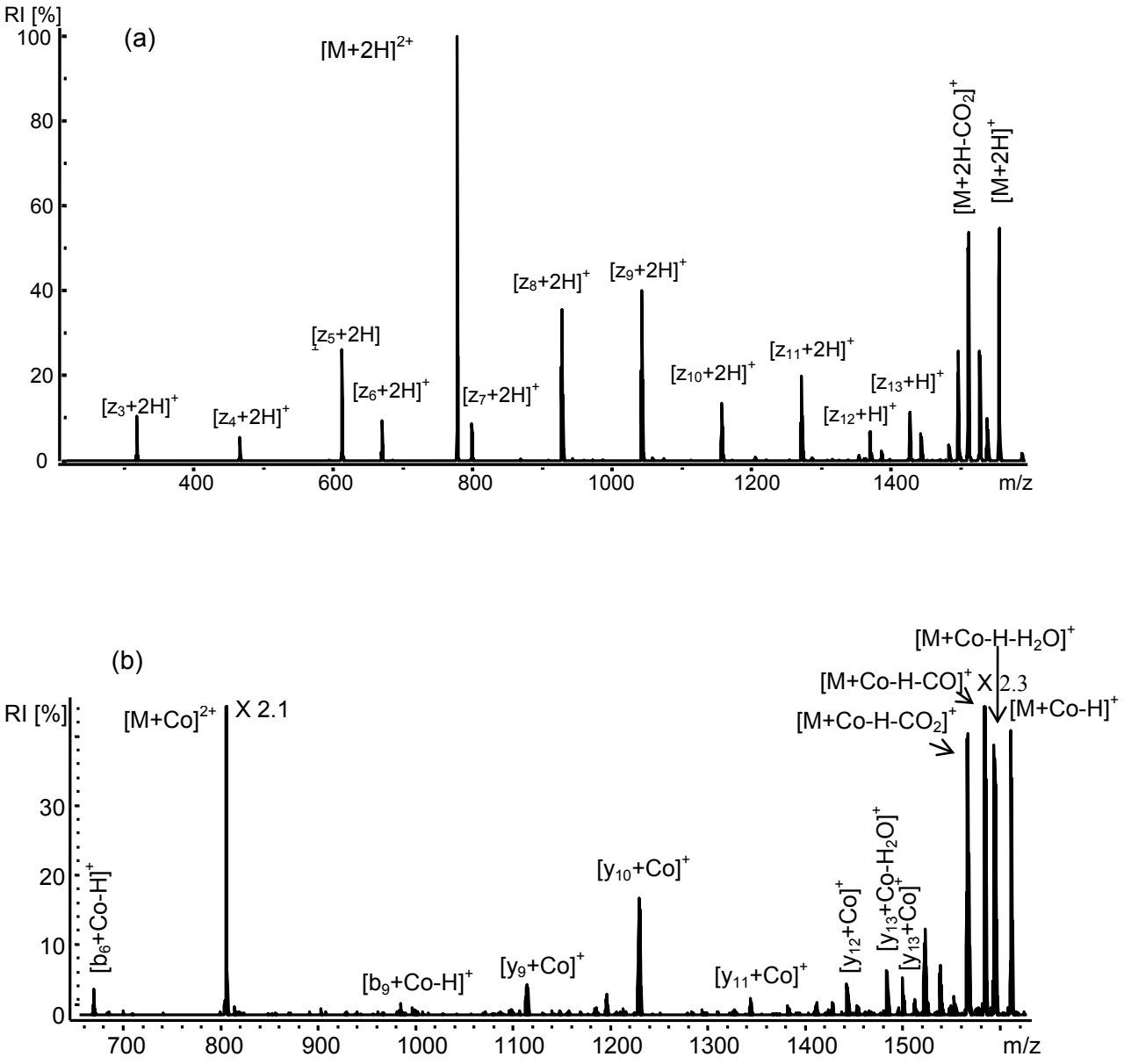

Figure 4.12. ETD spectra of (a) $[M + 2H]^{2+}$ and (b) $[M + Co]^{2+}$ from fibrinopeptide B.

produced with Fe(II) together gives a total of 4/6 backbone cleavages (Figure 4.5). Comparing ETD and CID of Co(II)-peptide complexes (Figure 4.6) reveals that CID results in identification at the second amino acid residue because of the formation of a_2^+ and $[c_2 + Co + H]^+$. Advantages of ETD include all singly charged, metallated products. Also, although both produce neutral losses (CO and H_2O), in CID these product ions are more prevalent and doubly charged, which increases complexity. ETD of Ni(II) peptide complexes result in increased fragmentation and complete sequence information. Consequently, Ni(II) may be useful as a cationization reagent in de novo sequencing. The results of this study support other findings[3] that ETD and CID should be used together to increase sequence coverage and accuracy when using search engines during high throughput proteomics.

4.3.3 Macrocyclic a- and b-Ions. Do They Exist? Do They Scramble Sequence Information?

In addition to increasing the number of backbone fragmentation sites, minimizing rearrangements is also important to prevent possible loss of sequence information caused by "scrambling." Sequence scrambling was first observed by Harrison *et al*. during CID from b-ions that were proposed to be macrocylic.[47] Studies have shown that macrocyclic b_n-ions ($n \geq 3$) can form in gas-phase CID experiments.[48] This could lead to possible ring opening of the macrocycle and elimination of an "internal" residue (see Figure 4.13). This "nonsequential" ion could complicate the sequencing process. Recently, macrocyclic a-ions have been observed and have been the subject of sequence scrambling research. In addition, the existence of macrocyclic a- and b-ions in CID has been the focus of several studies.[47-56] Investigations of large numbers of MS^n spectra have

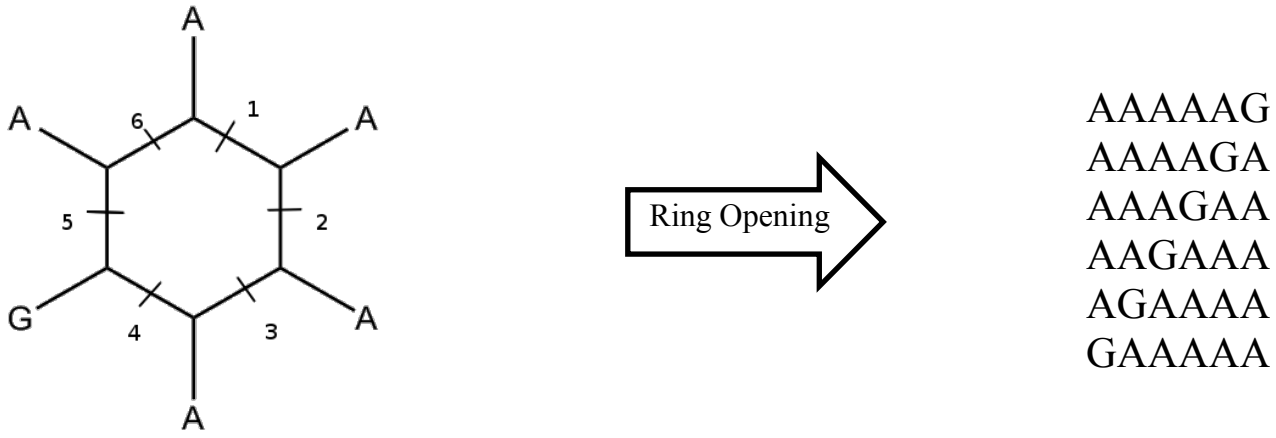

Figure 4.13. Different sequence scrambling possibilities that can follow ring opening from a macrocyclic ion. Amino acid residues can also be eliminated in the process.

concluded that b-ion scrambling during CID does not negatively impact the accuracy of database searches.[57, 58]

To determine if this type of nonsequential loss occurs during ETD of transition metal-cationized peptides, asymmetric polypeptides were synthesized and submitted to transition metal-cationization and ETD. Because most examples of sequence scrambling have been reported from protonated peptides during CID, the CID experiments on the protonated peptides were carried out for comparison. For example, CID of the $[M + H]^+$ formed by ESI of GGAAAAA, AGAGAAA, AAGGAAA, AAAGGAA, and AAAAAGA are shown in Figure 4.14. All peptides except GGAAAAA produce at least one nonsequential loss. For example, the peptide AAAAAGA forms an intense b_6^+ ion that eliminates an Ala to form $[b_6^+ - Ala]^+$, as shown in Figure 4.10. A b_5^+ forms 14 Da higher in mass (the difference being that of the Ala and Gly side chains CH_3 versus H). To produce $[b_6^+ - Ala]^+$ from AAAAAG (the amino acids remaining in b_6^+), a ring opening of a macrocyclic b_6^+ structure must occur.

Figures 4.9-4.11 are spectra produced from ETD on all AAAAAGA transition metal complexes. For ETD of $[M + Met]^{2+}$ with Met = Co and Ni, nonsequential ions form. For example, in Figure 4.12 $[a_6 + Co - H - Ala]^+$, and $[a_6 + Ni - H - Ala]^+$ and $[a_7 + Ni - Gly]^+$ are observed. Nonsequential product ion formation does not seem to occur with the other metal ions studied and goes undetected when using the simple heptaalanine model because all amino acid residues are the same. Without a mass label such as ^{13}C or a different amino acid present in the peptide sequence, there can be macrocycles forming and sequence scrambling as a result, but no way to detect them. Although the studies that have examined the nonsequential losses or sequence scrambling

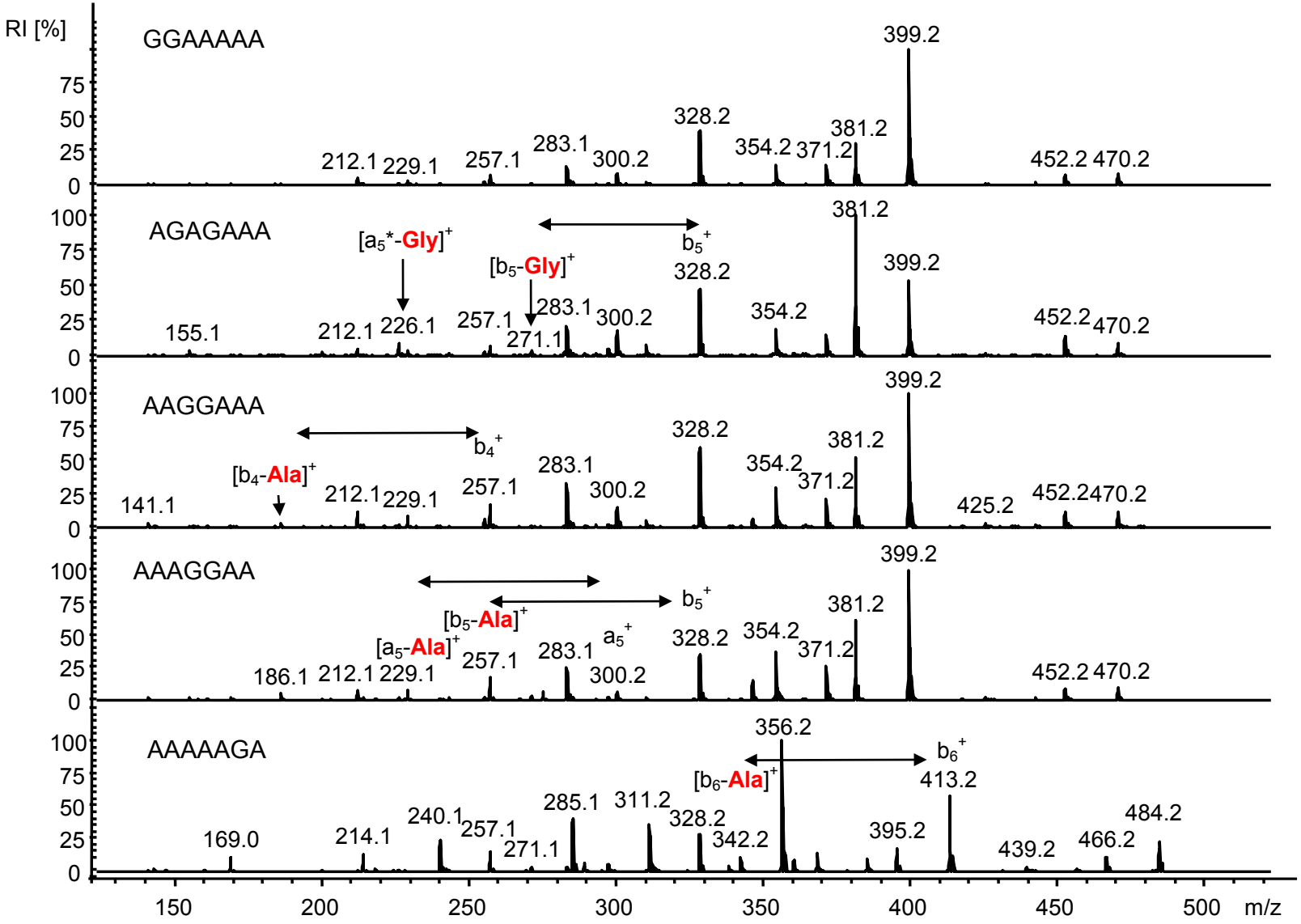

Figure 4.14. CID spectra obtained from five protonated, $[M + H]^+$, heptapeptides. Note the loss of nonsequential ions indicated in red (or bold).

have done so by CID, one study has recently shown evidence for macrocyclic b-ions during ECD.[59] This theoretical and experimental study of b-ions formed from ECD of substance P identifies several b-ion structures, including macrocyclic structures. To my knowledge the work presented in this dissertation is the only evidence for b- and a-ion macrocyclic structures forming during ETD.

4.4 Conclusions

Peptides that lack basic amino acid residues can not multiply protonate and thus can not be readily studied by ETD. Cationization by transition metals produces multiply charged ions by ESI (and nanoESI) that, when submitted to ETD, give sequence informative ions. The identity of the metal used for cationization determines its usefulness in sequencing. The results indicate that the ionization energies (IE2/IE3) of the metal ions may influence the dissociation behaviors after electron transfer. Transition metals with higher recombination energies tend to form fewer N-Cα cleavages and more b- and y-type ions. Metal ions with higher recombination energies may produce more b- and y-type ions due to vibrationally translated energy. Vibrational excitation is also the major pathway of energy distribution by CID. Consequently, metal cationization of peptides results in both ETD and CID exhibiting similar fragmentation pathways. The ions formed by ETD of the metallated peptides do not exhibit the typical c- or z-ion series typical of protonated peptides, but instead produce a-, b-, c-, and y-ion formation as produced by CID of the same complexes. Whether these differences relate to conformational differences or a result of the various characteristics of the metal ions themselves is not clear. Other trends such as ligand exchange rates, electronegativies,

and ionic radii may also be in play. The results presented in this work indicate that no single answer fully explains these behaviors.

For the ETD spectra produced here, all backbone cleavage products are singly charged. This makes product ion assignment less complex because the consideration of multiply charged product ions is unnecessary unlike the variously charged products formed by CID. As in CID, sequence coverage of the transition metal-cationized peptides by ETD is dependent on the identity of the metal. The additional y-ions that form after Ni(II) cationization lead to complete sequence coverage. These results indicate that N(II) may be the best cationizing reagent for peptide sequencing by ETD. During ETD, all product ions retain the metal. This is also unlike CID that produced both metallated and nonmetallated products with, which leads to increased spectral complexity and the need to manually inspect isotopic distributions for metal contributions where applicable.

Interesting product ions are found in the ETD spectra of peptides complexed with Co(II) and Ni(II). These metallated a- and b-ions are likely forming macrocycles and reopening to eliminate an amino acid residue. This appears as nonsequential losses in ETD spectra. This is the first time that evidence of macrocyclic ions has been reported in the ETD of metallated-peptides.

REFERENCES

1. M. Tyers; M. Mann, From genomics to proteomics. *Nature* **2003,** 422, 193-197.

2. R. Service, PROTEOMICS: New database to track protein locations. *Science* **2005,** 309, 1310.

3. R. Zubarev; A. Zubarev; M. Savitski, Electron capture/transfer versus collisionally activated/induced dissociations: Solo or duet? *J. Am. Soc. Mass Spectrom.* **2008,** 19, 753-761.

4. J. Wells; S. McLuckey, Collision-induced dissociation (CID) of peptides and proteins. *Methods Enzymol.* **2005,** 402, 148-185.

5. J. E. P. Syka; J. J. Coon; M. J. Schroeder; J. Shabanowitz; D. F. Hunt, Peptide and protein sequence analysis by electron transfer dissociation mass spectrometry. *Proc. Natl. Acad. Sci.* **2004,** 101, 9528-9533.

6. F. Kjeldsen; K. Haselmann; B. A. Budnik; F. Jensen; A. R. Zubarev, Dissociative capture of hot electrons by polypeptide polycations: an efficient process accompanied by secondary fragmentation. *Chem. Phys. Lett.* **2002,** 356, 201-206.

7. P. Roepstorff; J. Fohlman, Proposal for a common nomenclature for sequence ions in mass spectra of peptides. *Biol. Mass Spectrom.* **1984,** 11, 601-601.

8. H. J. Cooper; K. Hakansson; A. G. Marshall, The role of electron capture dissociation in biomolecular analysis. *Mass Spectrom. Rev.* **2005,** 24, 201-222.

9. A. T. Iavarone; K. Paech; E. R. Williams, Effects of charge state and cationizing agent on the electron capture dissociation of a peptide. *Anal. Chem.* **2004,** 76, 2231-2238.

10. A. R. Zubarev; N. A. Kruger; E. K. Fridriksson; M. A. Lewis; D. M. Horn; B. K. Carpenter; F. W. McLafferty, Electron capture dissociation of gaseous multiply-charged proteins is favored at disulfide bonds and other sites of high hydrogen atom affinity. *J. Am. Chem. Soc.* **1999**, 2857-2862.

11. R. A. Zubarev; D. M. Horn; E. K. Fridriksson; N. L. Kelleher; N. A. Kruger; M. A. Lewis; B. K. Carpenter; F. W. McLafferty, Electron capture dissociation for

structural characterization of multiply charged protein cations. *Anal. Chem.* **2000,** 72, 563-573.

12. H. Cooper; Hudgins; A. Marshall, Electron capture dissociation Fourier transform ion cyclotron resonance mass spectrometry of cyclodepsipeptides, branched peptides, and var epsilon-peptides. *Int. J. Mass Spectrom.* **2004,** 234, 23-35

13. S. J. Pitteri; P. A. Chrisman; J. M. Hogan; S. A. McLuckey, Electron transfer ion/ion reactions in a three-dimensional quadrupole ion trap: Reactions of doubly and triply protonated peptides with SO_2 dot$^-$. *Anal. Chem.* **2005,** 77, 1831-1839.

14. S. J. Pitteri; P. A. Chrisman; S. A. McLuckey, Electron-transfer ion/ion reactions of doubly protonated peptides: Effect of elevated bath gas temperature. *Anal. Chem.* **2005,** 77, 5662-5669.

15. A. R. Ledvina; N. A. Beauchene; G. C. McAlister; J. E. P. Syka; J. C. Schwartz; J. Griep-Raming; M. S. Westphall; J. J. Coon, Activated-ion electron transfer dissociation improves the ability of electron transfer dissociation to identify peptides in a complex mixture. *Anal. Chem.* **2010,** 82, 10068-10074.

16. I. A. Papayannopoulos, The interpretation of collision-induced dissociation tandem mass spectra of peptides. *Mass Spectrom. Rev* **1995,** 14, 49-73.

17. J. Axelsson; M. Palmblad; K. Hakansson; P. Hakansson, Electron capture dissociation of substance P using a commercially available Fourier transform ion cyclotron resonance mass spectrometer. *Rapid Commun. Mass Spectrom.* **1999,** 13, 474-477.

18. F. Meng; A. J. Forbes; L. Miller; N. L. Kelleher, Detection and localization of protein modifications by high resolution tandem mass spectrometry. *Mass Spectrom. Rev.* **2005**, 126-134.

19. R. A. Zubarev, Reactions of polypeptide ions with electrons in the gas phase. *Mass Spectrom. Rev.* **2003,** 22, 57-77.

20. R. A. Zubarev, Electron-capture dissociation tandem mass spectrometry. *Curr. Opin. Biotechnol.* **2004,** 15, 12-16.

21. R. Wu; T. B. McMahon, An investigation of protonation sites and conformations of protonated amino acids by IRMPD spectroscopy. *ChemPhysChem* **2008,** 9, 2826-2835.

22. H. Liu; K. Hakansson, Divalent metal ion-peptide interactions probed by electron capture dissociation of trications. *J. Am. Soc. Mass Spectrom.* **2006,** 17, 1731-1741.

23. J. P. Williams; J. M. Brown; I. Campuzano; P. J. Sadler, Identifying drug metallation sites on peptides using electron transfer dissociation (ETD), collision induced dissociation (CID) and ion mobility-mass spectrometry (IM-MS). *Chem. Commun.* **2010,** 46, 5458-5460.

24. Y. Eva Fung; H. Liu; T. Chan, Electron capture dissociation of peptides metalated with alkaline-earth metal ions. *J. Am. Soc. Mass Spectrom.* **2006,** 17, 757-771.

25. H. Liu; K. Hakansson, Electron Capture Dissociation of Tyrosine O-Sulfated Peptides Complexed with Divalent Metal Cations. *Anal. Chem.* **2006,** 78, 7570-7576.

26. A. J. Kleinnijenhuis; R. Mihalca; R. M. A. Heeren; A. J. R. Heck, Atypical behavior in the electron capture induced dissociation of biologically relevant transition metal ion complexes of the peptide hormone oxytocin. *Int. J. Mass Spectrom.* **2006,** 253, 217-224.

27. Y. E. M. van der Burgt; M. Palmblad; H. Dalebout; R. M. A. Heeren; A. M. Deelder, Electron capture dissociation of peptide hormone changes upon opening of the tocin ring and complexation with transition metal cations. *Rapid Commun. Mass Spectrom.* **2009,** 23, 31-38.

28. J. A. Mosely; B. S. Murray; D. Parker, Electron-capture dissociation and collision-induced dissociation of lanthanide metal-ligand complexes and lanthanide metal-ligand complexes bound to phosphopeptides. *Eur. Mass Spectrom.* **2009,** 15, 145-155.

29. F. Tureček; A. I. S. Holm; S. Panja; S. B. Nielsen; P. Hvelplund, Transition metals as electron traps. II. Structures, energetics and electron transfer dissociations of ternary Co, Ni and Zn–peptide complexes in the gas phase. *J. Mass Spectrom.* **2009,** 44, 1518-1531.

30. F. Tureček; J. W. Jones; A. I. S. Holm; S. Panja; S. B. Nielsen; P. Hvelplund, Transition metals as electron traps. I. Structures, energetics, electron capture, and electron-transfer-induced dissociations of ternary copper–peptide complexes in the gas phase. *J. Mass Spectrom.* **2009,** 44, 707-724.

31. L. Feketeová; V. Ryzhov; R. A. J. O'Hair, Comparison of collision- versus electron-induced dissociation of Pt(II) ternary complexes of histidine- and methionine-containing peptides. *Rapid Commun. Mass Spectrom.* **2009,** 23, 3133-3143.

32. B. S. Freiser (Ed.), *Organometallic Ion Chemistry*. Kluwer Academic Publishers: Dordrecht, Netherlands, 1996.

33. I. Bertini; A. Sigel; H. Sigel, *Handbook on Metalloproteins*. Marcel Dekker, Inc.: New York, 2001.

34. J. A. Gutierrez; Wessling-ResnickM, Molecular mechanisms of iron transport. *Crit. Rev. Eukaryot. Gene Expr.* **1996,** 6, 1.

35. E. I. Solomon; M. J. Baldwin; M. D. Lowery; , Electronic structures of active sites in copper proteins: contributions to reactivity. *Chem. Rev.* **1992**, 521-542.

36. H.-J. Thiesen; C. Bach, Transition metals modulate DNA-protein interactions of SP1 zinc finger domains with its cognate target site. *Biochem. Biophys. Res. Commun.* **1991,** 176, 551-557.

37. J. B. Vincent, The biochemistry of chromium. *J. Nutr.* **2000,** 130, 715-718.

38. W. Chan; P. White, *Fmoc Solid Phase Peptide Synthesis: A Practical Approach*. Oxford University Press: New York, 2000.

39. R. A. Zubarev; N. L. Kelleher; F. W. McLafferty, Electron capture dissociation of multiply charged protein cations. A nonergodic process. *J. Am. Chem. Soc.* **1998,** 120, 3265-3266.

40. C. Chanthamontri; J. Liu; S. A. McLuckey, Charge state dependent fragmentation of gaseous α-synuclein cations via ion trap and beam-type collisional activation. *Int J Mass Spectrom.* **2008,** 283, 1-3.

41. C. Jensen; A. Holm; H. Zettergren; J. Overgaard; P. Hvelplund; S. Nielsen, On the charge partitioning between c and z fragments formed after electron-capture induced dissociation of charge-tagged Lys-Lys and Ala-Lys dipeptide dications. *J. Am. Soc. for Mass Spectrom.* **2009,** 20, 1881-1889.

42. D. R. Lide, *CRC Handbook of Chemistry and Physics*. 84 ed.; CRC Press: Boca Raton, FL, 2003.

43. S. Lippard; J. Berg, *Principles Of Bioinorganic Chemistry*. University Science Books: Mill Valley, CA, 1994.

44. W. M. Haynes, *CRC Handbook of Chemistry and Physics*. 91st ed.; CRC Press: London, 2010-2011.

45. J. Simons, Mechanisms for S-S and N-C[alpha] bond cleavage in peptide ECD and ETD mass spectrometry. *Chem. Phys. Lett.* **2010,** 484, 81-95.

46. H. Liu; K. Håkansson, Abundant b-type ions produced in electron capture dissociation of peptides without basic amino acid residues. *J. Am. Soc. Mass Spectrom.* **2007,** 18, 2007-2013.

47. A. G. Harrison; A. B. Young; C. Bleiholder; S. Suhai; B. Paizs, Scrambling of sequence information in collision-induced dissociation of peptides. *J. Am. Chem. Soc.* **2006,** 128, 10364-10365.

48. S. Molesworth; S. Osburn; M. Van Stipdonk, Influence of size on apparent scrambling of sequence during CID of b-type ions. *J. Am. Soc. Mass Spectrom.* **2009,** 20, 2174-2181.

49. B. J. Bythell; P. Maitre; B. Paizs, Cyclization and Rearrangement Reactions of a_n Fragment Ions of Protonated Peptides. *J. Am. Chem. Soc.* **2010,** 132, 14766-14779.

50. B. J. Bythell; S. Molesworth; S. Osburn; T. Cooper; B. Paizs; M. Van Stipdonk, Structure and reactivity of a_n and a_n* peptide fragments investigated using isotope labeling, tandem mass spectrometry, and density functional theory calculations. *J. Am. Soc. Mass Spectrom.* **2008,** 19, 1788-1798.

51. N. C. Polfer; B. C. Bohrer; M. D. Plasencia; B. Paizs; D. E. Clemmer, On the dynamics of fragment isomerization in collision-induced dissociation of peptides. *J. Phys. Chem. A* **2008,** 112, 1286-1293.

52. N. C. Polfer; J. Oomens; S. Suhai; B. Paizs, Infrared spectroscopy and theoretical studies on gas-phase protonated Leu-enkephalin and its fragments: direct experimental evidence for the mobile proton. *J. Am. Chem. Soc.* **2007,** 129, 5887-5897.

53. A. G. Harrison, Peptide sequence scrambling through cyclization of b_5 ions. *J. Am. Soc. Mass Spectrom.* **2008,** 19, 1776-1780.

54. I. Riba-Garcia; K. Giles; R. H. Bateman; S. J. Gaskell, Evidence for structural variants of a- and b-type peptide fragment ions using combined ion mobility/mass spectrometry. *J. Am. Soc. Mass Spectrom.* **2008,** 19, 609-613.

55. A. Atik; T. Yalcin, A systematic study of acidic peptides for b-type sequence scrambling. *J. Am. Soc. Mass Spectrom.* **2011,** 22, 38-48.

56. C. Bleiholder; S. Osburn; T. D. Williams; S. Suhai; M. Van Stipdonk; A. G. Harrison; B. Paizs, Sequence-scrambling fragmentation pathways of protonated peptides. *J. Am. Chem. Soc.* **2008,** 130, 17774-17789.

57. A. Goloborodko; M. Gorshkov; D. Good; R. Zubarev, Sequence scrambling in shotgun proteomics is negligible. *J. Am. Soc. Mass Spectrom.* **2011,** 22, 1121-1124.

58. I. Saminathan; X. Wang; Y. Guo; O. Krakovska; S. Voisin; A. Hopkinson; K. Siu, The extent and effects of peptide sequence scrambling via formation of macrocyclic b-ions in model proteins. *J. Am. Soc. Mass Spectrom.* **2010,** 21, 2085-2094.

59. X. Li; Y. Huang; P. O'Connor; C. Lin, Structural heterogeneity of doubly-charged peptide b-Ions. *J. Am. Soc. Mass Spectrom.* **2011,** 22, 245-254.

CHAPTER 5

ELECTRON-TRANSFER COLLISIONALLY-ACTIVATED DISSOCIATION OF TRANSITION METAL-CATIONIZED PEPTIDES

5.1 Introduction

Electron-transfer dissociation (ETD) is a new MS/MS technique used in peptide sequencing.[1] ETD requires multiply charged precursor ions, $[M + nH]^{n+}$, because electron-transfer to the precursor produces the charged reduced product $[M + nH]^{(n-1)+\bullet}$. For a singly charged precursor, this would result in a neutral and therefore be useless in mass spectrometry, which can only detect charged species. The higher the initial charge of the precursor, the more efficient the dissociation process.[2, 3] The majority of peptides and proteins that need to be sequenced are generated by tryptic digests, which generally produce peptide ions with charges in the range of 1-4 and most commonly 2 by electrospray ionization (ESI).[4] As a result, the application of ETD to sequencing tryptic peptides would benefit from increasing the efficiency of ETD.

Electron-transfer collisionally-activated dissociation (ETcaD) was first described by Swaney *et al.* in 2007[4] as a method of applying supplemental activation to the intact electron-transfer (ET) product ion species, $[M + nH]^{(n-1)+\bullet}$, in an attempt to increase dissociation. This reduced (but not dissociated) product has also been referred to as electron-transfer no dissociation (ETnoD). Collisional-activated dissociation (CAD),

synonymous with collision-induced dissociation (CID), of the ETnoD product ions from 755 doubly charged tryptic peptides resulted in a 26% increase in sequence coverage over ETD and 12% over CID.[4] In another study,[5] supplemental activation of the non-dissociated electron-transfer product was applied to doubly and triply charged, tryptic digested peptide ions. The supplemental activation (from CID) was deemed "essential" to obtain a high quality ETD spectrum.[5] The addition of supplemental activation increased sequence coverage 35% over ETD alone. Interestingly, ETD leads to cleavage of covalent bonds of the peptide backbone without disrupting weaker noncovalent bonds. As a consequence, c- and z-ions may be produced following N-Cα cleavage, but noncovalent interactions between the c-and z-ion pairs can cause them to appear instead as the reduced molecular ion $[M + nH]^{n+\bullet}$.[6, 7] By subsequently performing CID on these c/z pairs, the noncovalent interactions are broken to yield a spectrum containing c- and z-ions.[4, 8]

For a dissociation technique to be useful in applied proteomics, the data sets generated from MS^n must be searched by search engines such as *Mascot* and *pFind*. This makes the large numbers of MS^n data generated in high-throughput MS a more manageable task. A study of ETcaD, CID, and ETD data sets from the yeast proteome were searched by different search engines and compared.[9] ETcaD was found to increase the effectiveness of the searches in identifying peptide sequences over ETD or CID alone.

To determine the efficacy of ETcaD for the sequencing of metallopeptides, peptides cationized by transition metal ions, Cr(III), Fe(II), Co(II), Ni(II), and Cu(II), were submitted to ETcaD. The resulting spectra were compared to CID and ETD spectra of the same transition metal-peptide complexes.

5.2 Experimental

Sample preparation and sample introduction for this work are previously described in Chapters 2-4. All ETcaD experiments were carried out on a high capacity ion trap (Bruker HCTultra PTM Discovery System; Bruker Daltonics, Billerica, NH, USA) For ETcaD, a 100-200 ms reaction of fluoranthene anions with the doubly charged peptides produced by ESI, $[M + Cr - H]^{2+}$ and $[M + Met]^{2+}$, for Met = Fe(II), Co(II), Ni(II), and Cu(II), forms the ETnoD products $[M + Cr - H]^{+\bullet}$ and $[M + Met]^{+\bullet}$. These ETnoD products were submitted to a supplemental activation through low energy CID in the quadrupole ion trap. The CID experiments were performed with He gas and a 30% - 200% collision energy sweep and amplitudes of 0.5 - 1.2 V. The low mass cut-off was set at *m/z* 50.

5.3 Results and Discussion

5.3.1 Effectiveness of ETcaD on Transition Metallated Peptides

ETcaD of the charge-reduced product ions, $[M + Cr - H]^{2+}$ and $[M + Met]^{+\bullet}$, result in increased sequence coverage and reduced spectral complexity when compared to ETD and CID. Figure 5.1 demonstrates the utility of the technique. ETD of $[M + Cr - H]^{2+}$ gives only 2 backbone cleavages, as shown in Figure 5.1a. CID on the same ion (Figure 5.1b) has some undesirable properties for peptide sequencing, such as intense neutral losses and spectral complexity. However, CID does increase backbone cleavage resulting in production of four out of a possible six sequence ions. As shown in Figure 5.1c, combining ETD with supplemental activation, ETcaD, of the same sample results in complete sequence coverage. The types of ions that form resemble those produced by

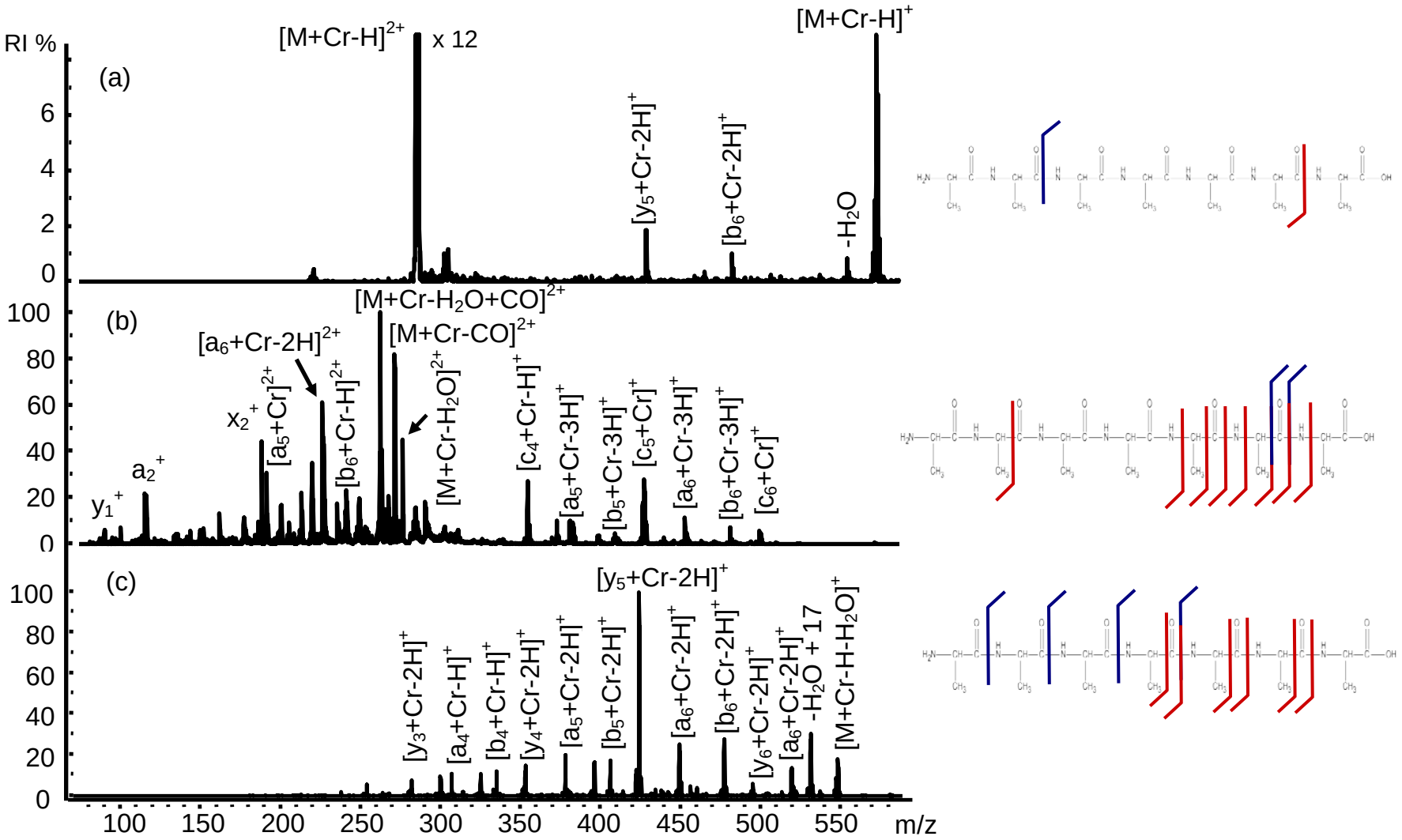

Figure 5.1 Comparing the sequencing efficacy of (a) ETD, (b) CID, and (c) ETcaD on Cr-cationized heptaalanine, $[M + Cr - H]^{2+}$. In the sequence diagram at right, cleavages that form C-terminal ions are shown in blue and cleavages that form N-terminal ions are shown in red.

ETD where the y- and b-ions incorporate Cr and lose 2 H as $[y_n + Cr - 2H]^+$ and $[b_n + Cr - 2H]^+$. The overall ETcaD spectrum is "clean" and easily interpretable. Most ions form in similar abundances, (see Figure 5.1c) unlike CID, where doubly charged neutral losses dominate (as illustrated in Figure 5.1b).

Similar results were found for all transition metal-cationized heptaalanine complexes; increased sequence coverage, and cleaner spectra. However, because heptaalanine contains only alanine residues, nonsequential losses (discussed in Chapter 4) are not observable using this peptide. If nonsequential losses occur, they would be undetected because all residues have the same *m/z*. Therefore, transition metal-cationized AAAAAGA complexes were also submitted to ETcaD in order to readily identify nonsequential losses. Figure 5.2 illustrates the effect of changing the cationizing reagent on backbone cleavages formed by ETcaD.

5.3.2 ETcaD of Cr(III)-AAAAAGA

Figures 5.3 - 5.7 show the results for ETcaD of transition metal-cationized AAAAAGA. ETcaD of AAAAAGA cationized by Cr(III) is a relatively clean spectra with intense a-, b-, and y-type ions, as shown in Figure 5.3. Like Cr-cationized heptaalanine, the AAAAAGA spectrum has full sequence coverage and is easier to interpret than the CID spectrum produced by the same complex. However, the production of $[b_6 + Cr - 2H - Ala]^+$ and $[a_6 + Cr - 2H - Ala]^+$ suggests that macrocyclic ions form during ETcaD as they do by ETD; this is discussed in Chapter 4, Section 3.3.

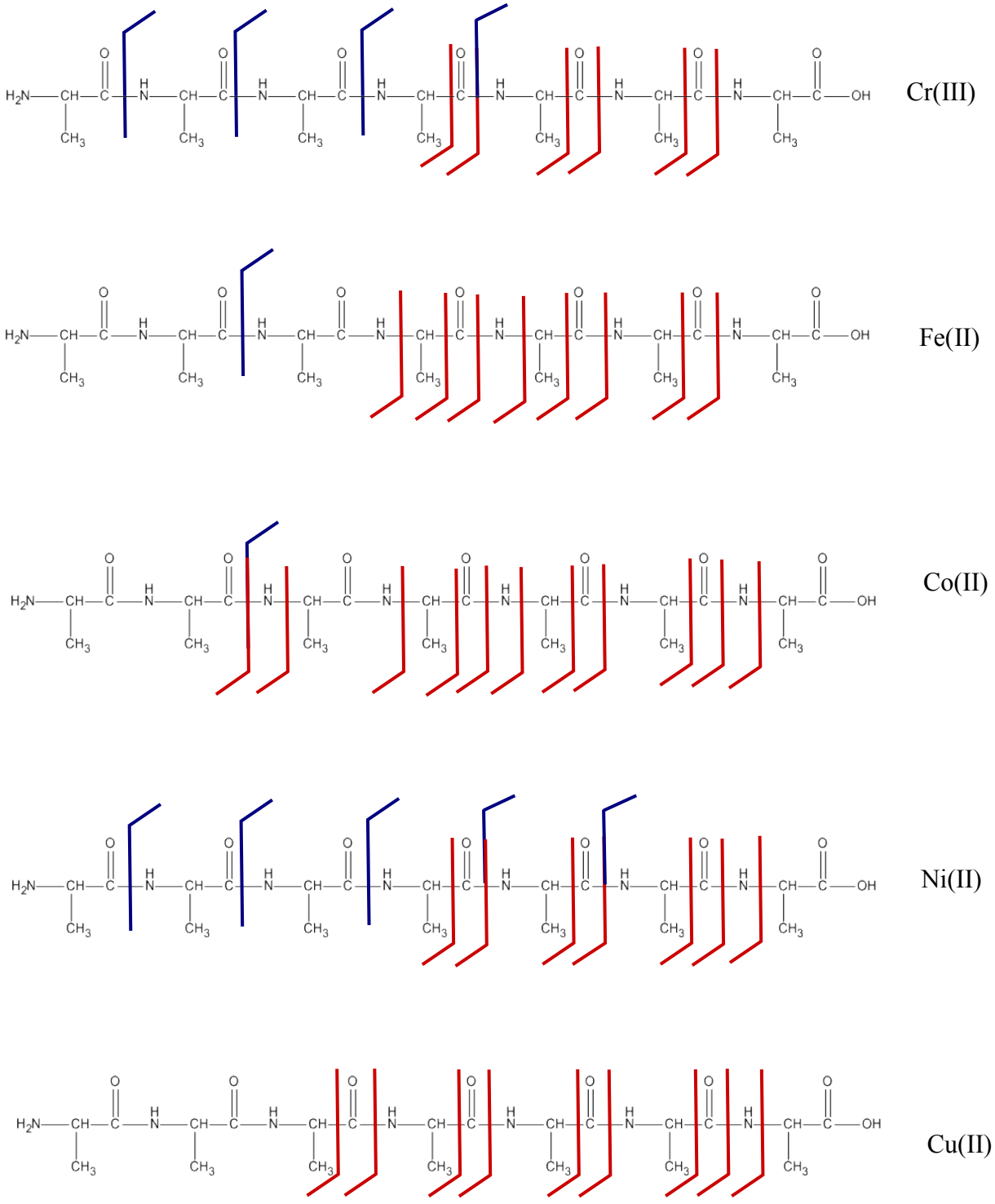

Figure 5.2. Backbone cleavages resulting from ETcaD of heptaalanine cationized by transition metals. Red indicates N-terminal products and blue indicates C-terminal products. All precursor ions are $[M + Met]^{2+}$ except for the ion from Cr(III), which is $[M + Cr - H]^{2+}$.

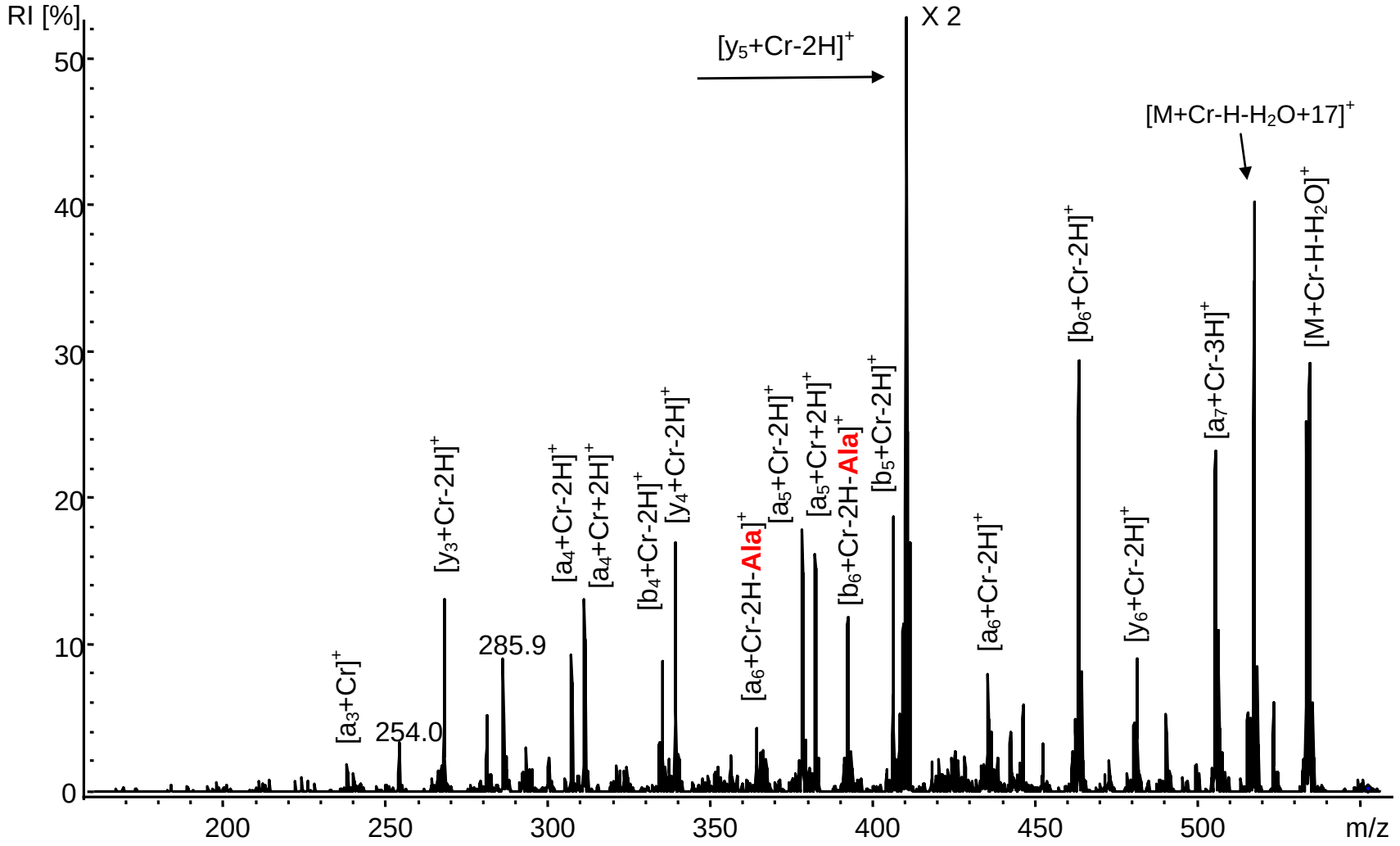

Figure 5.3 ETcaD spectrum obtained from ETD on $[M + Cr - H]^{2+}$, where M = AAAAAGA, followed by CID on the ETnoD product $[M + Cr - H]^{+}$. Nonsequential product ions are marked in red.

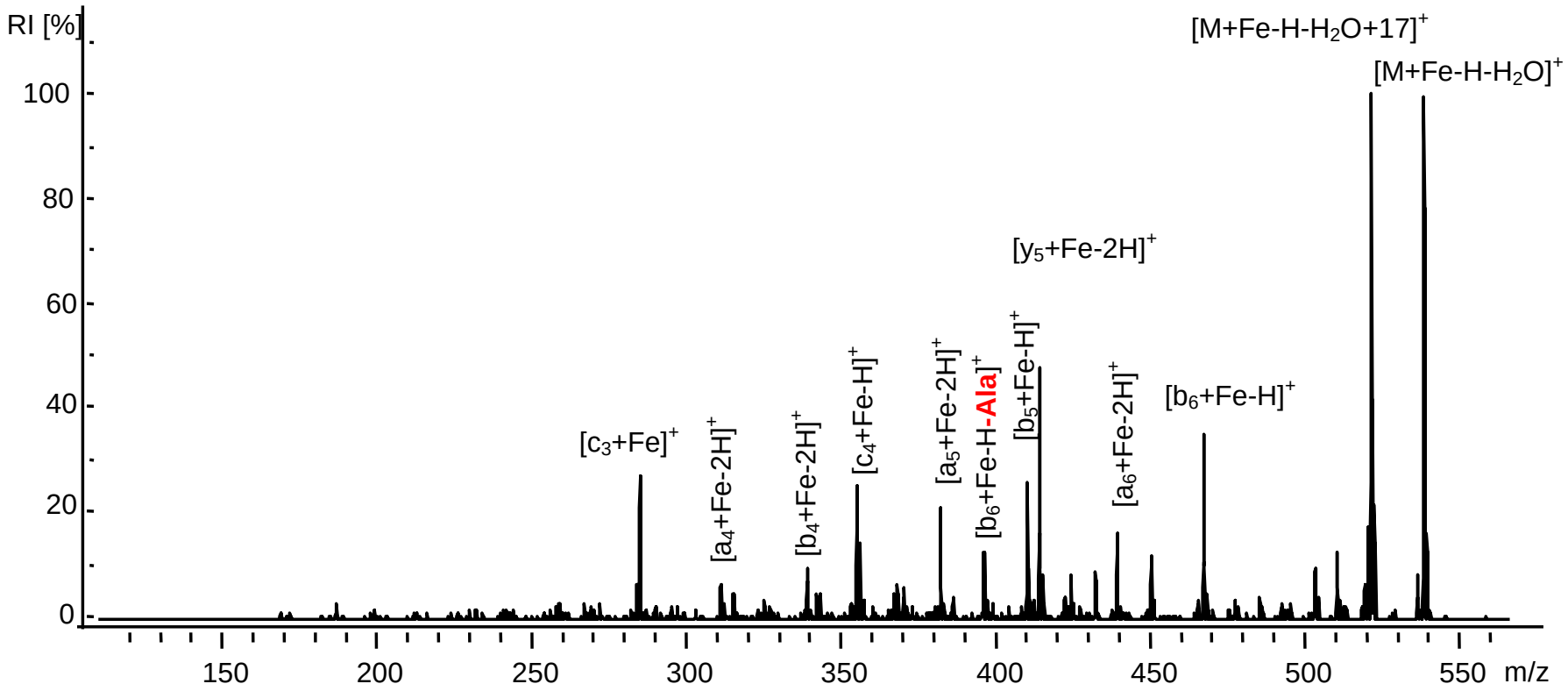

Figure 5.4 ETcaD spectrum obtained from ETD on $[M + Fe]^{2+}$, where M = AAAAAGA, followed by CID on the ETnoD product $[M + Fe]^{+}$. Nonsequential product ions are marked in red.

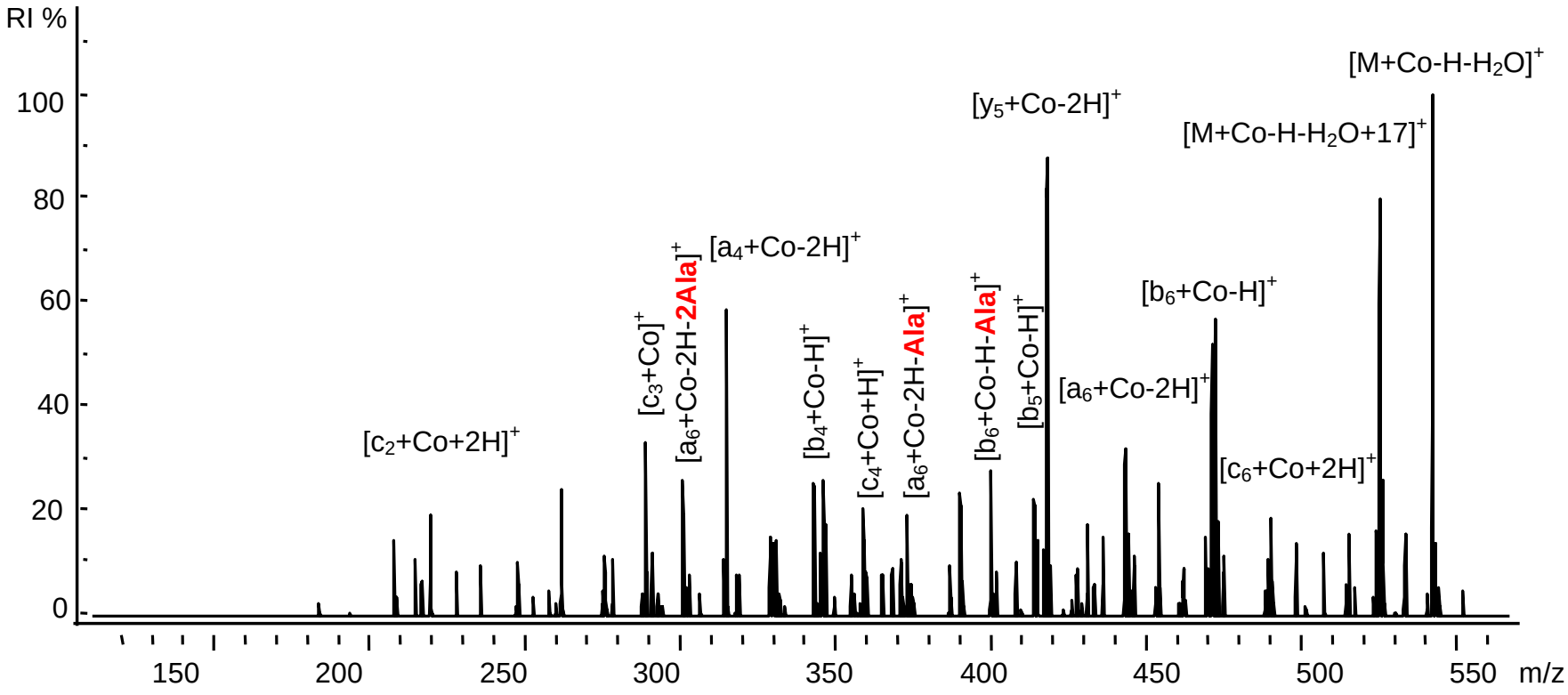

Figure 5.5 ETcaD spectrum obtained from ETD on $[M + Co]^{2+}$, where M = AAAAAGA, followed by CID on the ETnoD product $[M + Co]^{+}$. Nonsequential product ions are marked in red.

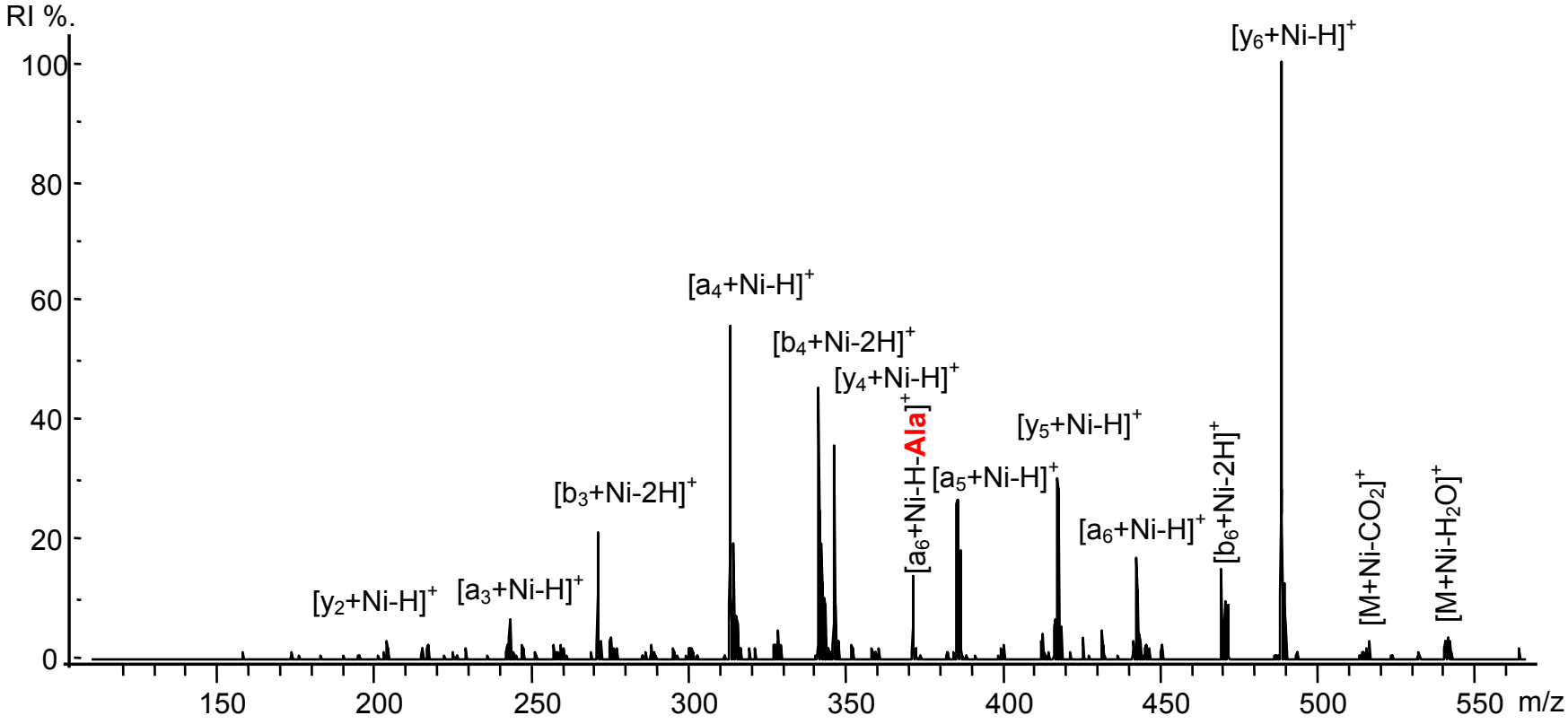

Figure 5.6. ETcaD spectrum obtained from ETD on $[M + Ni]^{2+}$, where M = AAAAAGA, followed by CID on the ETnoD product $[M + Ni]^{+}$. Nonsequential product ions are marked in red.

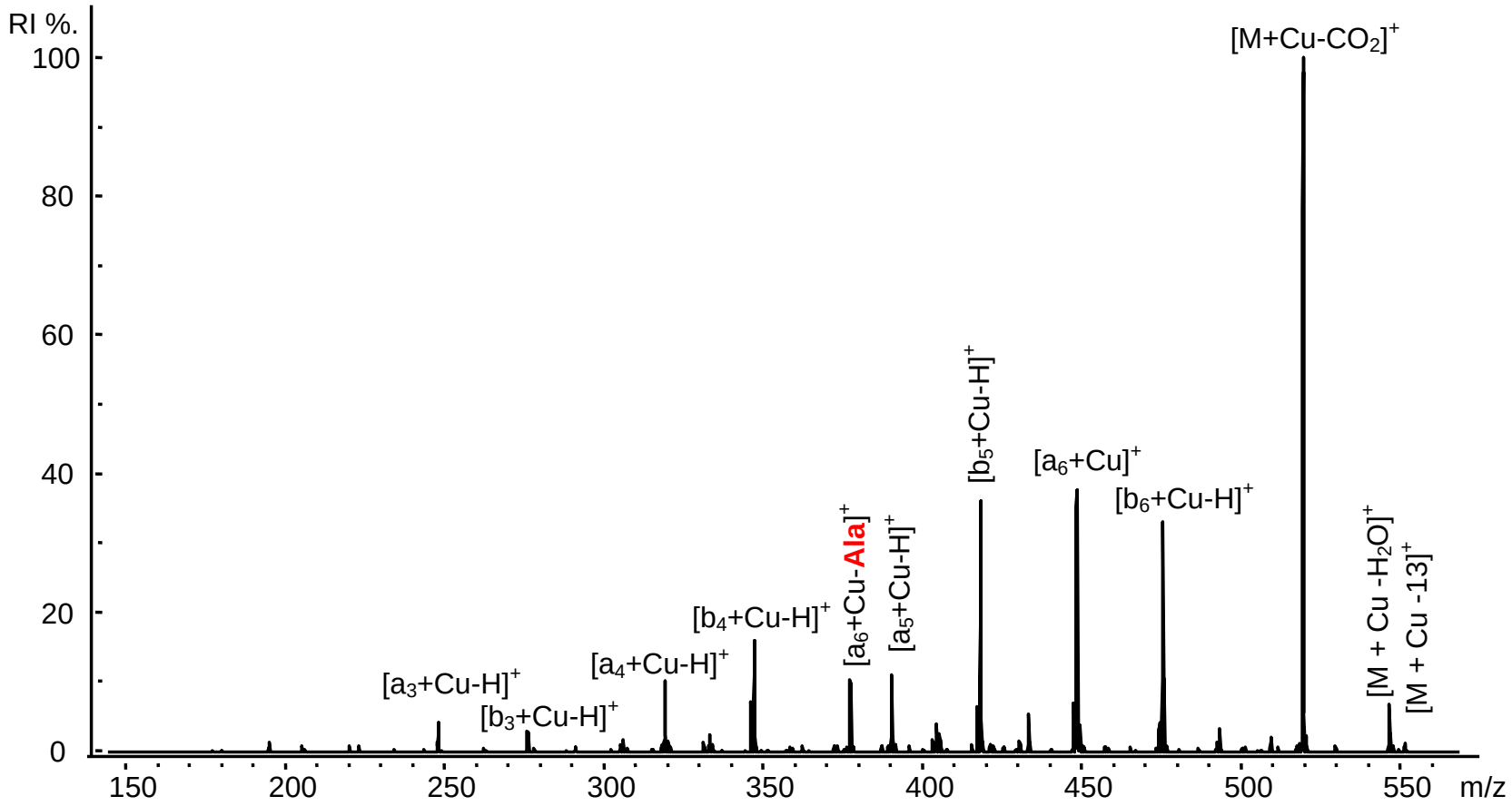

Figure 5.7 ETcaD spectrum obtained from ETD on $[M + Cu]^{2+}$, where M = AAAAAGA, followed by CID on the ETnoD product $[M + Cu]^{+}$. Nonsequential product ions are marked in red.

5.3.3 ETcaD of Fe(II)-AAAAAGA

ETcaD of AAAAAGA cationized by Fe(II) results in five out of six backbone cleavages and only one nonsequential loss, also from metallated b_6, as shown in Figure 5.4. The $[b_6 + Fe - H - Ala]^+$ and intense neutral losses are not desirable in peptide sequencing; however, the overall spectra is more readily interpretable than that formed by CID of $[M + Fe]^{2+}$ (Figure 3.5). Fe(II) formed more intense metallated c-ions during ETcaD than the other metal ions studied. The recombination energy (RE) of Fe(II) is lower than that of the other metals. The results shown in Figures 5.3-5.7 are consistent with those found by ETD (discussed in Chapter 4 Section 3.1), where c-type product ions are more abundant when metal ions of lower REs are used as the cationizing reagent.

5.3.4 ETcaD of Co(II)-AAAAAGA

Similar results occur with cationization by Co(II) as shown in Figure 5.5. ETcaD increases backbone cleavage relative to ETD and CID. Like Fe(II), Co(II) cationization produces five out of six backbone cleavages by ETcaD. However, also like Fe(II), ETcaD of the Co(II) complex exhibits more nonsequential losses than by ETD alone. In fact, Co(II) leads to more nonsequential losses than Fe(II): $[b_6 + Co - H - Ala]^+$, $[a_6 + Co - 2H - Ala]^+$, and $[a_6 + Co - 2H - 2Ala]^+$. The nonsequential loss of Gly is not observed with AAAAAGA. This is likely because typical a_n- and b_n-ion macrocycles occur for n = 4-6. For a_n- and b_n- ions with n = 4-6, Gly could only be eliminated from n = 6 due to the location of Gly in the sequence, AAAAAGA, forming expected a_5- and b_5- sequence ions. Therefore it is not necessarily the characteristic of Ala that is causing the nonsequential losses, but likely the size of the macrocyclic ion itself.

5.3.5 ETcaD of Ni(II)-AAAAAGA

Figure 5.6 reveals similar product ion formation with Ni(II) cationization. Notice that Ni(II) produces a base peak of $[y_6 + Ni - H]^+$. In contrast, metallated $[y_5 + Met - H]^+$ or neutral loss products are more common as base peaks in the ETcaD spectra of Cr(III), Fe(II), and Co(II). Ni(II)-metallated N- and C-terminal products form by CID, ETD, and ETcaD. In addition, neutral losses such as H_2O occur from the C-terminus and do not form as abundantly by Ni(II) cationization as by the other transition metals studied. Much of the precursor, $[M + Ni]^{2+}$ likely has Ni(II) coordinated to the C-terminus and several other backbone sites such as the carbonyl oxygen and/or the deprotonated amide. Coordination to the C-terminus could prevent facile loss of H_2O and increase $[y_n + Ni - H]^+$. The CID and ETD of $[M + Ni]^{2+}$ (See Figures 3.9 and 4.13c) also produce significantly more y-ions than the other metals studied. This is not without precedent. The coordination of Ni(II) to the C-terminus of Helicobacter pylori has been observed by X-ray absorption spectroscopy.[10] Like Cr(III), Ni(II)-cationization and ETcaD leads to complete sequence coverage and a relatively clean spectrum.

The Ni-metallated b-ions do not undergo nonsequential losses, however, $[a_6 + Ni - H - Ala]^+$, is produced as shown in Figure 5.6. Note that the b-ions form as $[b_n + Ni - 2H]^+$ whereas with Co(II) and Fe(II) b-ions form as $[b_n + Met - H]^+$. Recent studies of macrocyclic b-ions[11-15] that form by CID of protonated species indicate that these structures re-open as a result of a mobile proton on the ring. The loss of an additional hydrogen from the metallated b-ions may prevent re-opening and subsequent nonsequential losses.

5.3.6 ETcaD of Cu(II)-AAAAAGA

Figure 5.7 is the spectrum resulting from ETcaD of a Cu(II)-AAAAAGA ion. Unlike the other transition metals, Cu(II) leads to predominantly CO_2 loss and no C-terminal product ions. Overall the spectrum is cleaner than that produced by CID of the same ion and interpretation leads to five out of six sequence ions. As is the case with the other transition metals, Cu(II) does produce some nonsequential losses in the form of $[b_6 + Cu - H - Ala]^+$ and $[a_6 + Cu - H - Ala]^+$.

All transition metal ions studied led to some nonsequential losses by ETcaD and always from metallated a_n- or b_n-ions with $n \geq 5$. This may be because of the location of the metal ion coordination sites or steric limitations of smaller ring sizes. To further investigate this, the $[a_7 + Cu]^+$ product formed by ETcaD of $[M + Cu]^+$, M = AAAAAGA, was isolated and submitted to CID (MS^4). Products resulting from the loss of CO_2 and one to three alanines were produced. Note that these Ala losses are nonsequential and form as $[a_7 + Cu - Ala]^+$, $[a_6 + Cu - Ala]^+$, and $[a_6 + Cu - 2Ala]^+$. This further supports the existence of macrocyclic metallated a-ions.

5.3.7 Loss of Carbon by ETcaD of Cu(II)-Peptides

Another interesting feature of Cu(II) spectra is the loss of 13 Da from the precursor ion as $[M + Cu - CH]^+$. This is similar to the unusual loss of carbon following CID of $[M + Cu - H]^+$, which appears as $[M + Cu - H - C]^+$ found in Figure 3.10 of Chapter 3. This CH-elimination is unusual and was investigated further. The CH-loss product, $[M + Cu - CH]^+$ was isolated and submitted to CID (MS^4). The resulting

spectrum (not shown) reveals a loss of *m/z* 34 (likely the small neutrals H_2 and O_2 or H_2O_2) as did the carbon-loss products formed by CID of $[M + Cu - H]^+$, for M = heptaalanine and ^{13}C-labeled heptaalanine, both shown in Figure 3.12. Interestingly, the charge reduced $[M + Cu]^{+\bullet}$ loses CH and the singly charged precursor $[M + Cu - H]^+$ eliminates C. The CH-loss product occurs with each peptide studied when cationized by Cu(II). Each CID experiment on $[M + Cu - H]^+$ (M = AAGGGAA, GGAAAAA, AGAGAAA, GGAAAA, AAAAAAA, AAAAAGA, and ^{13}C-labeled side chains at the first and sixth positions of AAAAAAA) and produces $[M + Cu - H - C]^+$. Likewise, each ETcaD of $[M + Cu]^{+\bullet}$ produces $[M + Cu - CH]^+$. If the carbon eliminated were from a side chain of alanine, labeling with ^{13}C would indicate this by loss of 13 Da by ETD and loss of 14 Da by ETcaD. However, this does not occur. Therefore the side chain carbons are not the carbons lost in this process.

In a gas-phase ion chemistry study of the reactions of Cu(I) with organic aldehydes, ketones, carboxylic acids, and esters, Freiser and coworkers[16] found that a variety of small neutral molecules and radicals (e.g. H_2O, H_2, CO, CH_2O, and CH_2) were eliminated as the neutral product. A study by Adams and coworkers[17] of Co(II)- and Ni(II)-tetrapeptide complexes , $[M + Met^{2+} - 3H]^-$, found that these complexes primarily lose CO_2 and HCO_2H from the free C-terminus in negative mode metastable ion decomposition spectra. Similar processes may be occurring to cause elimination of C and H_2O_2 from the C-terminal carboxylic acid group during CID on peptides complexed to Cu(II). The unusual spectral characteristics produced by $[M + Cu]^{2+}$ may be due, in part, to the fast exchange rates of Cu(II) relative to the other metal ions investigated. The fast ligand exchange rates may affect both the initial solution-phase coordination chemistry

and later the gas-phase behavior of the Cu(II) complexes. The ease of Cu(II) to exchange ligands relative to the other metal ions may be beneficial in sequencing by increasing the number of sites that are cleaved. Whether the stability of the product ion $[M + Cu - CH]^+$ (or $[M + Cu - H - C]^+$ by ETD) or the gas-phase Cu(II) rearrangement at the C-terminus is driving this carbon elimination is not clear from these results.

5.4 Conclusions

Transition metal-cationized peptides yield more sequence information when submitted to ETcaD than by ETD alone. Supplemental activation of the ETnoD product increases overall backbone cleavage products and relative intensities. However, the additional energy may be driving the increase in nonsequential residue losses. These nonsequential losses occur from metallated a_n- and b_n- ions independent of the transition metal chosen for cationization and only from $n \geq 5$. The utility of the technique is evident when applied to Cr(III)-cationized peptides, which result in the least amount of sequence informative ions when submitted to either CID or ETD. When ETcaD is applied to Cr(III)-cationized peptides full sequence information is attained. The results presented in this dissertation indicate that Ni(II) is a promising cationizing reagent for increasing sequence informative ions by ETD and ETcaD.

REFERENCES

1. R. A. Zubarev, Reactions of polypeptide ions with electrons in the gas phase. *Mass Spectrom. Rev.* **2003,** 22, 57-77.

2. S. J. Pitteri; P. A. Chrisman; J. M. Hogan; S. A. McLuckey, Electron transfer ion/ion reactions in a three-dimensional quadrupole ion trap: Reactions of doubly and triply protonated peptides with SO_2 $\bullet^-$. *Anal. Chem.* **2005,** 77, 1831-1839.

3. S. J. Pitteri; P. A. Chrisman; S. A. McLuckey, Electron-transfer ion/ion reactions of doubly protonated peptides: Effect of elevated bath gas temperature. *Anal. Chem.* **2005,** 77, 5662-5669.

4. D. Swaney; G. C. McAlister; M. Wirtala; J. C. Schwartz; J. E. P. Syka; J. J. Coon, Supplemental activation method for high-efficiency electron-transfer dissociation of doubly protonated peptide precursors. *Anal. Chem.* **2007,** 79, 477-485.

5. W. Y. Kelly-Chan; T. W. Dominic-Chan; P. O'Connor, Electron transfer dissociation with supplemental activation to differentiate aspartic and isoaspartic residues in doubly charged peptide cations. *J. Am. Soc. Mass Spectrom.* **2010,** 21, 1012-1015.

6. K. Breuker; H. Oh; D. M. Horn; B. A. Cerda; F. W. McLafferty, Detailed unfolding and folding of gaseous ubiquitin ions characterized by electron capture dissociation. *J. Am. Chem. Soc.* **2002,** 124, 6407-6420.

7. D. M. Horn; K. Breuker; A. J. Frank; F. W. McLafferty, Kinetic intermediates in the folding of gaseous protein ions characterized by electron capture dissociation mass spectrometry. *J. Am. Chem. Soc.* **2001,** 123, 9792-9799.

8. Y. Xia; H. Han; S. A. McLuckey, Activation of intact electron-transfer products of polypeptides and proteins in cation transmission mode ion/ion reactions. *Anal. Chem.* **2008,** 80, 1111-1117.

9. R.-X. Sun; M.-Q. Dong; C.-Q. Song; H. Chi; B. Yang; L.-Y. Xiu; L. Tao; Z.-Y. Jing; C. Liu; L.-H. Wang; Y. Fu; S.-M. He, Improved Peptide Identification for Proteomic Analysis Based on Comprehensive Characterization of Electron Transfer Dissociation Spectra. *J. Proteome Res.* **2010,** 9, 6354-6367.

10. D. C. Kennedy; R. W. Herbst; J. S. Iwig; P. T. Chivers; M. J. Maroney, A dynamic Zn site in helicobacter pylori HypA: A potential mechanism for metal-specific protein activity. *J. Am. Chem. Soc.* **2006,** 129, 16-17.

11. C. Bleiholder; S. Osburn; T. D. Williams; S. Suhai; M. Van Stipdonk; A. G. Harrison; B. Paizs, Sequence-scrambling fragmentation pathways of protonated peptides. *J. Am. Chem. Soc.* **2008,** 130, 17774-17789.

12. A. G. Harrison, Peptide sequence scrambling through cyclization of b_5 ions. *J. Am. Soc. Mass Spectrom.* **2008,** 19, 1776-1780.

13. A. G. Harrison, To b or not to b: The ongoing saga of peptide b ions. *Mass Spectrom. Rev.* **2009,** 28, 640-654.

14. A. G. Harrison; A. B. Young; C. Bleiholder; S. Suhai; B. Paizs, Scrambling of sequence information in collision-induced dissociation of peptides. *J. Am. Chem. Soc.* **2006,** 128, 10364-10365.

15. C. Jia; W. Qi; Z. He, Cyclization reactions of peptide fragment ions during multistage collisionally activated decomposition: an inducement to lose internal residues. *J. Am. Soc. Mass Spectrom.* **2007,** 18, 663-678.

16. R. C. Burnier; G. D. Byrd; B. S. Freiser, Copper (I) chemical ionization-mass spectrometric analysis of esters and ketones. *Anal. Chem.* **1980,** 52, 1641-1650.

17. A. Reiter; J. Adams; H. Zhao, Intrinsic (gas-phase) binding of Co^{2+} and Ni^{2+} by peptides: A direct reflection of aqueous-phase chemistry. *J. Am. Chem. Soc.* **1994,** 116, 7827-7838.

CHAPTER 6

CHARACTERIZATION AND SEQUENCING OF LMWCr BY MASS SPECTROMETRY

6.1 Introduction

More than fifty years ago, chromium was proposed to be an essential trace element and was shown to have the potential to treat the symptoms of type 2 diabetes. Since that time research into chromium's action at the molecular level has been ongoing but futile.[1] One chromium binding molecule has been found to be biologically active and proposed as a potential candidate for the *in vivo* form of chromium, low-molecular weight chromium-binding substance (LMWCr or chromodulin).[2]

The identification of this molecule(s) and attempts at characterizing it and its complex with chromium were begun in the 1980s by Osamu Wada and coworkers.[2-9] In 1981, a low-molecular-weight chromium compound was identified by size exclusion chromatography of the cytosol of liver cells of male mice injected with a single dose of potassium chromate.[2] A similar low-molecular-weight compound was found in the feces and urine for hours after the intravenous administration. These researchers suggested that a low-molecular-weight chromium-binding substance (LMWCr) was formed in the liver and participates in retention and excretion of chromium from the body. Material from the livers of rabbits was treated similarly with chromate was partially purified and was found to be an anionic organic-chromium complex containing amino acids.[2] Also in 1981,

Wada and coworkers reported additional studies on LMWCr from urine. LMWCr was found to occur in urine normally, although the amounts were greatly increased after rats were injected with chromate.[4] Normal human and rat urine LMWCr was not found to be saturated with chromium. Human LMWCr was believed to be similar to that found in the liver and other organs of rabbits and dogs and to be involved in removing excess chromium from the body. The distribution of LMWCr in mice 2 hours after injection with potassium dichromate was also examined.[6] LMWCr was found in liver, kidney, spleen, intestine, testicle, brain, and blood plasma, with the greatest amount in liver followed by kidney. Supernatants of homogenates of the organs were found to possess more chromium bound to LMWCr when dichromate was added to the homogenate than when the mice were injected with dichromate. The time course of chromium binding to LMWCr after injection of dichromate was investigated.[3] Chromium was found to be associated with liver and kidney LMWCr only 2 minutes after injection and reached a maximum 1 to 2 hours after treatment. In these studies, LMWCr was again identified by its elution behavior in size exclusion chromatography and its Cr-binding ability.

Insulin dose response studies using rat adipocytes have indicated a potential intrinsic biological function for LMWCr. Isolated rat adipocytes in the presence of LMWCr and insulin display an increased ability to metabolize glucose to produce carbon dioxide or total lipids; this increase occurs without a change in the insulin concentration required for half maximal stimulation.[8-10] This lack of change in half-maximal insulin concentration suggests a role for LMWCr inside the insulin-sensitive cells after insulin binds externally to the insulin receptor.[10] The stimulation of glucose metabolism by LMWCr is proportional to the chromium content of the oligopeptide.[5] A role has been

proposed for LMWCr in the autoamplification of insulin signaling by binding to activated insulin receptor.[11]

Efforts continued to isolate and characterize LMWCr. To date LMWCr has been isolated and purified from several mammalian sources including rabbit liver,[8] bovine liver,[12] and porcine kidney,[13] The material from rabbit was loaded with Cr by injection of the animal with chromate (or Cr(III) which provides lower yields). For the materials from bovine liver and porcine kidney, chromate was added to the homogenized liver or kidney or suspended kidney powder. A Cr-loading procedure was required so that the material can be followed by its chromium content during the isolation and purification procedures. Amino acid analysis of the bovine LMWCr indicates the presence of 4 glutamate (glutamic acid and/or glutamine), 2 aspartate (aspartic acid and/or asparagine), 2 glycine, and 2 cysteine residues,[12] while the rabbit LMWCr possesses an additional glycine residue.[8] Thus, LMWCr appears to be a naturally occurring oligopeptide composed of glycine, cysteine, aspartate and glutamate with the carboxylates comprising more than half of the total amino acid residues. No amino acid sequence data has appeared, despite attempts at sequencing by Edman degradation, NMR, and mass spectrometry. The lack of additional characterization of the organic components of the materials has been a matter of concern, particularly since the rabbit LMWCr amino acid composition was reported over 20 years ago.

LMWCr is an acidic peptide that contains four tightly bound Cr(III). The presence of Cr(III) has prevented the sequencing of LMWCr by mass spectrometry in the past. The Cassady group has previously attempted to analyze bovine LMWCr by ESI, which gave no signal, and by MALDI/TOF, which gave a weak signal and produced a

difficult to interpret PSD spectrum.[14] Multiple tightly bound Cr(III) may hold the peptide together preventing facile fragmentation. Herein is a reported successful effort to sequence the oligopeptide of LMWCr by mass spectrometry.

6.2 Experimental

6.2.1 Preparation of Samples

To compare to chromodulin samples, commercially available biological acidic peptides and synthetically prepared acidic peptides were used to mimic properties of chromodulin. These include Fibrinopeptide B (human), which was purchased from Fisher Scientific (Pittsburg, PA, USA), DAADAAD, DAAAD, EAAEAAE, and suggested candidate sequences for LMWCr (EDGEECDCGE, DGEECDCGEE) and smaller heptapeptides fragments of LMWCr, (pEEEEGDD and pEEEGEDD), which were synthesized using the procedure discussed in Chapter 2 Section 3. Synthetic peptides were prepared according to standard solid phase Fmoc procedures using an Advanced ChemTech (Louisville, KY, USA) Model 90 peptide synthesizer. Biologically derived samples of LMWCr were received from John Vincent's group at the University of Alabama after isolation from several sources including bovine, alligator, and chicken liver, and human urine by methods described in previous publications.[12, 15, 16]

Additional procedures were carried out to desalt, purify and concentrate samples for this study.[17] For MALDI/TOF analysis, the resulting samples were prepared with and without MALDI matrix. Matrices studied include 2,5-dihydroxybenzoic acid (DHB) and α-cyano-4-hydroxycinnamic acid (CCA) prepared in (1:1 ACN:H_2O) with and without 0.1 and 1 % trifluoracetic acid (TFA) or formic acid (FA) used to assist in protonation.

Other attempts to optimize ionization include varying the ratio of sample to matrix including ratios of 1:1, 1:2, 1:4, 1:5, and 1:10. The type of plate used for sample spotting; for example, Anchorchip^{TM}, polished, and brushed steel were also varied until optimum signal was achieved. Sample spot sizes were 0.8-1.5 μL depending on sample plate used. For ESI/QIT MS analysis, samples were prepared in MeOH, ACN, water, or combinations of the three. For example, 1:1 MeOH:H_2O works well with EDGEECDCGE adducted with Cr(III).

6.2.2 Mass Spectrometry

MALDI/TOF MS experiments were carried out as described in Chapter 2. Positive and negative spectra were obtained using linear and reflectron modes with accelerating voltages of 20 kV. Post source decay (PSD) spectra were obtained in the negative mode after precursor isolation by stepping down the reflectron voltages in stages: -21.0, -19.55, -15.75, -11.82, -8.86, -6.64, -4.98, -3.74, and -2.80 kV. The resulting spectral segments were stitched together into a PSD spectrum with the processing software Flexanalysis.

On-line LC-MS analysis of chromodulin was carried out with an Agilent 1200 series liquid chromatograph. A Zorbax (150 × 0.5 mm) 5B-C18 column was interfaced to a Bruker HCTultra PTM discovery system high capacity quadrupole ion trap (QIT) mass spectrometer (Billerica, MA, USA) via electrospray ionization (ESI). Mobile phase A was doubly deionized water (ddH_2O), and mobile phase B was acetonitrile. A gradient elution at a flow rate of 10 μl/min was performed as follows: 0-5 min 2 % B (isocratic), 5-44 min 2 %-80 % B (linear gradient), and then 44-60 min 100 % B (isocratic).

A syringe pump was used for direct infusion of sample solution into the ESI source with a flow rate of 140 μL/h. The needle spray voltage was 4 kV; the ion transfer capillary temperature was 300 °C. The mass spectra were obtained within a range of *m/z* 100-2000 in the negative ion mode. Tandem mass spectrometry employed low energy collision-induced dissociation utilizing He as the collision gas. The fragmentation amplitude was set as 1.0 V, and the acquisition software's smart fragmentation was on (the start amplitude 30 % and the end amplitude 200 %).

6.3 Results and Discussion

6.3.1 Mass Spectrometric Analysis of Acidic and LMWCr Candidate Peptides

Previous work[14] demonstrates that once bound to Cr(III), acidic peptides lose large neutrals to produce minimal fragmentation and very little actual backbone cleavage. Initial studies into this phenomenon involved a small acidic peptide DAAAD and Cr(III) in an attempt to minimize side chain interactions with the metal. Figure 6.1 shows MALDI PSD spectra of (a) protonated (apo) DAAAD $[M + H]^+$ and (b) the Cr(III) adduct, $[M + Cr - 2H]^+$. The protonated peptide gives intense b-ions and three out of four possible backbone cleavages. In contrast, the Cr(III) metallated sample gives only one fragment, which is 154.2 Da lower in mass than the precursor. This fragment ion could not be identified. Similar large neutral loss had been observed in the Cassady group[18] previously in Cr(III)-adducted peptides and is attributed to the tight binding of metal to the peptide's acidic side chains. The metal "holds" the peptide together, preventing facile fragmentation and thus eliminating the possibility of sequencing. Possibly the peptides are fragmenting but not being detected because Cr ions can be bound at multiple sites and

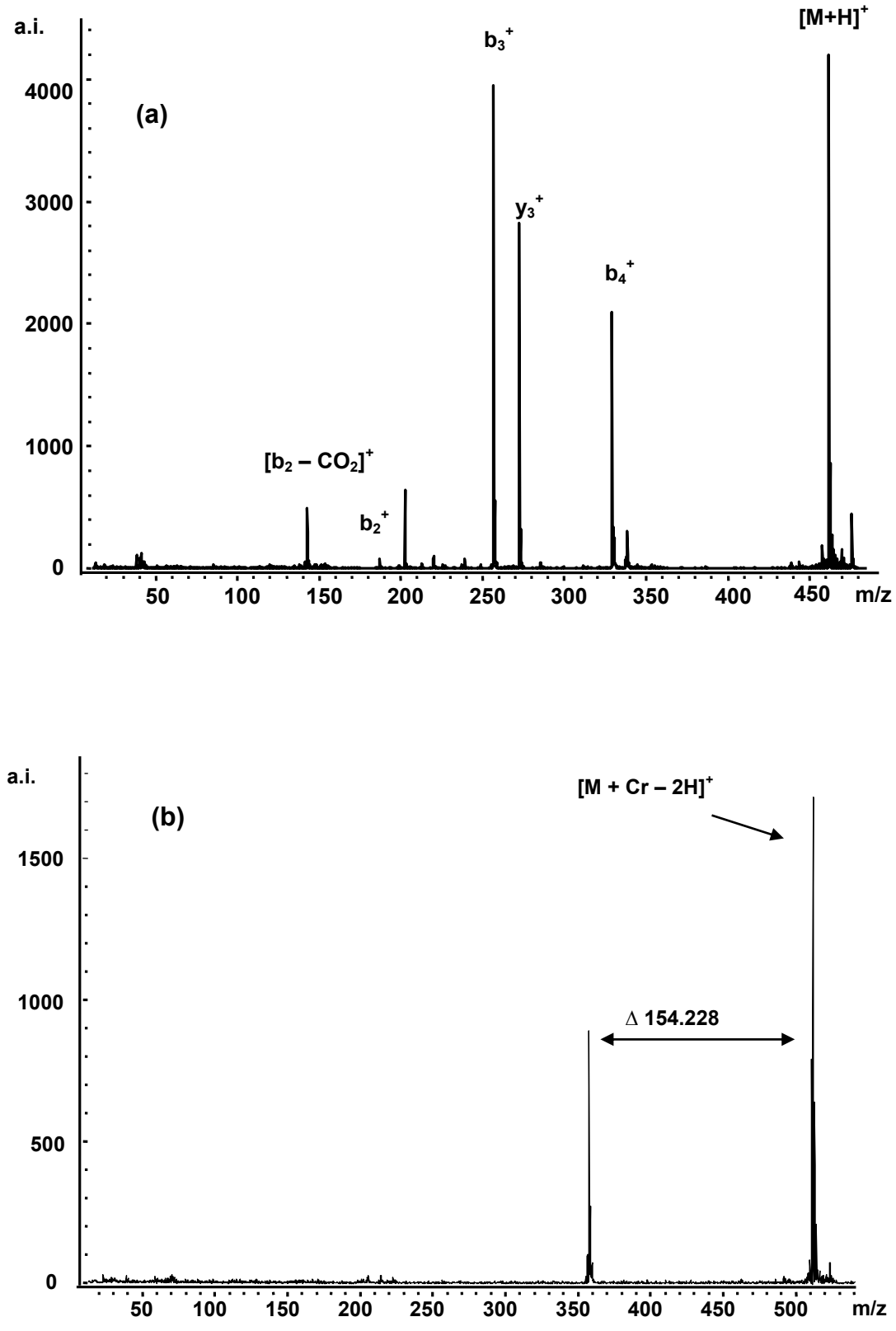

Figure 6.1. Positive MALDI PSD mass spectra obtained from (a) protonated DAAAD, $[M + H]^+$ and (b) the Cr(III)-adducted DAAAD, $[M + Cr - 2H]^+$.

hold the pieces of the peptide together. This could account for the unidentifiable peaks that form when fragmenting Cr-metallated peptides.

The biologically derived holo-peptide, LMWCr, contains four tightly bound Cr(III). To more closely model LMWCr, Cr(III) was added to its proposed candidate sequence[19, 20] EDGEECDCGE. Previous attempts to mimic LMWCr's multiple Cr attachments led to the attachment of only one Cr(III) to this peptide.[14] This limits the ability to study its PSD spectra as a model for the biologically derived holo-peptide.

To increase the number of Cr(III) bound to the candidate peptide, several conditions were tried. Chromium (III) chloride hexahydrate, $CrCl_3 \bullet 6\ H_2O$, was used in previous attempts to add Cr(III) to peptides. Trivalent chromium is substitutionally inert or very slow to exchange its ligands when coordinated to water. To increase binding to the peptide, the waters of hydration and chlorides were removed and replaced with more easily exchangeable ligands as described in Section 6.3.2. The Cr complex, hexakis(tetrahydrofuran)chromium(III) tris(tetrafluoroborate), was then reacted with the candidate peptide, and the more labile ligands were easily replaced by the peptide donor sites.

6.3.2 Synthesis of $Cr(THF)_6(BF_4)_3$ hexakis(tetrahydrofuran)chromium(III) tris(tetrafluoroborate)

To synthesize $Cr(THF)_6(BF_4)_3$, care should be taken to avoid water contamination in every step. To avoid water, a double neck, round bottom flask was fitted with a condenser and a septum to hold the starting material ($CrCl_3 \bullet 6H_2O$) and a stir bar. The Cr(III) salt was first ground by mortar and pestle to reduce the amount of water retained

by large pieces during the drying process. The system was heated in an oil bath under vacuum at ~ 80 °C for at least 12 hours. The initially dark green starting material turned purple indicating loss of the six coordinated water molecules.

Once the water molecules were removed, tetrahydrofuran (THF) was added through a septum via canula/syringe. The resulting dark purple solution was stirred and refluxed under vacuum for 24 hours. To displace the chloride ligands, silver tetrafluoroborate ($AgBF_4$) was added to the mixture in a 3:1 molar ratio (Ag:Cr) in a glove box. Alternatively, the $AgBF_4$ can be dissolved in the THF and transferred via canula through a septum. The solution was allowed to stir and reflux ~24 hours and then filtered through a glass fritted funnel under nitrogen and kept under vacuum overnight to remove excess THF. The reaction sequence is shown in equations 6.1-6.3.

$$CrCl_3 \bullet 6H_2O \ + \text{heat} \ \rightarrow \ CrCl_3 + 6H_2O \qquad (6.1)$$

$$CrCl_3 \ + 6THF \ \rightarrow \ CrCl_3 \bullet (THF)_6 \qquad (6.2)$$

$$CrCl_3 \bullet (THF)_6 \ + \ 3AgBF_4 \ \rightarrow \ \mathbf{Cr(THF)_6(BF_4)_3} \ + \ 3AgCl\,(s) \qquad (6.3)$$

6.3.3 Reactions of $Cr(THF)_6(BF_4)_3$ with EDGEECDCGE

The newly synthesized $Cr(THF)_6(BF_4)_3$ was added to the candidate sequence and compared to $CrCl_3 \bullet 6H_2O$ to its determine ability to increase Cr(III) adduction to acidic peptides. Previous results indicate that $CrCl_3 \bullet 6H_2O$ adds a maximum of one Cr(III) to EDGEECDCGE.[14] In this study, MALDI/TOF MS results show that when added as a 1:5 molar ratio of peptide to Cr(III) salt in dry MeOH, $CrCl_3 \bullet 6H_2O$ adds two, three, and four Cr(III) in small amounts. This is an improvement over previous work, which only

added one Cr(III).[14] Simply removing the water (previous peptides were all dissolved in water) may increase Cr(III) incorporation. The reactions of $Cr(THF)_6(BF_4)_3$ with EDGEECDCGE were carried out in dry MeOH and in dry 1:1 MeOH:ACN (v:v). Using $Cr(THF)_6(BF_4)_3$ increases the number of bound Cr(III) to six and increases the relative intensities of all chromium-bound peptide ions as shown in Figure 6.2. This indicates that the peptide has taken up more Cr(III). The acidic side chains of the peptide that may bind Cr(III) are visualized in Figure 6.3. This also demonstrates that the candidate peptide is capable of multiple Cr(III) attachments, which is consistent with the solution-phase behavior of LMWCr.

6.4 Smaller Heptapeptide Fragments of LMWCr

6.4.1 Production of Apo-Oligopeptide of LMWCr

In the past, only harsh methods had been successful in removing Cr from LMWCr because Cr(III) ions bind tightly to LMWCr[21] (and *vide infra*). Previous efforts to generate the apo (or metal free) form of the oligopeptide involved exposing the LMWCr to an excess of ethylenediaminetetraacetic acid (EDTA) at low pH (~3.5) and elevated temperatures for substantial periods of time.[5, 12] This process generated an appreciable amount of denatured, unrecoverable material when performed with milligram quantities of LMWCr. A new technique developed in the Vincent group[17] generated an apo-oligopeptide of LMWCr from a variety of sources (alligator liver, chicken liver, bovine liver, and human urine). Amino acid analysis showed that the component of bovine LMWCr had the composition 1.0 glycine: 4.5 glutamate: 2.2 aspartate: 0 cysteine. This indicates that LMWCr lost some of the amino acids during treatment and or processing.

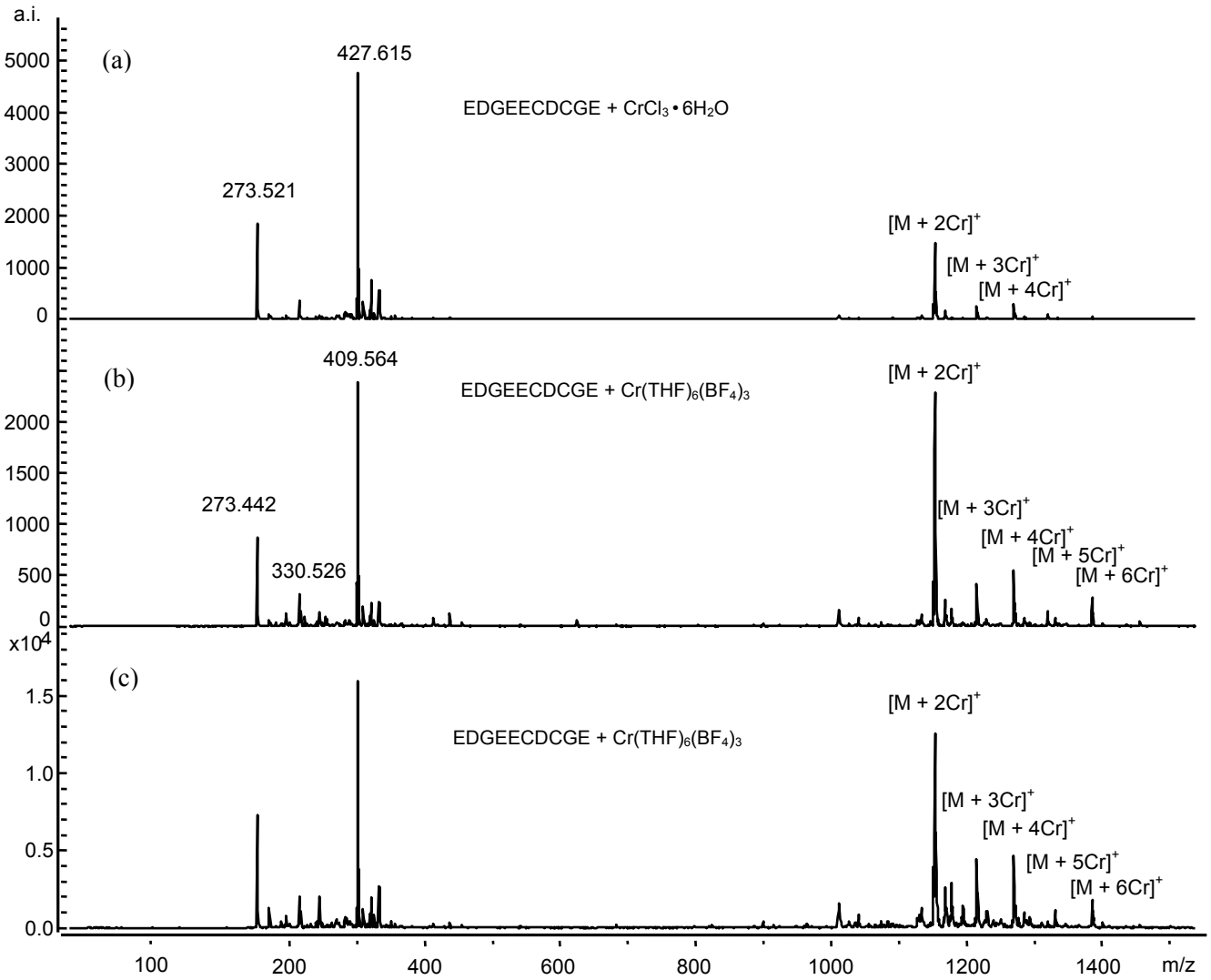

Figure 6.2. Positive MALDI MS spectra obtained after mixing EDGEECDCGE candidate peptide with (a) $CrCl_3 \bullet 6H_2O$, (b) $Cr(THF)_6(BF_4)_3$ (both in dry MeOH), and (c) $Cr(THF)_6(BF_4)_3$ (in dry MeOH/ACN).

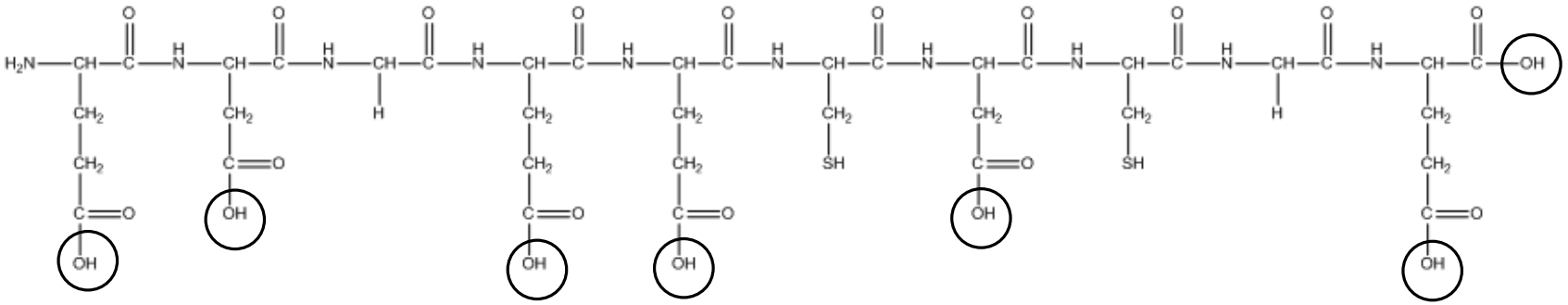

Figure 6.3. Structure of the LMWCr candidate sequence EDGEECDCGE with acidic sites circled.

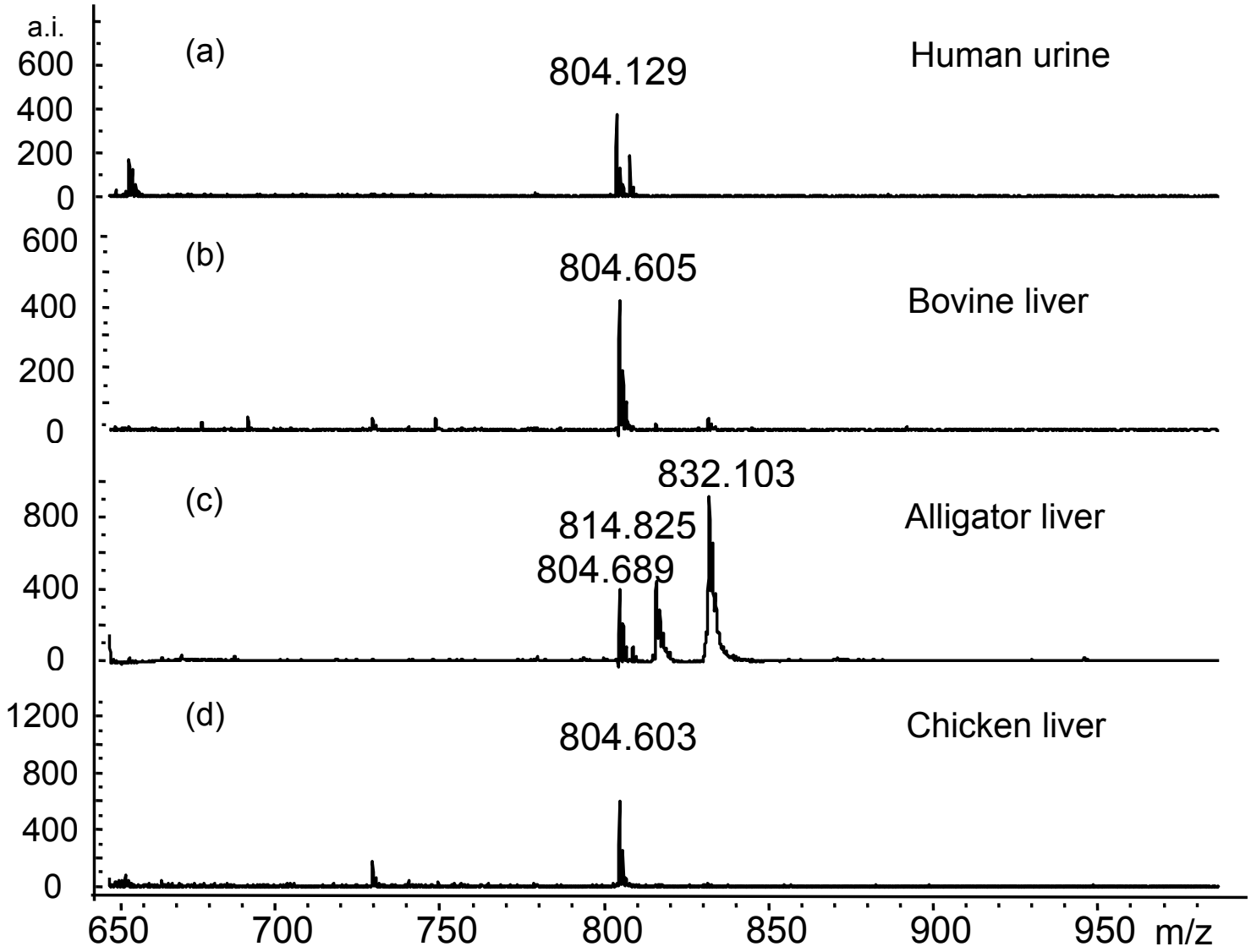

Figure 6.4. Negative mode MALDI/TOF MS of treated LMWCr samples from (a) human urine, (b) bovine liver, (c) alligator liver, and (d) chicken liver.

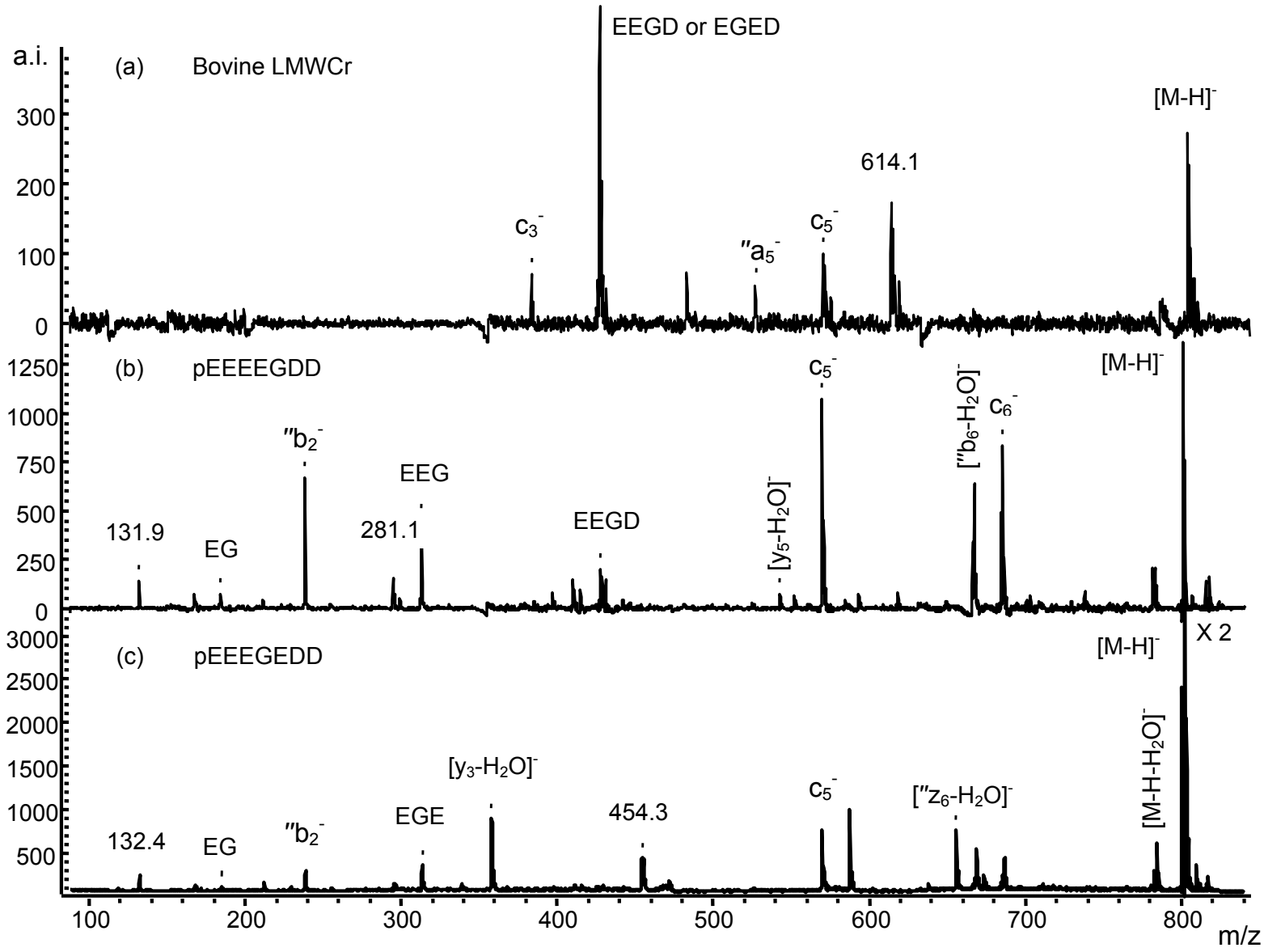

Figure 6.5. Negative PSD spectra of the [M - H]$^-$ from a) treated bovine LMWCr, and its candidate sequences b) pEEEEGDD, and pEEEGEDD

6.4.2 MALDI/TOF MS of Model Peptides and LMWCr

Samples received from the Vincent group after purification via graphite powder microcolumn were submitted to MS analysis. All samples produce a molecular ion, $[M - H]^-$ (*m/z* 804), when analyzed by negative mode by MALDI/TOF MS (Figure 6.4). The corresponding positive mode molecular ion, $[M + H]^+$ (*m/z* 806), was not observed. The lack of a positive signal is consistent with the highly acidic nature of LMWCr. The y-axis in Figure 6.4 shows the absolute intensity of the ion signals. The intensities for the ions of interest are only a few hundred detector counts, which is very low; a more typical value would be about ten times higher. The low signal intensities possibly resulted from low LMWCr concentration due to poor binding capacity of the microcolumn or inefficient LC elution using 70% acetonitrile/0.1% TFA or from difficulty of ionizing the samples by MALDI.

Post-source decay (PSD) of the *m/z* 804 ion of bovine LMWCr was performed (Figure 6.5) and two sequences were proposed based on this data: pEEEEGDD and pEEEGEDD (where pE is pyroglutamate). Peptide backbone cleavage ions were identified and are denoted with Roepstorff and Fohlman nomenclature.[22] All assigned product ions match the mass-to-charge of the predicted ions to within *m/z* ±1, which is within accepted accuracy of PSD. Several significant unassigned peaks are observed in the spectra that are not standard peptide cleavage fragments. Past work in the Cassady group[23] has indicated that non-standard cleavages frequently appear in negative mode MS/MS when adjacent acidic residues exist in a peptide. The precursor ion, $[M - H]^-$, at *m/z* 804 is 2 Da higher in mass than expected. The reason for this is unclear, but it occurs consistently in the MALDI/TOF experiments of the LMWCr samples. The extra 2 Da

may indicate that the biological peptides have been modified by the addition of two hydrogen atoms (e.g., hydrogenation across the double bond of a carbonyl) during the MALDI process; perhaps a trace component in the biological samples is facilitating the process. Sample modification during MALDI is unusual, but not without precedent. Tanaka and coworkers observed hydrogenation during MALDI on oligosaccharides tagged with 2-aminopyridine,[24] while Yamaguchi *et al*. found that MALDI induced dehydrogenation for a peptide derivatized with 2-hydrazino-2-imidazoline.[25]

Post-source decay spectra of the synthetic peptides were generated and compared to those produced by biological LMWCr's; the spectra are shown in Figure 6.5. The synthetic peptides produced the expected $[M - H]^-$ at *m/z* 802. The PSD spectra for the biological LMWCr samples were produced from *m/z* 804, while the PSD spectra for the synthetic peptides were generated from *m/z* 802. (MALDI/TOF MS analysis of mixtures of biological and synthetic peptides yielded both *m/z* 802 and *m/z* 804, showing that these were two distinct ions.) This mass discrepancy may prevent a strong match between the PSD spectra for the biological peptides and the model peptides. Spectra of the LMWCr's from different biological sources (bovine, human, alligator, and chicken) shared common features at *m/z* 384, 428, 482, and 570, which suggests a similarity in sequence. However, the PSD spectra of peptides pEEEEGDD and pEEEGEDD both showed only a few similar features to those of the LMWCr's at *m/z* 428, 482, and 570. The MALDI/TOF spectra did not share enough common features to positively identify the biological peptide.

6.4.3 Analysis of LMWCr Using ESI/QIT MS

No ESI response (*m/z* 802) could be observed when LMWCr was loaded into the LC portion of the ESI/QIT MS due to ionization interferences that result from biological samples.[17] Suppression of the signal at the time point that corresponds to the void volume of the column is common.[26] Consequently, for the experiments described below, LMWCr samples were introduced into the ESI source by infusion with a syringe pump rather than by LC.

As was the case for MALDI, no positive ion signal was observed when LMWCr samples were ionized by ESI. The negative mode ESI spectrum of bovine LMWCr (Figure 6.6) shows one peak at *m/z* 802 and another at *m/z* 401 corresponding to the singly and doubly charged species, $[M - H]^-$ and $[M - 2H]^{2-}$, respectively. Unlike the ions generated by MALDI, these ions generated by ESI (which is a much gentler ionization technique) exactly conform to the MW of pEEEEGDD or pEEEGEDD. Low-energy CID MS/MS (or MS^2) on *m/z* 802 ions, $[M - H]^-$, was carried out to elucidate the sequence. The synthetic peptides pEEEEGDD and pEEEGEDD were dissociated under the same conditions. The MS/MS spectra of *m/z* 802, $[M - H]^-$, from the bovine sample and the two synthetic peptides were dominated by a very intense water elimination ion at *m/z* 784, $[M - H - H_2O]^-$. Water loss during low-energy CID is common and abundant in the negative mode when a peptide has adjacent acidic residues.[23] Relative to this large *m/z* 784, other CID products were present with only a few percent relative intensity (or less), and no obvious differences existed among these low intensity ions. That is, CID on $[M - H]^-$ (MS/MS) can not distinguish between these two synthetic peptides, and both model spectra are a good match for the biological sample.

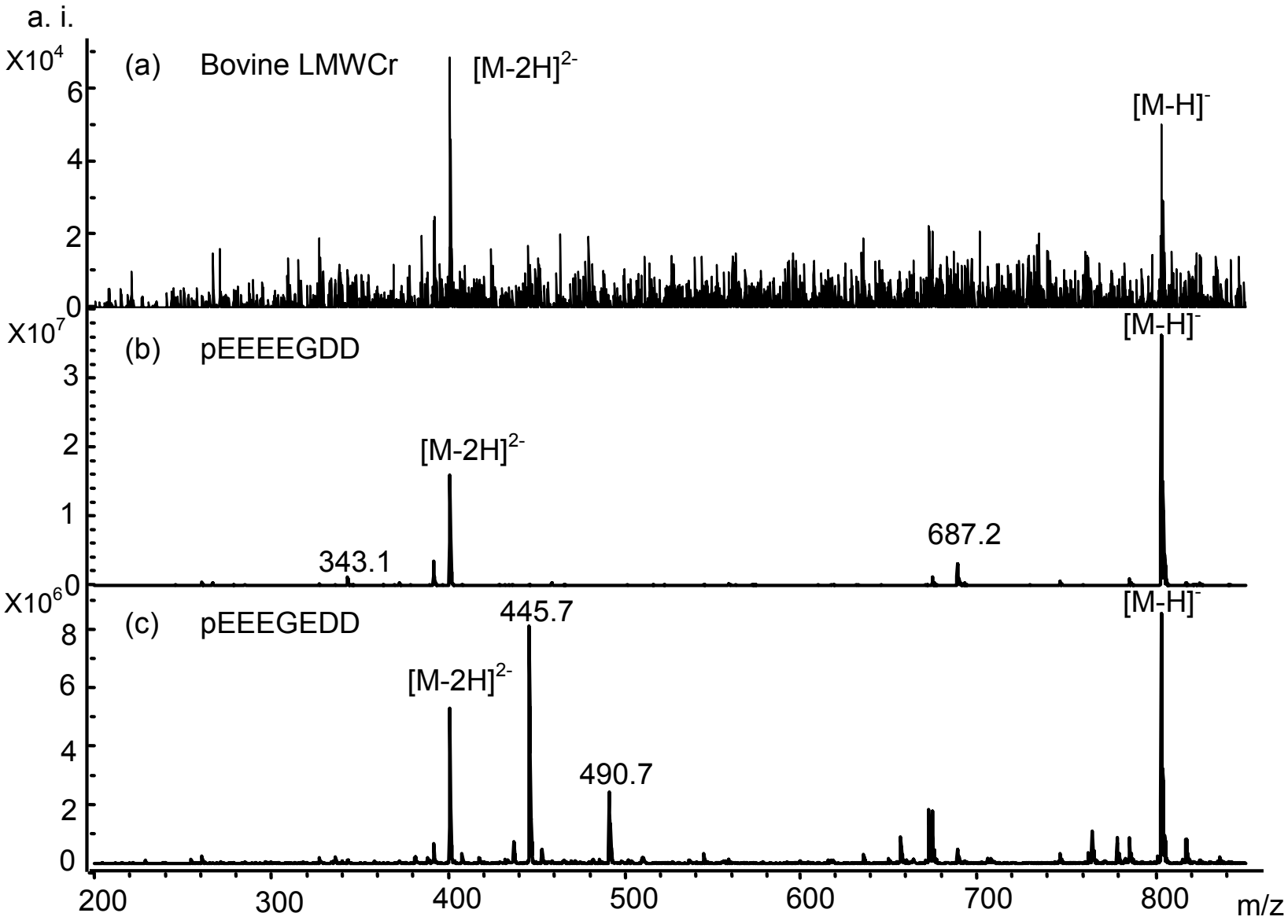

Figure 6.6. Negative mode ESI/QIT spectra of (a) bovine LMWCr and the candidate sequences (b) pEEEEGDD and (c) pEEEGEDD.

The intense peak at *m/z* 784, $[M - H - H_2O]^-$, which dominated the MS/MS spectra for both synthetic peptides and for bovine LMWCr, was subjected to a further stage of CID. The resulting MS^3 spectra are shown in Figure 6.7. Again, very similar spectral features were shared by the spectra of LMWCr and the two synthetic peptides. A few notable differences were observed in MS/MS/MS spectra of *m/z* 784 ions between the two synthetic peptides. A peak at *m/z* 397 (circle marked in Figure 6.7) is found in the spectrum from pEEEEGDD, which corresponds to an $''a_4^-$ fragment. Because $''a_4^-$ incorporates only the first four residues of the peptides (starting at the N-terminus), it will not form at the same *m/z* in the spectrum of pEEEGEDD. The CID spectrum from the fragment of bovine LMWCr also contains a peak at *m/z* 397 in roughly the same abundance as in the spectrum for pEEEEGDD. In addition, a peak at *m/z* 632, corresponding to $[''b_6 - 2H_2O]^-$, is found only in the spectra from pEEEGEDD, not in the spectra from pEEEEGDD or bovine LMWCr. In negative mode CID of peptides, adjacent acidic residues (aspartic acid or glutamic acid) promote water loss, and this is much more prevalent when one of the residues is aspartic acid.[23] Of the two model peptides, only pEEEGEDD has an aspartic acid residue (D at the sixth position) adjacent to another acidic residue (E at the fifth position) within the first six residues of the sequence, which comprise $[''b_6 - 2H_2O]^-$. Taking into account the two spectral features discussed here, the sequence of the fragment from bovine LMWCr is assigned as pEEEEGDD.

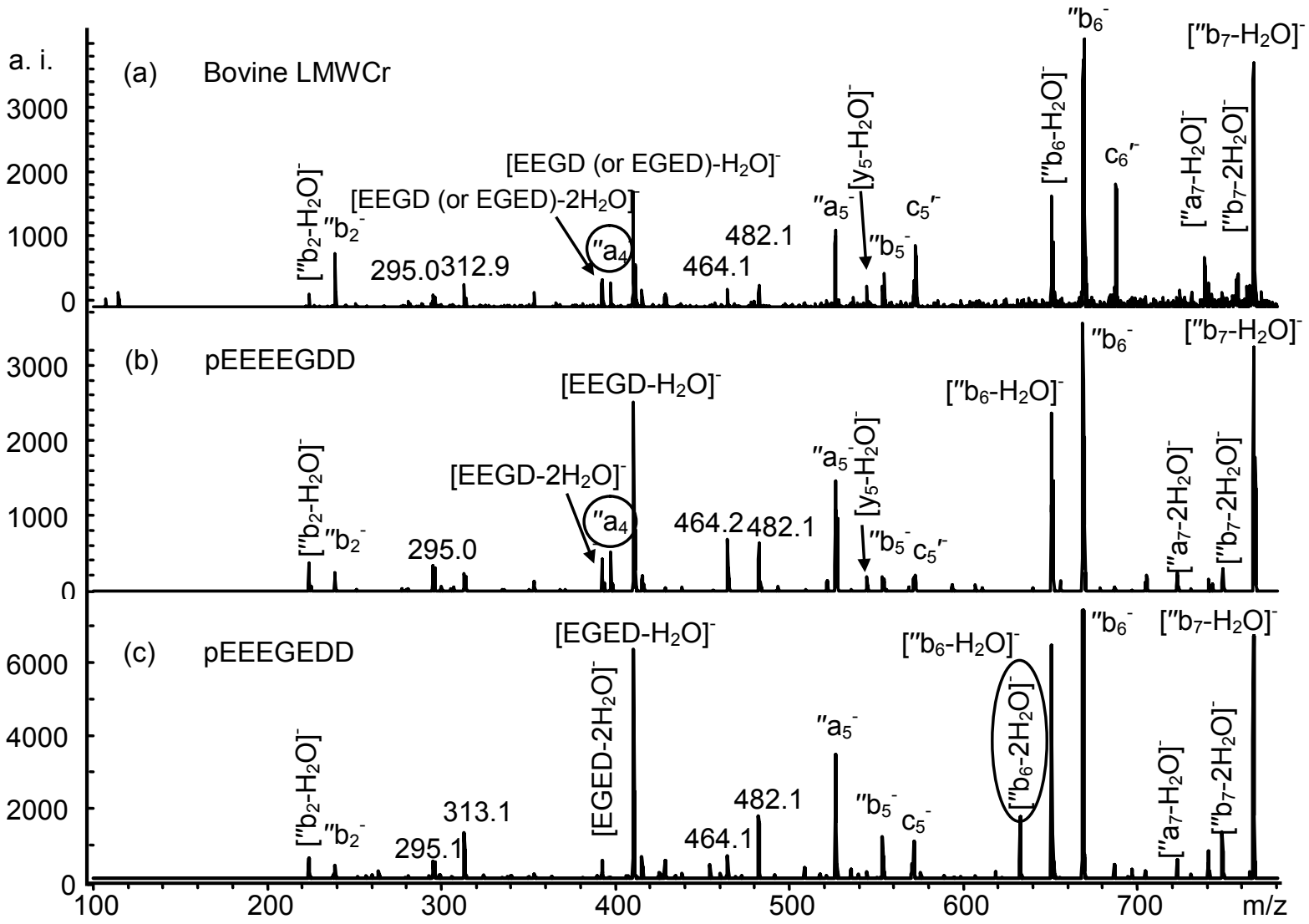

Figure 6.7. Negative mode MS^3 spectra obtained from CID of the $[M - H - H_2O]^+$ for M = (a) bovine LMWCr, (b) pEEEEGDD, and (c) pEEEGEDD.

6.4.4 Supporting Evidence for the Proposed Sequence Belonging to LMWCr

In the body, peptides, including numerous peptides with bioactivity, originate from the processing of proteins. Thus, the heptapeptide isolated from LMWCr should have at a point in its history been part of a larger protein. A genomic search against the databases of the National Center for Biotechnology Information (NCBI) using the sequence EEEEGDD was performed by the Vincent group to identify proteins containing this sequence motif. Multiple 100 % hits were found due to the short sequence and low complexity: seven sequences in *Homo sapiens*; two in *Bos taurus*; two in *Gallus gallus*; one in *Mus musculus*. Unfortunately, very little of the American alligator genome has been sequenced. None of the hits contain glycine and cysteine residues flanking the EEEEGDD sequence, suggesting that these residues are not part of a contiguous peptide and are attached to the heptapeptide in a non-standard fashion. This is consistent with NMR studies on holoLMWCr and acid-hydrolyzed LMWCr that suggested the presence of some other organic moiety.[12]

Curiously, several of the sequence hits correspond to genes for proteins involved in modifying chromatin. None of these hits correspond to a responsive gene in chromium treatment of mice (isolated adipocytes) or mouse testis (TM4 Sertoli-like) cells.[27, 28] This is an area worthy of continued investigation.

Further confirmation of the proposed sequence pEEEEGDD being that of LMWCr came from chromium-binding studies and Hill plots, which were performed by the Vincent group.[17] The chromium-binding of the proposed candidate sequences were compared to that of LMWCr. The binding of chromium to bovine apoLMWCr prepared by the low pH EDTA method,[12] to the heptapeptide pEEEEGDD, and to the two full

candidate acidic peptides was investigated. A variation on equilibrium dialysis using ultrafiltration was used to follow ^{51}Cr-binding to the peptides and Langmuir isotherms were used to estimate the number of Cr(III) ions that bind to synthetic and biologically derived LMWCr. The results indicate that the synthetic peptide pEEEEGDD tightly binds four Cr(III) ions. In addition, the Hill constants, which demonstrate cooperativity of Cr to peptide binding, of apo LMWCr and pEEEEGDD are identical within experimental error.[17]

6.5 Conclusions

LMWCr is a highly acidic peptide that has several tightly bound Cr(III) ions, which have prevented mass spectrometric sequencing in the past. Previous attempts to sequence LMWCr by MALDI/TOF PSD led to unidentifiable fragment ions and no useful sequence information, while attempts to ionize by ESI resulted in no signal.[14] In this work, extensive MS studies on a contiguous peptide component of biologically derived LMWCr resulted in sequence information by both MALDI/TOF and ESI/QIT MS. Comparison of LMWCr and candidate peptides revealed that the most likely sequence of the heptapeptide component of LMWCr is pEEEEGDD. This proposed sequence agrees with previous amino acid analysis and new chromium-binding studies. The new sequence also explains the failure to sequence this peptide by Edman degradation in that the N-terminus (pE) is cyclized, which prevents sequencing by this method.[29]

$Cr(THF)_6(BF_4)_3$ was used to increase the number of bound Cr(III) on acidic peptides and is presented as an alternative to the use of $CrCl_3 \cdot 6H_2O$ as a reagent to bind

Cr(III) to peptides. This may be useful in further studies of chromium-bound peptides where multiple bound chromium ions are desirable. The tight binding of Cr(III) to peptides, especially those with acidic amino acid side chains, greatly decreased fragmentation in tandem MS experiments. This greatly limits their ability to be sequenced by mass spectrometry.

In conclusion, the sequence of the contiguous peptide component of LMWCr represents a potentially significant milestone towards understanding the pharmacological role of chromium supplementation at a molecular level. Hopefully, this work will lead to further studies elucidating or eliminating a potential role for LMWCr in treating the symptoms of type 2 diabetes and other conditions resulting from improper carbohydrate and lipid metabolism.

REFERENCES

1. J. B. Vincent; D. Stearns, *The bioinorganic chemistry of chromium: essentiality, therapeutic agent, toxin, carcinogen?* Wiley-Blackwell: New York, 2011; in press.

2. A. Yamamoto; O. Wada; T. Ono, A low-molecular-weight, chromium-binding substance in mammals. *Toxicol. Appl. Pharmacol.* **1981,** 59, 515-523.

3. M. S. Wada O, Yamaguchi N, Ishikawa S, Yanagisawa H. , Low-molecular-weight, chromium-binding substance in rat lungs and its possible role in chromium movement. *Ind Health* **1983,** 21, 35-41.

4. G. Y. Wu; O. Wada, Studies on a specific chromium binding substance (a low-molecular-weight chromium binding substance) in urine. *Jpn. J. Ind. Health* **1981,** 23, 505-512.

5. A. Yamamoto; O. Wada; S. Manabe, Evidence that chromium is an essential factor for biological activity of low-molecular-weight, chromium-binding substance. *Biochem. Biophys. Res. Commun.* **1989,** 163, 189-193.

6. A. Yamamoto; O. Wada; T. Ono, Distribution and chromium-binding capacity of a low-molecular-weight, chromium-binding substance in mice. *Journal of Inorganic Biochemistry* **1984,** 22, 91-102.

7. W. O. Yamamoto A, Suzuki H., Separation of biologically active chromium complex from cow colostrum. *J Exp Med* **1987**, 152, 211-219.

8. W. O. Yamamoto A, Ono T, Isolation of a biologically active low-molecular-mass chromium compound from rabbit liver. *Eur J Biochem* **1987,** 165, 627-631.

9. W. O. Yamamoto A, Suzuki H., Purification and properties of biologically active chromium complex from bovine colostrum. *J. Nutr.* **1988,** 118, 39-45.

10. J. Vincent, Relationship between glucose tolerance factor and low-molecular-weight chromium-binding substance. *J Nutr.* **1994,** 124, 117-118.

11. J. B. Vincent, The Biochemistry of Chromium. *J. Nutr.* **2000,** 130, 715-718.

12. C. M. Davis; J. B. Vincent, Isolation and Characterization of a Biologically Active Chromium Oligopeptide from Bovine Liver. *Arch. Biochem. Biophys.* **1997,** 339, 335-343.

13. H. K. Sumrall; J. B. Vincent, Is glucose tolerance factor an artifact produced by acid hydrolysis of low-molecular-weight chromium-binding substance? *Polyhedron* **1997,** 16, 4171-4177.

14. J. Gao. Matrix-assisted laser desorption ionization time-of-flight studies of natural and synthetic peptides. PhD dissertation, Department of Chemistry, The University of Alabama, Tuscaloosa, 2008.

15. Y. Chen. Low-molecular-weight chromium-binding substance: Advanced studies from aves to human. PhD Dissertation, Department of Chemistry, University of Alabama, Tuscaloosa, 2009.

16. M. J. Hatfield; S. Gillespie; Y. Chen; Z. Li; C. J. Cassady; J. B. Vincent, Low-molecular-weight chromium-binding substance from chicken liver and American alligator liver. *Comp. Biochem. Physiol. B* **2006,** 144, 423-431.

17. Y. Chen; H. M. Watson; J. Gao; S. Sinha; C. J. Cassady; J. B. Vincent, Characterization of the organic component of low-molecular-weight chromium-binding substance and its binding to chromium *J. Nutr.* **2011,** 141, 1225-1232.

18. D. Pu; J. B. Vincent; C. J. Cassady, The effects of chromium(III) coordination on the dissociation of acidic peptides. *J. Mass Spectrom.* **2008,** 43, 773-781.

19. D. Dinakarpandian; V. Morrissette; S. Chaudhary; K. Amini; B. Bennett; J. D. Van Horn, An informatics search for the low-molecular weight chromium-binding peptide. *BMC Chemical Biology* **2004,** 4, 2.

20. J. B. Vincent; J. Hatfield; S. Burdette, Caracterizing chromium-containing oligopeptides. *Abstr. Paper Am. Chem. Soc.* **2004**, 227 U-459.

21. Y. Sun; J. Ramirez; S. A. Woski; J. B. Vincent, The binding of trivalent chromium to low-molecular-weight chromium-binding substance (LMWCr) and

the transfer of chromium from transferrin and chromium picolinate to LMWCr. *J. Biol. Inorg. Chem.* **2000,** 5, 129-136.

22. F. J. Roepstorff P, Proposal for a common nomenclature for sequence ions in mass spectra of peptides. *Biomed Mass Spectrom* **1984,** 11, 601.

23. T. Yalcin; C. J. Cassady, Unpublished results.

24. S. Sekiya; Y. Yamaguchi; K. Kato; K. Tanaka, Mechanistic elucidation of the formation of reduced 2-aminopyridine-derivatized oligosaccharides and their application in matrix-assisted laser desorption/ionization mass spectrometry. *Rapid Commun. Mass Spectrom.* **2005,** 19, 3607-3611.

25. M. Yamaguchi; M. Oka; K. Nishida; M. Ishida; A. Hamazaki; H. Kuyama; E. Ando; T.-a. Okamura; N. Ueyama; S. Norioka; O. Nishimura; S. Tsunasawa; T. Nakazawa, Enhancement of MALDI-MS Spectra of C-Terminal Peptides by the Modification of Proteins via an Active Ester Generated in Situ from an Oxazolone. *Anal. Chem.* **2006,** 78, 7861-7869.

26. R. Bonfiglio; R. C. King; T. V. Olah; K. Merkle, The effects of sample preparation methods on the variability of the electrospray ionization response for model drug compounds. *Rapid Commun. in Mass Spectrom.* **1999,** 13, 1175-1185.

27. R. Cheng; W. Alvord; D. Powell; K. Kasprzak; L. Anderson, Microarray analysis of altered gene expression in the TM4 Sertoli-like cell line exposed to chromium(III) chloride. *Reprod Toxicol.* **2002**, 223-236.

28. C. Rink; S. Roy; S. Khanna; T. Rink; D. Bagchi; S. CK, Transcriptome of the subcutaneous adipose tissue in response to oral supplementation of type 2 Leprdb obese diabetic mice with niacin-bound chromium. *Physiol genomics* **2006,** 27, 370-379.

29. F. Wold, In vivo chemical modification of proteins (post-translational modification). *Annu Rev Biochem.* **1981,** 50, 783-814.

CHAPTER 7

CONCLUDING REMARKS

The field of mass spectrometry is rapidly changing and adapting to the needs of analytical chemistry. The application of various configurations of mass spectrometry to the field of proteomics is charged with the daunting task of sequencing the human proteome. In order to analyze the vast amounts of MS^n data produced during high throughput MS processes, spectral interpretation by processing software is necessary. To improve the specificity of the algorithms used in peptide identification, fundamental studies into fragmentation of peptides by various techniques is essential. The analytical chemists' job is to seek out the fundamental understanding of the processes occurring during each stage of MS sequencing: sample ionization, the dissociation techniques, and the gas-phase chemistry that governs product ion pathways. The main objectives are to increase the efficiency and accuracy of peptide sequencing

The contributions of this dissertation and questions the work has provoked are many. The cationization of peptides with several transition metals was found to produce primarily doubly charged peptide ions. The dissociation of these complexes by various techniques was investigated. The identity of the transition metal ion chosen for cationization was found to directly affect the types and abundances of product ions formed independent of the dissociation technique used. In addition, the type of metal ion can alter the pathways of ion formation as shown with metallated a- and b-ions in

Chapters 2-4. The CID spectra of doubly and singly charged Cu-peptide complexes were found to be complementary and give complete sequence coverage when examined together.

As discussed in Chapters 3 and 5, Cu(II) was found to cause carbon elimination from singly charged peptide complexes. These results suggest that the lost carbon originates from the C-terminus. Future work could be done to determine a mechanism for the elimination of carbon by Cu(II) from singly charged peptides. Labeling the side chain of alanine with ^{13}C indicates that the carbon loss is not from a side chain methyl group. Labeling the C-terminal carbonyl carbon to determine if it is lost during Cu(II) insertion would be interesting. Intense loss of CO_2, as shown in Figure 5.7, suggests that this could be the case.

The ETD and ETcaD experiments on transition metallated-peptides result in less complex spectra that are more easily interpreted than those produced by CID of the same complexes. ETD spectra show decreasing N-Cα cleavage as the recombination energy (RE) of the metal ions increase, where the RE of Cr(III) > Cu(II) > Ni(II) > Co(II) > Fe(II). Evidence for macrocyclic, metallated a- and b-ions was found in spectra formed from ETD of Co(II) and Ni(II) cationized peptides in Chapter 4. These species result in the formation of nonsequential ions. Nonsequential ion formation was even more evident in the spectra formed by ETcaD of transition metal-cationized peptides. The presence of nonsequential ions in the MS^n data may not greatly affect the accuracy of search engines; however, investigating this further with large numbers of spectra would be interesting. These results could then be compared with studies of how nonsequential losses formed by CID of protonated species affect search engine results.

Studies of low-molecular-weight chromium-binding substance (LMWCr, a.k.a. chromodulin) and related peptides were carried out and discussed in Chapter 6. LMWCr is an acidic peptide that contains four tightly bound Cr(III). This peptide may be involved in carbohydrate metabolism and, thus, a knowledge of its sequence may be of importance in diabetes research. The candidate sequences that do not contain Cr(III) fragment more easily than the same peptides after metal ion incorporation. The presence of tightly bound Cr(III) has long been an obstacle in the sequencing of LMWCr. The existence of only a few studies into Cr-metallated peptides using mass spectrometry has resulted in limited understanding of how Cr(III) affects peptide fragmentation behavior. The removal of the Cr(III) by the Vincent group also removed some amino acid residues; however, a peptide component of LMWCr was submitted to extensive MS study. Comparisons of MS^n spectra obtained from biologically derived LMWCr to those of synthetic peptides allowed full sequence information of peptide to be obtained. The successful sequencing of a fragment of the apo-LMWCr by mass spectrometry is a good example of the application and necessity of investigations like those presented in Chapters 3-5.

Chapter 6 also describes the use of hexakis(tetrahydrofuran)chromium(III) tris(tetrafluoroborate), $Cr(THF)_6(BF_4)_3$, which when mixed with acidic peptides similar to LMWCr, greatly promotes the formation of complexes containing multiple Cr(III). The incorporation of multiple Cr(III) allows for more closely mimicking biologically derived LMWCr, which contains four Cr(III), when studying fragmentation of biologically derived LMWCr.

To further investigate the primary sequence of LMWCr, the newly formed complexes obtained with $Cr(THF)_6(BF_4)_3$, such as $[M + 4\ Cr - 11H]^+$, can now be dissociated alongside biologically derived holo-LMWCr. Comparing the resulting spectra may allow the full sequence to finally be attained. This would be a promising project for future researchers.